Numerical Modeling of the In-Plane Seismic Behavior of Unreinforced Masonry Wall Retrofitted with Bed Joint Reinforcements

Saeid Mahmoudimotlagh

TU Delft

Numerical Modeling of the In-Plane Seismic Behavior of Unreinforced Masonry Wall Retrofitted with Bed Joint Reinforcements

By

Saeid Mahmoudimotlagh

in partial fulfilment of the requirements for the degree of

Master of Science
in Civil Engineering

at the Delft University of Technology,
to be defended publicly on Monday March 30, 2020 at 14:00 PM

Student number:	4661710
Project duration:	July 17, 2019 – March 30, 2020
Thesis committee:	Prof. dr. ir. Jan. G. Rots, Chair of the Committee
	Dr. ir. Rita Esposito, Daily Supervisor
	Ir. Lambert J.M. Houben, Supervisor

TU Delft

Acknowledgement

It is with great pleasure to express my appreciation to Jan Rots, the chair of my thesis committee, who inspired my interest in the nonlinear finite element modeling of structures. It was an immense opportunity for me to have discussions with Prof. Rots which helped me a lot to learn from his critical remarks.

I would like to declare my extended gratitude to my daily supervisor, Rita Esposito. It was a chance to work with Dr. Esposito who provided constructive feedbacks in every step of the way that were the keys to the tackle with the obstacles. I am extremely delighted to have the chance of gaining experience in working with her. I would also thank Lambert Houben for his supportive recommendations.

Moreover, I am grateful to DIANA FEA BVs' staff and support team (Maziar Partovi, Kesio Palacio, Arjen de Putter, and Ab van den Bos) who kindly helped me for this graduation project.

I would also like to thank my family for their love and support during this period. My parents have continuously been a source of positive energy that helped me to work harder in the entire of the master thesis.

Saeid Mahmoudimotlagh
Delft, March 2020

Contents

Abstract

Gas-induced earthquakes are a major problem in the north of the Netherlands. This is due to the reason of having many unreinforced masonry (URM) buildings being located in this area. These types of buildings are vulnerable to seismic events and taking action is required to improve the seismic resilience of these structures. In order to achieve this purpose, existing structures must be retrofitted and if the aesthetic of the building is important (like heritage buildings), the implemented retrofitting technique must not alter the appearance of the property. An experimental campaign was conducted at Delft University of Technology (Licciardello & Esposito, 2019) to investigate whether bed joint reinforcement (BJR) can be used for seismic retrofitting of URM walls. BJR is often used to repair damage in URM structures caused by settlement. The behavior of a cantilever URM wall with an asymmetric opening retrofitted with 12 layers of BJR (single and double bars) and 8 diagonal anchors (around the corners of the window opening) was determined with a quasi-static cyclic in-plane test. Experimental results of the retrofitted wall showed that by applying this retrofitting technique the force capacity increased slightly and maximum crack width decreased compared with the unreinforced masonry (URM) wall, which was tested in another campaign at TU Delft.

In this thesis, the influence of BJR, diagonal anchors and reinforcement layout on the in-plane seismic behavior of the retrofitted wall is studied. To achieve this goal several nonlinear static analyses using DIANA software were performed. First, the case experimentally tested is adopted as a benchmark and a validation of the numerical model is performed. Afterwards, the validated numerical model is adopted to perform a parametric study considering different reinforcement layouts.

Since the global behavior of the wall is of interest, a macro-modeling approach is used in this research; 2D analyses were performed. Four-node 2D plane stress elements were used to model the masonry wall and the concrete lintel. Material nonlinearity was considered for the former, while linear elastic behavior was used for the latter as no damage in the concrete was expected. BJR and diagonal anchors were modeled as fully bonded reinforcement and von Mises plasticity criterion was adopted. A two-node, 2D class-III beam element was used to represent the steel beam located at the top of the wall. In contradiction with the experiment, a monotonic load-prescribed deformation (in two directions, $+44$ and -40 mm for the URM wall and $+81$ and -64 mm for the retrofitted wall) was applied in the plane of the walls. To consider the self-weight of the beam 0.12 MPa (12 N/mm) pre-compression load was applied vertically. The experimental test stopped because of the failure of the walls at the mentioned displacements. So, the numerical results beyond the mentioned displacements were not validated and analyses were stopped accordingly.

To validate the numerical results, the URM wall and the retrofitted wall were modeled with two smeared crack based material models: the Total Strain Crack Model (TSCM) and the Engineering Masonry Model (EMM). The former is an isotropic whilst the latter is an orthotropic material model. The trend of the capacity curve, as well as the initial stiffness of two material models, are in good agreement with the experiment. However, a convergence problem was experienced when EMM was applied and this led to obtaining unreliable numerical results. Although various iterative methods, different material properties, and extremely small load steps were applied, no convergent solution was found in this study. It must be mentioned that EMM was successfully implemented by other researchers at TU Delft and desirable results were achieved. With regard to the convergence issues, TSCM is decided to be applied in this research.

By applying TSCM (for the URM wall and the retrofitted wall) models were able to estimate the peak-load with an accuracy of 12%. Furthermore, crack patterns and failure modes were predicted accurately by TSCM. However, it was observed that the applied iterative method can affect the peak-load and the crack pattern of the models. At +50 mm displacement divergence occurred when the Regular Newton-Raphson Method (RNR) was applied and the crack pattern of the collapse phase (displacement = +81 mm) could not be studied. Therefore, it is necessary to use the Secant Method, which is suitable for post-peak, to solve the divergence problem. By implementing the Secant Method, up to quadruple cracked integration points were reported in comparison with RNR and this may lead to an issue related to the overestimation of the peak-load (around +25%). No localization of cracks in one finite element was another minor problem of the Secant Method that might be due to the mentioned problem. In this graduation assignment, a combination of two iterative methods was used to solve the mentioned problems. RNR was used to check the peak-load (since divergence occurs after peak-load) and the Secant Method was adopted to investigate the crack pattern and failure modes. In the latter, more attention is needed to interpret the cracks since a smeared out crack pattern is obtained. The crack pattern of the URM and the retrofitted wall can be found in Figure i.

The numerical study showed that BJR was able to improve the seismic performance of the retrofitted wall. Peak-load, maximum crack width, and failure modes were affected accordingly. The Peak-load was increased slightly (13%) in the retrofitted wall with the original reinforcement layout compared with the URM wall. BJR acts in tension to restrains the crack opening and by checking von Mises stress, the plasticity of steel was recognized. So, the maximum crack width is another factor that was affected remarkably: a difference of −110% in maximum crack width (at displacement = −68 mm) was observed after retrofitting. Finally, the crack pattern and failure mechanism of the structure was changed due to the presence of the horizontal bars. In the URM wall rocking of the piers was the main failure mechanism, however, in the retrofitted wall apart from rocking of the piers that occurred initially, an arch mechanism below the window level and toe-crushing were observed.

The sensitivity analysis showed that the results were sensitive to variation in tensile fracture energy and modulus of elasticity, while tensile strength, compressive strength, and compressive fracture energy were the other variations that did not affect the results considerably. A variation of ±50% in modulus of elasticity led to a variation of approximately ±20% in the stiffness of the wall, +14/−8% in terms of peak-load and +64/−45% in maximum crack width. A variation of ±50% in tensile fracture energy led to a variation of +10/−7% in terms of peak-load and +26/−24% in maximum crack width.

An extensive parametric study was carried out to study the influence of diagonal anchors, the length of the anchors, and different reinforcement layouts. According to the 12 analyzed cases (including the base case), it was concluded that double BJR was slightly more effective than single BJR in terms of peak-load and maximum crack width. By applying only 4 layers of double BJR almost the same peak-load and maximum crack width were obtained comparing the results of the retrofitted wall with the original layout (with 12 BJR layers). The location of the BJR, however, was the governing concern. In the URM wall cracks mostly developed diagonally from the window corners and by applying horizontal bars below and above the window opening, the diagonal cracks were restricted and failure modes of the wall changed.

Single BJR next to the opening (in piers) played an important role in the behavior of the wall. The absence of these single BJR might lead to the shear mechanism of the piers. The number of BJR is a function of the opening's dimension. For this study, it was observed that at least 3 layers of single BJR next to the opening were necessary.

By analyzing the numerical results, a proposed reinforcement layout can be presented. It is believed that the mentioned 4 layers of double BJR (above and below the opening) and 3 layers of single BJR (next to the opening) were a wise choice for retrofitting of the wall. Furthermore, diagonal anchors could be ignored. Not only diagonal anchors with original length but also anchors with extended length did not affect the performance of the wall. Conservatively, a layer of double BJR far above and below the window level could be applied. It is believed that the masonry portion above the lintel and below the opening should not leave unreinforced. With this proposed layout the amount of reinforcement was decreased by 30%, however, the force capacity, crack patterns and failure modes of the model were comparable with the retrofitted wall with original reinforcement layout.

Finally, it is recommended to investigate the application of micro-modeling to study the crack patterns and failure mechanisms of the wall more precisely. Besides, a cyclic load - similar to the experiment - can be applied to see if more accurate results can be observed. Engineering Masonry Model is a new and powerful orthotropic material model that allows the user to choose different head-joint failure types. It is recommended to solve the convergence problem of this material model as it is more useful for cyclic loads. Finally, by applying shell elements, the out-of-plane deformation of the walls, which was observed in the experiment, can be investigated. Although this did not lead to failure of the wall in the experimental test.

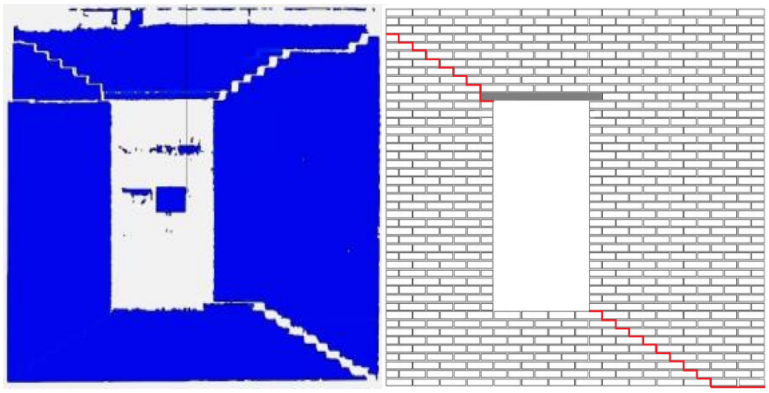

URM wall loaded in positive X-direction.
Test vs. analysis (displacement = +44 mm)

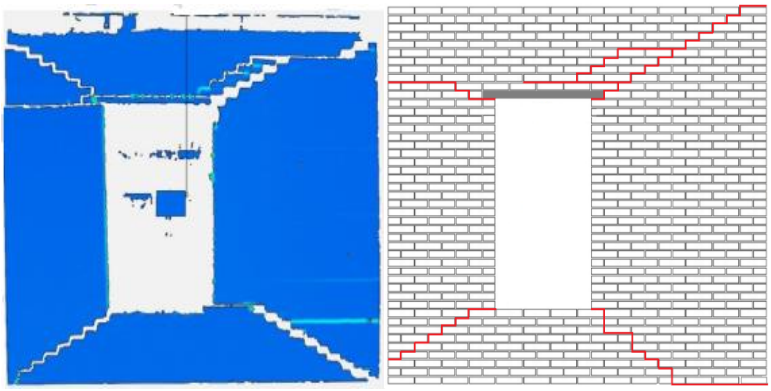

URM wall loaded in negative X-direction.
Test vs. analysis (displacement = -40 mm)

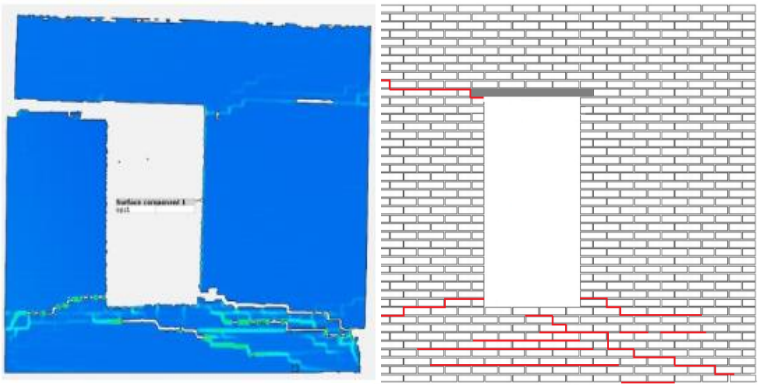

Retrofitted wall loaded in positive X-direction.
Test vs. analysis (displacement = +81 mm)

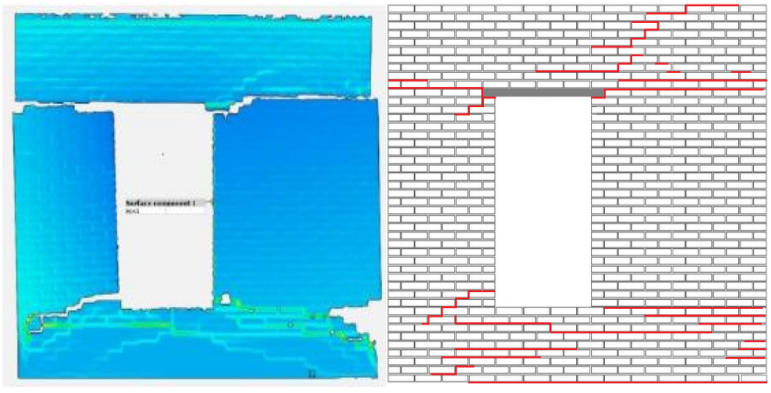

Retrofitted wall loaded in negative X-direction.
Test vs. analysis (displacement = -64 mm)

Figure i: Crack patterns. Test vs. analysis

List of Figures

List of Tables

1

INTRODUCTION

This chapter outlines the background problem and the main objectives of the research. The research questions and the step by step procedure adapted to answer the questions are provided in detail.

1.1 Background problem

According to Mulder and Perey (2018) publication, around 1000 minor earthquakes were recorded around the northern part of the Netherlands and particularly the Province of Groningen between 1986 and 2019 (Figure 1-1).

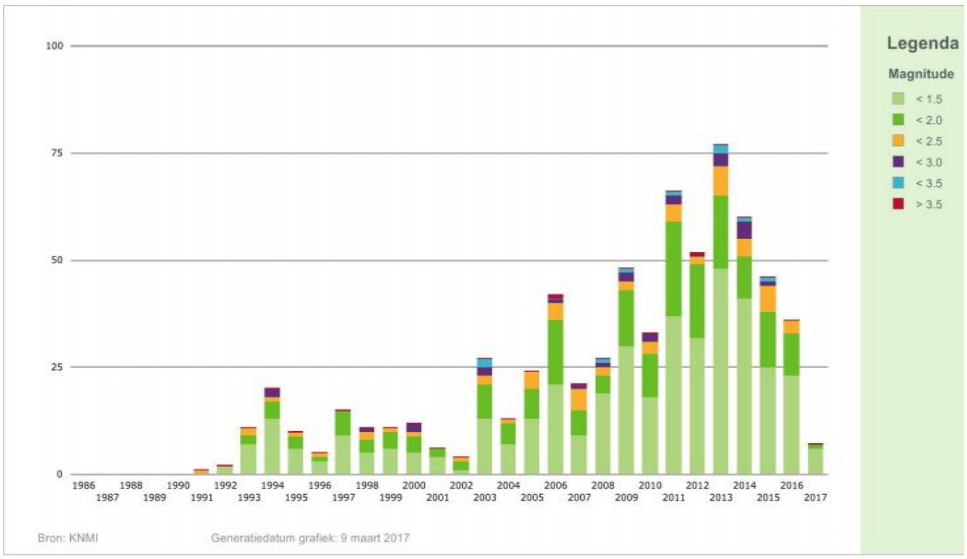

Figure 1-1: Earthquakes with a magnitude larger than 1.5 from 1991 to 2018 (Mulder & Perey, 2018)

The most severe earthquake had a magnitude of 3.6 on the scale of Richter which was occurred in Groningen on 16 August 2012. More than 1000 damage reports were received after seven days. After some investigations, it was deduced that the gas extraction resulted in this earthquake (Mulder & Perey, 2018).

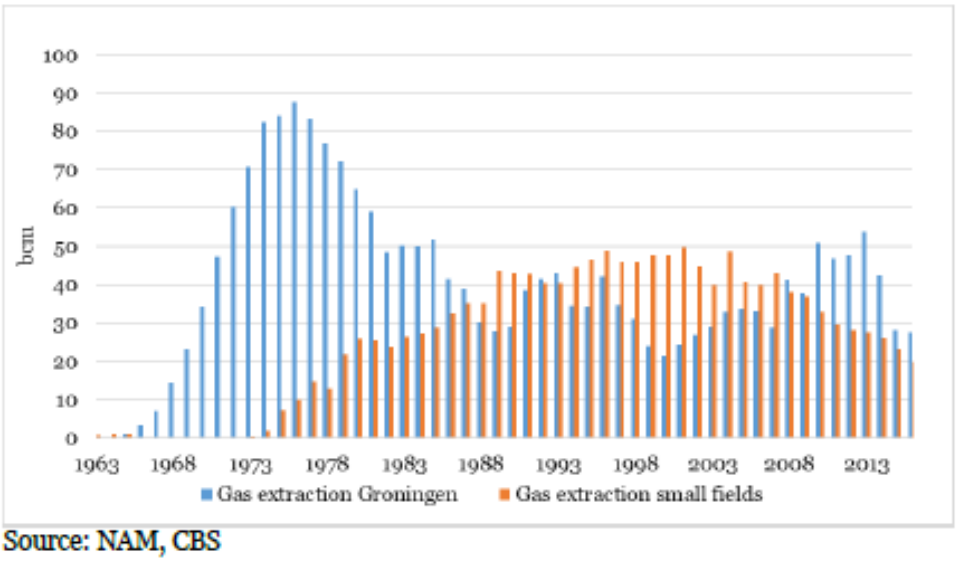

Figure 1-2: Gas extraction in the Netherlands, 1963-2016. 'bcm' stands for billion cubic meters (Mulder & Perey, 2018)

In geology point of view, the natural gas of Groningen can be found in the sandstone layer, at 3 Km below the ground, of this province. Sandstone is defined as a layer or layers of sand pressed

against each other under high pressure. Which regards to the high porosity, this is a good reservoir for gas.

Once the gas is pumped out, the sandstone pressure drops and the weight of the top layers cannot be carried anymore. As a result, soil subsides and layers are compressed. If this compression occurs in an irregular way soil subsidence leads to an earthquake. This type of earthquake has much more impact on the building since it occurs in shallow depth compared with the natural earthquakes that occur at 20-100 Km below the ground (Mulder & Perey, 2018).

Much more damage reports received from cities located in the center and north of the Groningen as shown in Figure 1-3. It reveals that the center and northern part of the Groningen are the most vulnerable parts (van der Voort & Vanclay, 2015).

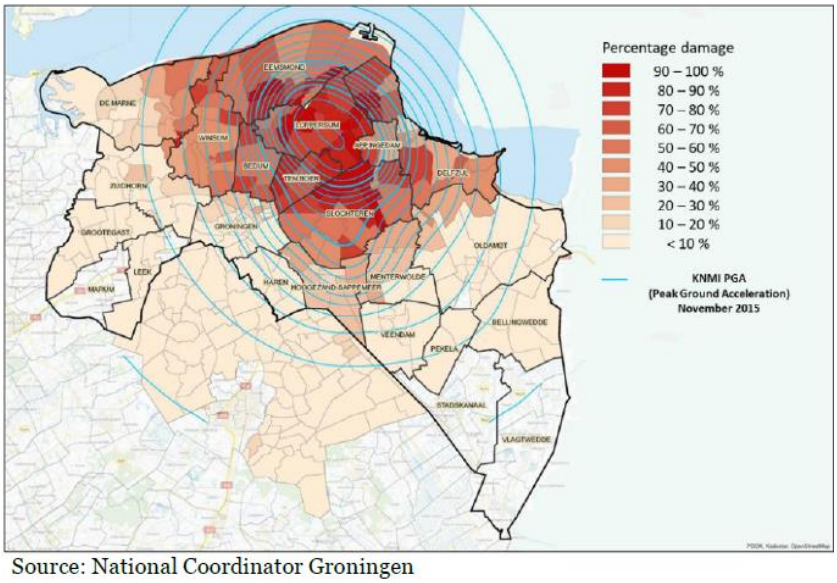

Source: National Coordinator Groningen

Figure 1-3: Percentage damage in Groningen (van der Voort & Vanclay, 2015)

The mentioned gas-induced earthquakes have a negative effect on the residents of the Groningen. Some notable *social* and *economic* consequences are: declining house prices and housing market; damage to property (17000 reported damages); dikes failure; mitigation; feeling of insecurity and anger (Mulder & Perey, 2018; van der Voort & Vanclay, 2015)

Since there are many unreinforced masonry (URM) buildings in the Groningen area, take action is required to improve the performance of these structures.

To increase the seismic performance of the damaged/undamaged URM buildings, several retrofitting (strengthening) techniques can be applied. We can study the performance of a structural URM wall retrofitted by an arbitrary technique under seismic loads. Once the results are satisfying, we can apply the technique for the similar building's structural walls to retrofit the structure and improve the global behavior of the building.

There are several retrofitting techniques that can be applied for the mentioned purpose in order to improve the seismic behavior of the URM structures. However, some of these techniques have a negative effect on the aesthetic of the façade. Some notable retrofitting techniques are mentioned here (Elgawady & Lestuzzi, 2004).

- Surface treatment

- Grout and epoxy injection
- External reinforcement by steel plate or tube (for building)
- Reinforced concrete tie columns
- Center core strengthening system

All the mentioned techniques are either not doable for existing buildings (like center core strengthening system) or are not appropriate if the aesthetic of the wall is important (for historical buildings, for instance). However, an experimental laboratory test conducted at Delft University of Technology (Licciardello & Esposito, 2019 and Licciardello et al., 2020) focused on applying bed joint reinforcement on the existing structural URM wall with an opening in order to study the seismic performance of the URM wall. In this test, some diagonal anchors are introduced around the opening to control the crack width. Bed joint reinforcement is generally implemented for repairing the damaged masonry buildings due to settlement.

1.2 Scope and Objectives of research

This MSc. project investigates the numerical modeling of an experimental laboratory test performed at Delft University of Technology by Lucia Licciardello et al., 2019-2020 funded by the *Cultural Heritage Agency of the Netherlands.* The objective of this research is to find the most accurate finite element model for both the URM wall and the retrofitted wall. The effect of diagonal anchors, bed joint reinforcement, and reinforcement layout on the performance of the wall is investigated.

The scope of this graduation project is the numerical modeling of the unreinforced masonry (URM) wall and the retrofitted wall with an opening. The results of the experimental test are implemented for this goal.

This project is performed in three main phases: in the first phase, several numerical models (for the URM wall and the retrofitted wall) are taken into account with different characteristics (material model, constitutive model, element type, load step, iterative method, boundary conditions and etc.). The outcome of this stage is several numerical models with different characteristics. In the second stage, all numerical models are compared with the result of the experimental test (validation) to find the most accurate model. Furthermore, a sensitivity analysis is conducted in this stage as well. In the last stage, a parametric study is carried out to examine the effect of diagonal anchors and their length, bed joint reinforcement, and reinforcement layout on the performance of the wall. Figure 1-4 shows the three main phases of the MSc project briefly.

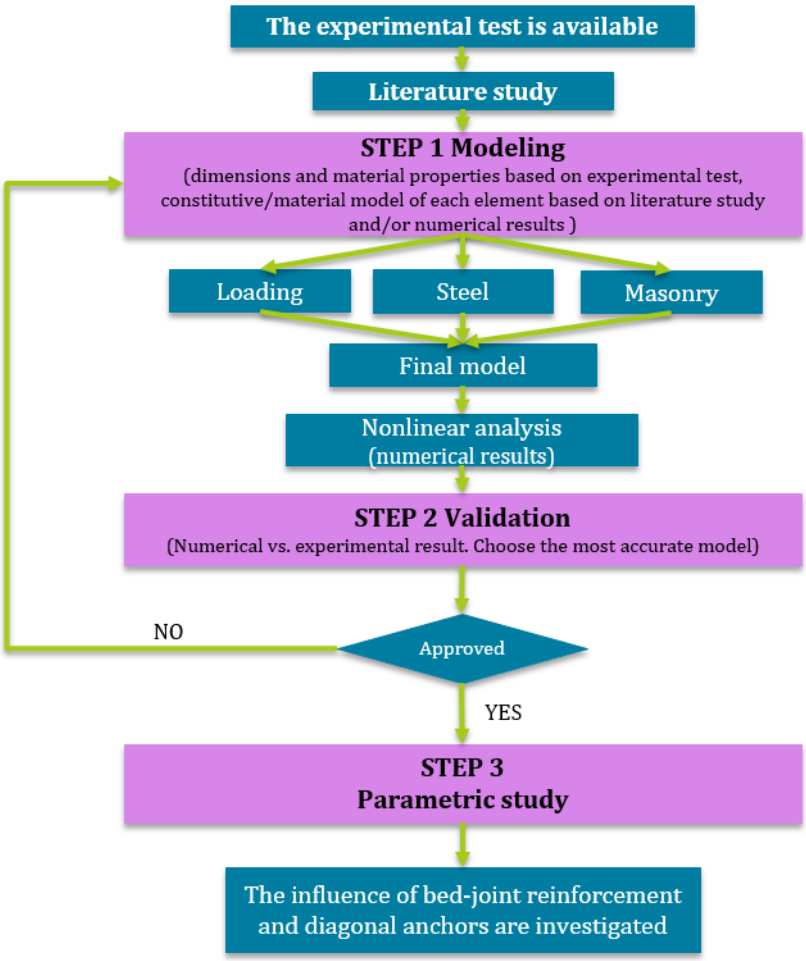

Figure 1-4: Research methodology

1.3 Research questions and methodology

The main research question is as follows.

❖ *What is the in-plane seismic behavior of the URM wall retrofitted with bed joint reinforcement and diagonal anchors using a numerical approach?*

To answer the main research question, the following sub-questions must be solved:

1. What finite element (FE) model simulates accurately the in-plane behavior of the retrofitted and URM wall? (For example, micro and macro-strategy are possible for modeling of the wall but the more suitable one must be considered)
   - Several nonlinear finite element (NLFE) models with a prescribed deformation load, a variety of characteristics and different material models are used to find the most accurate FE model. First the URM wall then the retrofitted wall is modeled. It is necessary to check if micro modeling or macro modeling is suitable for this research. Discrete and smeared crack model is another choice that is considered based on the aim of the project. In addition, material nonlinearity of steel, modeling of the reinforcement and mesh size affects the results that must be checked to evaluate the in-plane behavior of the wall.
   - The experimental results are used to validate the numerical models and find an accurate numerical model.

2. What is the effect of bed joint and diagonal reinforcement on the in-plane behavior of the retrofitted URM wall in terms of force capacity, crack width/pattern and failure modes?

- This question can be answered based on the numerical results that are obtained from point 1.

3. What is the effect of material properties of the masonry on the performance of the retrofitted wall?

- A sensitivity analysis is carried out for this part. Several NLFE models are developed to answer this question. Compressive and tensile strength, as well as fracture of masonry energy in tension and compression are increased then decreased by 50% to study the effect of material properties.

4. What is the influence of **only** diagonal anchors and their length on the behavior of the retrofitted URM wall?

- A similar NLFE model is developed for this part. However, only diagonal anchors are modeled and the results are compared with the URM wall.
- To find the effect of anchor length the same NLFE model with longer diagonal anchors is considered. The numerical results are compared with the URM wall.

5. What is the influence of **only** bed joint reinforcements on the behavior of the retrofitted URM wall?

- NLFE model with a prescribed deformation load is consumed to answer the mentioned questions. The validated FE model is used and only bed joint reinforcement is modeled.
- The numerical results are compared with the URM wall to find the answers.

6. What is the effect of different reinforcement layout on the wall performance? The number of the bed joint reinforcement can vary in the thickness and along with the height of the wall.

- To answer these questions, eleven retrofitted walls with different bed joint reinforcement layouts are modeled. The diameter of the rebar is kept constant (6 mm) but the number of rebar in the thickness and along the height of the wall is changed.
- The results are compared with the original retrofitted wall in terms of peak-load, maximum crack width, and crack pattern.

It is expected that this research addresses the following scientific gap:

Bed joint reinforcement is usually applied to repair the existing damaged unreinforced masonry walls due to the settlement. However, we do not know if this technique can be performed for seismic events or not. In this reach, the possibility of bed joint reinforcement and diagonal anchors application for seismic retrofitting of the existing URM wall is investigated.

1.4 Outline of the thesis

This report contains seven chapters. Chapter 1 describes the background problem, objective and scope of the research. Then research questions are provided. In chapter 2, the literature study, failure mechanisms of the URM wall with and without opening are discussed in detail. Common retrofitting techniques with their pros and cons are discussed as well. Finally, mechanical properties and numerical modeling that are necessary for the numerical analysis are presented. The case study (the result of the experimental test) is described in chapter 3. Chapter 4 shows what types of elements, constitutive models, and convergence criterion is implemented in this

research. Numerical results are discussed in chapter 5. In this chapter, the URM wall and retrofitted wall are modeled with two material models to choose the appropriate one. Then the effect of bed joint reinforcement and diagonal anchors on the performance of the wall is investigated. Finally, a sensitivity analysis is performed. In chapter 6, a parametric study is carried out to examine the effect of only the diagonal anchor and its length as well as bed joint reinforcement on the performance of the wall. In the end, 11 cases are checked to study the influence of the reinforcement layout on the wall performance and a proposed reinforcement layout is provided accordingly. Conclusion and recommendations are provided in chapter 7.

2

LITERATURE STUDY

This chapter describes the in-plane failure mechanisms of the unreinforced masonry (URM) wall. To improve the performance of the URM walls several common seismic retrofitting are discussed with their pros and cons. Finally, mechanical properties (material models) of masonry and steel, as well as numerical models, are investigated.

2.1 The vulnerability of unreinforced masonry structures

An unreinforced brick masonry building is a type of building that loads are carried by load-bearing elements, mostly load-bearing walls. The masonry material used in this type of structure can be tile, cinderblock, brick and etc., which are bound to each other by mortar to form an element.

These types of buildings are not reinforced by rebar and due to that, they are vulnerable to collapse in lateral loads: wind and earthquake.

Although masonry has a very good strength against compressive forces when it is subjected to seismic loads, its resistance is low both in-plane and out-of-plane of the element. There are three main reasons for that:

- Weak bonds
- Masonry has a very low tensile strength
- Masonry is a quasi-brittle material

To increase the performance of the URM structures, retrofitting techniques can be used. There are several methods for retrofitting of URM walls. Once a wall is strengthened, we can extend it to all walls to retrofit the whole building.

2.2 In-plane seismic response of URM walls

Under seismic loading, in-plane and out-of-plane failure of the URM wall might occur. Because this thesis focus on the in-plane behavior of the masonry wall, it is important to understand the failure mechanisms of the URM wall. This part investigates the in-plan failure modes of the URM wall with and without opening.

2.2.1 In-plane failure mechanisms of URM walls without opening

According to Elgawady and Lestuzzi (2004), four main in-plane failure mechanisms can be considered for URM walls: shear failure, bed joint sliding failure, rocking failure, and toe-crushing as can be seen in Figure 2-1. Other possible failure modes can be found in FEMA 306 (1998).

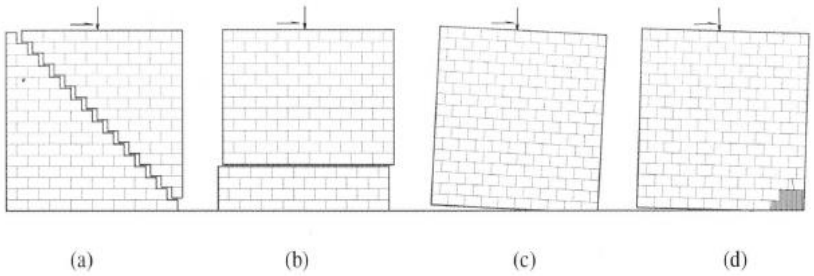

Figure 2-1: Major in-plane failure modes of URM walls: shear failure or diagonal tension cracking (a), bed joint sliding failure (b), rocking failure (c), and toe-crushing failure (d) (Elgawady & Lestuzzi, 2004)

The mentioned failure mechanisms can be explained by FEMA 306(1998) as follows.

- *Shear failure and bed joint sliding failure*: bed joint sliding failure can be recognized in the site and the experiment. It has two forms: 1- sliding in the horizontal direction (Figure 2-1 (b)) and 2- a stair-stepped diagonal crack (also known as shear failure or diagonal tension cracking) (Figure 2-1 (a)). During the staircase diagonal crack, the head joints open and close so, the bed joint is allowed to move. Pure bed joint sliding (Figure 2-1 (b)) is a ductile

failure and crack goes through the unit-mortar interface horizontally. Pure bed joint sliding occurs when the vertical load on the wall is low or applied mortar has a poor quality that leads to a low friction coefficient between masonry and mortar.

- *Rocking failure and toe-crushing failure:* the combination of two failures also is known as a flexural failure and occurs due to a combination of tension and compression failure. Because of lateral load, the bottom corner of the wall tends to uplift and simultaneously the other corner of the wall at the bottom is compressed. The former leads to tension failure (rocking, Figure 2-1 (c)) while the latter leads to compression failure (toe-crushing failure, Figure 2-1 (d)).

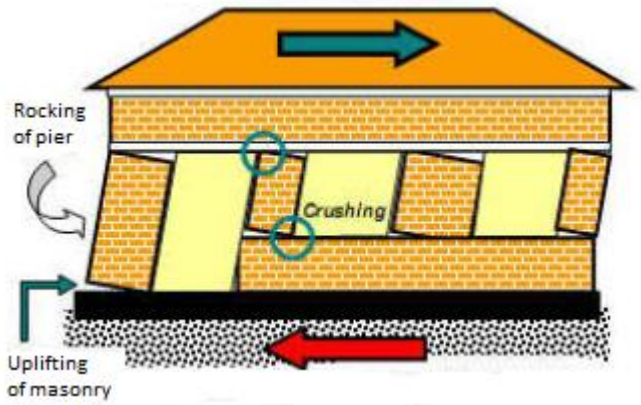

Figure 2-2: Flexural failure (rocking and toe-crushing failure)

The ductile or brittle behavior of the mentioned failures is explained by FEMA. According to FEMA 273(1997) and 356(2000), ductile and brittle action is defined as follows.

- Deformation-controlled action (ductile action): the component action reaches its capacity under the governing mechanism and a ductile behavior is expected for the element. The strength of the element does not change significantly. Bed joint sliding failure (Figure 2-1 (b)) and rocking failure (Figure 2-1 (c)) are categorized as deformation-controlled action (Ghiassi et al., 2012).
- Force-controlled action (brittle action): the component action does not reach its capacity under the governing mechanism and a brittle behavior with a rapid and complete loss of strength is expected for the element. Diagonal tension cracking (Figure 2-1 (a)) and toe-crushing failure (Figure 2-1 (d))are categorized as force-controlled action (Ghiassi et al., 2012).

2.2.2 In-plane failure mechanisms of URM walls with opening

On the one hand, window opening reduces the in-plane stiffness of the URM wall and on the other hand, the weakness of the piers and/or spandrels is important during the earthquake. Since the presence of the opening changes the stiffness of the URM wall, other failure modes/damages are possible for perforated URM walls. In addition, the corners of an opening are critical points. According to FEMA 306 (1998), all the mentioned failure modes in the previous part might occur in a perforated URM wall, however, the possibility of the following failure mechanisms is likely as well:

- *Wall-pier rocking:* Once the flexural cracking develops at the bottom, the rotation of the pier about the toe occurs. When the compressive stress is low, the shear capacity of the wall is high, and the piers are weak and/or slender then the possibility of this failure mechanism is likely.
- *Spandrel joint sliding:* this type of failure is a bed joint sliding (Figure 2-3(a)) that occurs at the end of the spandrels and as a result, pulling apart of the units happens. This failure mechanism occurs when spandrels are weak or when reaching the in-plane moment capacity of the wall despite the structure can resist more shear stresses. If a reliable lintel is applied, this mode can be a ductile failure and allows a remarkable drift.
- *Spandrel unit cracking:* This damage is observed in structures with weak spandrel. If the in-plane moment capacity of the wall is reached but cannot be revealed by sliding (like spandrel joint sliding) the energy is revealed by brittle vertical cracking at the end of the spandrels (Figure 2-4). In this case, if a reliable lintel is not constructed local failure occurs without warning.

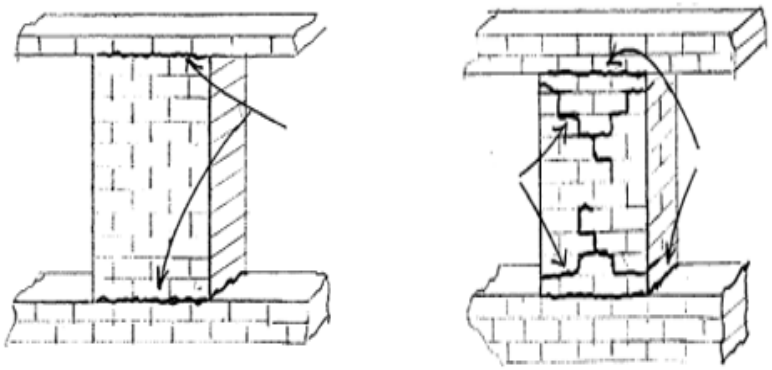

(a) (b)

Figure 2-3: Wall-pier rocking: hairline cracks in bed joints at top and bottom (a), possible hairline cracks in bed joints within pier (b) (FEMA 306(1998))

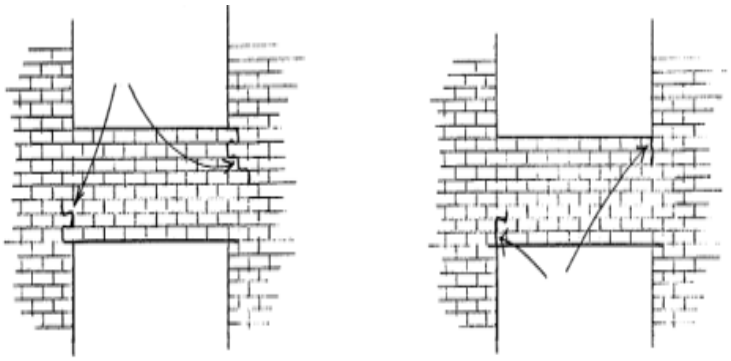

(a) (b)

Figure 2-4: Spandrel joint sliding (a) and Spandrel unit cracking (b) (FEMA 306(1998))

All the possible behavior and failure modes for the URM structures with/without opening with corresponding damage guide references, if available, can be found in FEMA 306(1998) as can be found in Figure 2-5 and Figure 2-6.

Ductility Category	Behavior Mode	Likelihood of Occurrence and Damage Guide Reference		
		Solid Wall (URM1)	Weak Piers (URM2)	Weak Spandrels (URM3)
Higher Ductility	Foundation Rocking	Common in field; no experiments; see text	NA	NA
	Wall-Pier Rocking	Possible; similar to URM2A Guide	Common in field; experiments done; see URM2A Guide	NA
	Bed Joint Sliding	Common in field; has experiments; similar to URM2B	Common in field; experiments done; see URM2B Guide	Unlikely; no guide
	Bed Joint Sliding at Wall Base	Possible; similar to URM2B Guide	NA	NA
	Spandrel Joint Sliding	NA	NA	Common in field; no experiments; see URM3D Guide
Moderate Ductility	Rocking/Toe Crushing	Seen in experiments; similar to URM2A Guide	Possible; similar to URM2A Guide	NA
	Flexural Cracking/Toe Crushing/Bed Joint Sliding	Seen in experiments; see URM1F Guide	Possible; similar to URM1F Guide	Unlikely; no guide
	Flexural Cracking/Diagonal Tension	Possible	Seen in experiments; similar to URM2K Guide	Unlikely
	Flexural Cracking/Toe Crushing	Seen in experiments; see URM1H Guide	Possible; similar to URM1H guide	Possible; no guide
	Spandrel Unit Cracking	NA	NA	Common in field; see URM3I guide
Little or No Ductility	Corner Damage	Common in field; no experiments; no specific guide; see text	NA	Common in outer pier of upper stories; no specific guide; see text
	Preemptive Diagonal Tension	Possible; similar to URM2K guide	May be common in field; seen in experiments; see URM2K Guide	May be common in field; no experiments; similar to URM2K Guide
	Preemptive Toe Crushing	Theoretical; similar to URM1H Guide	Theoretical; similar to URM1H Guide	Unlikely; no guide
	Out-of-Plane Flexural Response	Common in field; see URM1M Guide	Possible; similar to URM1M Guide	Unlikely; no guide

Figure 2-5: Summary of behavior modes for URM walls (FEMA 306(1998))

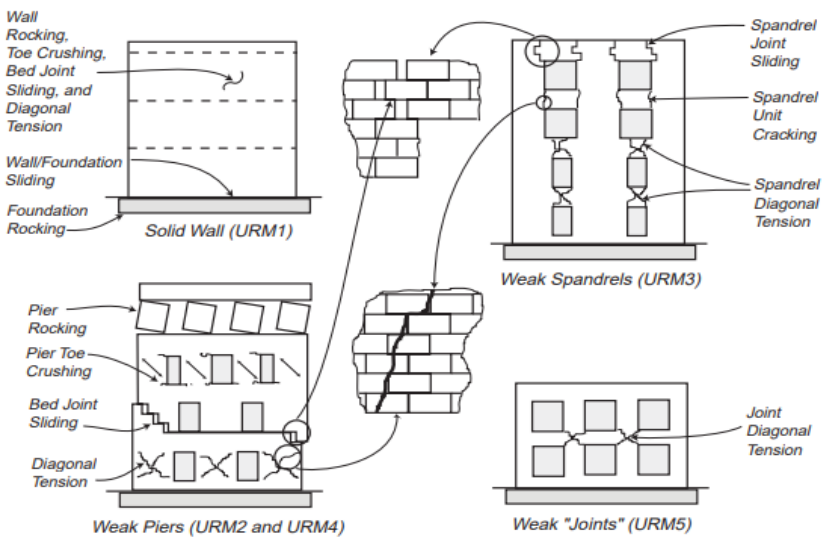

Figure 2-6: Summary of behavior modes for URM walls (FEMA 306(1998))

2.3 Common seismic retrofitting techniques for masonry structures

In this section, some conventional methods for retrofitting of the URM structures for seismic loads are reviewed. On one hand, a few of them are suitable only for buildings and the others are applied for walls. On the other hand, the retrofitted technique might affect the aesthetic of the building which is not desirable for heritage buildings.

2.3.1 Surface treatment

In this method, which has been developed mostly by experimental tests, a cover is put on the masonry exterior in order to improve the seismic behavior of the structure (Elgawady & Lestuzzi, 2004).

They continue that this technique can be ferrocement, reinforced plaster or shotcrete, a combination of steel mesh and concrete or purely cementitious materials, such as strain hardening cementitious composites (SHCC), can be used for retrofitting.

However, all the mentioned techniques affect the appearance of the walls and it must be considered for historical buildings.

- **Ferrocement**

Elgawady and Lestuzzi (2004) explain that ferrocement is a good choice for cheap buildings since it is not costly and can be performed by unskilled laborers. Ferrocement consists of several sheets of mesh (Figure 2-7) embedded in a cement with high strength of around 15-30 MPa and a mortar layer with a thickness of 10-50 mm.

Ferrocement improves both the in-plane (by a factor of 1.5) and the out-of-plane behavior of the URM wall. On the one hand, reduce in wall height-to-thickness (h/t) ratio leads to improvement in the out-of-plane behavior of the structure. On the other hand, once the bricks experience cracking, mesh plays a role as an aid to confine them and as a result, in-plane inelastic behavior of the structure is improved (Elgawady & Lestuzzi, 2004).

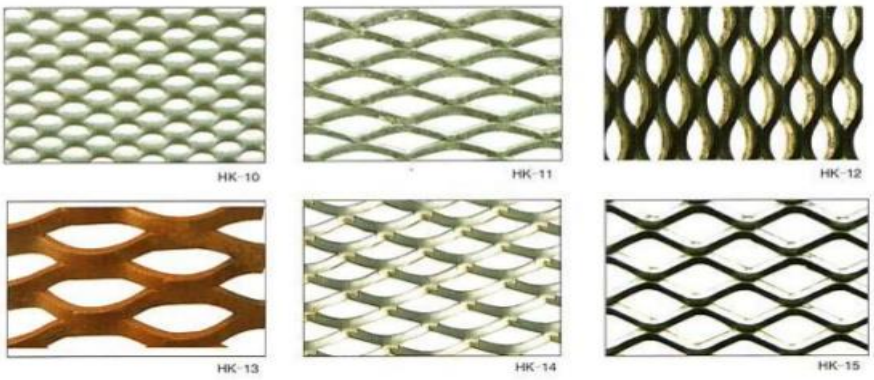

Figure 2-7: Mesh used in ferrocement method (Elgawady & Lestuzzi, 2004)

- **Reinforce plaster**

High strength steel reinforcement covered by cement plaster (Figure 2-8) is used for retrofitting in this method and different patterns of the reinforcement are possible in this technique: vertical, horizontal, or diagonal rebar (Elgawady & Lestuzzi, 2004).

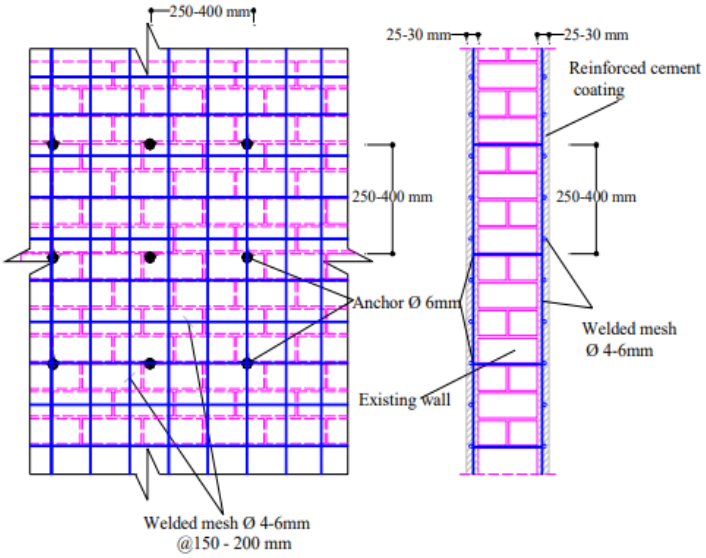

Figure 2-8: Pattern and detail of the steel reinforcement (Elgawady & Lestuzzi, 2004)

Elgawady and Lestuzzi (2004) continue that many factors can affect the result of the retrofitting: the cement mortar strength, the ratio of the rebar, reinforcement-retrofitted wall bonding and etc. Accordingly, the in-plane behavior of the structure is improved by a factor between 1.25-3 in diagonal tension tests and static cyclic tests (Elgawady & Lestuzzi, 2004).

It is clear that this technique has a negative effect on the appearance of the building too.

- **Shotcrete**

In this technique, the masonry structure is strengthened by steel welded mesh with sprayed shotcrete over it. The minimum thickness of shotcrete is 60 mm and can be increased based on the seismic demand. Transferring the shear stresses across the shotcrete-masonry interface is vital and can be controlled by applying shear dowel/connector which is fixed by resin epoxy into the holes which are drilled into the masonry wall (Elgawady & Lestuzzi, 2004).

They continue that the ultimate load of the retrofitted wall is the most notable improvement in this method. A cyclic test showed that a one-sided 90 mm thick shotcrete is able to increase the peak-load of the structure by 3 times. In addition, the strengthened composite element can dissipate the earthquake energy very well: reinforcement by yielding and shotcrete with elongation. (Elgawady & Lestuzzi, 2004).

Similar to other types of surface treatment methods, shotcrete has a negative effect on the aesthetic of the wall.

2.3.2 Grout and epoxy injection

Due to a seismic load, a masonry wall might lose its original integrity. Furthermore, there are some voids and cracks (because of an earthquake, manufacture imperfections, chemical or mechanical actions). By applying this technique, we can restore the original integrity of the masonry structure by filling all the cracks and voids. In addition, stiffness and strength of the structure improve substantially (Elgawady & Lestuzzi, 2004)

They explain that the injectability of the mix plays a vital role in the success of this method. Injectability is obtained by the physical and chemical compatibility of the mix's substances as well as its mechanical properties.

By applying this technique, lateral resistance of the retrofitted wall increases remarkably: 2-4 times more than the URM wall. Furthermore, both strength and stiffness are increased (Elgawady & Lestuzzi, 2004).

Since grout and epoxy injection does not vary the aesthetic and the building's architectural appearance, this type of retrofitting is a good option for the historical buildings.

2.3.3 External reinforcement by steel plate or tube

Several details with different profiles-plate and tubes can be implemented in this method. A conventional detail is two bracing and two vertical plate/tube steel elements (Figure 2-9). For the integrity of the retrofitted structure, the steel system must be attached directly to the load-bearing masonry wall and diaphragm of the storey (Elgawady & Lestuzzi, 2004).

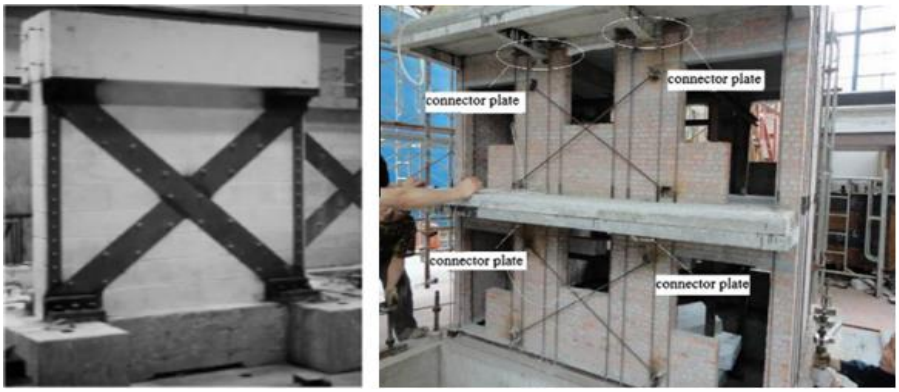

Figure 2-9: External reinforcement (Elgawady & Lestuzzi, 2004)

Elgawady and Lestuzzi (2004) explain that implementing vertical and diagonal bracing system can enhance the in-plane resistance of the retrofitted wall (by a factor of 4.5). This improvement is limited by toes crushing followed by buckling of the steel element.

This technique is favorable for historical buildings due to its effect on the aesthetic of the structure.

2.3.4 Reinforced concrete tie columns

Although it is not very easy to apply reinforced concrete tie columns in an existing masonry building, however, it is applied widely in Asia and Latin America for retrofitting of the building (Elgawady & Lestuzzi, 2004).

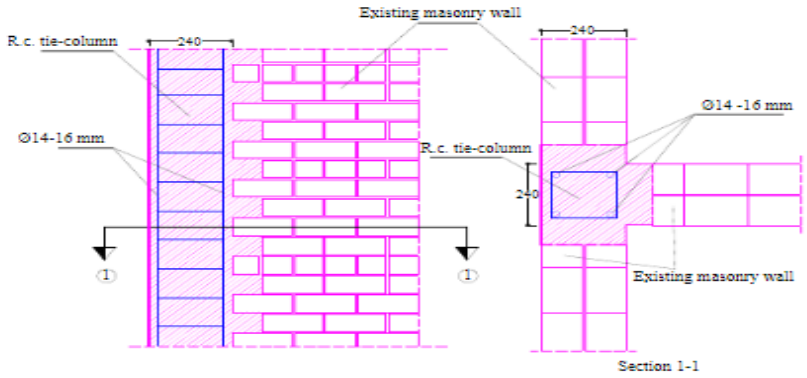

Figure 2-10: Confining URM using reinforced concrete column (Elgawady & Lestuzzi, 2004)

Elgawady and Lestuzzi (2004) explain that confining is the most notable feature of this method. Walls must be confined at all corners and wall intersections by vertical reinforced concrete columns as can be seen in Figure 2-10.

Researches have shown that applying this method without tie beams (horizontal reinforced concrete elements) does not affect the behavior of the masonry structure significantly under seismic loads. Therefore, to improve the system, tie columns should be connected to floor levels by tie beams along the wall (Elgawady & Lestuzzi, 2004).

They continue that this technique does not have a remarkable effect on the ultimate load resistance of the URM but increases the integration of the structure- due to confinement- ductility, and energy dissipation (damping characteristics) of URM structures.

This technique not only has a negative effect on the appearance of the structure but can only be applied for buildings and not walls.

2.3.5 Center core strengthening system

Non-destructive strengthening of the masonry wall is the most notable advantage of the center core which makes it popular for historical URM buildings. This oil-well technique has been used successfully in several projects in the word in order to save the URM buildings against earthquake hazards (Elgawady & Lestuzzi, 2004).

According to Elgawady and Lestuzzi (2004), a reinforced grouted core is placed in the middle of the structural wall in this method. Since this is a drying drill method, a vacuum with filters is used to control the dust. The wall is drilled and a vertical hole is generated continuously from the roof to the foundation. Based on the thickness of the existing masonry wall the diameter of the hole is between 50-150 mm. Then reinforcement is placed in such a way that it locates in hole center and grout is pumped to fill the hole. The strong bonding between grout and bricks makes an integrated wall with a high in-plane and out-of-plane capacity as it is shown in Figure 2-11.

This technique does not affect the aesthetic of the structure but is only applied for the building.

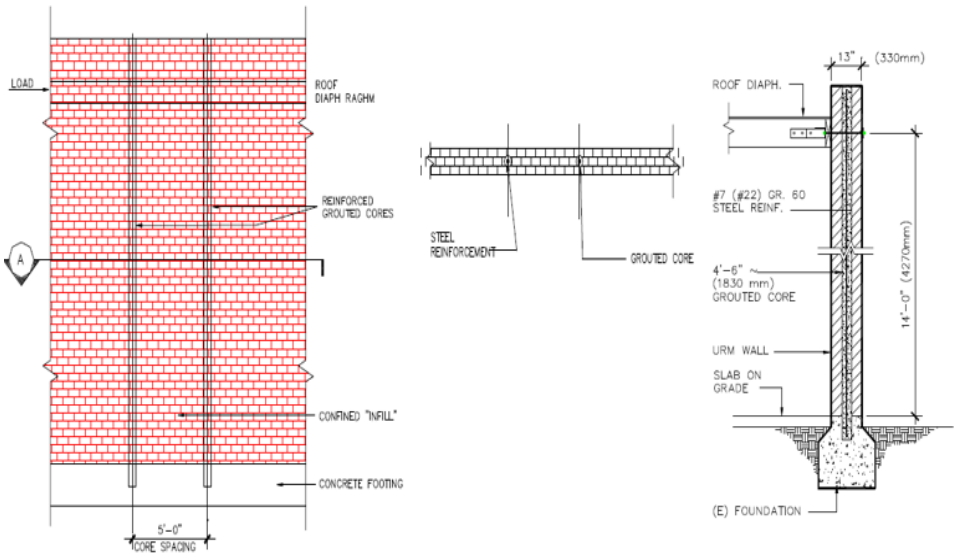

(a) (b) (c)

Figure 2-11: Center core detail. Elevation view (a), top view (b), cross-sectional view (c) (Breiholz, 1993)

2.3.6 **Bed joint reinforcement**

This method is usually implemented as a repair method for damaged walls due to settlement. Usually, a spiral stainless steel bar for reinforcing and cement-based repair mortar for installation of the steel is used for strengthening.

However, an experimental campaign conducted at Delft University of Technology (Licciardello & Esposito, 2019) focused on applying bed joint reinforcement on the existing structural URM wall with an opening to study the seismic performance of the URM wall.
This method can be performed for both damaged and undamaged existing URM buildings.

The bed joint reinforcement installation procedure is as follows (Licciardello & Esposito, 2019).

- Cut a slot in the masonry joint for 1/3 of its thickness.
- Then clean the slot with a vacuum cleaner.
- Wet the bed joint in order to have a more effective repair mortar-brick bond.
- Inject the repair mortar into the slot.
- Insert the twisted stainless-steel bar.
- Fill the slot with repair mortar completely.

It is expected that the reinforcement acts in tension and restrain crack opening and improves the shear behavior in the plane of the retrofitted masonry walls. Also, this method can improve the capacity of the structure for lateral loads (Petersen et al., 2012).

Since this technique does not affect the appearance of the old buildings, it is a good choice for retrofitting of the URM walls.

Figure 2-12: Procedures for applying bed joint reinforcement performed at Stevin lab, TU Delft: cutting the mortar (a), vacuuming the slot (b), wetting the slut (c), injecting repair mortar (d), introducing twisted steel bar. (Licciardello & Esposito, 2019)

Figure 2-13: Repair mortar and twisted steel bar (Licciardello & Esposito, 2019)

2.3.7 **Summary of retrofitting techniques**

Form the mentioned retrofitting techniques, only bed joint reinforcement and grout/epoxy injection are suitable for retrofitting the heritage buildings since they do not alter the aesthetic of the walls.

Table 2-1: Summary of the retrofitting techniques

Retrofitted Technique	Alter the Aesthetic of the Wall	Appropriate for Wall	Improvement in Lateral In-Plane Resistance of the Wall
Surface treatment	Yes	Yes	By a factor of 1-3
Grout and epoxy injection	No	Yes	By a factor of 2-4
External reinforcement by steel plate or tube	Yes	Yes	By a factor of 4.5
Reinforced concrete tie columns	Yes	No	-
Center core strengthening system	No	No	-
Bed joint reinforcement	No	Yes	Not available

2.4 **Mechanical properties of materials**

In this research, the behavior of retrofitted masonry wall with bed joint reinforcement and diagonal anchors is studied. To model the material nonlinearity in masonry (cracking and crushing), the Total Strain crack Model (TSCM, an isotropic material model) and Engineering Masonry Model (EMM, an orthotropic material model) can be implemented. The constitutive law of the mentioned models is discussed in the section. Moreover, the nonlinearity of the steel is presented shortly.

2.4.1 **Masonry; material model (mechanical properties)**

In numerical modeling, the mechanical properties of masonry can be vary based on the research objective.

The behavior of masonry in tension and compression can be shown by the constitutive model (stress-strain curve). Both elastic and plastic behavior can be consumed by the user based on the problem. When damage and cracking are studying, the nonlinear behavior of material must be considered.

There are two approaches to modeling cracking and damage in masonry structures:

- *Discrete cracking model*: localized cracks can be checked and predefined cracks must be introduced by the user. Usually, the continuum element with linear elastic behavior and interface element with discrete cracking is used for this model (all nonlinearity is lumped in the interface element). It means crack cannot occur everywhere and it must be defined by the user before analysis. In this model, the predefining of the cracks might be a bit difficult, but the interpretation of the results is easier than the smeared cracking model.
- *Smeared cracking model*: continuum element with a smeared crack approach is defined and cracks can occur everywhere in any direction in the element. As a result, the interpretation of the result is difficult. Furthermore, crushing of the units can be investigated in smeared crack modeling (by a softening stress-strain law in compression).

Since in this thesis all possible cracks in the URM wall and the retrofitted wall must be checked, the *smeared crack approach* is used. Consequently, the TSCM and EMM that uses a smeared approach are discussed in detail in the following paragraphs.

- **Total strain-based crack model:**

According to the Modified Compression Field Theory, the constitutive model with regards to the total strain is established. The Total Strain Crack Model uses a smeared approach for fracture energy. Integration points (a point in an element where stresses and strains are calculated) play an important role in this method. Stresses and strains are calculated in each integration point which is extrapolated over a certain area (red area in Figure 2-14). If an integration point is set to be cracked then crack will be smeared out over the corresponding area which is related to the cracked integration point.

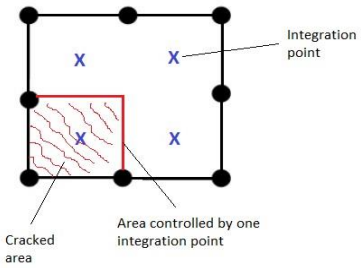

Figure 2-14: Integration points

If the principal stresses rotate, open cracks will be loaded in shear direction (Figure 2-15). This occurs because of: non-proportional loading of structure and/or redistribution of force in the structure.

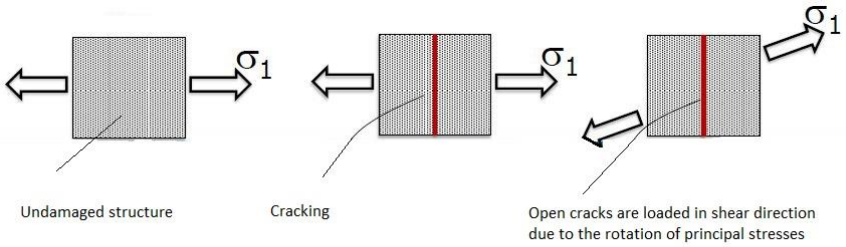

Figure 2-15 Rotation of principal stresses

There are two options for considering this phenomenon as can be seen in Figure 2-16:

- Fixed Crack Model: due to cracking of the material the shear stiffness usually reduced. This reduction is known as shear retention. In Fixed Crack Model this reduction must be taken into account since it is assumed that crack is fixed and does not rotate with principal stress.
- Rotating Crack Model: in this model crack rotates with principal stresses. The modeling of shear behavior is not necessary for this model since crack is not fixed.

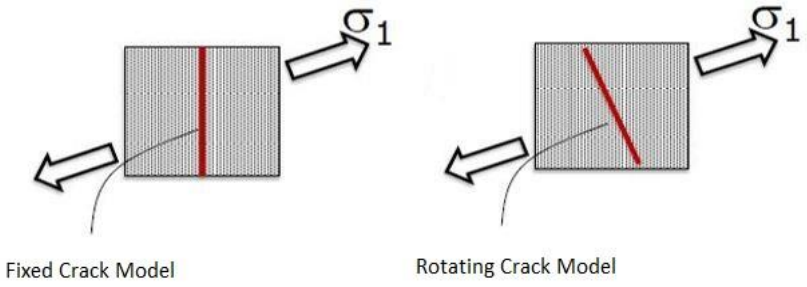

Figure 2-16: Fixed and rotating Crack Model

By applying cyclic loads energy absorption is underestimated in the masonry if TSCM is applied since this material model is based on secant unloading and reloading. To solve this problem EMM was developed (DIANA FEA, 2019).

There are several defined tensile and compressive stress-strain curves that can be implemented for this material model based on the problem as can be found in Figure 2-17, 18.

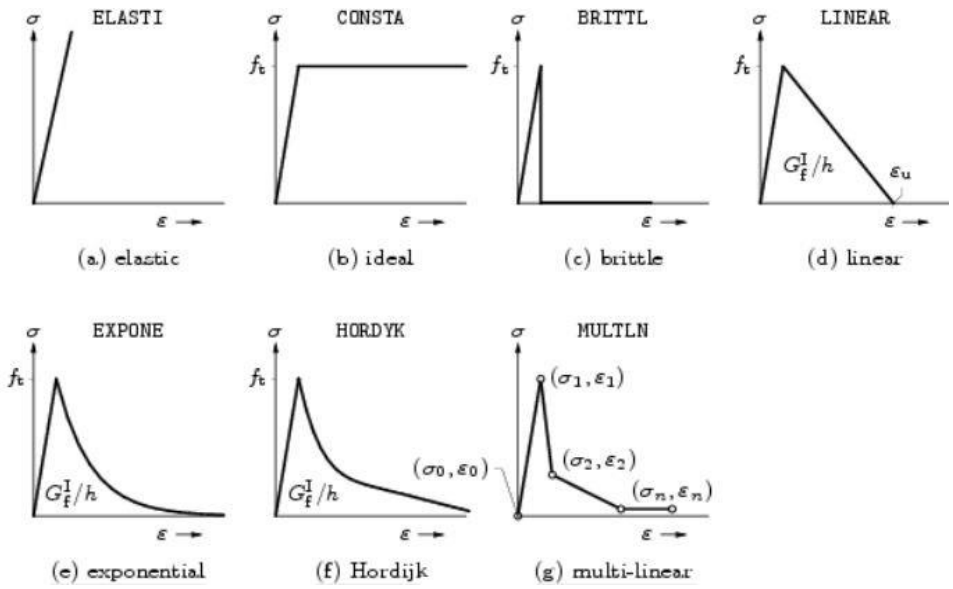

Figure 2-17: Material models in tension, smeared cracking model (DIANA FEA, 2019)

$G_f, h, f_t, \sigma_{nn}, and\ \varepsilon_{nn}^{cr}$ refer to fracture energy in tension, the crack bandwidth, tensile strength of the material, tensile stress, and ultimate crack strain of material respectively.

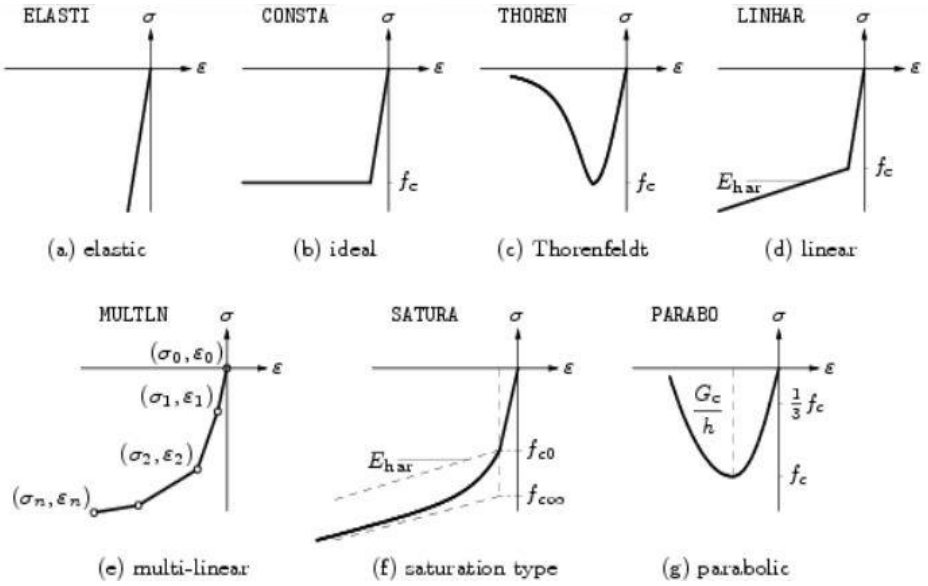

Figure 2-18: Material models in compression, smeared cracking model (DIANA FEA, 2019)

$G_c, h, and\ f_c$ refer to fracture energy in compression, the crack bandwidth, and the compressive strength of material respectively.

- **Engineering masonry model:**

As mentioned, energy dissipation is underestimated by applying the Total Strain Cracks Model when cyclic loading is used. To solve this problem Engineering Masonry Model (that is based on the smeared failure model) was developed in a joint project by DIANA FEA BV and Professor J.G. Rots in 2016 (Schreppers et al., 2017). This material model was used in DIANA FEA 10.1 for the first time.

This model is a total-strain based continuum model that behaves as an anisotropic material with zero Poisson's ratio. It covers compression, tension, and shear failure modes and can consider cracks in both bed joint (X-direction) and head-joint (Y-direction) as well as diagonal stair-case cracks. This model also covers elastic and mixed hysteresis loops for the different failure modes.

- *Cracking:*

Stresses are defined by the respective strain component, ε, and the highest value of the strain which is has been reached during the loading history. The maximum strain ever reached is called $\alpha_{tensile}$ and the corresponding stress is $\sigma_{rf,tensile}$.

Modulus of elasticity (E), tensile strength (f_t), and fracture energy in tension (G_{ft}) define the stress-stress curve in X- and Y-direction. In addition, the softening part of the curve is assumed to be linear (Figure 2-19) and the ultimate strain (ϵ_{ult}) is defined as follows.

$$\varepsilon_{ult} = \frac{2G_{ft}}{hf_t}$$

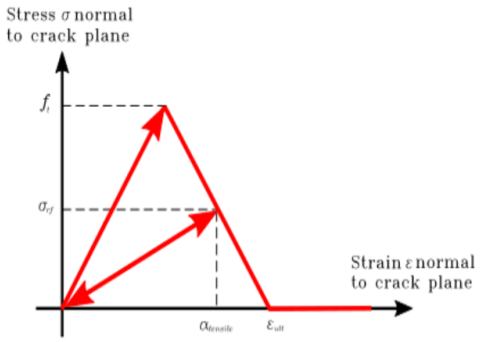

Figure 2-19: Engineering Masonry Model. Tensile behavior of the material model (DIANA FEA, 2019)

- *Compression (crushing):*

The normal compressive stresses are defined by the respective strain component, ε, and the lowest value of the strain which is has been reached during the loading history. The minimum strain ever reached is called α_{comp} and the corresponding stress is $\sigma_{rf,compressive}$.

Modulus of elasticity (E), strength in compression (f_c), and compressive fracture energy (G_c) define the stress-stress curve in X- and Y-direction. Furthermore, the softening part of the curve is assumed to be linear as can be found in Figure 2-20.

The compression curve is considered as a combination of a parabolic curve and a linear softening curve. The ultimate strain (ϵ_{ult}) can be obtained by the following equation:

$$\varepsilon_{ult} = \varepsilon_{peak} + \max[0, \frac{2G}{hf_c} - \frac{f_c}{A^2E} - \frac{A+1}{A}\left(\varepsilon_{peak} - \frac{f_c}{E}\right)]$$

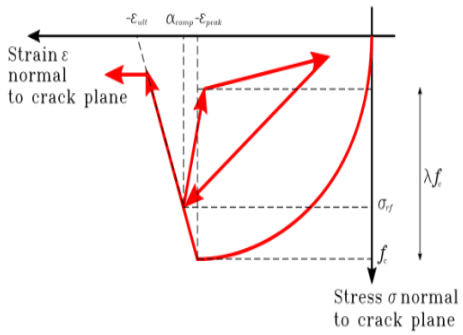

Figure 2-20: Engineering Masonry Model. Compressive behavior of the material model (DIANA FEA, 2019)

- *Shearing:*

In-plane shear strain, $\boldsymbol{\gamma}$, and the stress which is normal to the bed joint, σ_{yy}, are defined the in-plane shear stress, τ. In addition, the initial shear stiffness is defined by shear modulus (G) in this model. The shear stress is limited by the maximum stress, τ_{max}, that is defined by Coulomb friction as the following equation:

$$\tau_{max} = \max[0, c - \sigma_{yy}\tan(\varphi)]$$

Where, c the cohesion and φ is the friction angle.

The user can define either fracture energy in shear (G_{fs}) or magnitude for cohesion (c). If G_{fs} is defined, the cohesion reduces continuously linearly with the cumulative frictional shear strain,

γ_{cum}, until it reaches zero at a total shear strain of $\gamma = \gamma_{ult}$. In the other case, if cohesion is defined it will be used for all shear strains, $\boldsymbol{\gamma}$. When an integration point is cracked ($\alpha_{tensile} > f_t/E$) the cohesion immediately reduces to zero. γ_{cum} is the sum of incremental shear strains over all steps in which the shear stress is equal to τ_{max} or $-\tau_{max}$.

$$\gamma_{ult} = \frac{2G_{fs}}{h.c} - \frac{c}{G}$$

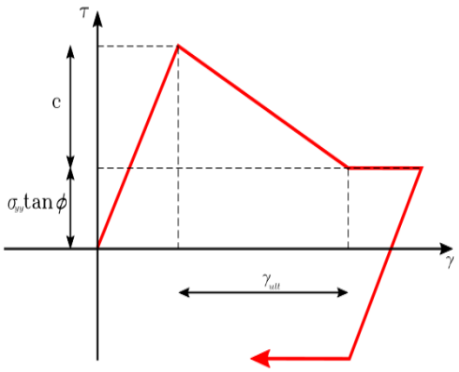

Figure 2-21: Engineering Masonry Model. Shear behavior of the material model (DIANA FEA, 2019)

2.4.2 Reinforcement; material model (mechanical properties):

Due to the lateral load, steel applied for retrofitting might reach yield stress. If plasticity occurs, the material nonlinearity of steel must be considered by applying *von Mises plasticity* in the material model.

2.5 Numerical modeling

Numerical analysis is the study of algorithms that use a numerical approximation to simulate the behavior of different phenomenon. Numerical modeling uses mathematical models to describe the problems.

Different numerical methods can be used for the modeling based on the problem and objective of the research: Discrete Element Method, Finite Element Method, Boundary Element Method, Finite Difference Method, Equivalent Frame Model, etc. Among all mentioned methods, Finite Element Method is the most suitable one for this research that is used in many commercial software like, DIANA, ANSYS, and ABAQUS.

The modeling of a structure strongly depends on the objective of the analysis. Consider a URM wall, for instance. If local failures are investigated more details must be modeled, however, this is not the case for understanding the global behavior of the wall. For a URM wall retrofitted with steel reinforcement, modeling of the masonry and steel reinforcement is a must, but modeling of the mortar and masonry-mortar interface can be ignored if their behavior is not the goal of the analysis.

2.5.1 Numerical modeling of URM wall and reinforcement

There are different alternatives for modeling of masonry structures numerically. With regard to the required accuracy and the required types of failure, the structure can be modeled. Usually, the alternatives are classified as are explained in the following paragraphs.

- *Detailed micro-modeling:* bricks and mortar are considered as continuum elements with defined failure modes while the brick-mortar interfaces are modeled as discontinuous elements by special elements. Since this is the most detailed modeling, modulus of elasticity, Poisson's effect, and nonlinear behavior of units and mortars are considered. In this case, the computational cost is high because both the modeling and analysis are time-consuming. The hardware of the computer (especially memory) must be sufficient (Campbell & Durán, 2017; Lourenço et al., 1995)
- *Simplified micro-modeling:* bricks are modeled by continuum elements. The mortar and the interface between brick and joint are modeled as discontinuous elements. This type of modeling is used to decrease the difficulties of modeling. According to the figure, each joint consists of 1- mortar, 2- interfaces as well as not including the Poisson's effect of the mortar. Although the general geometry is maintained the accuracy of the model is lesser than the previous case and all possible failure modes cannot be checked (Campbell & Durán, 2017; Lourenço et al., 1995)
- *Macro-modeling:* Unit, mortar and unit-mortar interface are lumped into the continuum. The masonry panel/wall is considered as a homogeneous element and as a result, all failure modes cannot be checked. This is a simple and enough accurate model when the global behavior of the element is in interest (Campbell & Durán, 2017; Lourenço et al., 1995)

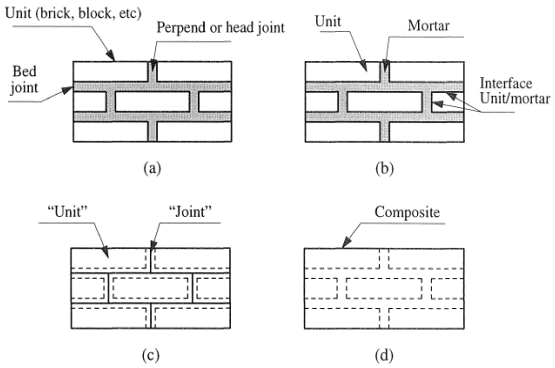

Figure 2-22: Numerical modeling of URM wall. URM wall (a), detailed micro-modeling (b), simplified micro-modeling (c), macro-modeling (d) (Lourenço et al., 1995)

2.5.2 Numerical modeling of steel reinforcement

In order to perform numerical modeling, two techniques can be implemented to model reinforcement (Dashti et al., 2017): discrete steel model and embedded steel model.

- *Discrete steel model:* truss or beam elements can be applied for the modeling of the reinforcement. Shear and bending stiffness can be introduced for the latter based on the problem. Interface elements can be implemented to model the bond-slip relationships at the interface with steel bars (nonlinear relation between shear traction (tension) t_t and shear slip Δu_t). For generating finite element mesh predicting the location of the reinforcement is important so it is a notable disadvantage of this approach.
- *Embedded steel model:* reinforcing bars are fixed in the structural elements. By using this method the degree of freedom of the system is kept constant. The displacement field of the mother element determines the strains in the reinforcement. As a result, a perfect bond between the surrounding material and reinforcement can be obtained. In this

method regardless of the location of the reinforcement, generating of finite element mesh is allowed.

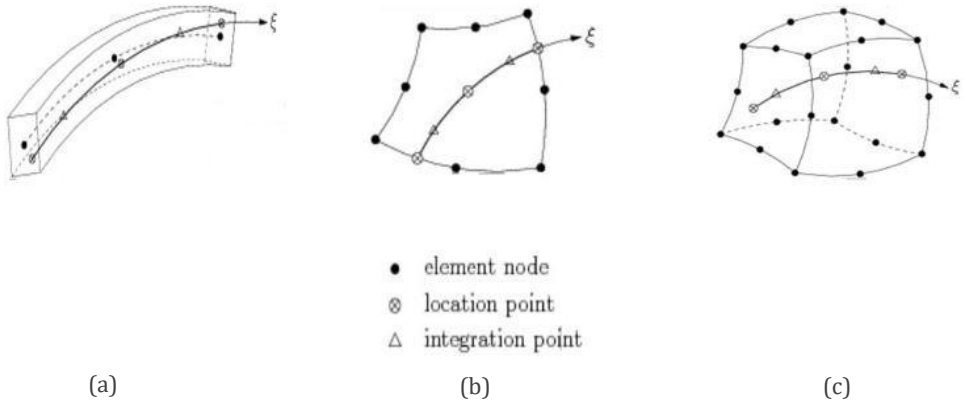

Figure 2-23: Embedded steel model: beam element (a), plane stress element (b) and solid element (c) (DIANA FEA, 2019)

3

CASE STUDY: UNREINFORCED MASONRY STRENGTHENED WITH BED JOINT REINFORCEMENT AND DIAGONAL ANCHORS

This chapter briefly describes an experimental laboratory test conducted at the Delft University of Technology (Licciardello & Esposito, 2019), which is here adopted as a case study. The geometry, boundary conditions, loading, material properties, reinforcement layout as well as experimental results of both unreinforced masonry and retrofitted wall are discussed.

3.1 Introduction

As mentioned before, the gas-induced earthquake leads to damage in the unreinforced masonry (URM) buildings located in the Groningen province. An experimental campaign (Licciardello & Esposito, 2019 and Licciardello et al., 2020) conducted at Delft University of Technology investigated (TU Delft) to understand if a combination of diagonal anchors and bed joint reinforcement improve the seismic behavior of the URM wall with an opening or not.

The performance of the retrofitted wall is compared with another experimental campaign performed at TU Delft for a URM wall with the same geometry and properties (Korswagen et al., 2019).

3.2 Material and method

A cantilever wall with an asymmetric opening with a prefabricated reinforced concrete lintel is used for the lab test. The width, height, and thickness of the wall is 3.1 m, 2.7 m and 0.1 m respectively. An overburden pressure of 0.12 MPa was applied at the top of the wall. The wall was strengthened with twisted steel bars embedded in the bed joint of the masonry.

Table 3-1: Wall Dimensions

Sample Name	Units Type and Size (mm)	L_w (mm)	H_w (mm)	T_w (mm)	Overburden (MPa)	Boundary Conditions
TUD-COMP 45	210x100x50	3070	2690	100	0.12	Cantilever

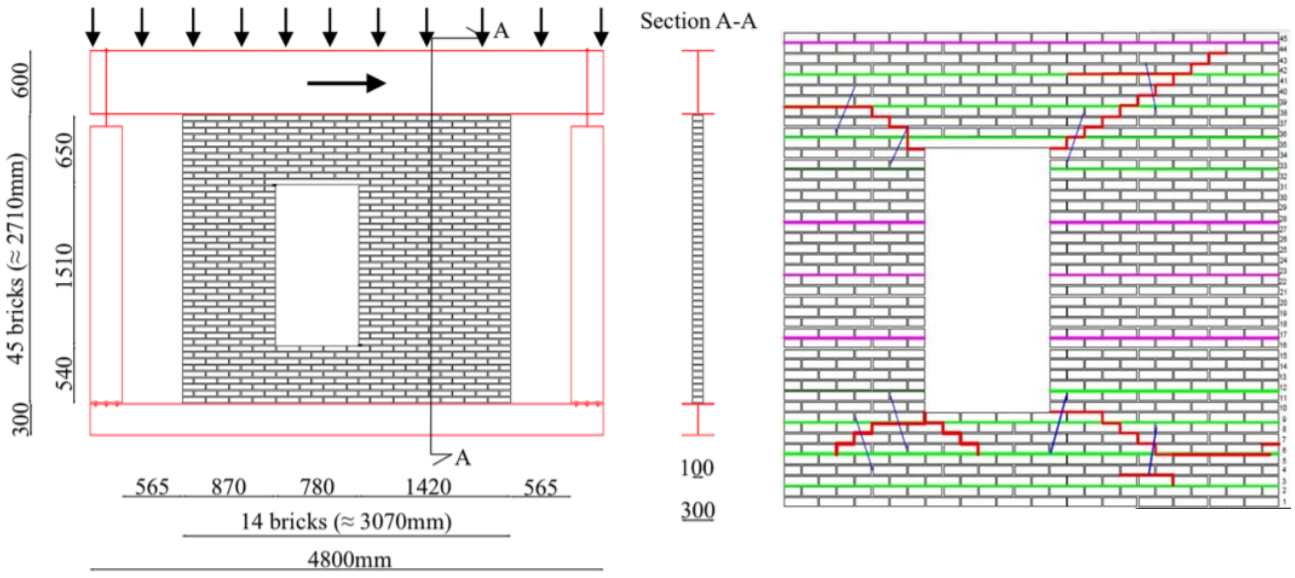

(a) (b)

Figure 3-1: Geometry of the masonry wall (a). Reinforcement layout that is designed based on the crack pattern (b) (Korswagen et al., 2019; Licciardello & Esposito, 2019)

Furthermore, the following material properties (Table 3-2) are obtained from the experiment.

Table 3-2: Overview of material properties (Licciardello & Esposito, 2019)

Property	Symbol	Unit	Average
Elastic modulus of masonry unit	E_b	MPa	8049
Density of masonry	ρ	kg/m^3	1708
Compressive strength of masonry in the direction perpendicular to bed joints	f_m	MPa	12.93
Elastic modulus of masonry in the direction perpendicular to bed joints calculated between 1/3 and 1/10 of the maximum stress	E_y	MPa	4590
Elastic modulus of masonry in the direction parallel to bed joints calculated between 1/3 and 1/10 of the maximum stress	E_x	MPa	3207
Masonry (bed joint) initial shear strength	f_{v0}	MPa	0.13
Masonry flexural strength with the moment vector parallel to the bed joints and in the plane of the wall	f_{x1}	MPa	0.16
Masonry (bed joint) shear friction coefficient	μ	-	0.82

The properties of repair mortar found by a three-point bending test and a compression test under the hydraulic jack. The former determines the flexural strength of the repair mortar while the latter determines the compressive strength of the mortar (Licciardello & Esposito, 2019).

Table 3-3: Repair mortar properties (Licciardello & Esposito, 2019)

Batch	Density kg/m^3	Flexural Strength $f_{mt,r}(MPa)$	Compressive Strength $f_{m,r}(MPa)$
Average	1922	7.68	46.95
Standard deviation	58	1.84	4.14
Coefficient of variation	0.03	0.24	0.09

3.3 Loading scheme

A cyclic horizontal load was applied to the top beam. The overburden pressure with a magnitude of 0.12 MPa which demonstrates the weight of the top beam was kept constant during the test.

For the URM wall, a cyclic in-plane load was applied in three phases to simulate a seismic event. Phase 1 and phase 2 consists of five and seven cycles respectively (Licciardello & Esposito, 2019).

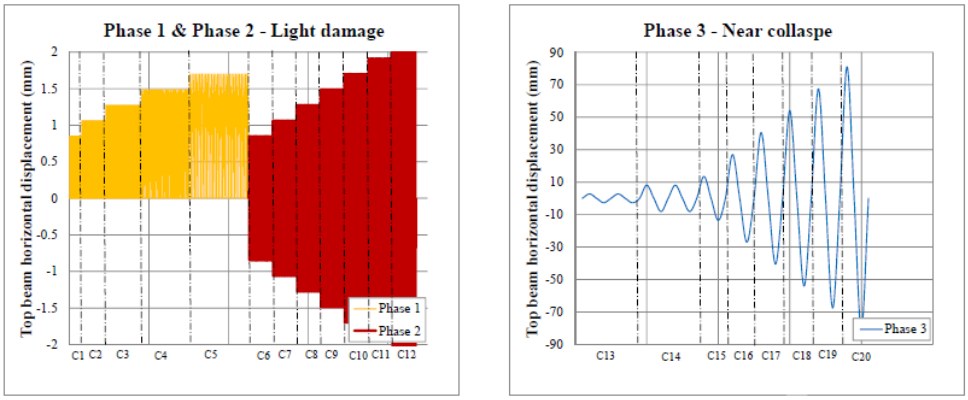

Figure 3-2: Cyclic in-plane load scheme (Licciardello & Esposito, 2019)

Table 3-4: Load scheme, phase 1 (Licciardello & Esposito, 2019)

	Unstrengthened		**Strengthened**	
Cycle	Horizontal Displacement (mm)	Drift (%)	Horizontal Displacement (mm)	Drift (%)
1	0.72	0.03	0.73	0.03
2	0.91	0.03	0.92	0.03
3	1.12	0.04	1.09	0.04
4	1.33	0.05	1.28	0.05
5	1.55	0.06	1.51	0.06

Table 3-5: Load scheme, phase 2 (Licciardello & Esposito, 2019)

	Unstrengthened				**Strengthened**			
Cycle	Horizontal Displacement (mm)		Drift (%)		Horizontal Displacement (mm)		Drift (%)	
1	-0.77	0.75	-0.03	0.03	-0.75	0.73	-0.03	0.03
2	-0.96	0.94	-0.04	0.03	-0.96	0.92	-0.04	0.03
3	-1.17	1.14	-0.04	0.04	-1.15	1.13	-0.04	0.04
4	-1.38	1.33	-0.05	0.05	-1.37	1.33	-0.05	0.05
5	-1.60	1.56	-0.06	0.06	-1.58	1.54	-0.06	0.06
6	-1.81	1.77	-0.07	0.07	-1.77	1.73	-0.07	0.06
7	-2.01	1.99	-0.07	0.07	-1.98	1.93	-0.07	0.07

An additional load phase was considered for the retrofitted wall. The first two phases were the same as the URM wall test. Then, the third phase brought the retrofitted wall to collapse. Phase 3 for the strengthened wall was according to the Groningen type loading (Licciardello & Esposito, 2019).

Table 3-6: Load scheme, phase 3 (Licciardello & Esposito, 2019)

	Unstrengthened				Strengthened			
Cycle	Horizontal Displacement (mm)		Drift (%)		Horizontal Displacement (mm)		Drift (%)	
1	-2.57	2.51	-0.10	0.09	-2.52	2.49	-0.09	0.09
2	-7.97	7.89	-0.30	0.29	-2.52	2.49	-0.09	0.09
3	-7.98	7.89	-0.30	0.29	-7.90	7.87	-0.29	0.29
4	-12.82	11.11	-0.47	0.41	-7.91	7.88	-0.29	0.29
5	-26.58	23.08	-0.98	0.85	-13.29	13.28	-0.49	0.49
6	-40.30	35.04	-1.49	1.30	-26.79	26.77	-0.99	0.99
7		43.63	0.00	1.62	-40.30	40.26	-1.49	1.49
8					-53.80	53.77	-1.99	1.99
9					-67.28	67.26	-2.49	2.49
10					-63.31	80.76	-2.34	2.99

3.4 Experimental results

The force-displacement (capacity curve) with the corresponding crack pattern is shown in Figure 3-3 to Figure 3-5. As a result, of the retrofitting the shape of the crack was changed which is indicated with a star in the figures.

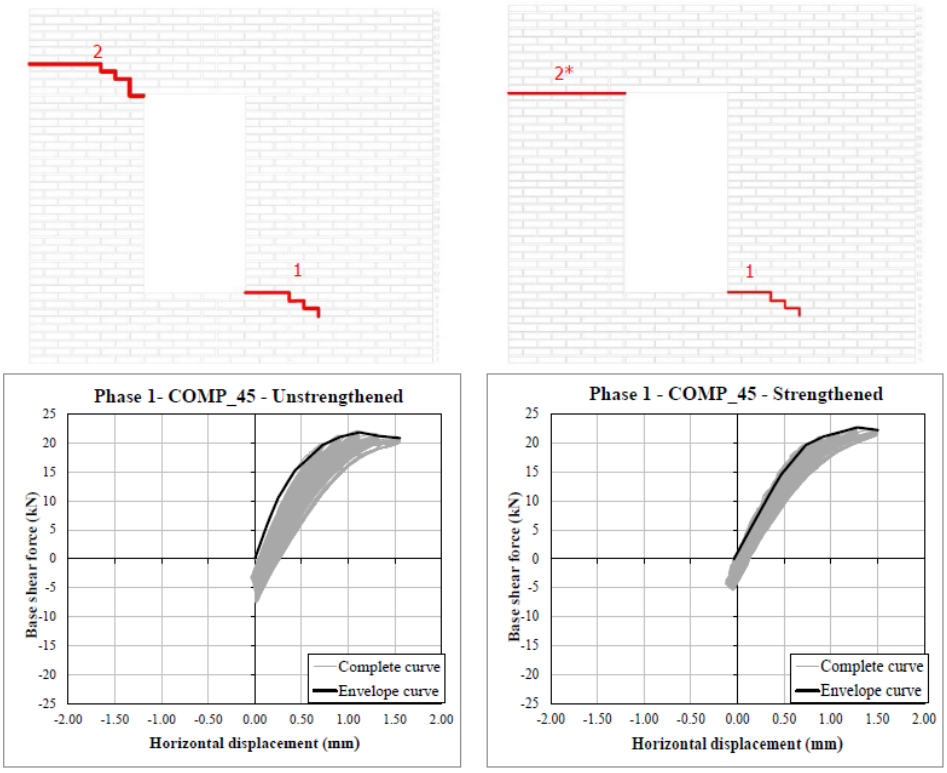

Figure 3-3: Phase 1, crack pattern and capacity curve (Licciardello & Esposito, 2019)

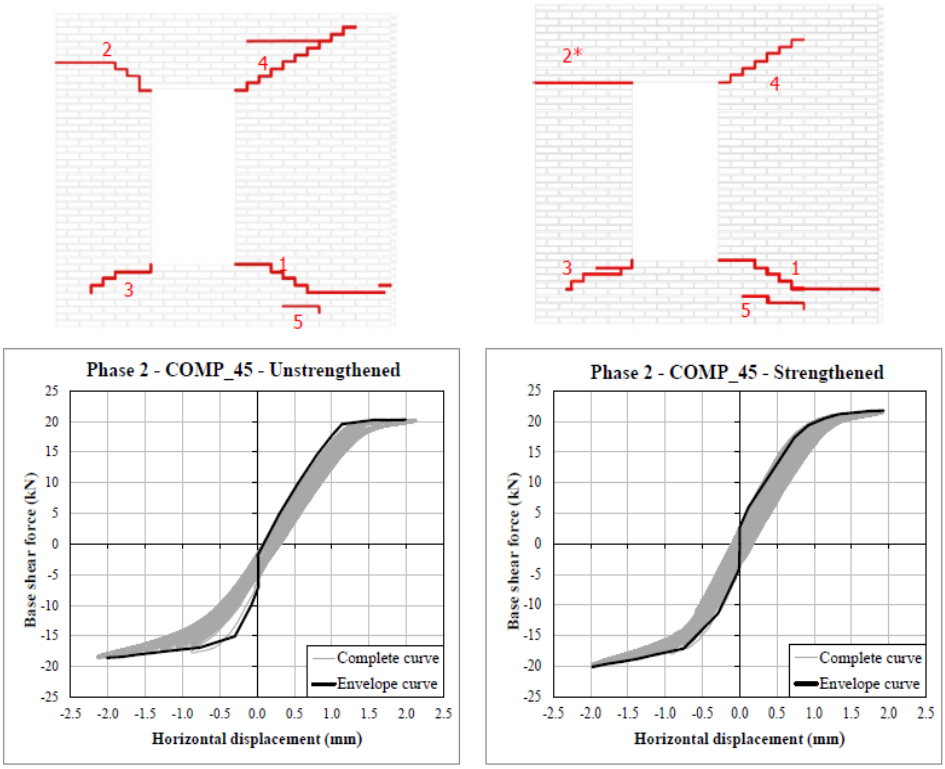

Figure 3-4: Phase 2, crack pattern and capacity curve (Licciardello & Esposito, 2019)

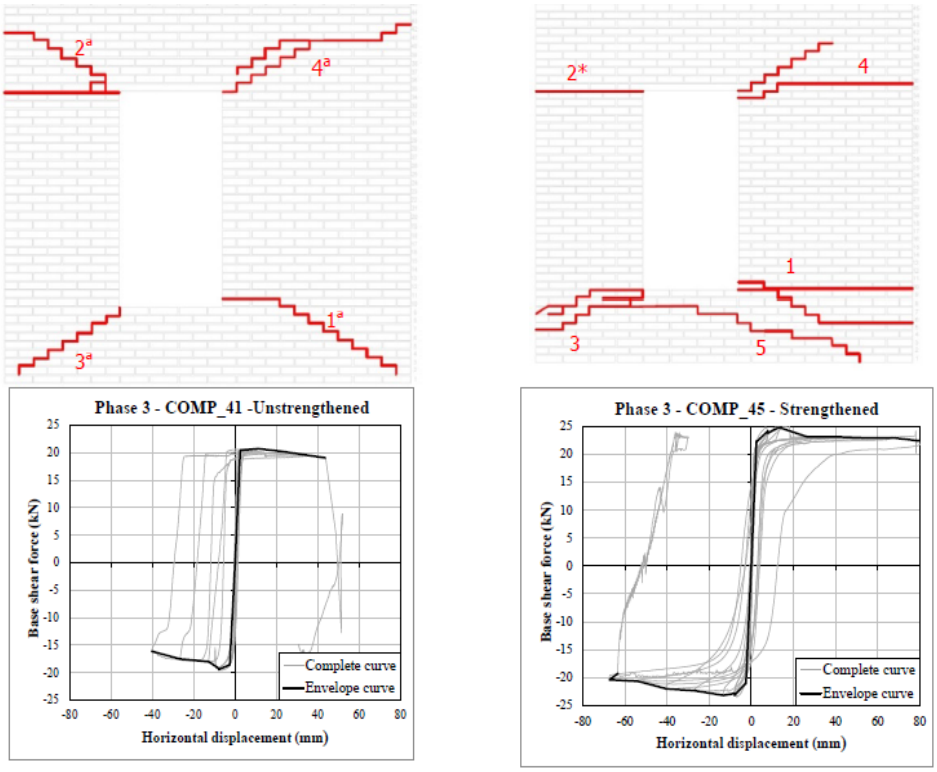

Figure 3-5: Phase 3, crack pattern and capacity curve (Licciardello & Esposito, 2019)

As mentioned before phase 3 is the near-collapse phase.

Figure 3-6 shows the evolution of cracks in all three phases. It can be seen that the rack pattern is changed when the wall is strengthened.

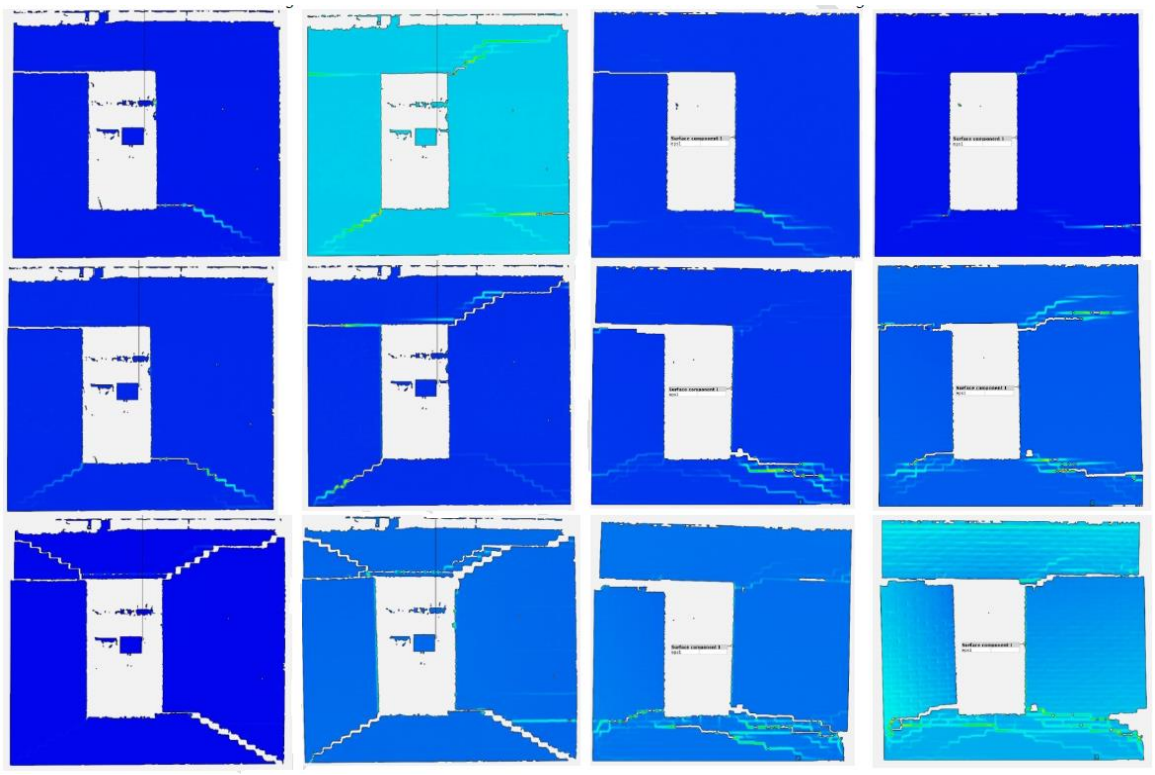

(a) (b)

Figure 3-6: Phase 3. Unstrengthened wall (a) and strengthened wall (b) (Licciardello & Esposito, 2019)

Figure 3-7 presents the backbone force-displacement diagram for both the unreinforced masonry wall and the strengthened wall.

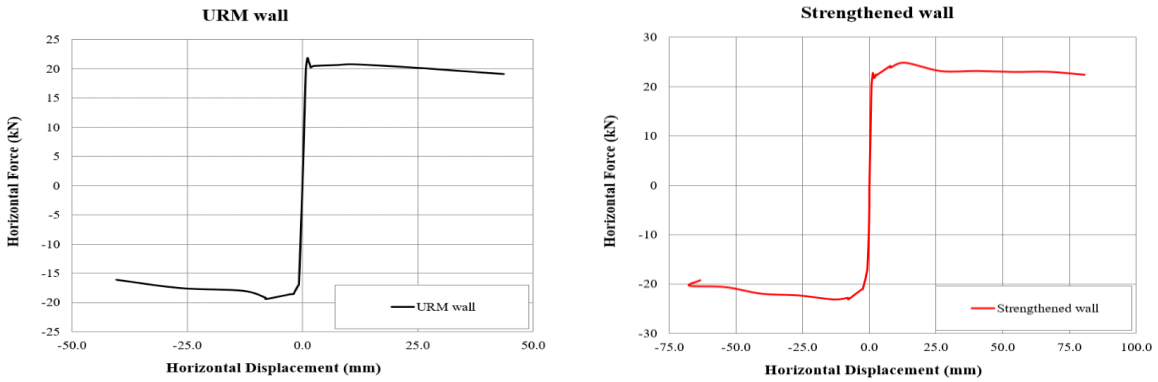

Figure 3-7: Unstrengthened wall capacity curve, left. Strengthen wall capacity curve, right (Licciardello & Esposito, 2019)

4

NUMERICAL MODELLING

This chapter describes, in detail, the finite elements, boundary conditions, material models, load scheme, analysis procedure, and convergence criterion used in this research. For all models, DIANA 10.3 (DIANA FEA, 2019) has been used.

4.1 Introduction

Recently, finite element modeling has become more and more popular in engineering firms due to the speed of the calculation and reliable results. One of the main applications of the nonlinear finite element analysis is to analyze the existing structures which are already tested in the laboratory. For all nonlinear analyses in this report, a commercial version of DIANA 10.3 (release date 2019-07-25) provided by TU Delft is implemented.

To perform the analyses, walls are modeled the same as the experimental specimen in terms of dimensions, material properties, boundary conditions, and etc. It must be mentioned that in the experiment a cyclic load was applied while a monotonic load is considered for the numerical modeling.

In this thesis, the influence of BJR, diagonal anchors and reinforcement layout on the in-plane seismic behavior of the retrofitted wall is studied. First, the case experimentally tested is adopted as a benchmark and a validation of the numerical model is performed, results can be found in chapter 5. Afterwards, the validated numerical model is adopted to perform a sensitivity analysis (chapter 5) and a parametric study considering different reinforcement layouts. Finally, a proposed reinforcement layout for retrofitting of the URM wall is presented. The numerical results of the parametric study and suggested reinforcement layout are presented in chapter 6.

In the following paragraphs, finite element models, constitutive laws, loading conditions, analysis procedure and convergence criterion are discussed in detail.

4.2 Finite element model

The finite element (FE) model of both the URM wall and the retrofitted wall is described in this part. The geometry, mesh, boundary conditions (B.C.), load scheme, iterative method, finite elements, constitutive model and material models used in the FE model are explained in detail.

4.2.1 Geometry and boundary conditions of the models

- **URM wall**

The wall is modeled by three components. Masonry wall (3070 mm length, 2690 mm height and 100 mm thickness), concrete lintel (980 mm length and 100 mm height) and a steel beam with a length of 3070 mm. The dimensions and location of the opening are based on the experimental test explained in chapter 3.

In the experimental test, an actuator which applies the horizontal load is attached to the center of the top beam (HEB 600 with a height of 600 mm). To consider the accurate moment arm of the load, a line that represents the top beam with an offset of 300 mm is modeled above the masonry wall.

A linear interface is used to connect the beam to the masonry wall to simulate the glue used in the experimental test.

Regarding the boundary condition, linear support is applied at the bottom to simulate the cantilever wall. Since this is a 2D model, displacement in X- and Y-direction is closed.

For the pushover analysis, a monotonic prescribed deformation is implemented to the beam. Since the wall is not symmetric it should be loaded in both negative and positive X-direction. To apply a prescribe deformation at the loading point, DIANA FEA requires additional support that restrains the displacement in the loading direction. In both cases, a point roller support is applied and displacement in X-direction is fixed which can be seen in Figure 4-1.

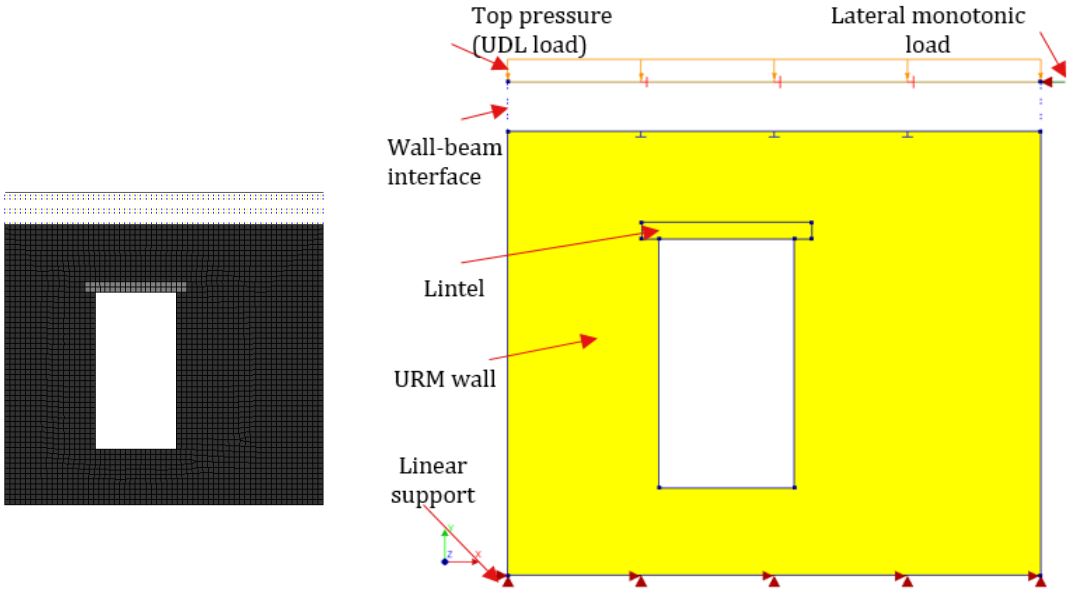

Figure 4-1: URM wall modeled in DIANA

- **Retrofitted wall**

The retrofitted wall, Figure 4-2, is molded as same as the URM wall explained in the previous part. The only difference is the bed joint reinforcement and diagonal anchors which are added to the model. The layout of the reinforcement is based on the experimental test.

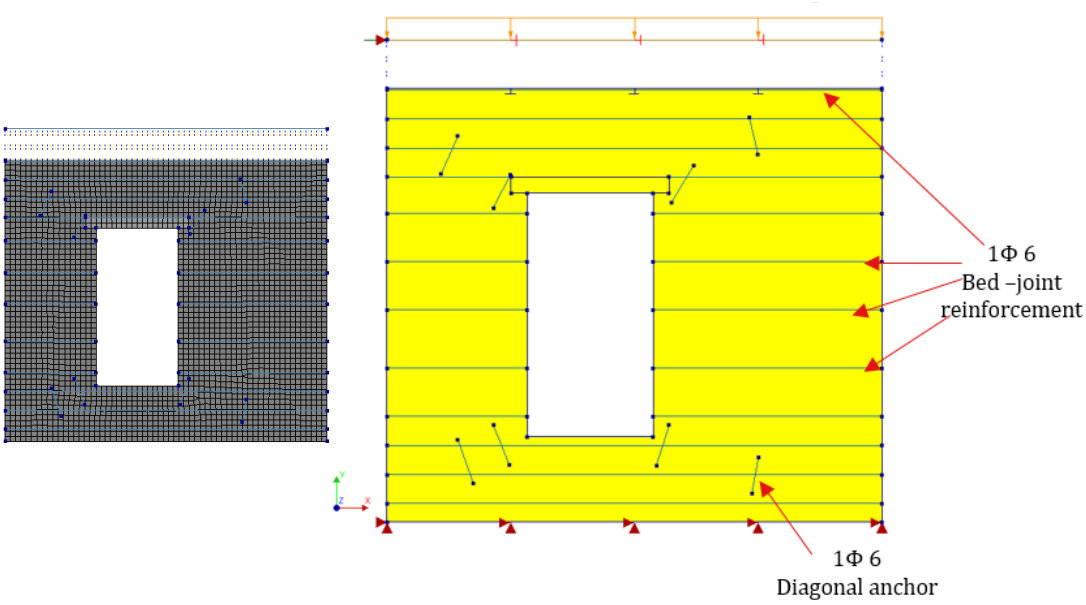

Figure 4-2: Retrofitted wall modeled in DIANA

4.2.2 Finite element discretization and element type

In this part, finite elements and their characteristics used for the numerical simulation are discussed for every single component (masonry, lintel, beam, and reinforcement).

Since load is applied in the plane of the wall and two dimensions (width and height) of the wall is considerably larger than the third dimension (thickness) of the wall, plane stress element can be used for numerical modeling.

- **Masonry wall and concrete lintel**

8QMEM, which is a four-node quadrilateral isoperimetric plane stress element, is used to model the masonry wall and concrete lintel. This element is based on linear interpolation and Gauss integration. Each node has two degrees of freedom in this element (X- and Y-direction). The polynomial for the displacement u_x and u_y is shown in Figure 4-3. A mesh size of 50 mm is used for this element.

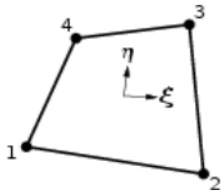

$$u_i(\xi, \eta) = a_0 + a_1 \xi + a_2 \eta + a_3 \xi \eta$$

Figure 4-3: Element Q8MEM (DIANA FEA, 2019)

- **Steel beam**

L6BEA, that is a two-node, two-dimensional class-III beam element, is implemented to model the I-shaped beam. An interface element is used for the wall-beam contact line.

Each node of the beam has three degrees of freedom: displacement in the horizontal and vertical direction as well as rotation around the Z-axis. Rotation around Z-axis is free in this model to simulate the cantilever behavior of the wall.

The polynomial for the displacement u_x, u_y and $\emptyset_z$ is shown in Figure 4-4.

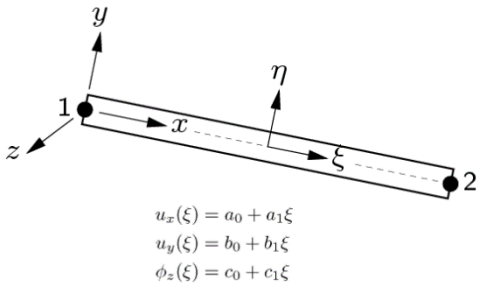

Figure 4-4: Element L6BEA (DIANA FEA, 2019)

- **Interface**

L8IF, is a line, 2+2 nodes, and 2D element. This element is a structural interface between two lines. It is based on linear interpolation and a 2-point Newton-Cotes integration scheme is applied for this element by DIANA.

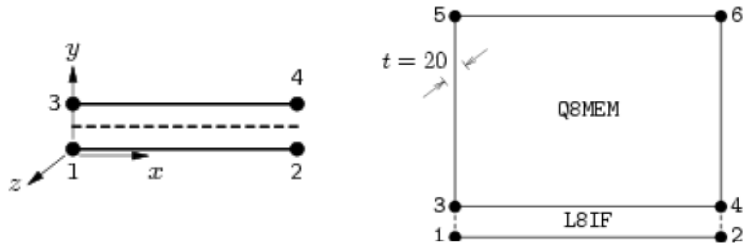

Figure 4-5: Element L8IF (DIANA FEA, 2019)

- **Bed joint reinforcement and diagonal anchor**

Bed joint reinforcement and diagonal anchor can be modeled in two ways: we can consider that reinforcement is fixed in its adjacent continuum element, fully bonded reinforcement, then embedded reinforcement can be applied. In this case, strain is derived from the nodal displacement of the mother continuum element. In another method, we can consider that there is a slip between reinforcement and its adjacent element. To simulate this behavior, bond-slip reinforcement can be chosen for the material model.

Table 4-1: Finite element models, DOF, integration scheme and dimension (DIANA FEA, 2019)

Component	Finite Element Types	DOF	Interpolation Scheme	Integration Scheme	Topological Dimension	Shape Dimension	Number of Elements for 50mm Mesh Size
Masonry wall	Quadrilateral 4-noded plane stress element (CQMEM)	8	linear	Gauss	2D	2D	2766
Top beam	2-noded beam element (class III-L6BEA)	6	linear	Gauss	2D	2D	61
Wall-beam interface	2+2 nodes interface element (L8IF)	8	linear	2-point Newton-Cotes	2D	2D	61

Table 4-2: Cross-section of the components

Element	Width (mm)	Length (mm)
Beam	300	3070
Wall	100	3070
Interface	100	3070

4.3 Constitutive and material models

Different components must be modeled with different constitutive laws according to the behavior of the component.

Since the masonry is supposed to crack, a nonlinear material should be considered for it. As the lintel is made of reinforced concrete, we do not expect any cracks in lintel as it is stiffer than masonry so, a linear concrete is chosen. The top beam, as well as its interface with masonry, is considered as a linear material in this research. The bead-joint and diagonal anchors might yield during loading. According to the experimental test, both reinforcements yielded. However, it is

essential to conduct a linear analysis to check the stress in the steel. If necessary, steel with nonlinear properties can be defined.

All the mentioned components and their corresponding constitutive and material models are discussed in detail in the following paragraphs.

- **Masonry wall**

Since the failure modes and crack pattern of the wall are investigated, masonry must be modeled with a nonlinear material. Two different material models are studied for masonry: Total Strain Crack Model (TSCM) and Engineering Masonry Model (EMM). Both models are based on the smeared crack model and are discussed in detail in chapter 2. Thus, in this part, material properties are deliberated and magnitudes are based on the experimental results provided in chapter 3.

- Total Strain Crack Model

Linear Material Properties: Modulus of elasticity, Poisson's ratio, and mass density of the masonry are chosen based on the experiment.

Tensile Behavior: different tensile curves can be chosen to show the softening of the masonry. However, as this model is compared with Engineering Masonry Model, providing the linear-crack energy only, the same tensile curve is used for the Total Strain Crack Model. Tensile strength and tensile fracture energy can be calculated as follows:

$$G_{ft} = 0.025(2f_t)^{0.7} = 0.0085$$

$$f_t = \frac{f_{x1}}{1.5} = \frac{0.16}{1.5} = 0.107\ MPa$$

Where,

f_{x1} is masonry flexural strength with the moment vector parallel to the bed joints and in the plane of the wall.

Compression Behavior: for the compression curve, meanwhile, a parabolic curve which models the softening of the masonry is used. This is due to the fact that the Engineering Masonry Model has almost the same behavior in compression.

Table 4-3: Applied material properties for Total Strain Crack Model

Linear material properties	
Material Model	Total Strain Based Crack Model
E_x	3207 (MPa)
$\boldsymbol{\nu}$	0.16
Mass Density	1708 (kg/m^3)
Tensile behavior	
Tensile Curve	Linear Crack Energy
Tensile Strength	0.107 (MPa)
G_{ft}	0.0085 (N/mm)
Compressive behavior	
Compression Curve	Parabolic
Compressive Strength	12.93 (MPa)
Fracture Energy in Compression	28.63 (N/mm)

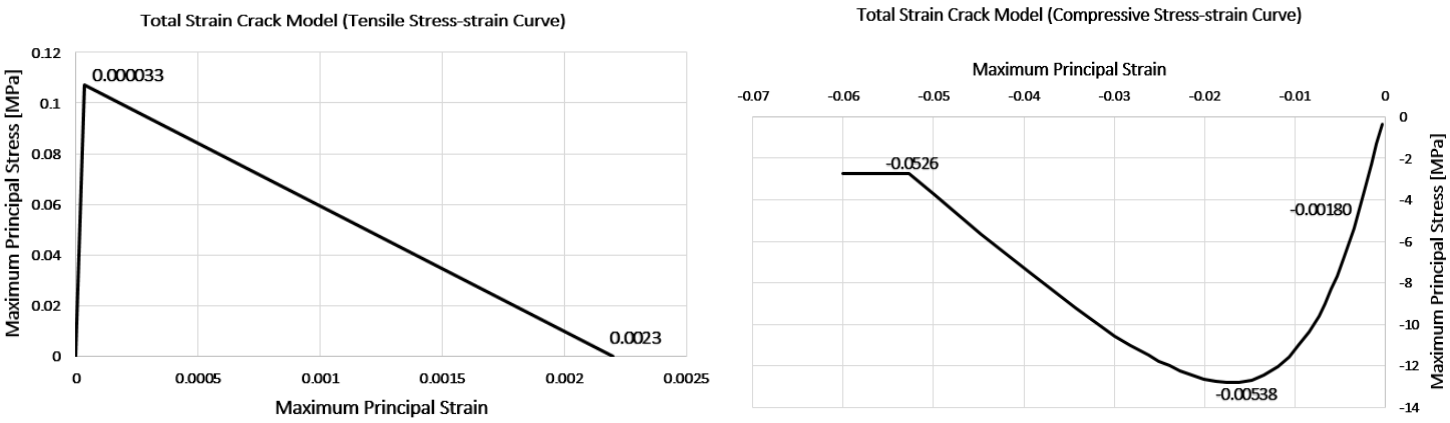

(a) (b)

Figure 4-6: Total Strain Crack Model. Tensile stress-strain curve (a) and compressive stress-strain curve (b)

- Engineering Masonry Model

Since this material model is an orthotropic model, material properties differ in X- and Y- direction. In this model, the shear failure is considered, yet, Poisson's effect is not taken into account. Tension and compression curves, by default, are linear and parabolic respectively. Since this material model is to be compared with the Total Strain Crack Model, the inputs must be identical as much as possible.

Linear Material Properties: Young's modulus in X-and Y-direction, shear modulus, and mass density are chosen from experimental data.

Tensile Behavior: three head-joint failure types can be checked in this part: direct input head-joint tensile strength, diagonal stair-case cracks, and tensile strength head-joint defined by friction. All cases are studied to find the most accurate model in terms of peak-load and crack pattern.

Compression Behavior: compressive strength and fracture energy in compression must be introduced for this part. Factor to strain and unloading factor are another two important parameters that determine the shape of the stress-strain curve in compression and unloading scheme.

Shear Behavior: fracture energy in shear, cohesion and friction angle should be considered for this part. The friction angle can be calculated based on the masonry shear friction coefficient ($\propto$) as follow:

$$\tan \propto = 0.82 \quad \rightarrow \propto = 39.35\ degree\ (0.686787\ radian)$$

As an example, since the failure type of the head joint is defined by *tensile strength head-joint defined by friction,* inputs would be as follows:

Table 4-4: Applied material properties for EMM. Failure type of the head-joint: tensile strength head-joint defined by friction

Linear material properties	
Material Model	Engineering Masonry Model
E_x	3207 (MPa)
E_y	4590 (MPa)
G_{xy}	1627 (MPa)
$\boldsymbol{\nu}$	Not Valid
Mass Density	1708 (Kg/m^3)
Cracking parameters	
Head-Joint Failure Type	**Tensile Strength Head-Joint Defined by Friction**
Bed Joint Tensile Strength	0.107 (MPa)
Minimum Tensile Strength Head-Joint	0.107 (MPa)
Fracture Energy in Tension (G_{ft})	0.0085 (N/mm)
Angle Between Stepped Diagonal Crack and Bed Joint	0.5 rad
Crushing Parameters	
Compressive Strength	12.93 (MPa)
Fracture Energy in Compression	28.63 (N/mm)
Factor to Strain at Compressive Strength	4
Unloading Factor	0.25
Shear failure parameters	
Friction Angle	0.686787 rad
Cohesion	0.14 (MPa)
Fracture Energy in Shear	0.15 (N/mm)

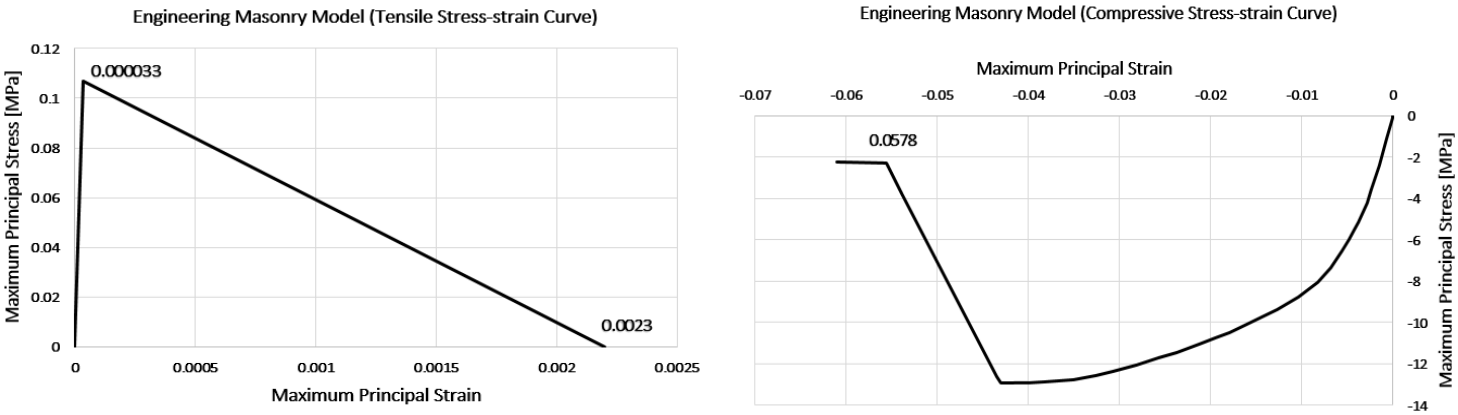

(a) (b)

Figure 4-7: Engineering Masonry Model. Tensile stress-strain curve (a) and compressive stress-strain curve (b)

- **Bed joint reinforcement and diagonal anchor**

For the bed joint reinforcement and diagonal anchor, first, we should check the linearity/nonlinearity of material and in the next step, the interaction of reinforcement with its adjacent element must be considered by an appropriate material model: embedded reinforcement and bond-slip of reinforcement. In this research, the former is implemented.

- *Embedded reinforcement*: when embedded reinforcement (i.e. fully bonded) is chosen as the material model we can select both linear and nonlinear steel.

Following properties can be consumed for linear steel:

Table 4-5: Material properties for embedded reinforcement, linear steel

Material Model	Young's Modulus $(\frac{N}{mm^2})$	Poisson's Ratio	Mass Density $(\frac{kg}{m^3})$
Embedded-linear elasticity	210000	0.3	7870

For nonlinear steel, the stress-strain curve with von Mises plasticity is used based on the experimental results.

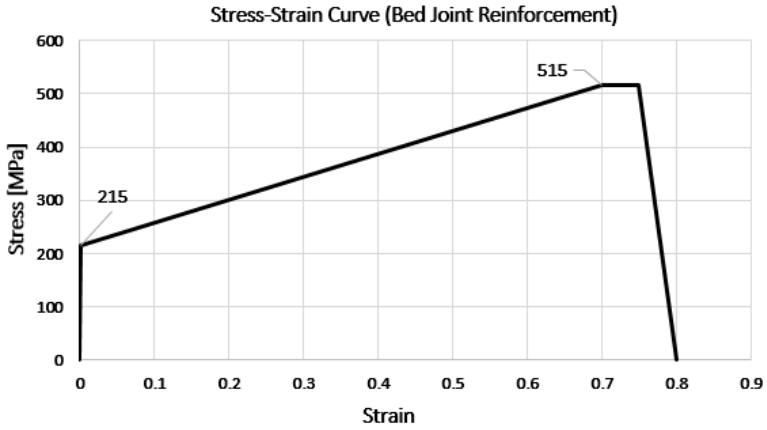

Figure 4-8: Stress-strain curve for bed joint reinforcement and diagonal anchor (provided by Dr. Tasos Drougkas, TU Delft)

Table 4-6: Material properties for embedded reinforcement, nonlinear steel

Material Model	Hardening Hypothesis	Hardening Function	Young's Modulus $(\frac{N}{mm^2})$	Poisson's Ratio	Mass Density $(\frac{kg}{m^3})$
Embedded-von Mises Plasticity	Strain hardening	Total strain-stress	210000	0.3	7870

- **Concrete lintel**

Since concrete is much stronger than masonry, linear concrete is used for the lintel. This results in the assurance of not observing any cracks in the lintel. For simplification, concrete is modeled as plain concrete since we do not expect its failure. The material properties used in DIANA is based on the experimental test as follows.

Table 4-7: Concrete lintel material properties

Element Type	Young's Modulus $(\frac{N}{mm^2})$	Poisson's Ratio	Mass Density $(\frac{kg}{m^3})$
Plane stress element	20000	0.2	2400

- **Beam-Wall Interface**

For this project, a 2-D linear interface is used for the wall-beam connection. In order to prevent interface slip, a high stiffness (dummy stiffness) is considered for the interface element. Normal stiffness (K_n) and shear stiffness (K_t) of the interface is calculated as follows.

$$K_n = \frac{1000 * E_{steel}}{l_{mesh}} = 4200000 \ \ N/mm$$

$$K_t = \frac{1000 * G_{steel}}{l_{mesh}} = 1650000 \ \ N/mm$$

Where l_{mesh} is 50 mm

Table 4-8: Interface material properties

Element Type	Normal Stiffness $(\frac{N}{mm^3})$	Shear Stiffness $(\frac{N}{mm^3})$
2-D line interface	4200000	165000

- **Steel beam**

The prescribed deformation is applied to the top beam and linear steel is chosen for this component. The self-weight of the beam is applied as an overburden pressure at the top, so self-weight is not considered for the beam.

Table 4-9: Material properties for top beam, linear steel

Element Type	Young's Modulus $(\frac{N}{mm^2})$	Poisson's Ratio	Mass Density $(\frac{kg}{m^3})$
Beam	210000	0.3	0

4.4 Loading conditions

The experimental test was a *quasi-static cyclic in-plane shear-compression test*. To simulate the same load scheme a nonlinear pushover analysis can be performed in software.

In general, three types of load are implemented: the self-weight of the wall and lintel, the pre-compression load and the prescribed deformation (lateral load).

Self-weight is calculated by DIANA based on the dimensions of the element (wall and lintel) and its mass density. The self-weight of the top beam is not considered here since it is applied as a pre-compression load at the top of the beam.

The self-weight of the top beam is applied as a **pre-compression load**: vertical force with a total magnitude of 0.12 MPa based on the experimental report. In the numerical model, this is replaced with a uniform distributed load (UDL) with a magnitude of 12 N/mm.

$$F = \sigma * A = 12 * 3070 * 100 = 36840 \quad N$$

$$UDL = \frac{force}{length\ of\ the\ beam} = \frac{36840}{3070} = 12 \quad \frac{N}{mm}$$

Where,
'A' is the cross-section of the wall where pressure is applied in the test.

Since this is a nonlinear analysis, the post-peak behavior of the wall is important and applying displacement control is more reasonable. As a result, a horizontal point load with a prescribed deformation type is applied to the top beam in negative and positive X- directions.

The loading history of the model affects the numerical results. Since the experimental test is based on a cyclic load, the effect of the cyclic load must be checked as well. Generally, by applying a cyclic load, more energy dissipates by opening and closing of the cracks so, masonry might carry a lower load and we can reach to more accurate force capacity curve for the models. However, applying a cyclic load is too time-consuming forasmuch as more than a hundred analyzes are supposed to be performed. A good solution to reduce the computational time is monotonic pushover analysis. As a result, we can analyze the models much faster and eliminate ineffective models.

For the monotonic pushover analysis, the prescribed deformation is set to 44 mm for positive X-direction and 40 mm for the opposite direction for the URM wall based on the experimental tests. These values for the strengthened wall are 81 mm and 64 mm for positive and negative X-direction respectively.

4.5 Convergence criterion

Two iterative methods (Regular Newton-Raphson and Secant Method) are implemented. Convergence criterion is considered based on a report provided by Rijkswaterstaat Central for Infrastructure (M.A.N. Hendriks et al., 2017).

> "Load increments are considered as converged if at least one of the force or energy norms is satisfied. Load increments that do not fully comply it might be still acceptable since they are followed by converged load increments".

According to the mentioned report, for all analyses, a maximum of 100 iterations is used with the force and energy convergence norm. Convergence tolerance is 0.01 and 0.001 respectively.

All the peak-loads reported in the analyses are the load magnitude of the last load step before divergence (numerical failure) upon the occurrence of the divergence.

4.6 Analysis procedure

An extensive study on the variations (parameters) is performed to examine their influences on the numerical results in terms of force capacity (capacity curve) and crack pattern. Then the results of the most accurate models are presented in chapter 5. To achieve this goal, several analyses are carried out. Many parameters are checked individually for two material models (TSCM and EMM). However, only the most accurate and/or important results are mentioned in the report. Material and geometrical nonlinearities are considered for all models.

Parameters that are checked are as follows.

General parameters for both material models:

- Mesh size
- Load step
- Iterative method

- Element type (linear vs. quadratic)

TSCM parameters:

- Crack orientation
- Poisson's ratio reduction model
- Residual compressive strength reduction due to lateral cracking
- Stress confinement

EMM parameters:

- Different head-joint failure types

By collecting the most accurate model based on the mentioned analyses, sensitivity and parametric study can be conducted.

5

NUMERICAL RESULTS

This chapter describes the most suitable numerical model that can be implemented for this project. Accordingly, two material models (i.e. the Total Strain Crack Model and the Engineering Masonry Model) are compared for the URM wall and retrofitted wall. Finally, an extensive sensitivity analysis is performed to study the effect of different parameters on the performance of the wall.

5.1 Post-processing of Results

In order to compare the numerical results with the experiment, peak-load, crack patter, and failure mechanisms are considered. To show the crack pattern, the maximum first principal strain (E1) and scaled E1 (as it is called in this research) are chosen. The former is used to show the maximum principal strain and its location while the latter is related to the constitutive law of the masonry wall and it is used to present the evolution of crack pattern in the wall.

To show the scaled E1, contour plot setting is modified and three colors are introduced to show the uncracked, partially cracked and fully cracked spots of the wall modeled with original material properties as shown in

Figure 5-1. Cracking strain (ε_{cr}) and ultimate strain (ε_{ult}) are calculated as follows.

$$\varepsilon_{cr} = \frac{f_t}{E} = \frac{0.107}{3207} = 0.0000333$$

$$\varepsilon_{ult} = \frac{2G_f}{f_t h} = 2 * \frac{2 * 0.0085}{0.107 * \sqrt{2 * 50 * 50}} = 0.0023$$

Where,

G_f is tensile fracture energy

f_t is tensile strength

h is crack bandwidth. For a 2D plane stress element, it can be calculated as $\sqrt{2A}$, where A is the area of the finite element (DIANA FEA, 2019). According to adaptive mesh refinement, 50 mm is a good choice for element size. (see appendix A for adaptive mesh refinement).

In the sensitivity analysis section, this curve will be changed by changing the parameters (modulus of elasticity, tensile strength, etc.).

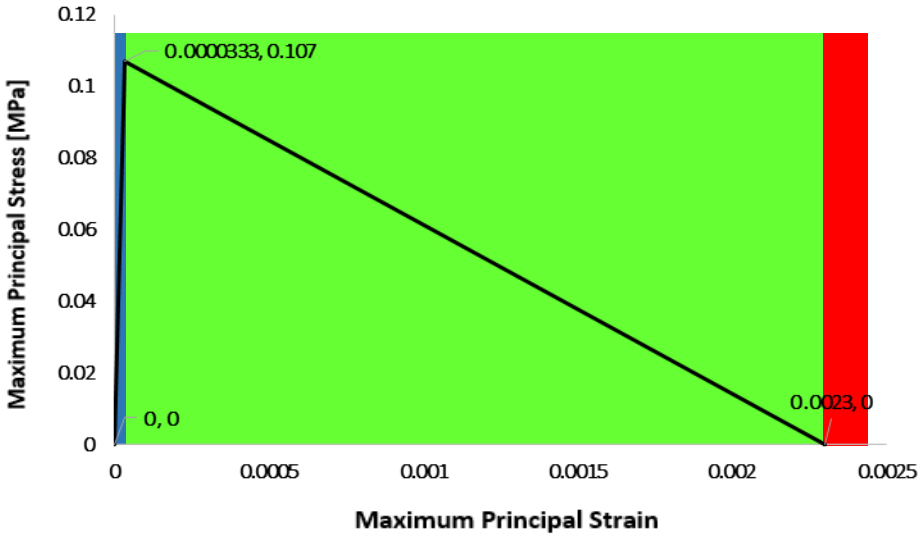

Figure 5-1: Tensile stress-strain curve for scaled E1

- Blue contour if $E1 < E_{cr}$ (uncracked)
- Green contour if $E_{cr} < E1 < E_{ult}$ (partially cracked)
- Red contour if $E1 > E_{ult}$ (fully cracked)

In order to find and plot the force-displacement curve of the model, applied deformation and corresponding support reaction are taken into account. The specific node (in top beam), where force and displacement are checked can be found in Figure 5-2

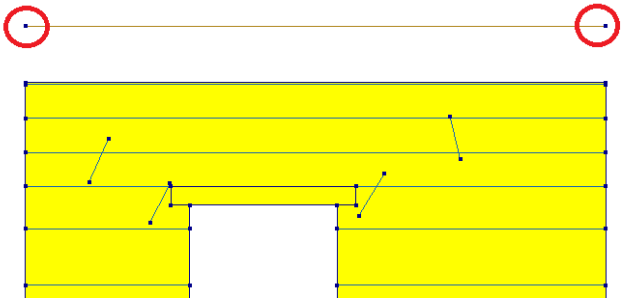

Figure 5-2: Selected nodes for force-displacement curve in two directions

5.2 Pushover analysis of the URM wall

This section, reports the results of the numerical simulation for the URM wall. Two analyses are performed: monotonic analyses in the positive and negative X-direction since the wall is not symmetric. The result of two material models (i.e. TSCM and EMM) are discussed separately.

Different parameters can be chosen for both material models. The most desirable parameters are selected based on the explanation in section 4.6.

The effect of mesh size, adaptive mesh refinement, is studied and analysis results can be found in Appendix A.

The computational time increases with a smaller load step significantly. In this research several models are analyzed so, managing the computational time is vital. As a result, while the force and displacement that corresponds to the first crack are studied, a small load step (0.04 mm) is applied. In this case, it is not necessary to run the model completely. However, whenever the models are fully analyzed, a bigger load step (0.4 mm) is used to decrease the computational time.

Table 5-1: Computational time vs. load step

Material Model	Load Step	Computational Time (Minutes)
TSCM	0.4 mm	29
TSCM	0.04 mm	1553

5.2.1 URM wall modeled by Total Strain Crack Model (TSCM)

A prescribed deformation with a magnitude of 44 and -40 mm is applied for the positive and negative X-direction respectively.

Figure 5-3 presents the capacity curve obtained from the FE analysis. There are seven important points shown by letters A to G on the curve that can be the aids to understand the behavior of the wall in terms of crack initiation and propagation, crack types, peak load, and failure mechanisms.

Table 5-2 shows parameters that are chosen for the URM wall molded with TSCM to get the most accurate results in terms of the capacity curve and crack pattern.

Table 5-2: Applied material properties, loading, convergence norm, mesh size, iterative method and element type for TSCM that is used in DIANA

Linear material properties	
Material Model	Total Strain Based Crack Model
E_x	3207 (MPa)
$\boldsymbol{\nu}$	0.16
Mass Density	1708 (kg/m^3)
Crack Orientation	Rotating
Tensile behavior	
Tensile Curve	Linear Crack Energy
Tensile Strength	0.107 (MPa)
G_{ft} (Fracture Energy in Tension)	0.0085 (N/mm)
Crack Bandwidth Specification	Rots
Poisson's Ratio Reduction model	No Reduction
Compressive behavior	
Compression Curve	Parabolic
Compressive Strength	12.93 (MPa)
Fracture Energy in Compression	28.63 (N/mm)
Reduction Due to Lateral Cracking	Vecchio and Collins 1986
Stress Confinement	No Increase
Others	
Prescribed Deformation	Positive X : 44 (mm) Negative X : 40 (mm)
Load Step	0.4 mm [0.01(100)]
Number of Iteration	100
Iterative Method	Regular Newton-Raphson
Convergence Norm and Tolerance	Energy (0.001) or Force (0.01) with Continuation Method
Mesh Size	50 (mm)
Element Type	Plane Stress-linear element (Q8MEM)
Structural Nonlinearity	Material and Geometry

When the wall is loaded in positive X-direction, the first cracks occur once the load reaches 8.09 kN with a relative deformation of 0.2 mm. It should be noted that the wall starts to crack diagonally from the bottom right corner of the window. By increasing the prescribed deformation to 1.79 mm, point B, two diagonal cracks that propagated from 2 window corners are recognized. In addition, a bed joint crack is recognized at the bottom of the left pier. At the final load step, point D, the top left crack opens significantly when 23.47 kN load is applied. As shown in

Figure 5-4, by increasing the load, the crack width grows and as a result, a fully separated boundary between the left pier and spandrel occurs. Therefore, the left pier turns to the undeformed state and the bed joint crack in the pier gets closed. Consequently, the rocking of the pier (at the bottom) cannot be seen anymore at the end of the analysis. By increasing the deformation toe, crushing is possible at the right bottom of the wall since compressive stress (12.73 MPa) is very close to the compressive strength (12.93 MPa) of the masonry wall.

The result is a bit different when the wall is loaded in the negative X-direction. This is due to the unsymmetrical shape of the wall and that the dimensions of the piers that are not the same so, the crack patterns of the wall are different in two directions. Cracks initiate at a lower load and displacement: -5.18 kN which corresponds with -0.16 mm deformation, point E, and again

corner of the window is the most vulnerable spot. At point F, the maximum load, -22 kN, is observed when the deformation reaches -9.80 mm. In this stage, stair-case cracks (diagonal cracks) are observed in 4 corners. Furthermore, a bed joint crack at the top of the left pier and rocking mechanism at the bottom of the wall is recognized. The crack pattern is the same in the last load step, point G, as can be seen in Figure 5-4. However, crack width and principal strain increases dramatically. The maximum strain values are in order of 0.58.

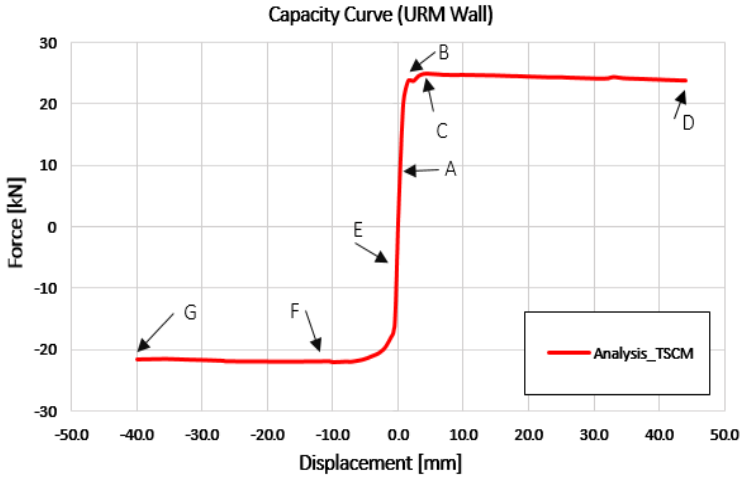

Figure 5-3: Capacity curve. URM wall modeled with Total Strain Crack Model (TSCM)

Table 5-3: URM wall model with TSCM. Crack initiation, crack propagation and peak-load

Point	Description	Force (kN)	Displacement (mm)
A	Crack initiation	8.10	0.2
B	Crack propagation	24.50	1.80
C	Peak-load	24.85	4.70
D	End of analysis	23.50	44
E	Crack initiation	-5.20	-0.15
F	Peak load	-22	-9.80
G	End of analysis	-21.60	-40

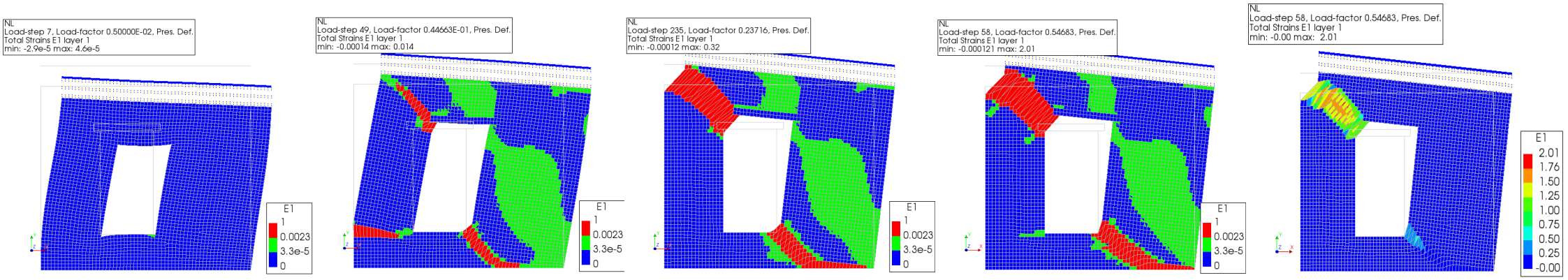

(a) Point A (b) Pint B (c) Point C (d) Point D (e) Point D. Maximum strain

Figure 5-4: URM wall modeled with TSCM, positive X-direction. Scaled first principal strain.

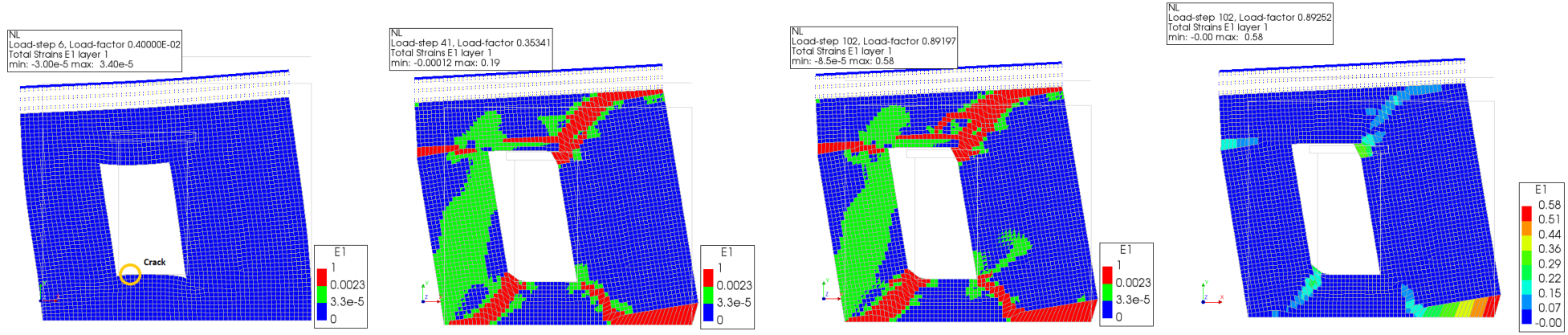

(a) Point E (b) Pint F (c) Point G (d) Point G. Maximum strain

Figure 5-5: URM wall modeled with TSCM, negative X-direction. Scaled first principal strain.

5.2.2 URM wall modeled by Engineering Masonry Model (EMM)

Similar to the TSCM, a prescribed deformation with a magnitude of 44 and -40 mm is applied for the positive and negative X-direction respectively.

In Engineering Masonry Model (EMM), three types of failure can be set for the head-joint: direct input head-joint tensile strength, diagonal stair-case cracks, and tensile strength head-joint defined by friction. Furthermore, it can be considered that the head-joint does not fail. All four options are checked one by one to find the most appropriate model. All cases have almost the same results. The result of the *tensile strength head-joint defined by friction* is explained in this section and other head-joint failure type results can be seen in Appendix B.

Figure 5-6 shows the capacity curve obtained from the analysis. Five important points that are shown by letters A to E on the curve are used to understand the behavior of the wall in terms of crack initiation and propagation, crack types, peak load, and failure mechanisms.

Table 5-4 shows the parameters that are chosen as the best options for the URM wall molded by EMM to get the most accurate results in terms of the capacity curve and crack pattern.

Table 5-4: Applied material properties, loading, convergence norm, mesh size, iterative method and element type for EMM that is used in DIANA

Linear material properties	
Material Model	Engineering Masonry Model
E_x	3207 (MPa)
E_y	4590 (MPa)
G_{xy}	1627 (MPa)
$\boldsymbol{\nu}$	0
Mass Density	1708 (Kg/m^3)
Cracking parameters	
Head-Joint Failure Type	**Tensile Strength Head-Joint Defined by Friction**
Bed joint Tensile Strength	0.107 (MPa)
Minimum Tensile Strength Head-Joint	0.107 (MPa)
Fracture Energy in Tension (G_{ft})	0.0085 (N/mm)
Angle Between Stepped Diagonal Crack and Bed joint	0.5 rad
Crushing Parameters	
Compressive Strength	12.93 (MPa)
Fracture Energy in Compression	28.63 (N/mm)
Factor to Strain at Compressive Strength	4
Unloading Factor	0.25
Shear failure parameters	
Friction Angle	0.686787 rad
Cohesion	0.14 (MPa)
Fracture Energy in Shear	0.15 (N/mm)
Crack bandwidth specification	Rots
Others	
Prescribed Deformation	40 (mm)
Load Step	0.4 mm [0.01(100)]
Number of Iteration	100
Iterative Method	Quasi-Newton Method

	(Secant Method)
Convergence Norm and Tolerance	Energy (0.001) or Force (0.01) with Continuation Method
Mesh Size	50 (mm)
Element Type	Plane Stress-linear element (Q8MEM)
Structural Nonlinearity	Material and Geometry

By applying EMM around 90% of load steps (in both directions) are not converged as can be found in Figure 5-6 so, numerical results are not valid anymore. So, it is not reasonable to discuss the results in detail. Several parameters are considered and changed to solve the convergence problem, however, no convincing results are obtained. It also must be mentioned that EMM was applied in some models by other researchers and the results were acceptable.

Studied parameters to solve the convergence problem are listed as follows.

- Different shear cohesion (0.3, 0.5, 0.8, and 1.2 N/mm^2).
- Not only similar but different modulus of elasticity in X and Y-direction.
- Different shear fracture energy (0.3, 0.6, 1.2, 2.4, and 5 N/mm).
- Different inputs for bed joint and head joint strength (head=0.107 and bed=0.107, head=0.107 and bed=0.05, head=0.07 and bed=0.05, head=0.25 and bed=0.03 MPa).
- The angle between stepped diagonal crack and bed joint (0.4, 0.5 and 0.75 rad).
- Very small load steps.
- Different iterative methods (Secant Method, Regular Newton-Raphson, Modified Newton-Raphson, Linear Stiffness, and Constant Stiffness).
- Arc length control.
- Different convergence norms.
- Different element type (linear and quadratic).
- Model with multiple execute blocks.
- Model without beam-wall interface at the top.

Regardless of the convergence problem, force capacity and crack pattern of the model are presented in Figure 5-6 and 5-8.

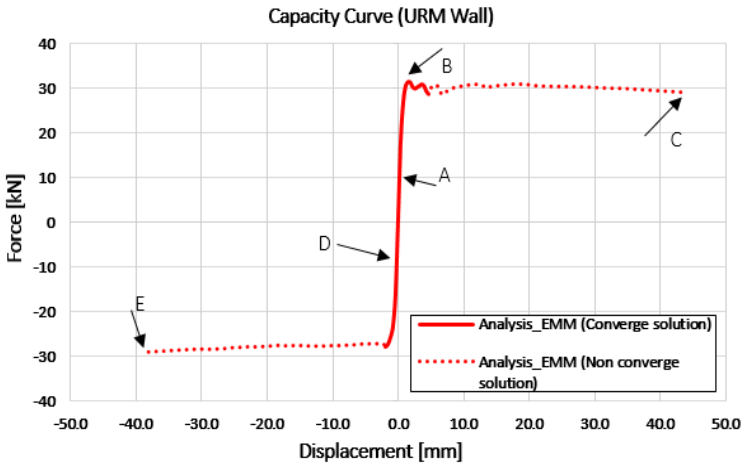

Figure 5-6: Capacity curve. URM wall modeled with Engineering Masonry Model

Table 5-5: URM wall model with EMM. Crack initiation, crack propagation and peak-load

Point	Description	Force (kN)	Displacement (mm)
A	Crack initiation	10.15	0.2
B	Peak-load	31.33	1.5
C	End of analysis (non-convergence solution)	28.85	44
D	Crack initiation	-8.85	-0.2
E	End of analysis and peak-load (**non-convergence solution**)	-28.40	-40

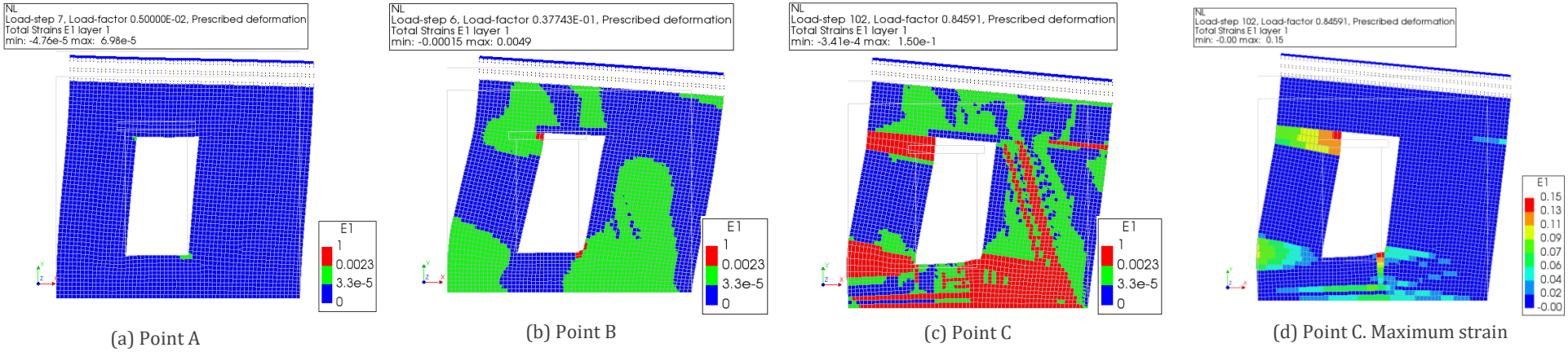

(a) Point A (b) Point B (c) Point C (d) Point C. Maximum strain

Figure 5-7: URM wall modeled with EMM, positive X-direction. Scaled first principal strain

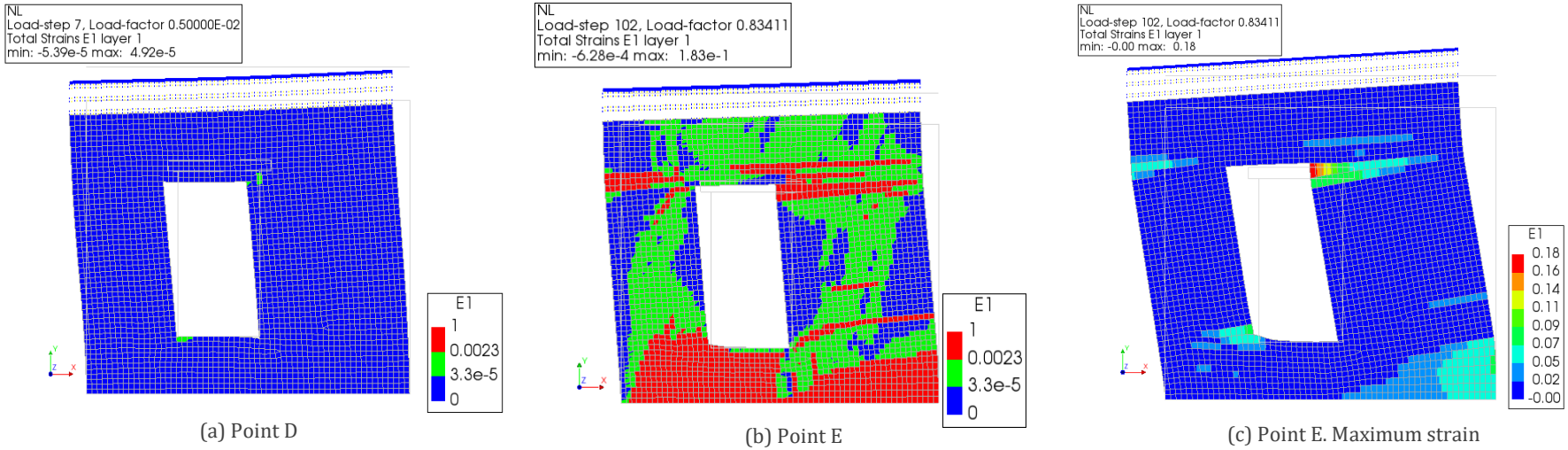

(a) Point D (b) Point E (c) Point E. Maximum strain

Figure 5-8: URM wall modeled with EMM, negative X-direction. Scaled first principal strain

5.2.3 Experimental vs. numerical: URM wall

In this part, numerical results are compared with the experiments in terms of crack pattern and capacity curve. For EMM, the head-joint failure type - chosen in part 5.2.2 is used - however, due to many non-converge solutions results are not valid and will not be discussed in detail. For crack patterns, first, the experimental result, failure mechanisms, and their causes are discussed in detail. Then, the numerical results are interpreted accordingly.

- **Capacity curve:**

Both material models follow the pattern of the capacity curve obtained by the experiment. The initial stiffness of the models can be seen in Figure 5-9. By choosing original material properties both EMM and TSCM simulate the stiffness of the wall in a good agreement with the experiment.

By applying TSCM, the model is converged in both directions very well. Considering the positive X-direction, the result is reliable. This material model predicts the peak-load with a difference of +5.75%. In the negative direction, TSCM estimates the peak load with slightly a higher difference, +12.41%. The experimental result is based on a cyclic load. However, a monotonic load is applied in the numerical models so, this can be a reason for the mentioned differences for the peak loads.

In contrast, by applying EMM, many load steps are not converged that lead to invalid results. The peak-load is overestimated by +33.55% (converge solution) in positive X-direction and +46% (non-converge solution) in the opposite direction.

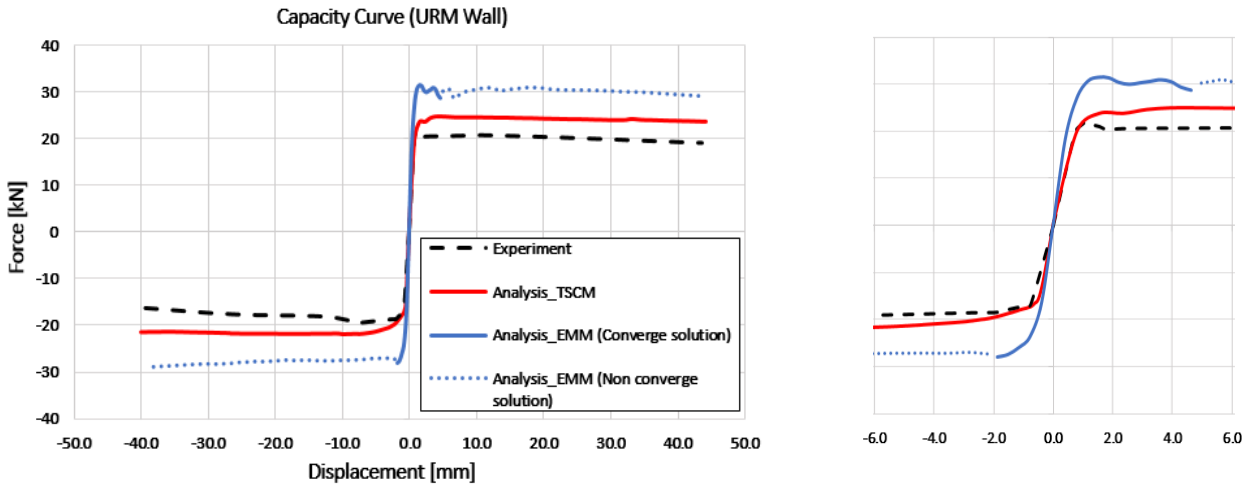

(a) (b)

Figure 5-9: Capacity curve (a) and stiffness (b) for URM wall. TSCM vs. EMM

- **Crack pattern:**

In order to organize the comparison, cracks are numbered from 1 to 4. The original and scaled first principal strain (E1) calculated by DIANA is used for comparing the results. The un-deformed shape of the contour is selected in order to study the crack pattern as accurate as possible, owing to the fact that the experimental data are based on absolute deformations and crack width is out of interest at this time. The deformed shape of the models can be found in the previous part.

Figure 5-11, 12 show the crack pattern in both directions observed in the **experimental tests**.

When the wall is loaded in the positive X-direction, cracks number 1 and 2 were observed by applying 7.89 mm displacement. A pure horizontal crack led to the separation of the spandrel and the left pier at this stage (crack number 2). A combination of bed joint and staircase crack was noticed in crack number 1 which was responsible for the rocking of the pier. By increasing the deformation (11.11 mm) at crack number 3, a staircase crack at the bottom left corner of the opening was observed. Finally, the wall failed when 43.63 mm displacement was applied in the test. As a result, the masonry portion on the above of the window level slides respect to the rest of the wall. Furthermore, crack number 4 was propagated from the top right corner of the opening while crack number 3 got closed because the left pier turned to its unreformed state as a result of the collapse of the wall.

Considering the negative X direction, the same diagonal staircase cracks were observed in the wall. The rocking of the right pier occurred by applying -7.97 mm displacement (crack number 1). Diagonal staircase cracks were recognized in 3 corners of the opening: crack numbers 1, 3 and 4. In addition, the horizontal crack at the top of the left pier was observed in this direction. By increasing the deformation to -12.82 mm, the same crack patterns were perceived, however, spandrel slipped leftwards with respect to the piers. In the collapse phase (-40.22 mm), the same crack patterns, with much wider crack width and a fully sliding of the spandrel were observed. Both piers were separated entirely respect to the window bank and spandrel by 4 diagonal cracks.

As can be seen in Figure 5-13, 14, the **Total Strain Crack Model** simulates the crack pattern and failure mechanisms properly when the wall is loaded in negative X-direction. The unreformed shape of the URM wall is shown at three load levels correspond to a displacement of -8.08, -12.72 and -40 mm. Diagonal cracks (crack numbers 3 and 4) can be recognized in all steps which are in line with the experimental test accurately. The initiation and propagation of these cracks are estimated very well. Cracks number 2 is molded properly, however, separation of the pier with respect to the spandrel cannot be seen in the model. Rocking of the wall (bottom right corner) is simulated numerically, however, it did not occur in the tests.

Considering the positive X-direction, four stages are shown for the interpretation of the numerical results. By applying a small deformation (+1.64 mm) rocking of the left pier is observed due to crack number 3. In the experimental results, no crack pattern for 1.64 mm displacement is presented so, this stage cannot be validated with the test. The diagonal crack that is labeled by number 1, meanwhile, is predicted precisely. Furthermore, crack number 2 initiates at the top left corner of the opening and continues horizontally. However, it then divers diagonally (stair-case crack) which does not match the experimental result perfectly. By increasing the deformation (+7.87 mm) results are almost comparable with the experiment: both cracks numbers 1 and 2 are modeled. Separation of the left pier and spandrel is simulated, however, with a diagonal crack. It means that the propagation of the crack does not match the test and the pattern of the crack is different for crack number 2 (horizontal and diagonal in the analysis but purely horizontal in the experiment). Crack number 3 cannot be seen anymore and this follows the experimental result accurately. Apart from crack number 4 that is not predicted in analysis, the other cracks are estimated by DIANA when +11.10 mm and +44 mm displacement is applied. In the last step, the masonry portion above the opening level and right pier rotate with respect to the rest of the wall. This failure can be seen in the deformed shape of the wall more clearly, Figure 5-10.

Considering both directions, it is fair to say that TSCM can predict the crack pattern as well as the evolution of the cracks in a good agreement with the experiment when the URM wall is studied.

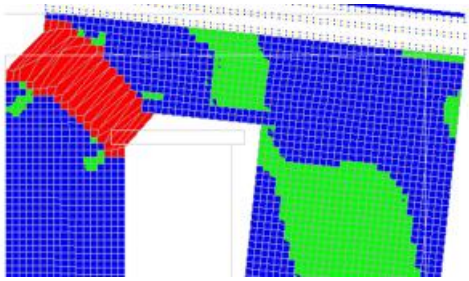

Figure 5-10: URM wall. Rotation of the spandrel and right pier with respect to the rest of the wall

Figure 5-15, 16 show the crack pattern in both directions observed in the **Engineering Masonry Model**. The prediction of the crack patterns and force capacity of the wall is not reliable since the model is not converged (Appendix C).

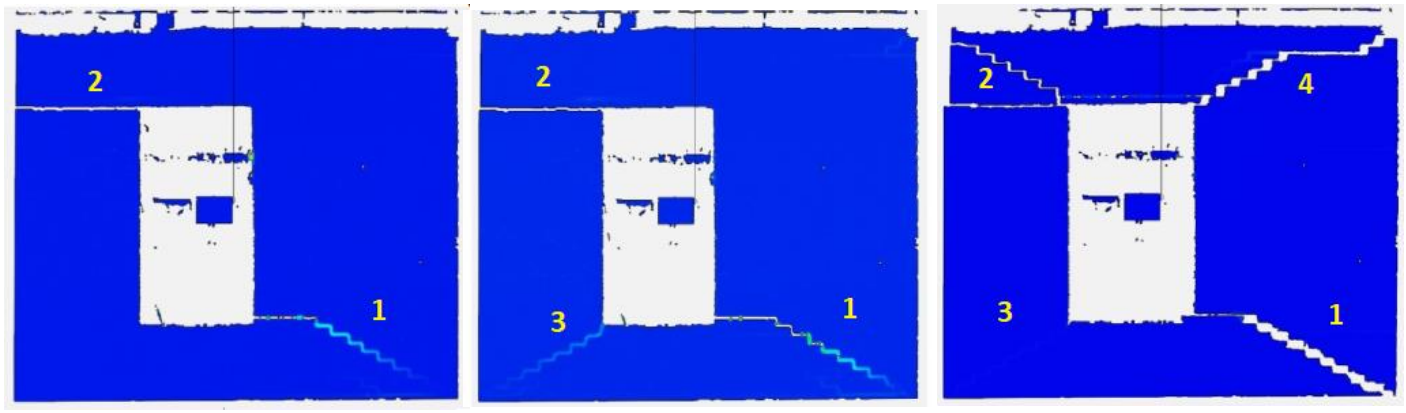

(a) Displacement = +7.89 mm (b) Displacement = +11.11 mm (c) Displacement = +43.63 mm

Figure 5-11: Phase 3, experimental result of URM wall. Wall is loaded in positive X-direction (Licciardello & Esposito, 2019)

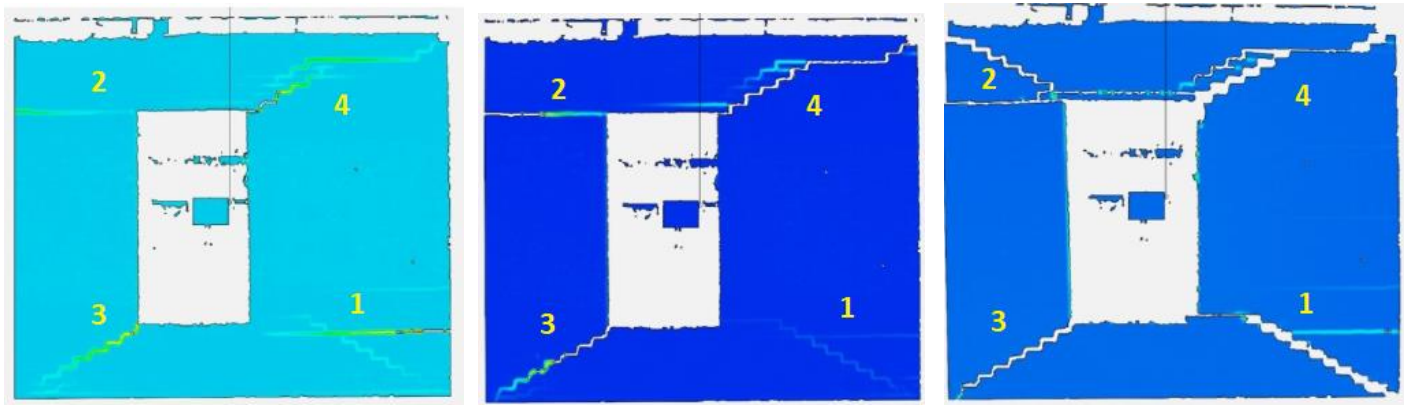

(a) Displacement = -7.97 mm (b) Displacement = -12.82 mm (c) Displacement = -40.2 mm

Figure 5-12: Phase 3, experimental result of URM wall. Wall is loaded in negative X-direction (Licciardello & Esposito, 2019)

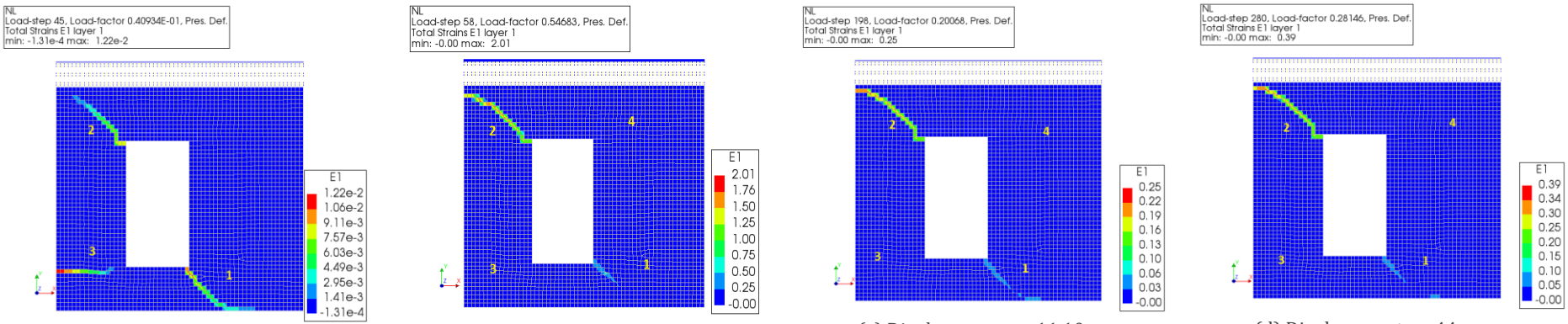

(a) Displacement = +1.64 mm (b) Displacement = +7.87 mm (c) Displacement = +11.10 mm (d) Displacement = +44 mm

Figure 5-13: URM wall modeled with TSCM, positive X-direction. First principal strain.

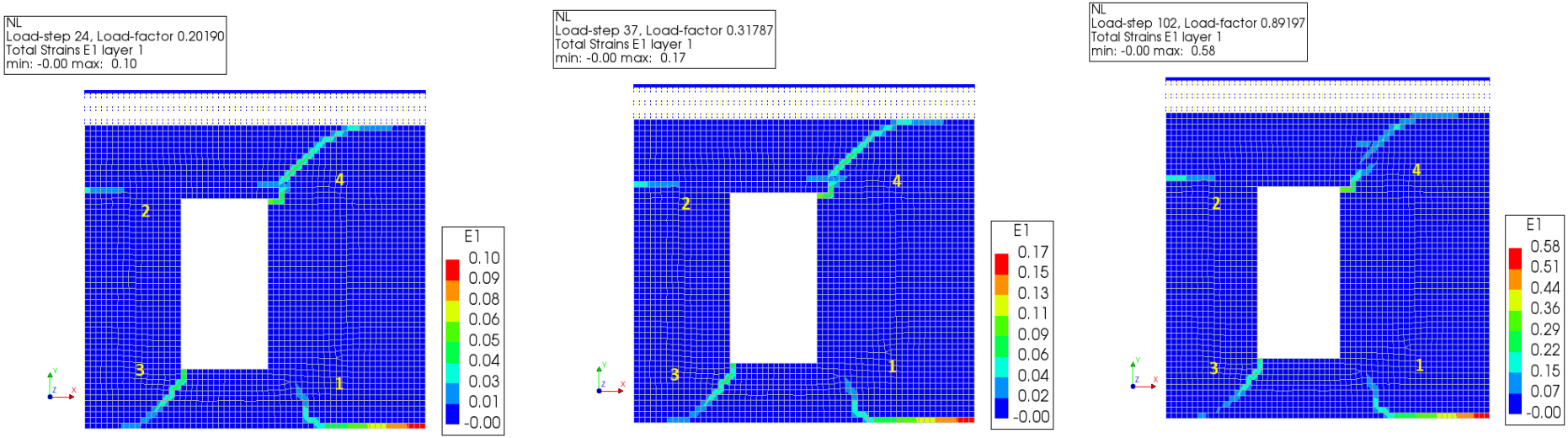

(a) Displacement = -8.08 mm (b) Displacement = -12.72 mm (c) Displacement = -40 mm

Figure 5-14: URM wall modeled with TSCM, negative X-direction. First principal strain.

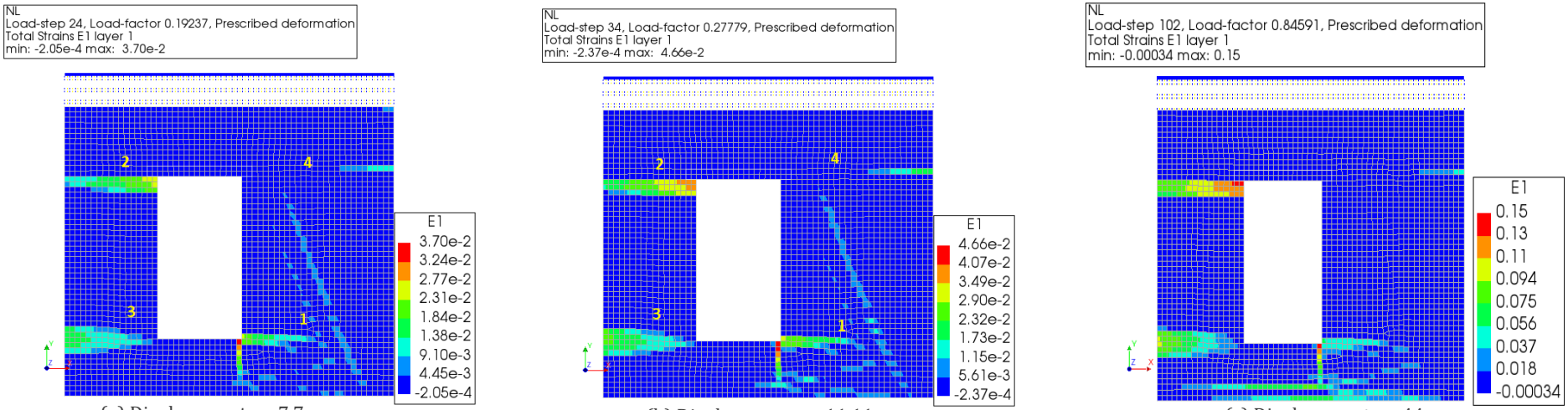

(a) Displacement = +7.7 mm (b) Displacement = +11.11 mm (c) Displacement = +44 mm

Figure 5-15: URM wall modeled with EMM, positive X-direction. First principal strain

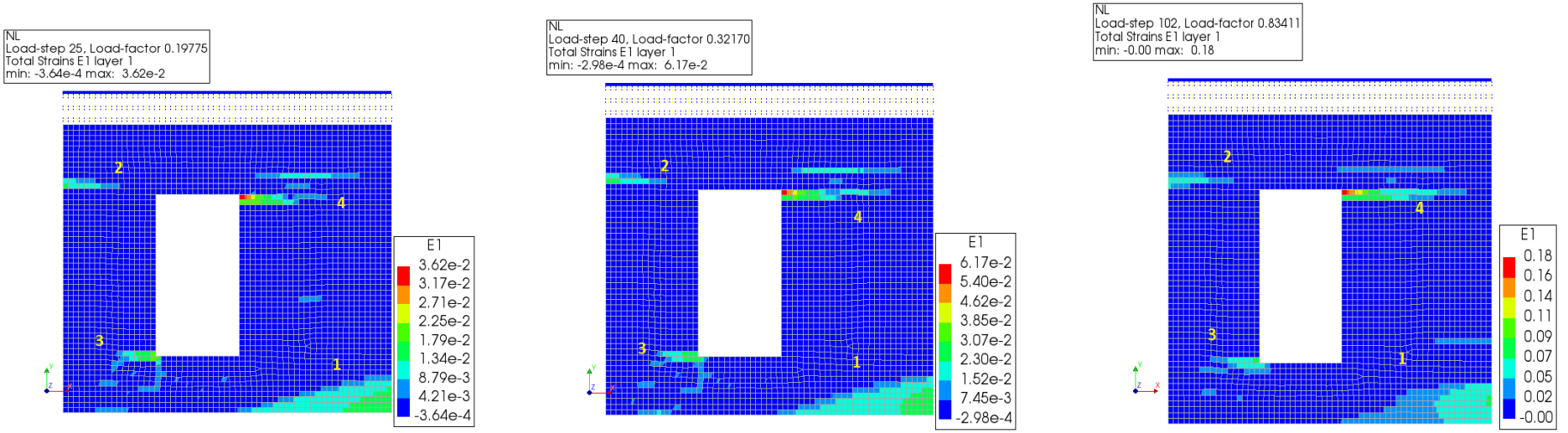

(a) Displacement = -8.08 mm (b) Displacement = -12.72 mm (c) Displacement = -40 mm

Figure 5-16: URM wall modeled with EMM, negative X-direction. First principal strain.

By comparing the crack pattern and capacity curves obtained from two material models we can conclude that TSCM predicts the behavior of the wall in a good agreement with the test. The numerical results obtained by EMM do not match the test because of the convergence problem of the analysis.

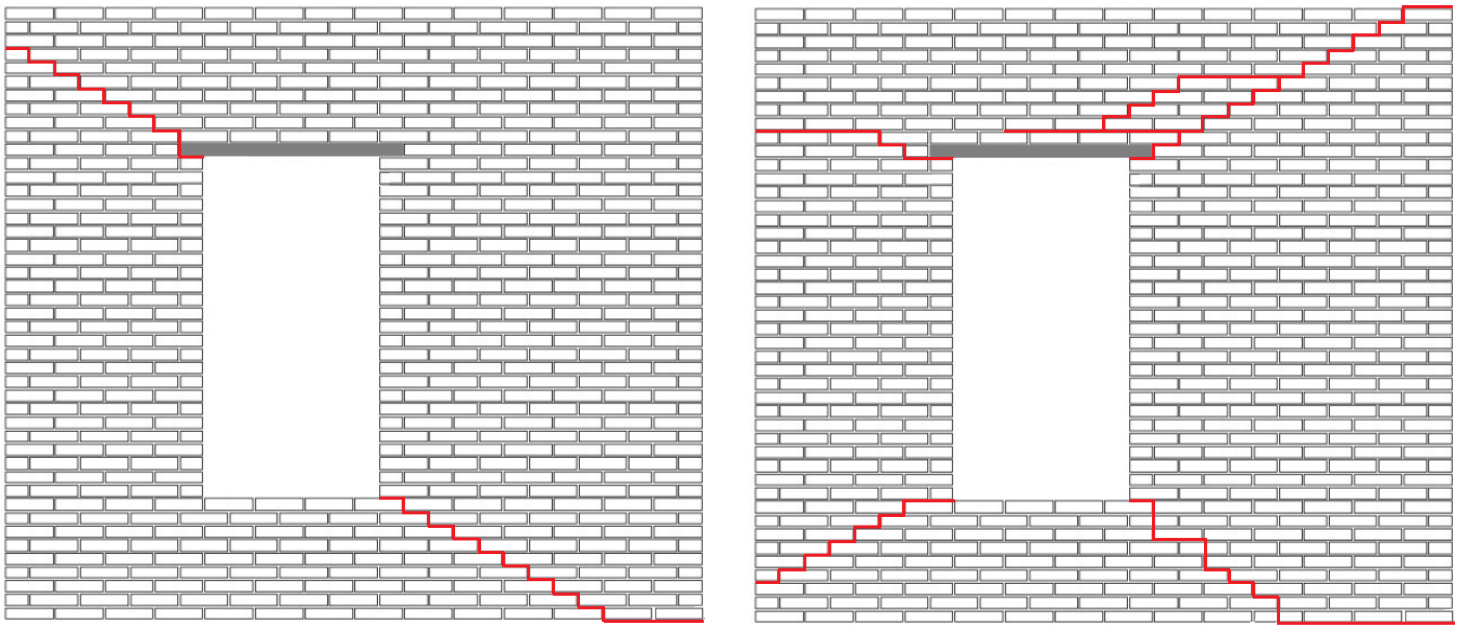

(a) Displacement = +44 mm

(b) Displacement = -40 mm

Figure 5-17: URM wall. Numerical results (TSCM), crack pattern

Table 5-6: Numerical result summary. URM wall, TSCM vs. EMM

Model	Load Step	Head-Joint Failure Type	Peak-Load (+X) (kN)	Difference to Test (+X)	Peak-Load (-X) (kN)	Difference to Test (-X)	Loading Capacity	Initial Stiffness	Crack Pattern
Experiment	N/A	N/A	23.45	N/A	19.45	N/A	N/A	N/A	N/A
EMM	0.4 mm [0.01(100)]	Tensile Strength Head-Joint Defined by Friction	31.35	**+33.55%**	28.40	**+46% (non-converge solution)**	**Non-converge solution**	**good agreement**	**Non-converge solution**
TSCM	0.4 mm [0.01(100]	N/A	24.85	**+5.75%**	22.00	**+12.40%**	**Good agreement**	**Very good agreement**	**Good agreement**

5.3 Pushover analysis of the retrofitted wall

This section reports the results of the numerical simulation for the retrofitted wall subjected to monotonic load. Once more, both TSCM and EMM are checked to find whether TSCM is still a better choice even for the retrofitted wall.

The same material properties that were used for the URM wall are chosen for the modeling of the retrofitted wall as well.

A full bond between mortar/masonry and steel is considered at this stage. This means that the steel is completely fixed to its adjacent. To model this behavior, embedded reinforcement is used for modeling.

Since a 2D plane stress element is considered for masonry, only one rebar can be modeled in the thickness of the wall. Therefore, wherever a double 6 mm rebar is applied for bed joint reinforcement, one rebar with a cross-section of 56.52 mm^2 is implemented. This value represents the summation of the cross-section of two 6 mm rebar.

To check the plasticity in steel, reinforcement is molded as an elastic material, however, the numerical results have shown that the stress in steel is higher than its yielding point. As can be found in Figure 5-18 and according to the stress-strain curve presented in chapter 3, steel yields at 215 MPa. Bed joint reinforcements applied bellow the window level yield since they act in tension to restrict cracks. So, we can conclude that the plasticity of steel must be considered in models. Rupture, however, does not occur in steel since rupture stress (515 MPa) is higher than maximum stress (502 MPa) obtained from numerical analysis.

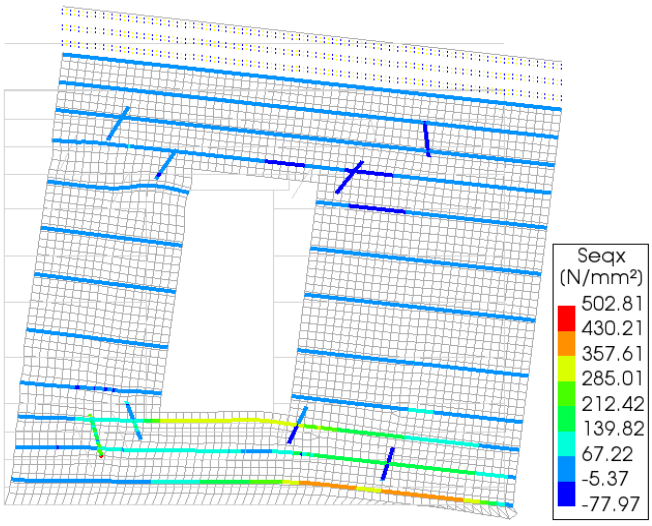

Figure 5-18: Reinforcement plasticity

5.3.1 Retrofitted wall modeled with TSCM

A prescribed deformation with a magnitude of 81 mm for the positive X-direction and -64 mm for the opposite direction is applied similar to the experiment.

Figure 5-20, presents the capacity curve obtained from the analysis. Six letters (A to F) are chosen on the graph to show the important events. Peak-load, crack initiation and crack patterns are discussed accordingly.

When the wall is loaded in positive X-direction, a force with a magnitude of 9.70 kN that corresponds with 0.24 mm deformation results in the first crack, point A. The corners of the opening are the most vulnerable spots so, cracks initiate from these points as it is shown in Figure 5-21. The crack width and length increase continuously by increasing the deformation to

1.55 mm, point B, and the peak-load (31.41 kN) is recorded at this stage. Similar to the URM wall, several diagonal partially cracks are observed in the right pier. Rocking failure is observed at the top and bottom of the left pier. Furthermore, a network of partial cracks is recognized in the spandrel and window bank. In the last load step, point C, left pier fails because of rocking and a fully separated boundary between the left pier and spandrel is noticed. In addition, several horizontal cracks are observed in the window bank and its surroundings. This network of cracks occurs due to the arch mechanism. Bed joint reinforcement acts in tension and compressive stress in masonry leads to this type of failure.

Taken into account the negative direction, cracks initiate at a lower load and displacement: 7.18 kN and 0.21 mm, point D, and as it was expected the bottom left corner of the window start cracking. At point E, a peak-load of 27.08 kN, is observed. Rocking failure is recognized at two spots: the bottom right corner of the wall and the top of the right pier. Sliding of the spandrel with respect to the piers is not modeled numerically since macro-modeling is implemented but as can be seen in

Figure 5-19 separation of piers with respect to the masonry portion above the opening is obvious. So, by applying more load sliding of the masonry above the window level occurs. Toe crushing is another failure mode that can be seen at the bottom left corner of the wall which is compressed at point F. Compressive stress (12.84 MPa) reaches the compressive strength (12.93 MPa) of the masonry as can be found in Figure 5-19.

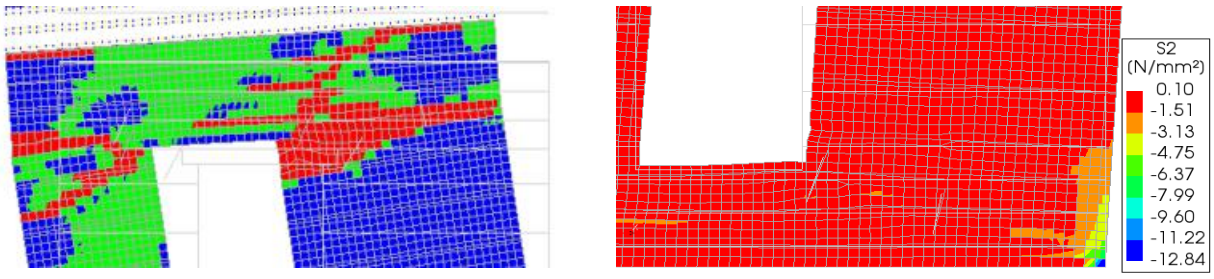

(a) (b)

Figure 5-19: Retrofitted wall. Sliding of the masonry portion above the window level with respect to the rest of the wall (a) and toe-crushing of the wall (b)

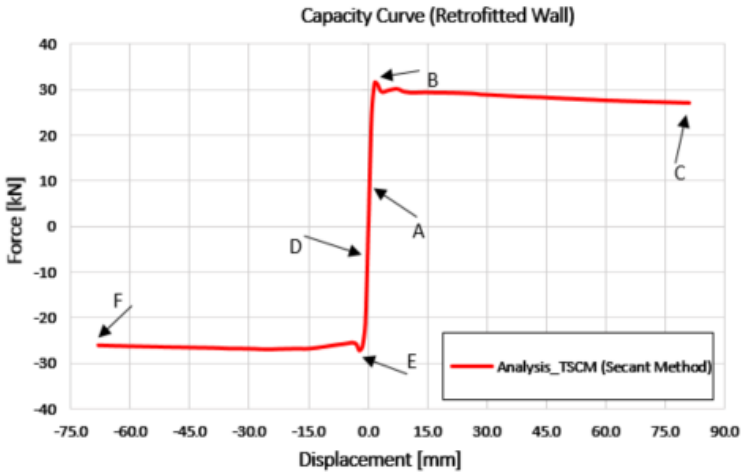

Figure 5-20: Capacity curve. Retrofitted wall modeled with Total Strain Crack Model (Secant Method)

Table 5-7: Retrofitted wall model with TSCM. Crack initiation, crack propagation and peak-load

Point	Description	Force (kN)	Displacement (mm)
A	Crack initiation	9.70	0.25
B	Peak load	31.40	1.55
C	End of analysis	27	81
D	Crack initiation	-7.20	-0.20
E	Peak load	-27.10	-2
F	End of analysis	-26.25	-64

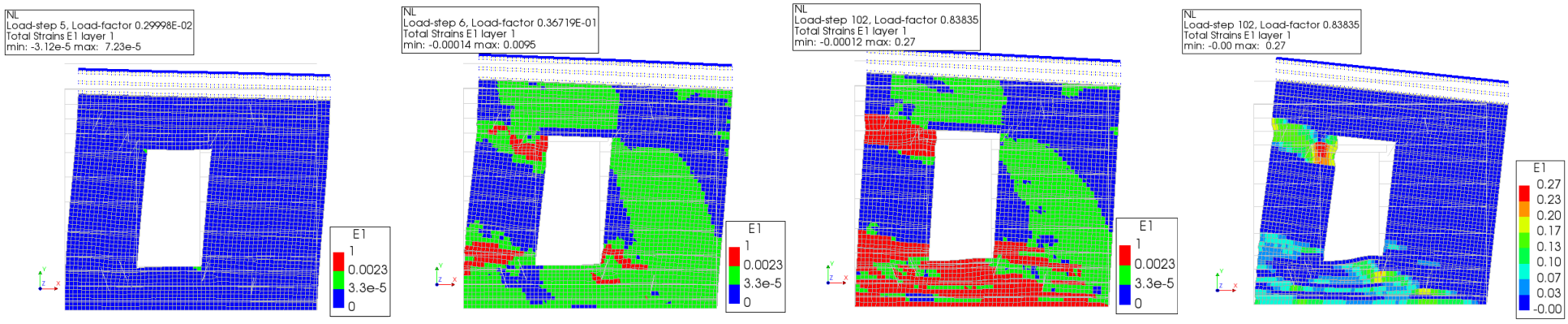

(a) Point A (b) Point B (c) Point C (d) Point C. Maximum Strain

Figure 5-21: Retrofitted wall modeled with TSCM, positive X-direction. Scaled first principal strain

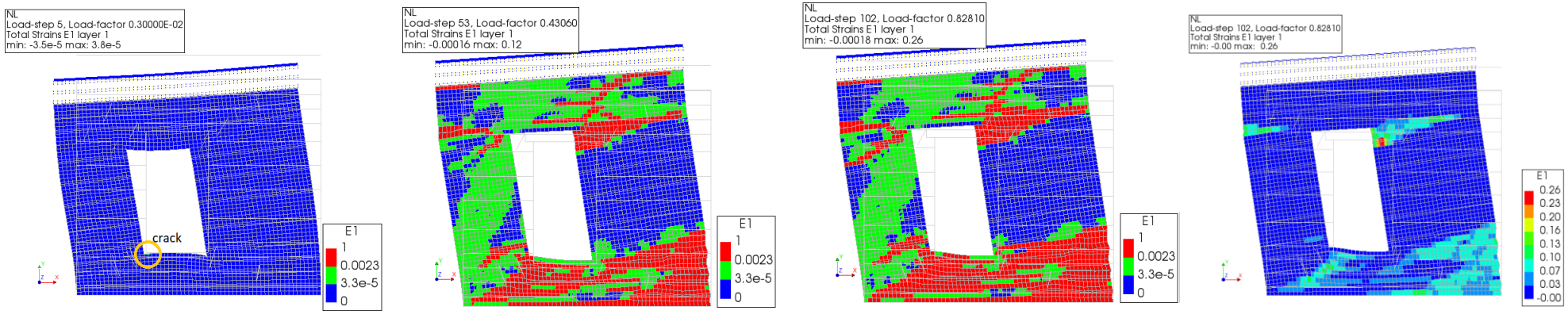

(a) Point D (b) Point E (c) Point F (d) Point F. Maximum Strain

Figure 5-22: Retrofitted wall modeled with TSCM, negative X-direction. Scaled first principal strain

5.3.2 **Retrofitted wall modeled with EMM**

Prescribed deformations with a magnitude of 81 and -64 mm are applied for the positive and negative X-direction respectively. According to the URM wall studied in the previous part, Tensile Strength Head-Joint Defined by Friction is used for the retrofitted case.

Figure 5-23, presents the force-displacement diagram obtained from the FE model. There are six remarkable points shown by letters A to F on the curve. The behavior of the wall at each point is discussed in the following paragraphs.

By applying EMM around 90% of load steps (in both directions) are not converged as can be found in Figure 5-23. So, numerical results are not valid anymore. As we could solve the convergence problem neither for the URM wall nor the retrofitted wall, TSCM will be implemented for the rest of the analyses.

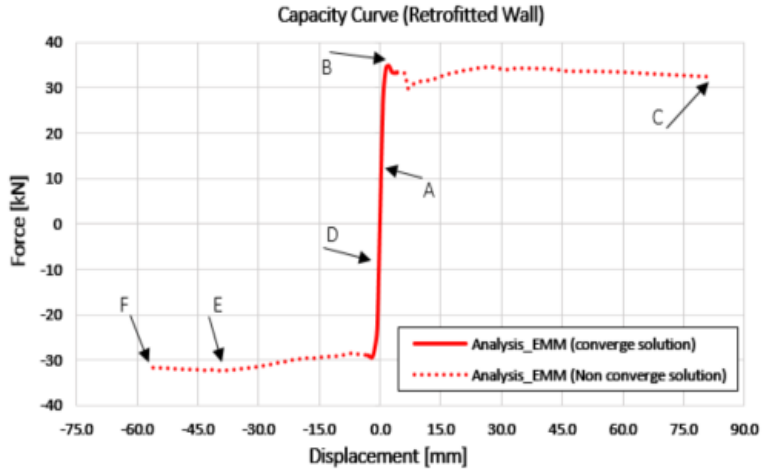

Figure 5-23: Capacity curve. Retrofitted wall modeled with Engineering Masonry Model

Table 5-8: Retrofitted wall model with EMM. Crack initiation, crack propagation and peak-load

Point	Description	Force (kN)	Displacement (mm)
A	Crack initiation	12.10	0.25
B	Peak-load	34.90	2.20
C	End of the analysis	32.30	81
D	Crack initiation	-9.50	-0.20
E	Peak-load	-32.35	-39.40
F	End of the analysis	-31.40	-64

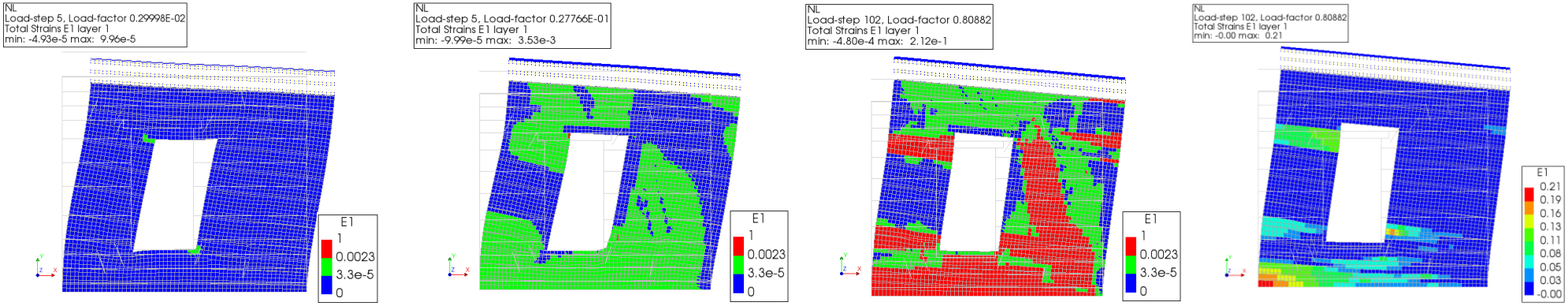

(a) Point A (b) Point B (c) Point C (d) Point C. Maximum Strain

Figure 5-24: Retrofitted wall modeled with EMM, positive X-direction. Scaled first principal strain

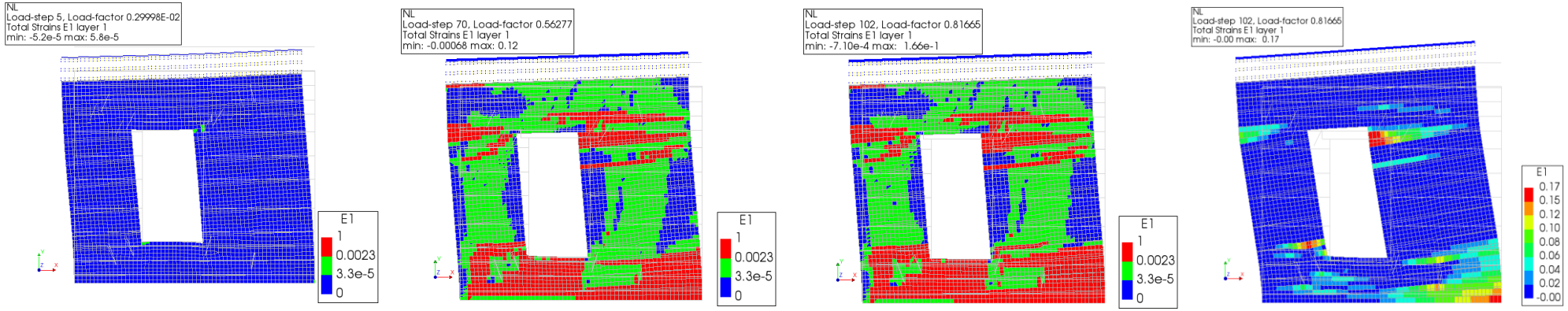

(a) Point D (b) Point E (c) Point F (d) Point F. Maximum Strain

Figure 5-25: Retrofitted wall modeled with EMM, negative X-direction. Scaled first principal strain

5.3.3 Experiment vs. numerical: retrofitted wall

In this part, numerical results are compared with the experiments in terms of crack patterns, crack types, failure mechanisms, and capacity curve. For EMM, the head-joint failure type is used. For crack pattern, first, the experimental result, failure mechanisms, and their causes are discussed in detail. Secondly, the numerical results are compared accordingly.

- **Capacity curve:**

Both material models follow the pattern of the capacity curve obtained by the experimental test. Initial stiffness for both models has a very good agreement with the test as can be seen in Figure 5-26.

By applying TSCM, the iterative method affects the results. This will be discussed in the sensitivity analysis section but results are presented in By comparing the crack pattern and capacity curves of the retrofitted wall we can conclude that the numerical results obtained by EMM are not in good agreement with the experiment due to the *convergence problem*, however, results obtained by TSCM match the test. As a result, TSCM will be applied for the rest of the analyses.

In this material model, the Secant Method completely converges all load levels but peak-load is overestimated (+22.7% in positive and +15.69% in negative X-direction). By choosing EMM, however, 90% of the load steps are not converged. As a result, numerical results are not valid in order to be compared with the test. Appendix C shows the divergence history for both material models.

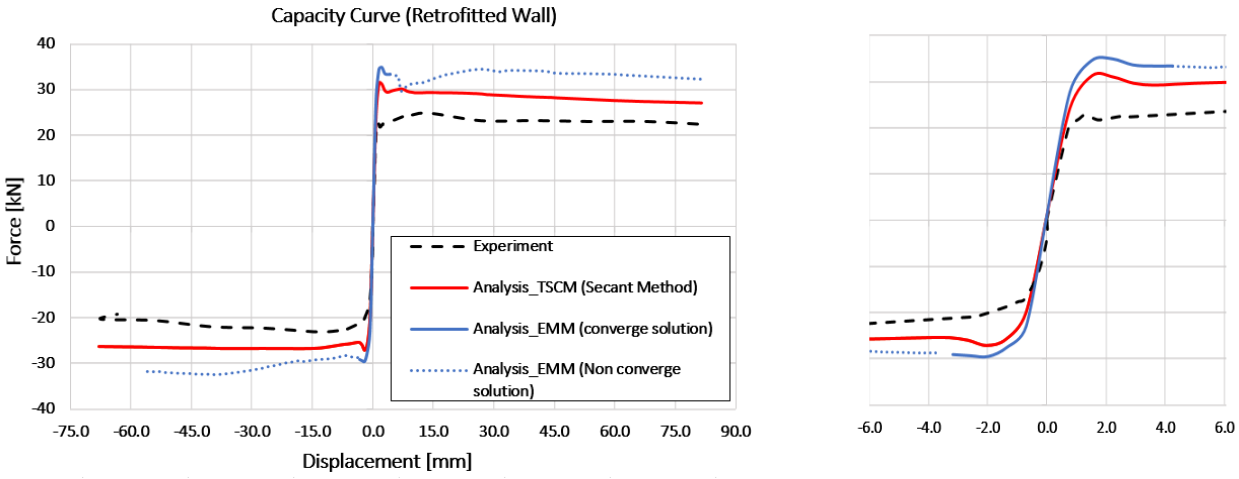

(a) (b)

Figure 5-26: Capacity curve (a) and stiffness (b) of the retrofitted wall. TSCM vs. EMM

- **Crack pattern:**

To simplify the comparison, cracks are labeled from 1 to 5. The original and scaled first principal strain (E1) obtained from DIANA is used for showing the crack patterns and failure modes. The un-deformed shape of the contour is more suitable for comparison since the experimental crack pattern is based on absolute deformations.

Figure 5-27, 28 show the crack pattern in both directions observed in the **experimental test**. As can be seen, crack patterns are completely different in the retrofitted wall.

Considering positive X-direction, two types of crack can be seen as a result of +7.87 mm displacement: a pure horizontal crack at the top of the left pier (crack number 2) that leads to the rocking failure in the left pier and two staircase cracks at the bottom of the piers (crack number 1 and 3). The same type of crack can be seen in the window bank. By increasing the deformation to +53.77 mm, the mentioned cracks propagated with a notable increment in terms of crack width. Failure of the left pier was observed due to the separation of the pier-spandrel interface. Moreover, crack Number 4 initiated from the top right corner of the opening and then propagated to the top right corner of the wall in this stage. Finally, in the collapse phase (+80.96 mm displacement) rotating of the spandrel and the right pier with respect to the rest of the wall occurred. Crack width increased in all cracks and a network of staircase and horizontal cracks were produced below the window level. In addition, toe crushing failure was observed at the bottom right side of the wall.

Studying the negative X-direction, by applying -7.90 mm displacement rocking of the right pier was observed (crack number 1) and staircase cracks formed at 2 corners of the opening (crack numbers 3 and 4). In the next stage (-53.80 mm displacement), cracks propagated but kept the same pattern. As a result of wider crack width, separation of the left pier and spandrel is recognized due to the rocking failure, crack number 2 in the figure. By increasing the ultimate deformation (-63.31 mm displacement), spandrel slipped with respect to the piers and wall failed.

Figure 5-29, 30, shows the estimated crack pattern of the wall modeled by the **Total Strain Crack Model**.

Taken into account the positive direction, all cracks are predicted when +7.87 mm displacement is applied. Separation of the left pier (crack number 2) is predicted. Staircase cracks (crack number 1 and 5), are molded in a good agreement with the test, however, crack number 5 is overestimated. By increasing the deformation from 7.87 to 53.65 crack width increases in all cracks which were observed in the test as well. The initiation of crack number 1 is not as same as the experiment but it is acceptable. By applying the collapse phase (81 mm displacement), the same crack patterns can be seen but with a larger crack width. The arch mechanism is recognized in the window bank and its adjacent that matches the test. Crack number 4, however, is not predicted in the numerical model.

Considering the negative direction, numerical results follow the experiment well acceptable. The first figure from left shows -8.13 mm deformation and all cracks, apart from crack number 5, have a good agreement with the test. Cracks numbers 1, 2, 3 and 4 are modeled as same as the test. Crack patterns are the same when the deformation is increased to -53.98 then -64 but crack width increases. Separation of the spandrel with respect to the piers is estimated very well in the collapse phase as can be seen in Figure 5-19. Crack number 5 shows a network of crack below the window level which matches the experimental results. Similar to what was concluded for the URM wall, TSCM has a good agreement with the experiment after retrofitting as well.

Figure 5-31, 32 present the crack pattern in both directions observed in the wall modeled by **Engineering Masonry Model**. However, models are not converged and results will not be discussed further.

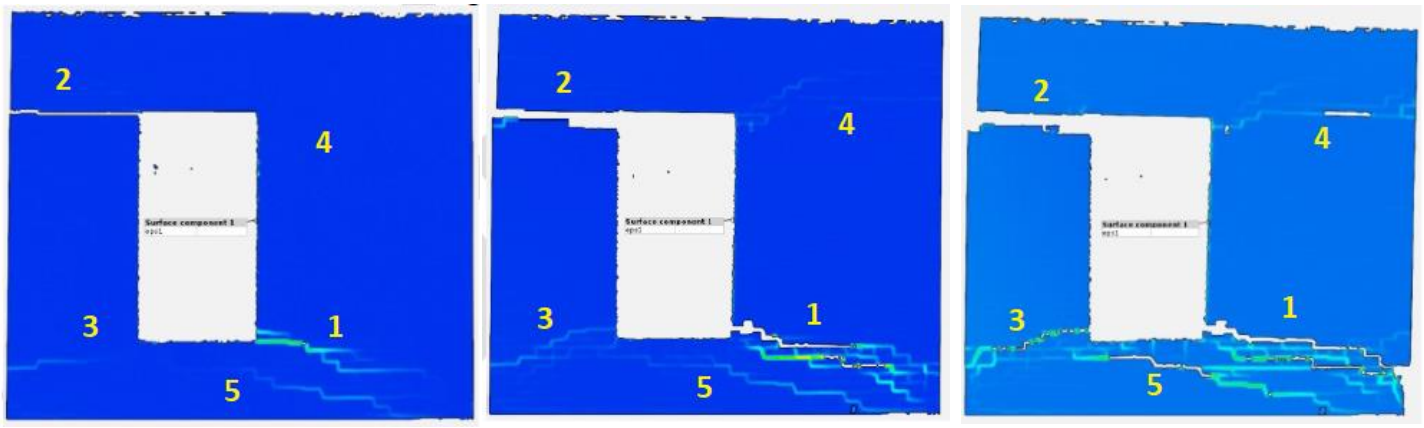

(a) Displacement = +7.89 mm (b) Displacement = +53.77 mm (c) Displacement = +80.96 mm

Figure 5-27: Phase 3, experimental result of the retrofitted wall. Wall is loaded in positive X-direction (Licciardello & Esposito, 2019)

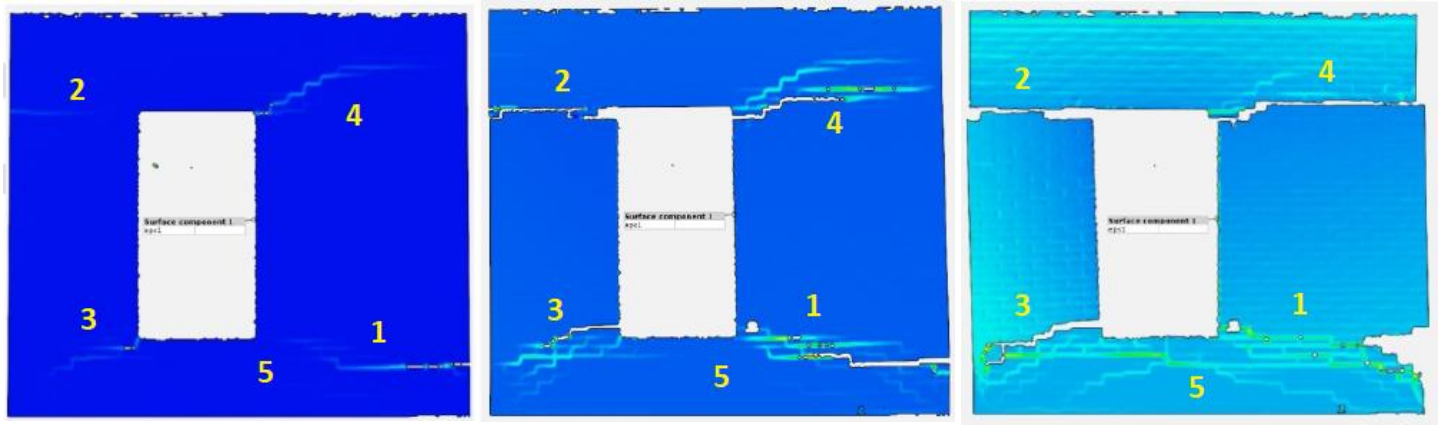

(a) Displacement = -7.9 mm (b) Displacement = -53.8 mm (c) Displacement = -63.31 mm

Figure 5-28: Phase 3, experimental result of the retrofitted wall. Wall is loaded in negative X-direction (Licciardello & Esposito, 2019)

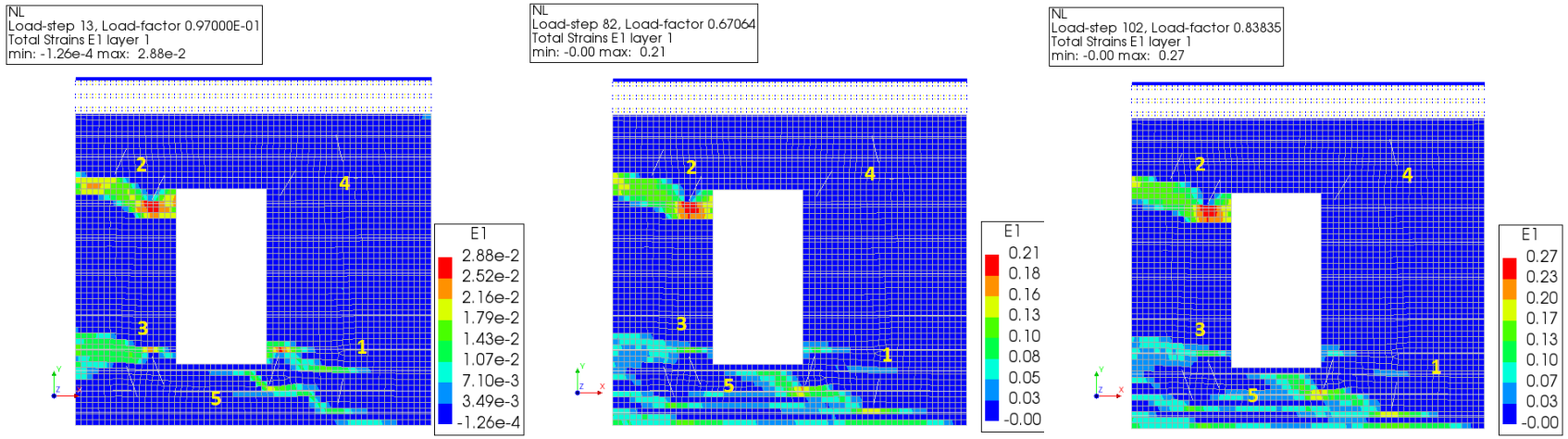

(a) Displacement = +7.76 mm (b) Displacement = +53.65 mm (c) Displacement = +81 mm

Figure 5-29: Retrofitted wall modeled with TSCM, positive X-direction. Maximum principal strain

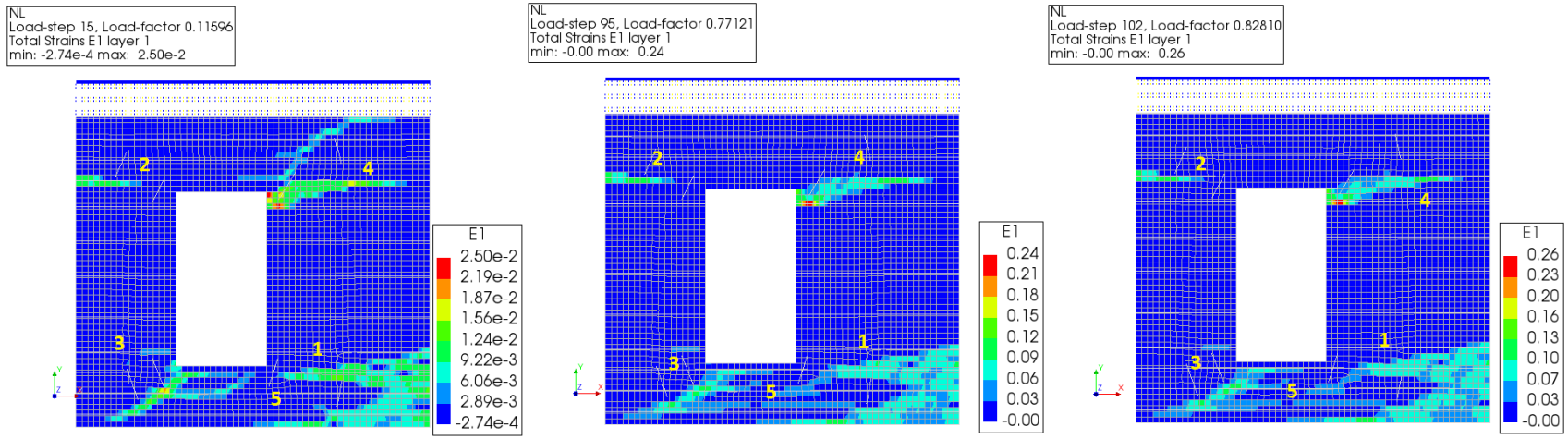

(a) Displacement = -8.12 mm (b) Displacement = -53.98 mm (c) Displacement = -64 mm

Figure 5-30: Retrofitted wall modeled with TSCM, negative X-direction. Maximum principal strain

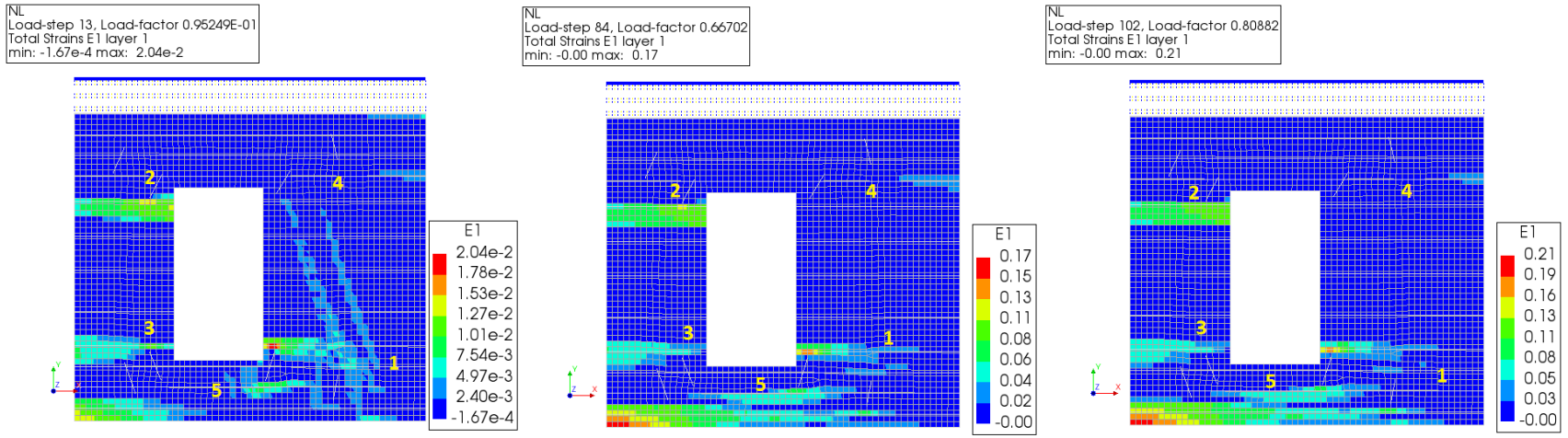

(a) Displacement = +7.26 mm (b) Displacement = +53.36 mm (c) Displacement = +81 mm

Figure 5-31: Retrofitted wall modeled with EMM, positive X-direction. First principal strain. From left to right: 7.26, 53.36, and 81 mm

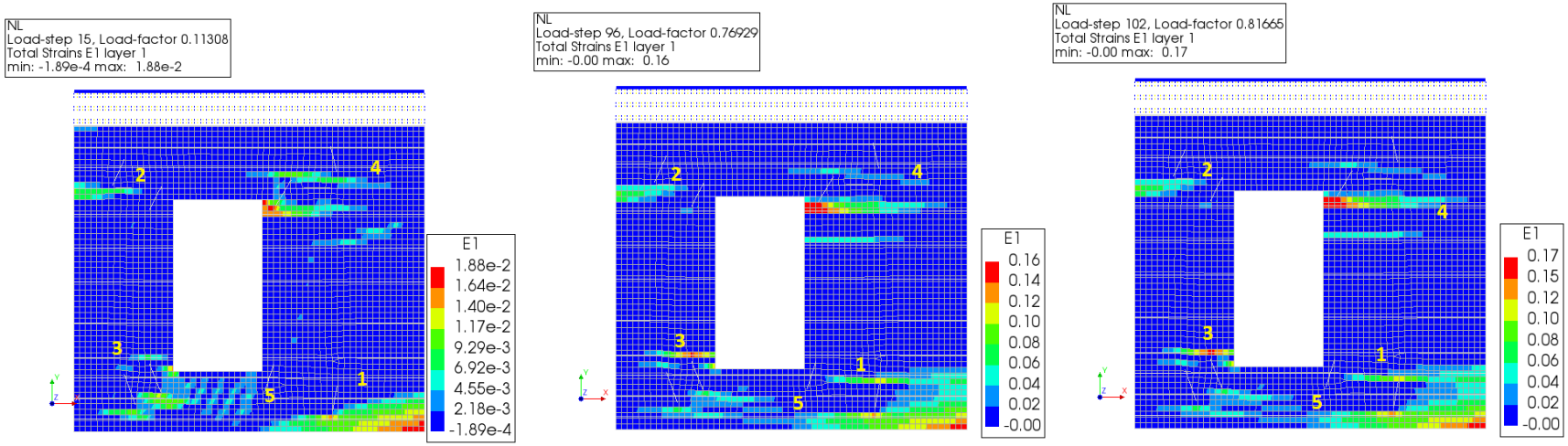

(a) Displacement = -7.92 mm (b) Displacement = -53.85 mm (c) Displacement = -64 mm

Figure 5-32: Retrofitted wall modeled with EMM, positive X-direction. First principal strain

By comparing the crack pattern and capacity curves of the retrofitted wall we can conclude that the numerical results obtained by EMM are not in good agreement with the experiment due to the convergence problem, however, results obtained by TSCM match the test. As a result, TSCM will be applied for the rest of the analyses.

(a) Displacement = +81 mm

(b) Displacement = -64 mm

Figure 5-33: Retrofitted wall. Numerical results (TSCM), crack pattern

Table 5-9: Numerical result summary. Retrofitted wall, TSCM vs. EMM

Model	Load Step	Head-Joint Failure Type	Peak-Load (+X) (kN)	Difference to test (+X)	Peak-Load (-X) (kN)	Difference to Test (-X)	Loading Capacity	Initial Stiffness	Crack Pattern
Experiment	N/A	N/A	25	N/A	23.15	N/A	N/A	N/A	N/A
EMM	0.4 mm [0.01(100)]	Tensile Strength Head-Joint Defined by Friction	34.90	**+32.90%**	32.35	**+33.20% (non-converge solution)**	**Non-convergence solution**	**Very good agreement**	**Non-convergence solution**
TSCM (Secant)	0.4 mm [0.01(100)]	N/A	31.40	**+22.75%**	27.10	**+15.70%**	**Moderate agreement**	**Very good agreement**	**Good agreement**
TSCM (RNR)	0.4 mm [0.01(100)]	N/A	28.20	**+12%**	26.30	**+12.80%**	**Good agreement**	**Very good agreement**	**Moderate agreement**

5.4 The effect of bed joint reinforcement and diagonal anchor on the seismic performance of the wall

In this section, the effect of bed joint reinforcement and diagonal anchor is studied in detail to figure out the seismic behavior of the retrofitted wall. The maximum crack width, crack patterns, and failure modes of the models are investigated in detail.

From the previous analyses, we know that the convergence problem does not occur by applying the Total Strain Crack Model (TSCM). Hence, this material model is applied to this section. As a result, the maximum crack width must be calculated in the principal direction. Strain crack ($Eknn$ (ε_{nn}^{cr})) is calculated by DIANA. It gives the strain crack in the principal direction. Crack width in principal can be found as follows (DIANA FEA, 2019).

$$Crack\ width\ in\ principal\ diredtion = \varepsilon_{nn}^{cr} * crack\ abndwidth$$

Where, crack bandwidth for a 2D plane stress element is $\sqrt{2A}$

Section 5.5.1 describes that the applied iterative method affects the numerical results considerably so, a combination of the Secant Method and Regular Newton Raphson Method must be applied to find the most accurate numerical results in terms of peak-load and crack patterns with the following details;

- URM wall, for peak-load: the result of Regular Newton Raphson Method
- URM wall, for crack patterns and failure modes: the result of Regular Newton Raphson Method
- Retrofitted wall, for peak-load: the result of Regular Newton Raphson Method (divergence occurs at +50mm)
- Retrofitted wall, for crack patterns and failure modes: Secant Method (no convergence/divergence problem)

Figure 5-34 shows the peak-loads which is calculated by applying Regular Newton Raphson iteration. Diverges occurs at +50 mm deformation in the retrofitted wall but the peak-load is already reached. We consider the peak-load obtained by the Regular Newton-Raphson Method since it is closer to the test compared with the Secant Method (it will be discussed in the sensitivity analysis section in detail)

By applying bed joint reinforcement and diagonal anchor, peak loads are increased from 22 kN to 26.30 kN in the negative X-direction (a difference of 17.80%) and from 24.85 kN to 28.20 kN in the positive X-direction (a difference of 12.93%).

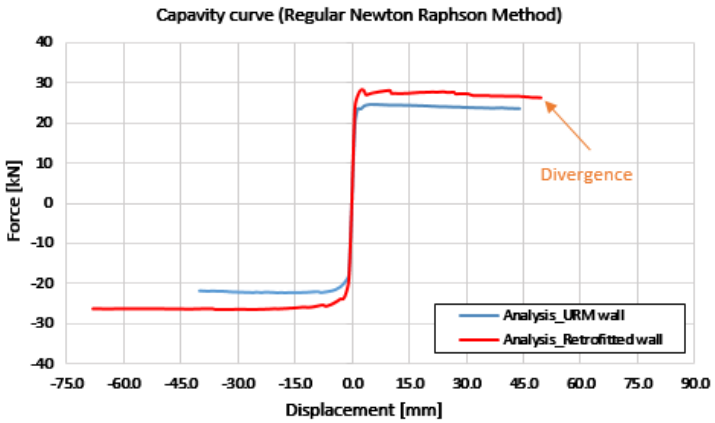

Figure 5-34: Capacity curve to show the peak-load. URM wall vs. retrofitted wall

As a result of bed joint reinforcement and diagonal anchor, the failure modes of the wall is changed. Figure 5-35 shows the failure modes that are recognized in the models in two directions. In the URM wall, the main mechanism is rocking of the piers; for the retrofitted wall initially rocking of the piers is observed but by increasing the deformation arch mechanism occurs in window bank and its adjacent. The arch effect is due to the bed joint reinforcement. Another failure mode that is observed only in the retrofitted wall is toe-crushing failure that occurs at the bottom right corner of the wall when it is loaded rightwards.

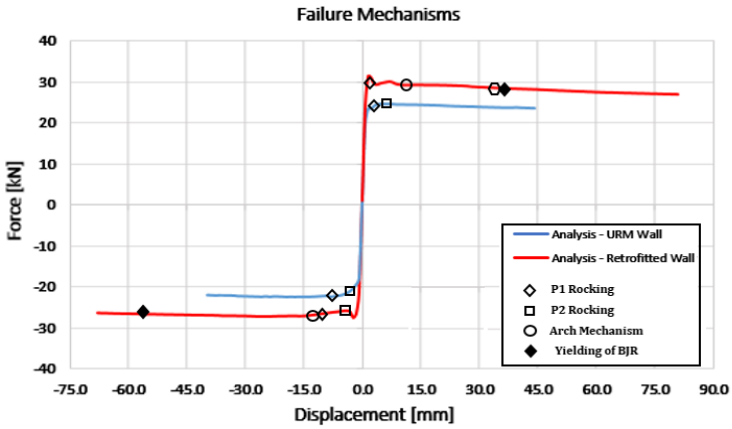

Figure 5-35: Capacity curve (Regular Newton-Raphson Method for the URM wall and Secant Method for the retrofitted wall is applied). P1 and P2 stand for pier1 (left pier) and pier 2 (right pier)

The crack pattern is another factor that is a function of the reinforcement layout. Arch mechanism (a network of a staircase and horizontal cracks) is recognized below the window level due to tensile force in steel. Plasticity of reinforcement is observed in the model as can be found in Figure 5-36. Stress in steel (220.49 MPa) is higher than the yielding stress in this element (215 MPA). In addition, wide shear cracks are recognized in the piers. The pure diagonal cracks observed in the URM wall can be seen in the retrofitted wall but with a smaller angle with respect to the horizon. Finally, toe-crushing (crushing of the masonry due to compressive stress) is observed at the bottom right corner of the wall when it is loaded rightwards as can be found in Figure 5-36. Compressive stress (-12.84 MPa) reaches compressive strength (-12.93 MPa) of masonry. Furthermore, crack width is dropped significantly as a result of bed joint reinforcement.

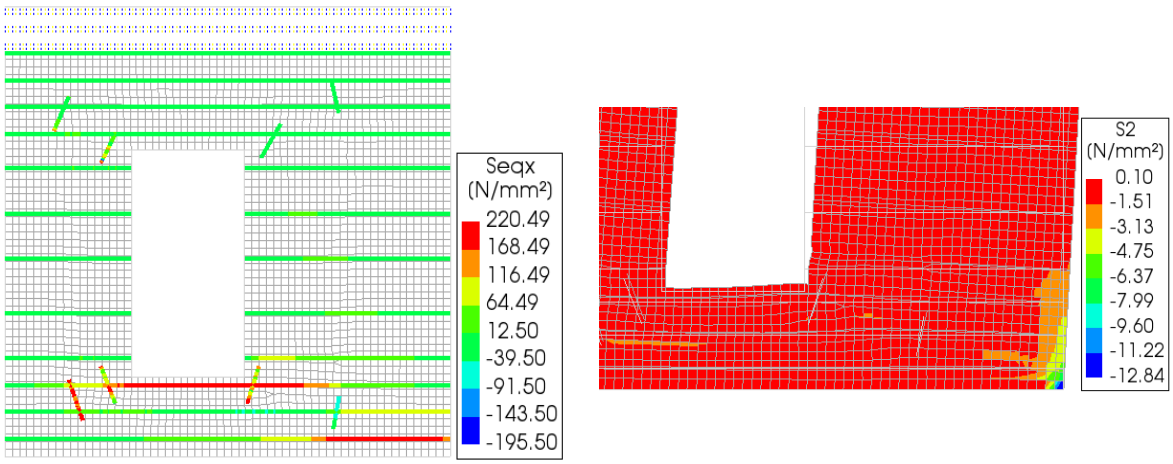

Figure 5-36: von Mises stress in stess (a) and toe-crushing (b)

Crack width is another factor that decreases dramatically by applying the reinforcement. As explained before bed joint reinforcement restrains cracks. Before retrofitting, the maximum crack width in principal direction in positive and negative X-direction is 147 mm ($2.08 * \sqrt{2 * 50 * 50}$) and 48.80 mm respectively. The crack width is calculated by strain crack ($Eknn$ (ε_{nn}^{cr}))) as can be seen in Figure 5-37, 38. By applying the reinforcement crack width drops to 19 mm in positive and 14.14 mm in negative direction.

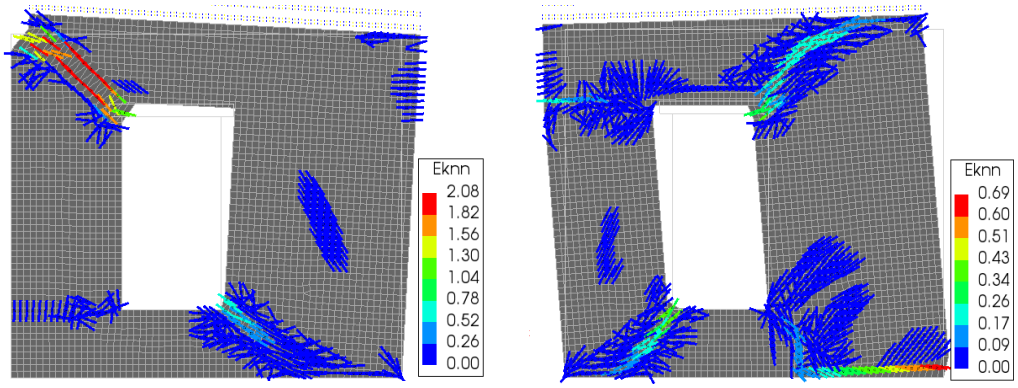

Figure 5-37: Strain crack in the URM wall

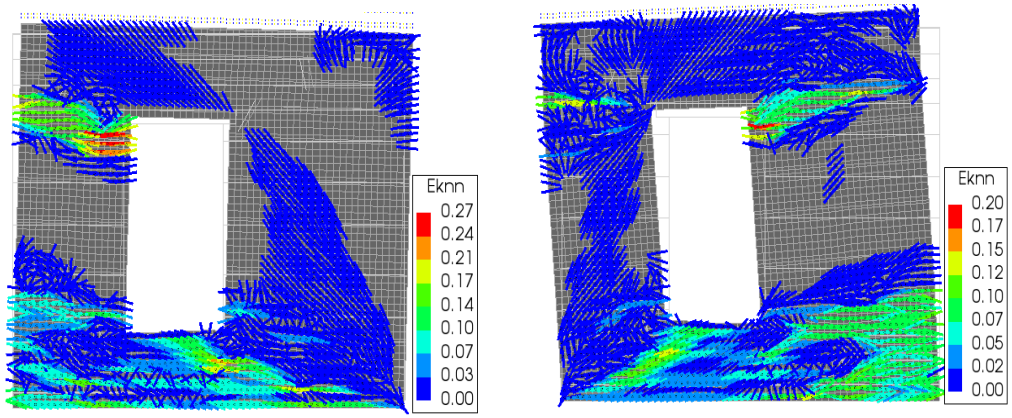

Figure 5-38: Strain crack in the retrofitted wall with original reinforcement layout

In conclusion, by applying bed joint reinforcement and diagonal anchors, the maximum crack width is restricted in the retrofitted wall and much smaller crack width, compared with the URM wall, is observed both locally and globally. The pattern of the cracks and failure modes are changed remarkably as well. In the URM wall rocking failure of the piers is the primary mechanism but after retrofitting apart from pier rocking that is recognized in higher lateral load, arch mechanism and toe crushing are observed. In addition, the force capacity of the wall is improved.

Table 5-10: Numerical result summary. URM wall vs. Wall retrofitted with bed joint reinforcement and anchor

Wall	Iterative method	Peak load (+X) (kN)	Peak load (-X) (kN)	Crack Width Max. (+X) (mm)	Crack Width Max. (-X) (mm)
URM wall	Combination of RNR and Secant Method	24.85	22	147	48.80
Retrofitted wall with diagonal anchors and bed joint reinforcement	Combination of RNR and Secant Method	28.20	26.30	19	14.14
Difference	**-**	**+12.93%**	**+17.80**	**-154.22%**	**-109.56%**

Table 5-11: Failure modes: URM wall vs. Wall retrofitted with bed joint reinforcement and anchor

Wall	Unstrengthened	Strengthened
Failure mechanisms	• Rocking of the piers • Right pier and masonry above the window level rotate with respect to the other portion of the wall	• Rocking of the piers • Arch mechanism • Toe-crushing • Sliding of the masonry above the window level with respect to the other portion of the wall

5.5 Sensitivity analysis

The importance of the iterative method and material parameters and their effect on the behavior of the wall is investigated in this part. The iterative method, modulus of elasticity of masonry wall, compressive strength of masonry wall, tensile strength of masonry wall, compressive fracture energy of masonry wall and tensile fracture energy of masonry wall are investigated in detail.

Based on the previous results, it is approved that by applying the Total Strain Crack Model, numerical results are much more accurate. As a result, this material model is used for this part and the rest of the research.

5.5.1 Iterative method

The previous analyses have revealed that the iterative method significantly affects the results in terms of divergence of the analysis, crack pattern and peak-load. So, the URM wall and retrofitted wall are analyzed by Regular Newton-Raphson and the Secant Method (Quasi-Newton method) to illustrate the differences. The convergence criterion and norm are the same as section 4.5.

By applying Regular Newton-Raphson and Total Strain Crack Model (TSCM), crack pattern, failure modes, and capacity curve of the **URM wall** are in good agreement with the experiment as shown

in Figure 5-39, 41. Models are fully converged in both directions and almost all diagonal staircase cracks are accurately modeled. Force capacity of the URM wall is calculated with acceptable numerical errors (+5.75% and 12.41% for positive and negative X-direction).

However, by applying the Secant Method results are slightly different. As shown in

Figure 5-40, 41, the crack pattern does not match the experimental results perfectly. In addition, larger peak-load reaches in the capacity curve of the URM wall (+24% and 25.97% in the positive and negative X-direction).

Since the results were not comparable it was decided to contact *DIANA FEA* support team to identify the issue. The number of cracks reported in analysis with the Secant Method is about 4 times larger than analysis with the Regular Newton-Raphson (RNR). This problem should be investigated further by software developers but it seems that there is a close correlation between number of cracks, different peak-load and the crack pattern in the models. Table 2-1 reports the number of cracks in both iterative methods (data are extracted from *.out file).

In conclusion, Regular Newton-Raphson is more effective for modeling the URM wall in terms of crack pattern, failure mechanism, and force capacity.

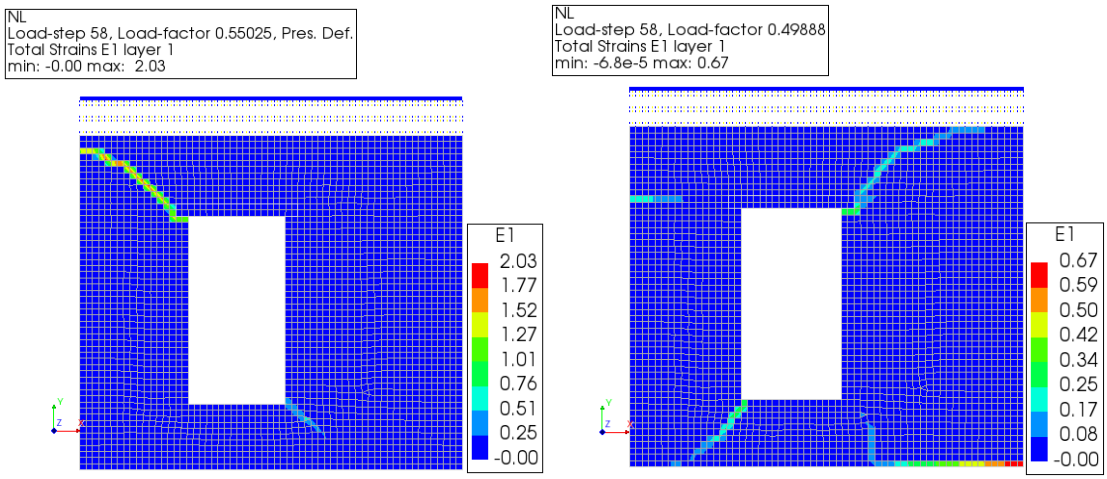

(a) Displacement = +44 mm (b) Displacement = -40 mm

Figure 5-39: URM wall (Regular Newton-Raphson Method)

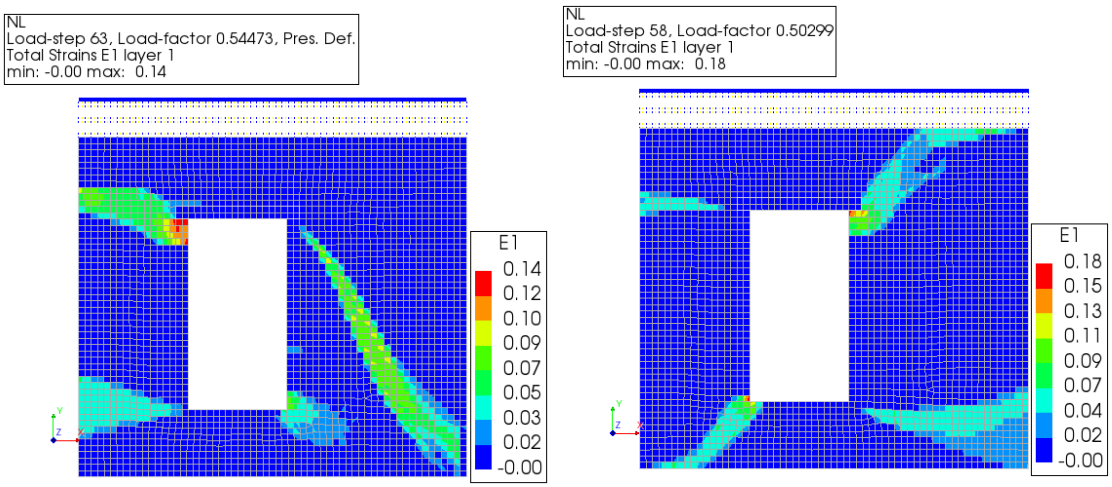

(a) Displacement = +44 mm (b) Displacement = -40 mm

Figure 5-40: URM wall (Secant Method)

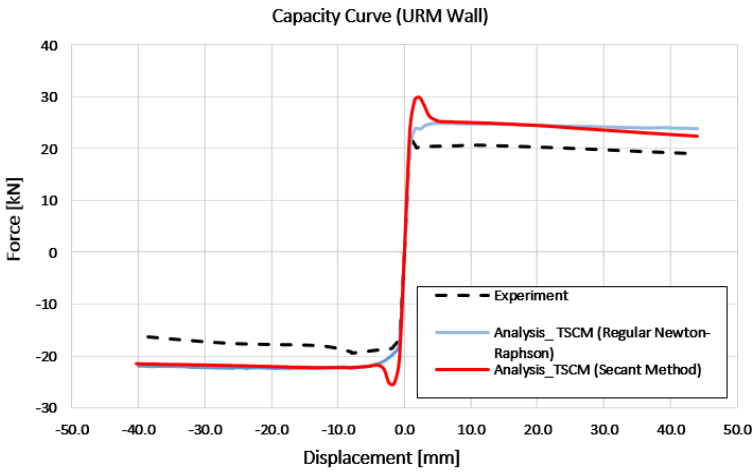

Figure 5-41: Capacity curve for the URM wall. Regular Newton-Raphson Method vs. Secant Method

Table 5-12: Numerical result, summary of sensitivity analysis. URM wall, Secant Method vs. Regular Newton Raphson Method

URM wall	Load Step	Peak-Load (+X) (kN)	Difference to Test (+X)	Peak-Load (-X) (kN)	Difference to Test (-X)	Loading Capacity	Initial Stiffness	Crack Pattern
Experiment	N/A	23.45	N/A	19.45	N/A	N/A	N/A	N/A
TSCM (Secant)	0.4 mm [0.01(100)]	29.85	**24%**	25.25	**26%**	**Moderate agreement**	**Very good agreement**	**Moderate agreement**
TSCM (RNR)	0.4mm [0.01(100)]	24.85	**+5.75%**	22.00	**+12.40%**	**Good agreement**	**Very good agreement**	**Good agreement**

Table 5-13: Number of cracks reported in analysis (positive X-direction). Secant Method (a) and RNR method (b)

(a)

Load Step	Number of Cracks
1	0
2	0
3	1652
4	3540
5	4243
6	4752
7	5240
8	5601
9	5857
10	6053
11	6218
12	6368
13	6488
14	6619
15	6716
16	6815
17	6890
18	6956
19	7023
20	7077
21	7154
22	7204
23	7234
24	7271
25	7298
26	7337
27	7378
28	7412
29	7438
30	7466
31	7488
32	7521
33	7541
34	7577
35	7600
36	7629
37	7646
38	7668
39	7692
40	7722
41	7740
42	7766
43	7785
44	7795
45	7809
46	7824
47	7849
48	7863
49	7879
50	7895
51	7909
52	7921
53	7935
54	7951
55	7965
56	7980
57	8000
58	8016

(b)

Load Step	Number of Cracks
1	0
2	0
3	495
4	897
5	1011
6	1112
7	1189
8	1237
9	1269
10	1306
11	1325
12	1352
13	1373
14	1392
15	1410
16	1431
17	1446
18	1465
19	1478
20	1486
21	1495
22	1500
23	1511
24	1529
25	1540
26	1552
27	1574
28	1589
29	1604
30	1617
31	1627
32	1630
33	1641
34	1647
35	1652
36	1659
37	1661
38	1665
39	1669
40	1677
41	1679
42	1681
43	1683
44	1689
45	1690
46	1690
47	1693
48	1695
49	1697
50	1701
51	1740
52	1764
53	1784
54	1804
55	1830
56	1846
57	1863
58	1883

As a result of larger deformations of the **retrofitted wall** (81 mm and -64 mm for the positive and negative X-direction) and the applied reinforcement, the numerical results changed.

By applying Regular Newton-Raphson, DIANA predicts crack patterns and failure modes in a moderate agreement with the experiment as can be seen in Figure 5-42. In addition, divergence occurs when the retrofitted wall is loaded rightwards. However, a low error is observed in the obtained peak-loads (+12.03% and +12.78% in the positive and negative X-direction respectively).

In contrast, the Secant Method predicts the crack patterns more accurately, but the force capacity of the wall is a bit overestimated in both directions (+22.73% in positive X-direction and +15.69% in negative X-direction).

Considering the scope of this project, the mathematics producer involved in these two iterative methods is not studied but a possible reason for the divergence is discussed here. In the Regular Newton-Raphson Method the stiffness matrix of the system is evaluated in every iteration. The level of the nonlinearity of the model is high since many integration points crack. As a result, the stiffness decreases substantially and this leads to an ill-conditioned stiffness matrix and divergence. In contrast, the Secant Method does not evaluate a completely new stiffness matrix in every iteration and the possibility of divergence decreases.

In conclusion, Regular Newton-Raphson is much more effective for finding the force capacity of the retrofitted wall, however, the Secant Method simulates the crack pattern accurately. It is advised to use both iterative methods, once for peak-load of the retrofitted wall and another time for the crack patterns and failure modes.

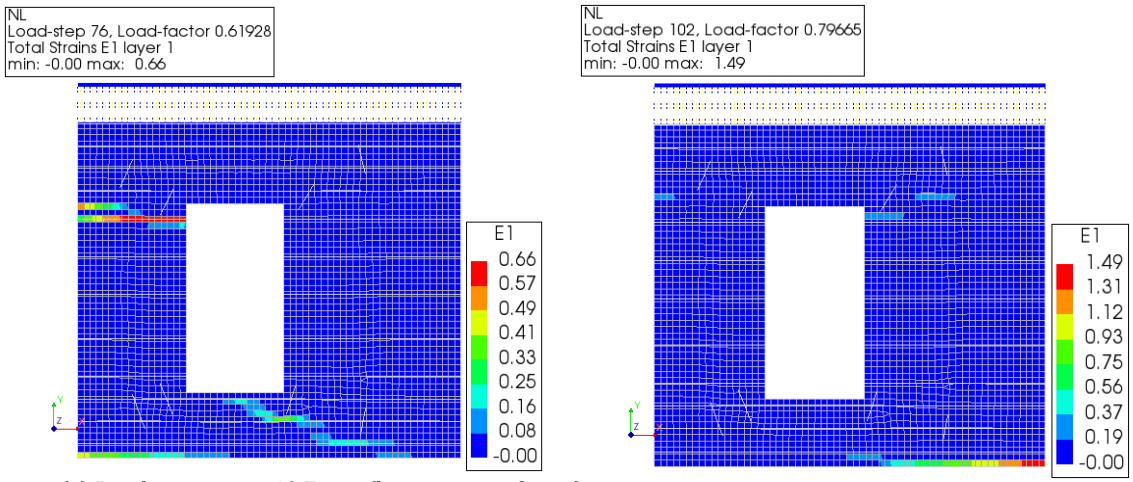

(a) Displacement = +49.7 mm (last converged step)

(b) Displacement = -64 mm

Figure 5-42: Retrofitted wall (Regular Newton-Raphson Method)

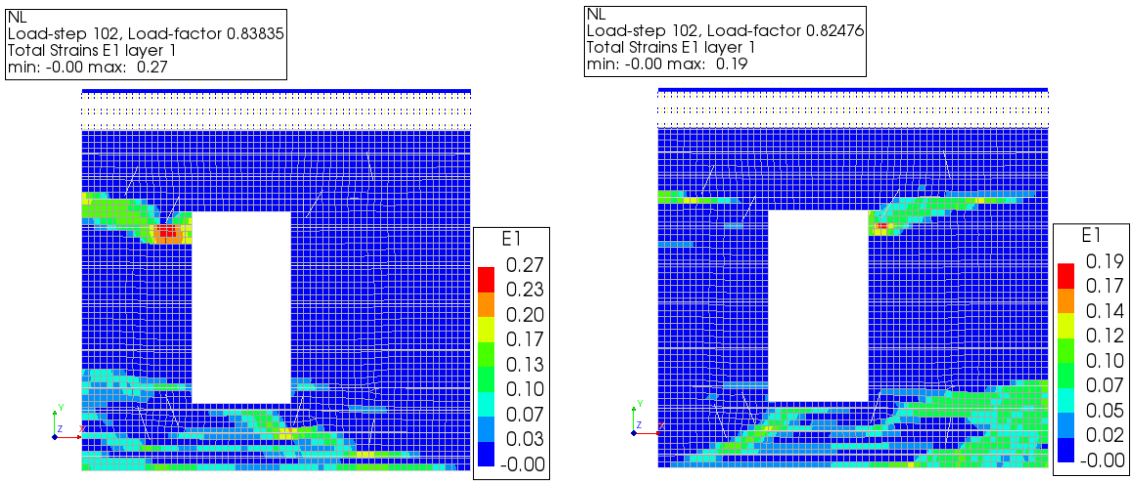

(a) Displacement = +49.7 mm (b) Displacement = -64 mm

Figure 5-43: Retrofitted wall (Secant Method)

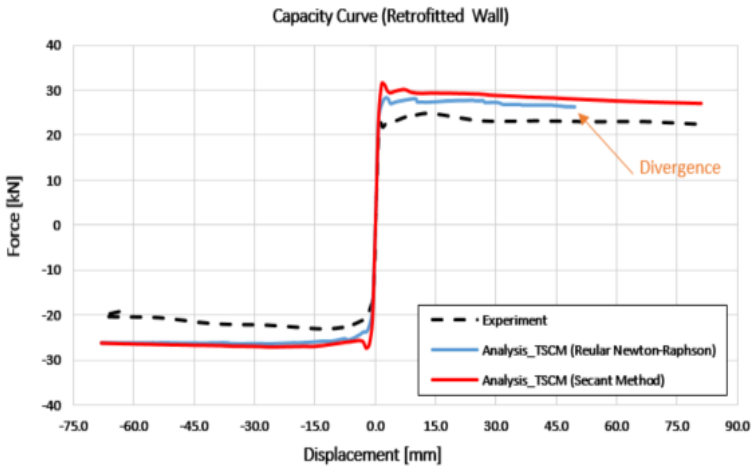

Figure 5-44: Capacity curve for the retrofitted wall. Regular Newton-Raphson Method vs. Secant Method

Table 5-14: Numerical result, summary of sensitivity analysis. Retrofitted wall, Secant Method vs. Regular Newton Raphson Method

Retrofitted wall	Load Step	Head-Joint Failure Type	Peak-Load (+X) (kN)	Difference to Test (+X)	Peak-Load (-X) (kN)	Difference to Test (-X)	Loading Capacity	Initial Stiffness	Crack Pattern
Experiment	N/A	N/A	25	N/A	N/A	N/A	N/A	N/A	N/A
TSCM (Secant)	0.4 mm [0.01(100)]	N/A	31.40	**+22.75%**	27.10	**+15.70%**	**Moderate agreement**	**Very good agreement**	**Good agreement**
TSCM (RNR)	0.4 mm [0.01(100)]	N/A	28.20	**+12%**	26.30	**+12.80%**	**Good agreement**	**Very good agreement**	**Moderate agreement**

5.5.2 The effect of material properties on the wall performance

In this section, five important elastic and inelastic material parameters of the model are investigated to find the sensitivity of material properties on the wall performance. The elastic parameter is the modulus of elasticity (represented by E) and the inelastic parameters are:

compressive strength (f_c), tensile strength (f_t), compressive fracture energy (G_c) and tensile fracture energy (G_f). The values of the original parameters are increased and decreased by 50%.

Table 5-15: Applied material properties for sensitivity analysis

Parameter	E	f_t	f_c	G_f	G_c
Original	3207	0.107	12.93	0.0085	28.63
Multiplied by 0.5	1603.5	0.0535	6.465	0.00425	14.315
Multiplied by 1.5	4810.5	0.1605	19.395	0.01275	42.945

To show the location of the maximum crack width, the wall is divided into 8 parts as can be seen in Figure 5-45.

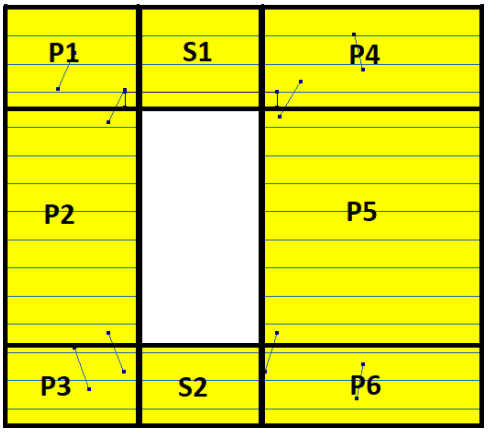

Figure 5-45: Division of the wall

The numerical analyses have shown that results are sensitive to the **modulus of elasticity**, in terms of peak-load, maximum crack width, and stiffness. However, the failure mechanism of the models does not change.

By decreasing the modulus of elasticity by 50%, the stiffness of the retrofitted wall decreases as well (Figure 5-46). A difference of -18.13% and -23.41% in positive and negative X-direction is observed. By contrast, a difference of +15.5% and +21% is recognized by increasing the modulus of elasticity.

It is reasonable that a stiffer wall reaches a higher peak-load and vice versa. As can be found in Figure 5-46, the force capacity of the wall is sensitive to the modulus of elasticity. By increasing the modulus of elasticity, a difference of +14.06% and +7.50% in positive and negative directions are observed. However, a smaller modulus of elasticity leads to a decrease in peak-load (-8.36% and -4.07% difference in positive and negative X-direction respectively).

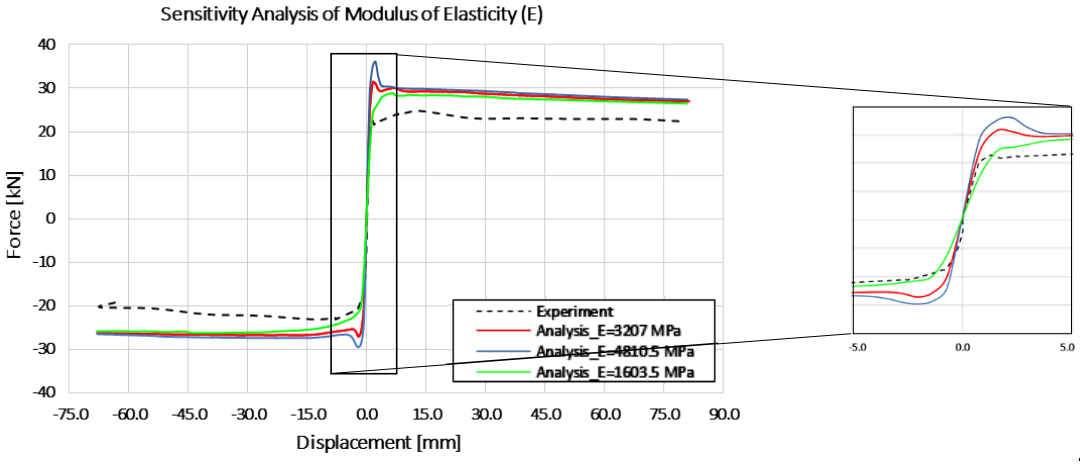

Figure 5-46: Capacity curve. Sensitivity of modulus of elasticity

The maximum crack width of the retrofitted wall is changed by changing the modulus of elasticity remarkably. Softer wall cracks sooner and finally larger crack width is obtained. A difference of +63.73% and +29.70% in the positive and negative direction is predicted in models while by decreasing the modulus of elasticity a difference of -45.16% and -35% is obtained.

As explained before, by changing the modulus of elasticity, the failure modes of the retrofitted wall do not change and crack patterns remain nearly the same. A diagonal shear crack can be seen in both piers. This crack is noticeably restrained by reinforcement and shear mechanism of the piers is prevented. By increasing the modulus of elasticity, the diagonal shear cracks decrease while by decreasing the modulus of elasticity wider cracks are estimated.

The magnitude of the first principal strain (E1) is another factor that is affected by changing the modulus of elasticity significantly. The larger crack width leads to the larger relative displacement of the cracked element and its nodes. Consequently, a larger strain is observed (0.16 for stiffer and 0.50 for the softer model). In addition, cracking strain is a function of the modulus of elasticity $(\varepsilon_{cr} = \frac{f_t}{E})$. By changing the modulus of elasticity, as can be seen in Figure 5-47, cracking strain changes as well.

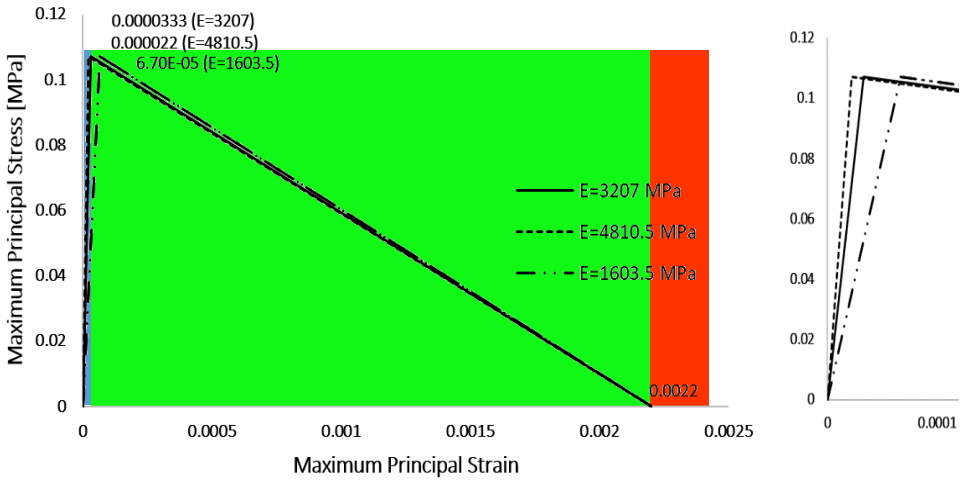

Figure 5-47: Tensile stress strain curve obtained by different modulus of elasticity

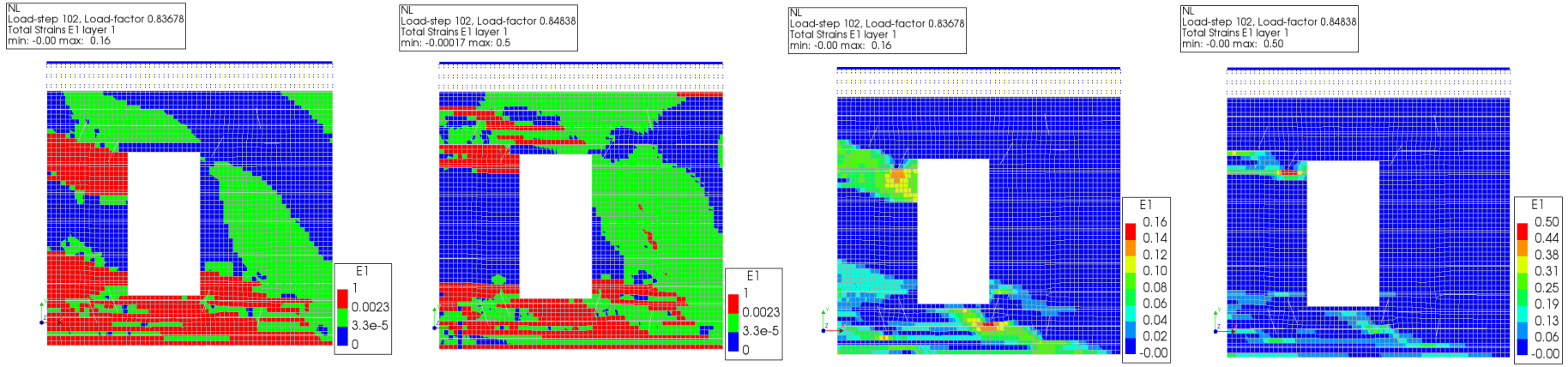

(a) E = 4810.5 MPa (b) E = 1603.5 MPa (c) E = 4810.5 MPa (d) E = 1603.5 MPa

Figure 5-48: Retrofitted wall. Sensitivity of modulus of elasticity, positive X-direction. First principal strain

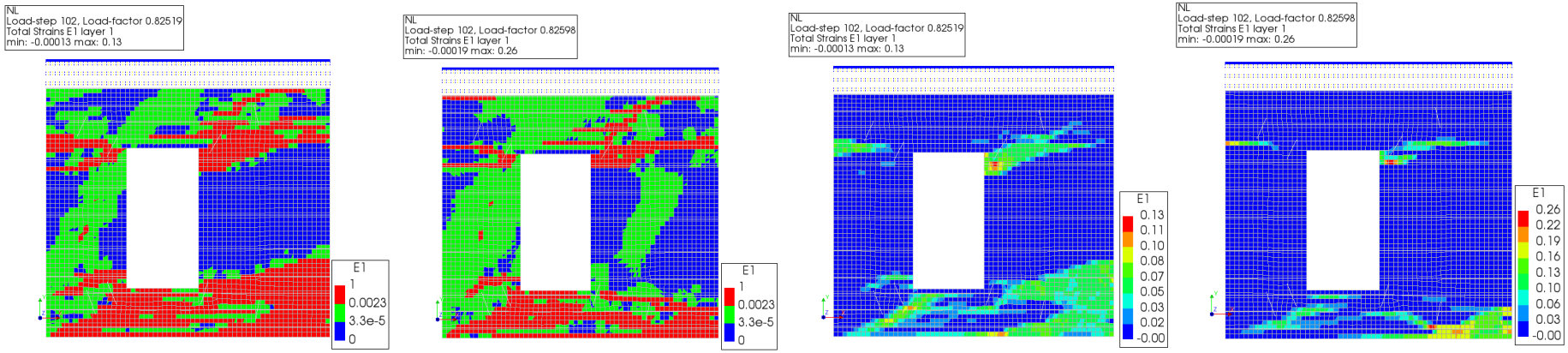

(a) E = 4810.5 MPa (b) E = 1603.5 MPa (c) E = 4810.5 MPa (d) E = 1603.5 MPa

Figure 5-49: Retrofitted wall. Sensitivity of modulus of elasticity, negative X-direction. First principal strain.

Table 5-16: Sensitivity of Modulus of elasticity

Modulus of Elasticity (MPa)	Crack Width at u=81 mm Positive X-direction (mm)	Crack Width at u=-64 mm Negative X-direction (mm)	Peak-load Positive X-direction (kN)	Peak-load Negative X-direction (kN)	Stiffness Positive X-direction (kN/mm)	Stiffness Negative X-direction (kN/mm)
3207 (original)	19 (at P2)	14.14 (at P5)	31.40	-27.30	26.95	25
1603.5 (50%decreased)	36.77 (at P2) (+63.73%)	18.34 (at P5) (+29.70%)	28.90 (-8.36%)	-26.25 (-4.07%)	22.50 (-18.13%)	19.80 (-23.41%)
4810.5 (50%increased)	12 (at S2) (-45.16%)	9.19 (at P5) (-35%)	36.15 (+14.06%)	-29.45 (+7.50%)	31.45 (+15.5%)	30.90 (+21%)

The results are almost insensitive to the **compressive strength** of the model. The Peak-load and failure mechanism of the models are not changed. The maximum crack width is completely the same in the positive direction but slightly different (around 30%) in the negative direction.

This statement is believed to be reasonable as failure mechanism and peak-load of the masonry are usually determined by tensile strength and tensile fracture energy. Force capacity of the retrofitted wall and a summary of numerical results can be seen in Figure 5-50and Table 5-17 respectively.

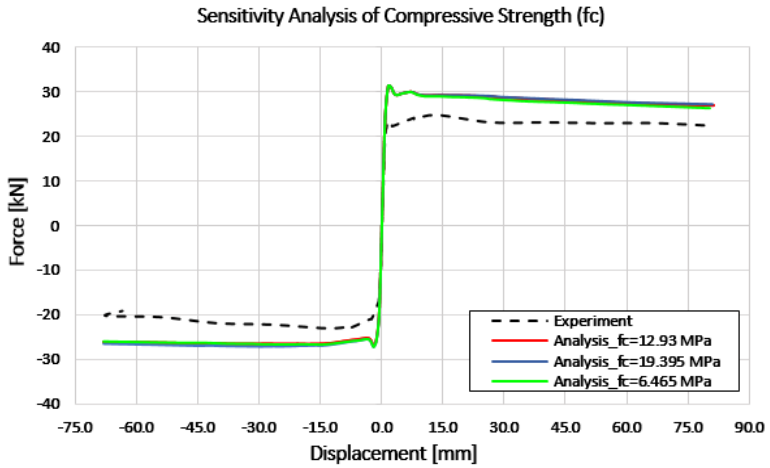

Figure 5-50: Capacity curve. Sensitivity of modulus of compressive strength

Table 5-17: Sensitivity of compressive strength

Compressive Strength (MPa)	Crack Width at u=81 mm Positive X-direction (mm)	Crack Width at u=-64 mm Negative X-direction (mm)	Peak-load Positive X-direction (kN)	Peak-load Negative X-direction (kN)
12.93 (original)	19 (at P2)	14.14 (at P5)	31.40	27.30
6.465 (50% decreased)	19 (at P2)	19 (at P5) (+34%)	31.40 (0%)	27.15 (-0.70%)
19.395 (50% increased)	19 (at P2)	18.90 (at P5) (+33.66%)	31.40 (0%)	27.15 (-0.70%)

Tensile strength is another material property that affects the results. Tensile strength is a parameter that usually determines the failure mechanism and force capacity of the wall.

However, the force capacity of the wall is not affected noticeably by changing the tensile strength in this model. This can be found in Figure 5-51 and Table 5-18. Differences are in a range of 1%~3% that is negligible.

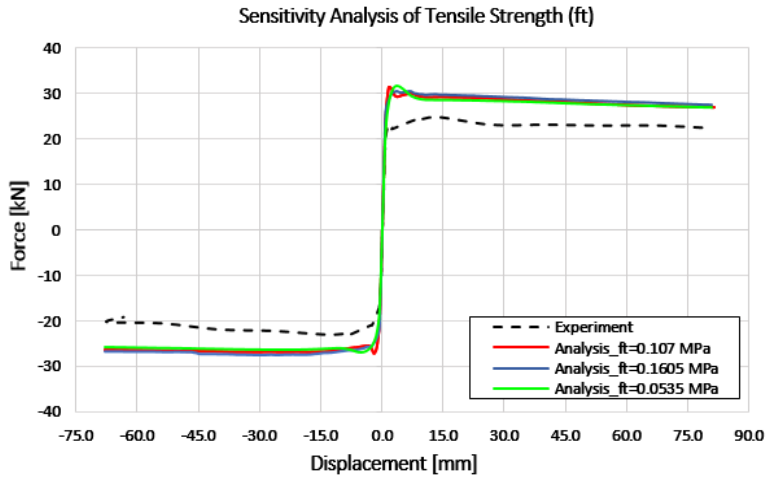

Figure 5-51: Capacity curve. Sensitivity of tensile strength

In general, by changing the tensile strength, the wall starts cracking at different stress and corresponding cracking strain, ε_{cr}. As a result, ultimate strain (ε_{ult}) will be changed based on the fact that it is not only a function of tensile strength but also tensile fracture energy ($\varepsilon_{ult} = \frac{2G_f}{f_t h}$). In the sensitivity analysis, only one parameter is changed each time. In another word, for studying the effect of tensile strength, the tensile fracture energy remains the same while it is a function of tensile strength: $G_f = 0.025 * (2f_t)^{0.7}$. With this assumption wall with the highest tensile strength reaches to *fully open crack stage* sooner since G_f remains the same and ε_{ult} is reached in a smaller strain. Consequently, a higher crack width can be observed in the wall with higher tensile strength. This does not occur in reality and it is expected that higher tensile strength leads to smaller crack width. Figure 5-52 shows how a *fully open crack stage* is observed in the stronger models.

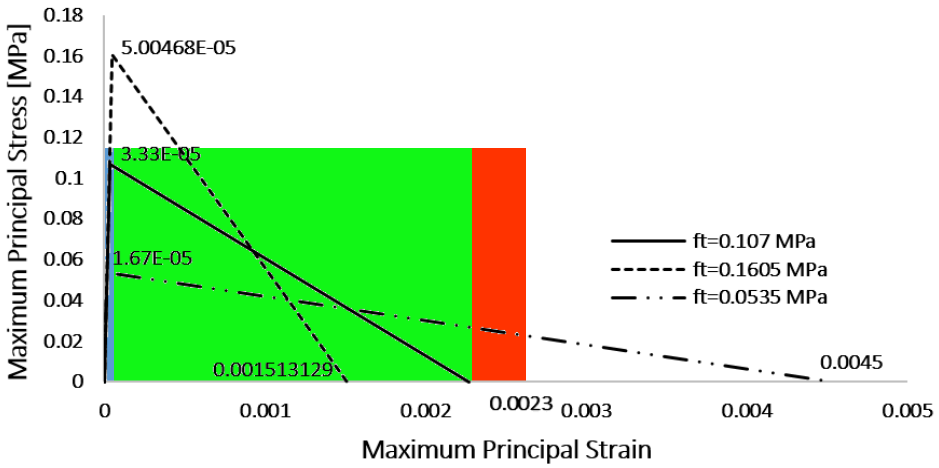

Figure 5-52: Tensile stress strain curve obtained by different tensile strength

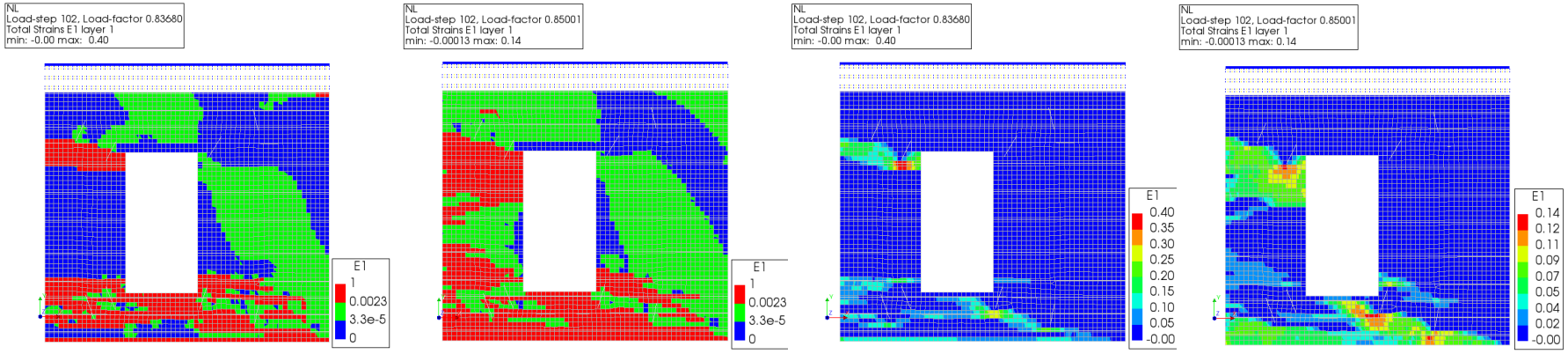

(a) ft = 0.1605 MPa (b) ft = 0.0535 MPa (c) ft = 0.1605 MPa (d) ft = 0.0535 MPa

Figure 5-53: Retrofitted wall. Sensitivity of tensile strength, positive X-direction. First principal strain

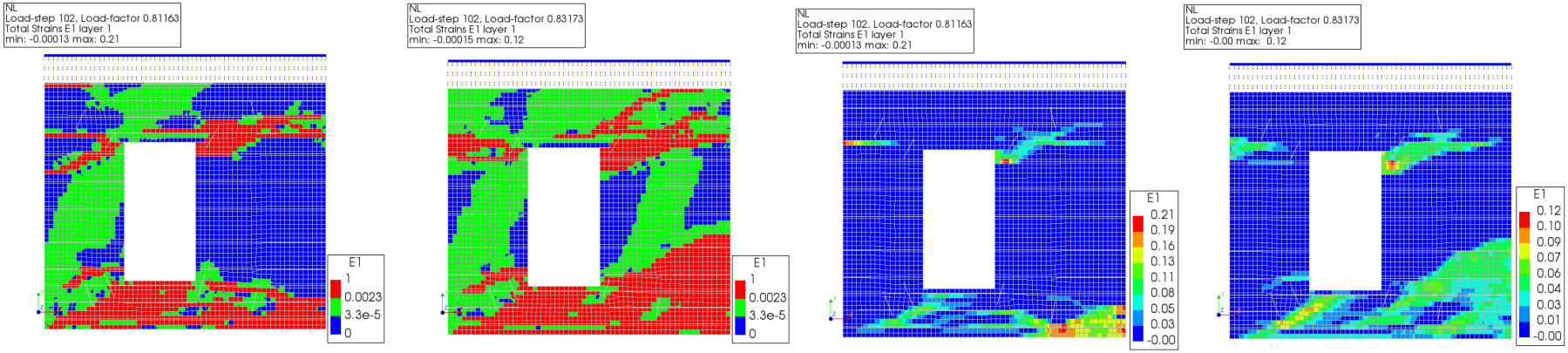

(a) ft = 0.1605 MPa (b) ft = 0.0535 MPa (c) ft = 0.1605 MPa (d) ft = 0.0535 MPa

Figure 5-54: Retrofitted wall. Sensitivity of tensile strength, negative X-direction. First principal strain

Table 5-18: Sensitivity of tensile strength

Tensile Strength (MPa)	Crack Width at u=81 mm Positive X-direction (mm)	Crack Width at u=-64 mm Negative X-direction (mm)	Peak-load Positive X-direction (kN)	Peak-load Negative X-direction (kN)
0.107 (original)	19 (at P2)	14.14 (at P5)	31.40	27.30
0.0535 (50% decreased)	10.6 (at P2) (-56.75%)	8.48 (at P5) (-40%)	31.80 (+1.1%)	26.90 (-1.62%)
0.1605 (50% increased)	29 (at P2) (+41.67%)	15.56 (at P5) (+10%)	30.40 (-3.20%)	27.50 (+0.69%)

Tensile fracture energy is another important material property that normally affects the results. Tensile fracture energy is a parameter that usually determines the failure mechanism, force capacity, and crack width of the brittle materials. In this research, however, this parameter does not change the failure modes of the retrofitted wall.

As can be seen in Figure 5-55, the force capacity is a function of fracture energy in tension. By decreasing the energy by 50% a difference of -7.22% (+X) and -2.41% (-X) and by increasing this parameter, a difference of +9.95% (+X) and +5.65% (-X) is observed in the models. These differences are reasonable. When the parameter is increased, more energy is required for crack growth and thus, the wall reaches a higher peak-load. By decreasing the fracture energy in tension a lower peak-load is observed since less energy leads to crack growth in the material.

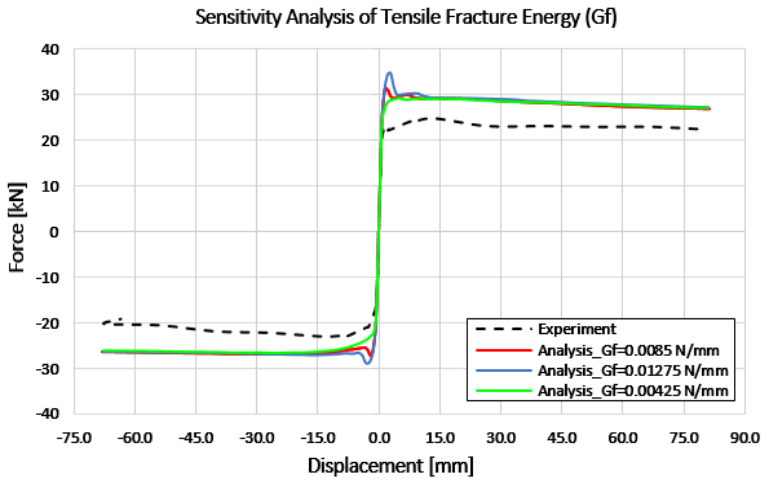

Figure 5-55: Capacity curve. Sensitivity of tensile fracture energy

The above statement explains why crack width decreases by increasing the tensile fracture energy and vice versa. Table 5-19 shows the maximum crack width in both directions. It should be noticed that the ultimate strain (ε_{ult}) is a function of G_f and by changing the tensile fracture energy, the stress-strain curve will be changed as well as can be found in Figure 5-56. Tensile strength remains the same (0.107 MPa).

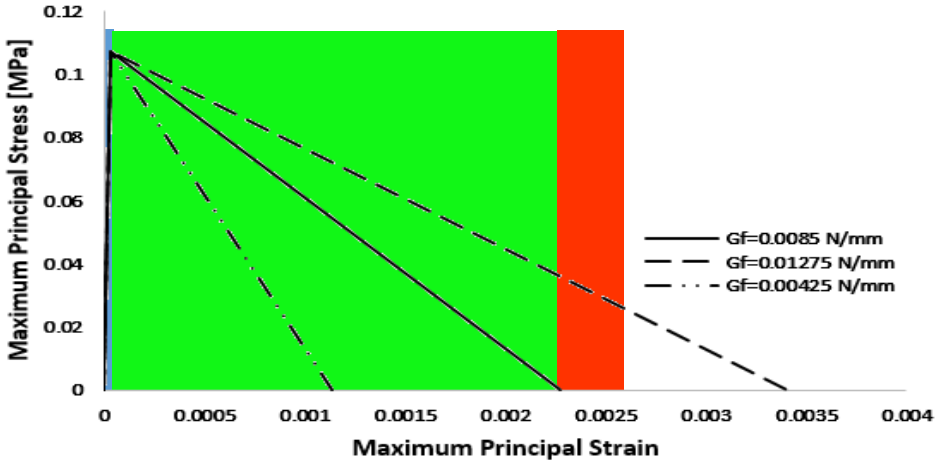

Figure 5-56: Tensile stress strain curve obtained by different tensile fracture energy

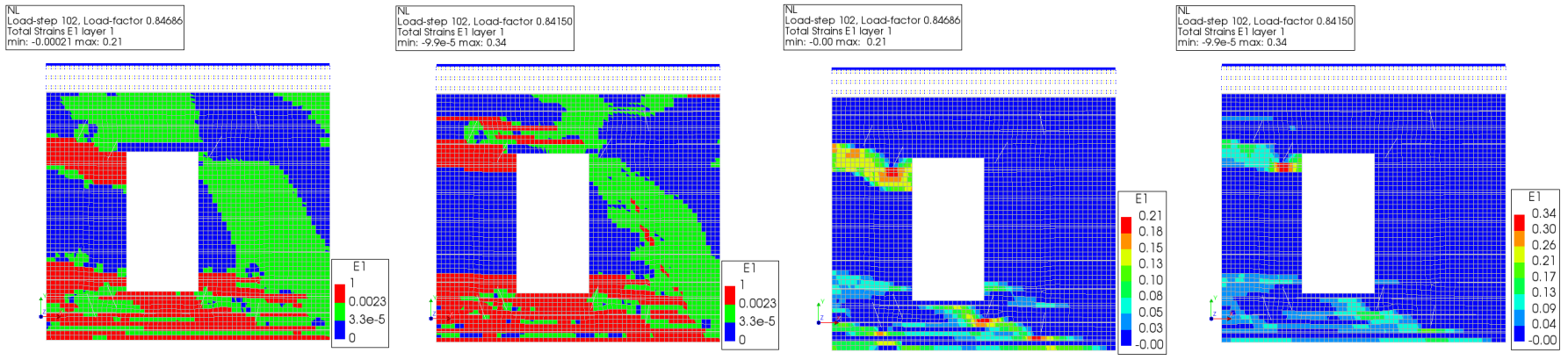

(a) Gf = 0.01275 N/mm (b) Gf = 0.00425 N/mm (c) Gf = 0.01275 N/mm (d) Gf = 0.00425 N/mm

Figure 5-57: Retrofitted wall. Sensitivity of tensile fracture energy, positive X-direction. First principal strain

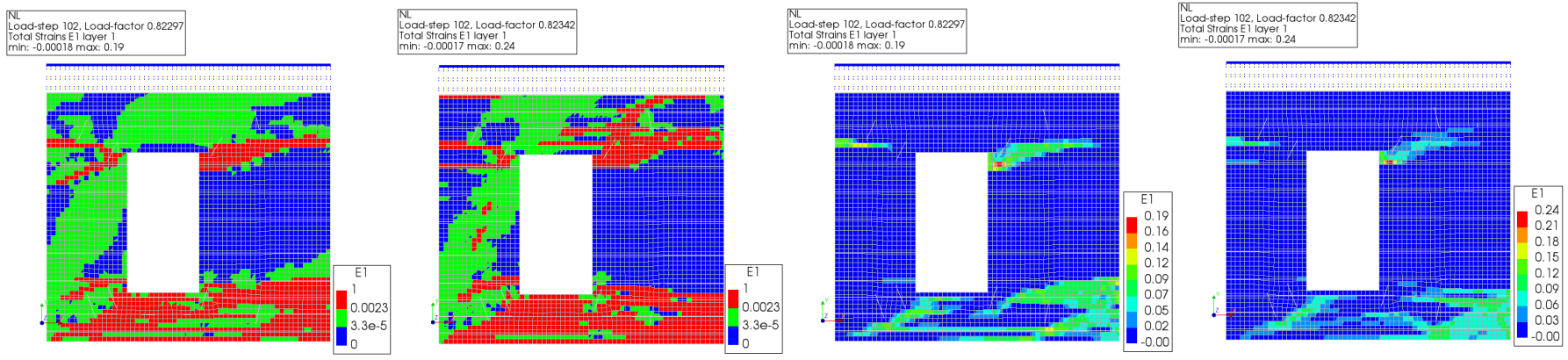

(a) Gf = 0.01275 N/mm (b) Gf = 0.00425 N/mm (c) Gf = 0.01275 N/mm (d) Gf = 0.00425 N/mm

Figure 5-58: Retrofitted wall. Sensitivity of tensile fracture energy, negative X-direction. First principal strain

Table 5-19: Sensitivity of tensile fracture energy

Tensile Fracture Energy (N/mm)	Crack Width at u=81 mm Positive X-direction (mm)	Crack Width at u=-64 mm Negative X-direction (mm)	Peak-load Positive X-direction (kN)	Peak-load Negative X-direction (kN)
0.0085 (original)	19 (at P2)	14.14 (at P5)	31.40	27.30
0.00425 (50% decreased)	24.75 (at P2) (+26.28%)	16.97 (at P5) (+20%)	29.20 (-7.22%)	26.70 (-2.41%)
0.01275 (50% increased)	14.85 (at P2) (-24.52%)	13.43 (at P5) (-5%)	34.70 (+9.95%)	28.90 (+5.65%)

Similar to compressive strength, the results are almost insensitive to the **compressive fracture energy** of the model. The Peak-load and failure mechanism of the models are not changed. The maximum crack width, however, is a bit different when the wall is loaded in the negative X-direction.

This statement is acceptable as failure mechanism and peak-load of the masonry are usually determined by tensile strength and tensile fracture energy.

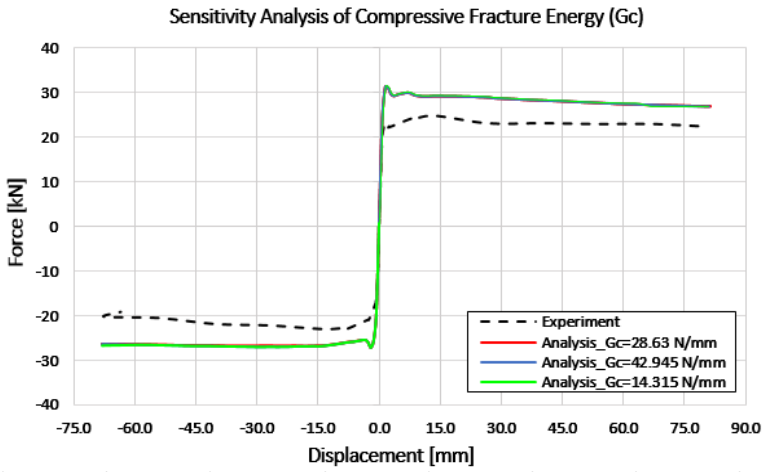

Figure 5-59: Capacity curve. Sensitivity of modulus of compressive fracture energy

Table 5-20: Sensitivity of compressive fracture energy

Compressive Fracture Energy (N/mm)	Crack Width at u=81 mm Positive X-direction (mm)	Crack Width at u=-64 mm Negative X-direction (mm)	Peak-load Positive X-direction (kN)	Peak-load Negative X-direction (kN)
28.63 (original)	19 (at P2)	14.14 (at P5)	31.40	27.30
14.315 (50% decreased)	19 (at P2)	19.80 (at P5) (+40%)	31.40 (0%)	27.15 (-0.7%)
42.945 (50% increased)	19 (at P2)	19.80 (at P5) (+40%)	31.40 (0%)	27.15 (-0.7%)

5.6 Conclusions

Two material models, Total Strain Crack Model (TSCM) and Engineering Masonry Model (EMM) are implemented to model the unreinforced masonry (URM) wall and the retrofitted wall. Results are compared in terms of peak-load, crack pattern and failure modes. The analyses with EMM do not converge in several load steps after the peak-load (Appendix C) and consequently, the results are not valid. In contrast, by applying TSCM, no convergence problem is experienced and the results are in good agreement with the tests. However, it is recognized that the applied iterative method can affect the results and divergence of the analysis, so it is essential to choose an appropriate iterative method.

The seismic performance of the wall improves by applying the reinforcement. A difference of +13% and +18% in the peak-load of the retrofitted wall is observed when the wall is loaded in positive and negative X-direction respectively. The maximum crack width of 147 mm (+X) and 49 mm (-X) reduced to 19 mm (+X) and 14 mm (-X) after retrofitting. Furthermore, the failure mode is another factor that changes in the retrofitted wall. In the unstrengthened wall, rocking of the piers is the main mechanism however in the strengthened wall apart from rocking of the piers, that occurs initially but in a higher peak-load, an arch mechanism (a network of cracks bellow the window level) is recognized due to horizontal bars. In addition, a diagonal shear crack in the piers, as well as toe-crushing that happens at the bottom right corner of the retrofitted wall is recognized.

The sensitivity analysis reveals that results are insensitive to the variation of compressive strength and compressive fracture energy. Since the global behavior of the wall usually is not determined by these two parameters, these results seem to be reasonable for the masonry walls. A similar trend is observed for tensile strength. By contrast, results were sensitive to the variation of modulus of elasticity and tensile fracture energy. Changing the modulus of elasticity affects the linear stiffness, peak-load, and maximum crack width. However, the failure mode of the retrofitted wall does not alter. Similarly, for the tensile fracture energy, the failure mode of the retrofitted wall is insensitive to this parameter. However, peak-load and crack width are affected.

6

PARAMETRIC STUDY

This chapter focuses on the seismic performance of the wall that is retrofitted with only bed joint reinforcement and only diagonal anchors (with two lengths). In addition, different reinforcement layouts are modeled to study the effect of the number of bars in the thickness as well as the height of the wall

6.1 The effect of only diagonal anchor on the seismic performance of the URM wall

In this section, the influence of *only* diagonal anchors in terms of seismic performance is studied. Thus, the same diagonal anchors (Figure 6-1) that were used in the experiment are applied (i.e. eight anchors) and the results are compared with the numerical results of the URM wall. Material parameters and properties are the same as the previous chapter. Then the influence of anchors on the capacity curve, failure mechanisms, and crack width are checked.

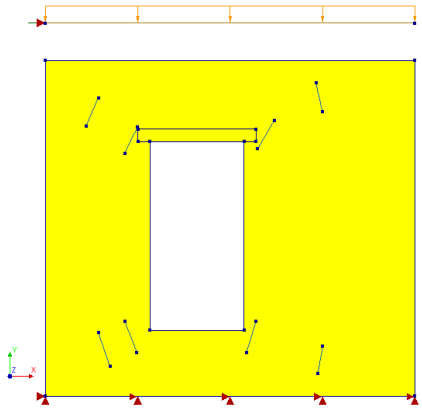

Figure 6-1: Diagonal anchor layout

Capacity curves have revealed that diagonal anchors do not affect the force capacity of the wall as can be seen in Figure 6-2. Both capacity curves have the same pattern without any remarkable changes in peak-loads.

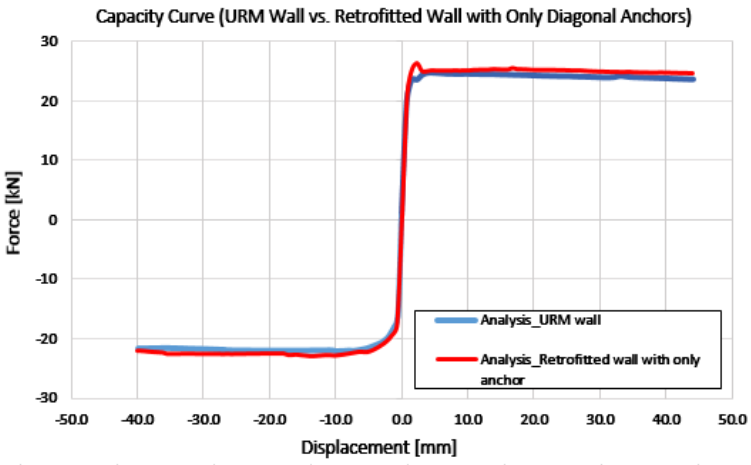

Figure 6-2: Capacity curve (Regular Newton-Raphson Method is used for iteration). Analysis is stopped manually at +44 and -40 mm

However, diagonal anchors have a significant effect on the location, initiation, and propagation of the cracks and also crack width.

Figure 6-3 and Figure 6-5 clearly show the influence of the diagonal anchors. In the retrofitted wall with only anchor (in positive X-direction), the wall starts cracking at different points and cracks propagate in different directions compared with the URM wall. Due to the diagonal anchors, cracks cannot propagate through the bars and they intend to smear from above

and below the anchors. Crack number 2 is completely diagonal for the URM wall, however, after applying the anchors, a combination of diagonal and horizontal crack is recognized. A shift in the location of the crack number 1 is observed after retrofitting: instead of the corner of the opening crack initiate and propagate from the middle of the opening.

In the negative direction, the location and pattern of the cracks nearly the same. However, propagation of the cracks in all quarters has been changed a bit once more which is due to the applied anchors.

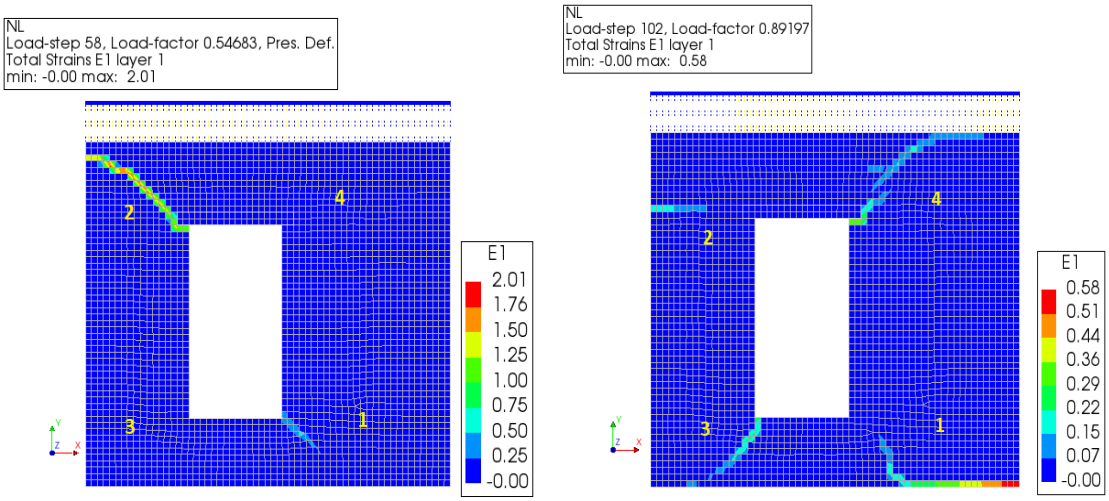

(a) Displacement = +44 mm (b) Displacement = -40 mm

Figure 6-3: URM wall, maximum principal strain

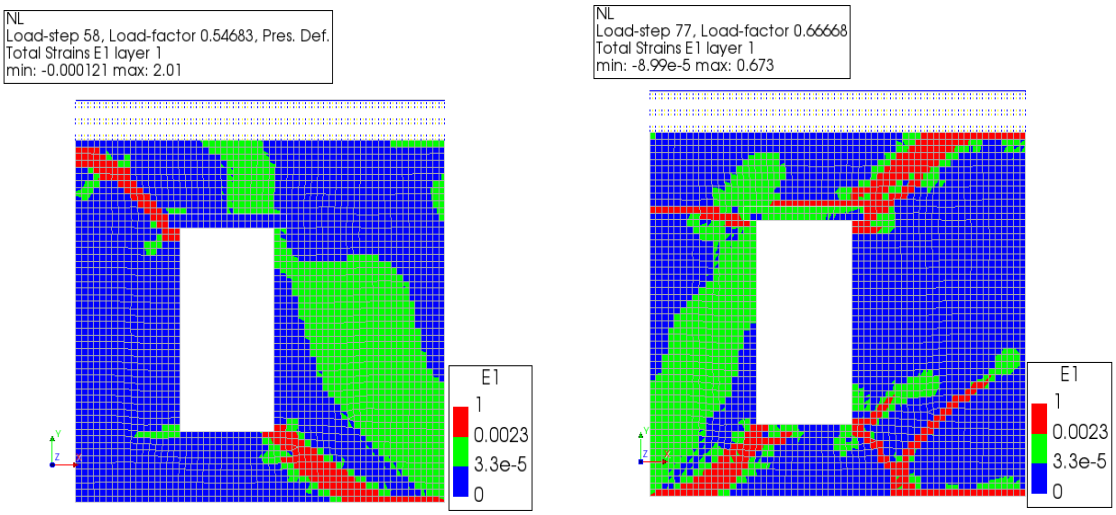

(a) Displacement = +44 mm (b) Displacement = -40 mm

Figure 6-4: URM wall, scaled principal strain

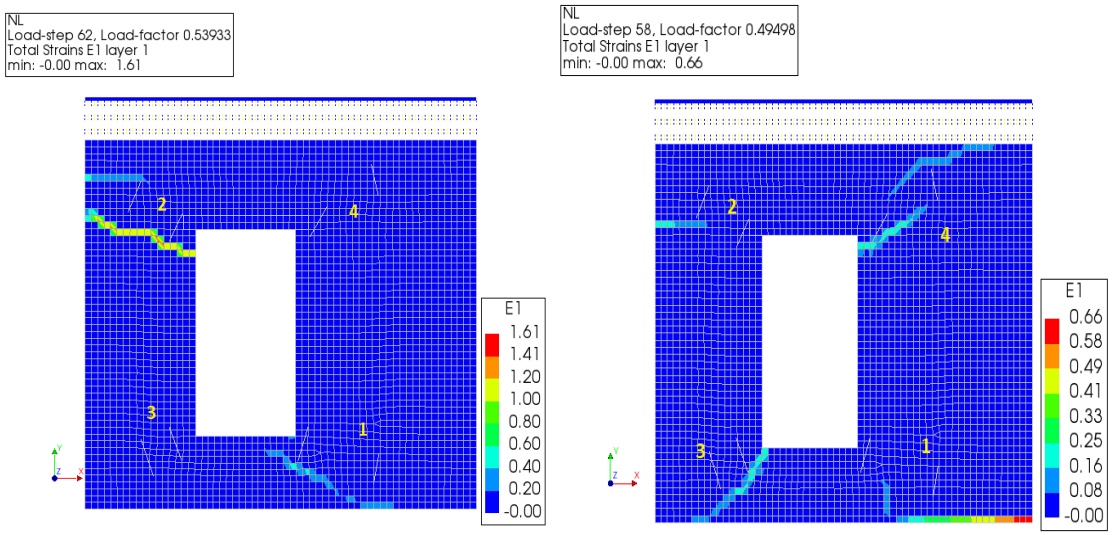

(a) Displacement = +44 mm (b) Displacement = -40 mm

Figure 6-5: Retrofitted wall with only diagonal anchors, maximum principal strain

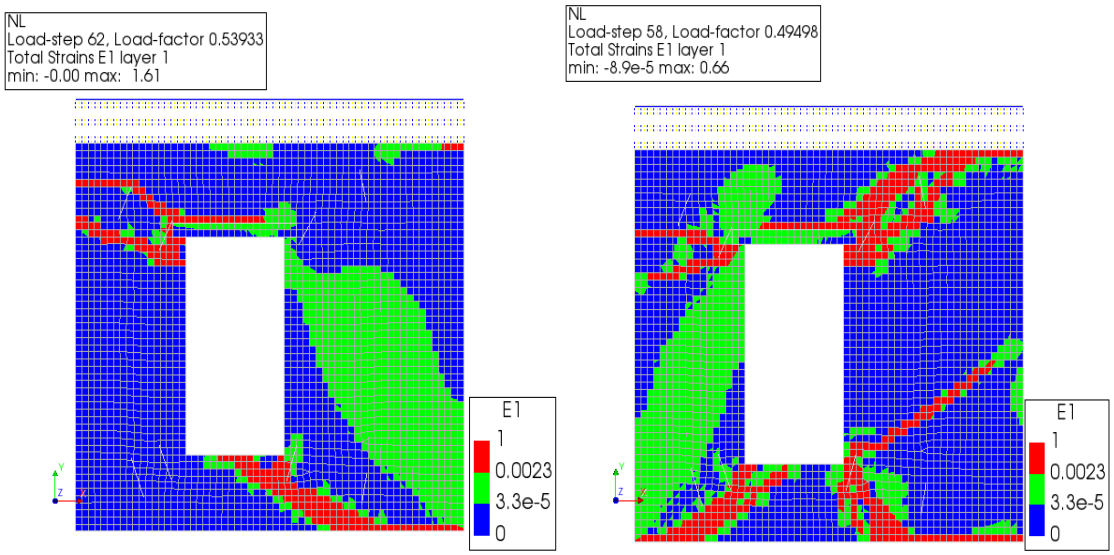

(a) Displacement = +44 mm (b) Displacement = -40 mm

Figure 6-6: Retrofitted wall with only diagonal anchors, scaled principal strain

In conclusion, it can be stated that by applying only diagonal anchors the crack width cannot be reduced. It can be said that a large crack width can even be observed after retrofitting since initiation and propagation of the cracks might change based on the location of the diagonal anchor. The same failure modes, compared with the URM wall, are recognized in the retrofitted wall with only diagonal anchors and the force capacity of the structure increases negligibly.

Table 6-1: Numerical result summary. URM wall vs. Wall retrofitted with only anchor

Model	Iterative Method	Peak-Load (+X) (kN)	Peak-Load (-X) (kN)	Crack Width Max. (+X) (mm)	Crack Width Max. (-X) (mm)
URM wall	Regular Newton-Raphson	24.85	22	147	48.80
Wall retrofitted with only anchor	Regular Newton-Raphson	25.65	22.90	116.15	48.80
Difference	-	**+3.09%**	**+4.01%**	**-20.63%**	**0%**

6.2 The effect of the diagonal anchor's length on the seismic performance of the URM wall

From previous analyses, we have realized that by applying the diagonal anchors, cracks intend to propagate from above and below the anchors. So, the length of the diagonal anchors might affect the results. To study the influence of the anchors' length, bars are modeled two times longer (540 mm) than the original case (Figure 6-7).

For both models, Regular Newton Raphson method is applied. Divergence occurs when the wall is loaded in negative X-direction. However, as around 85% of deformation is applied, the results can be interpreted. To solve the divergence problem, Secant Method can be used, although this method predicts the peak-load with a higher numerical error.

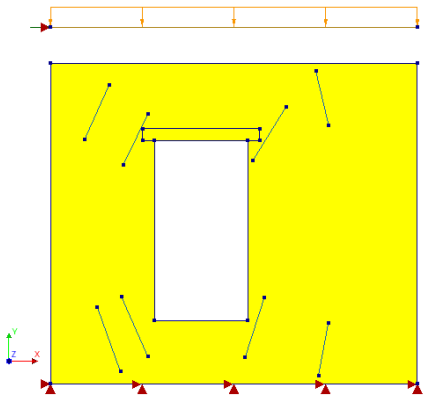

Figure 6-7: Diagonal anchor (longer length, 540 mm) layout

Capacity curves show that longer diagonal anchors inconsiderably increase the force capacity of the wall (+4.52% and +8.15% difference in positive and negative X-direction respectively), Figure 6-8. However, divergence occurs when the wall is loaded in negative X-direction. As explained before, the Secant Method can be applied to solve this numerical problem it overestimates the peak – load.

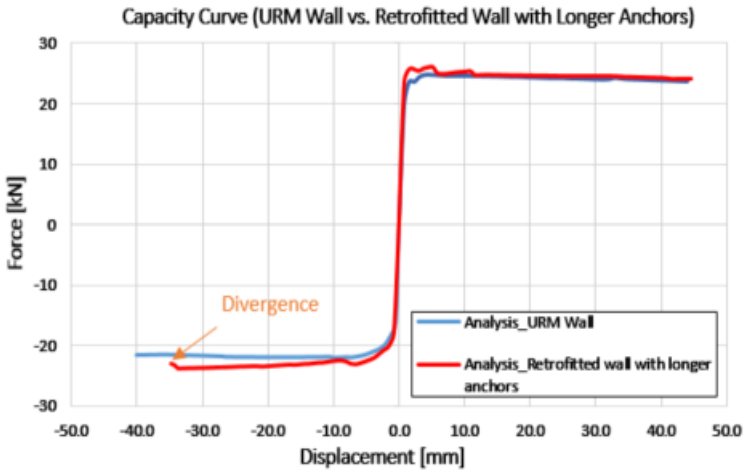

Figure 6-8: Capacity curve (Regular Newton-Raphson Method is used for iteration)

Similar to the original diagonal anchor case, longer bars in the retrofitted wall changes the location, initiation, and propagation of the cracks.

Figure 6-9, 10 show the influence of the longer diagonal anchors. In the retrofitted wall with longer anchors (positive X-direction), the wall starts cracking at different points and cracks propagate in different directions compared with the URM wall and retrofitted wall with original anchor length. As a result of the longer anchors, cracks intend to propagate from above and below the bars. In quarter D (crack number 1), a substantial change in the location of the diagonal crack is observed. Crack is completely shifted upward as a result of the longer anchors.

We can see the same behavior in the opposite direction, the location of the cracks are shifted a bit and cracks intend to smear from above and below the anchors.

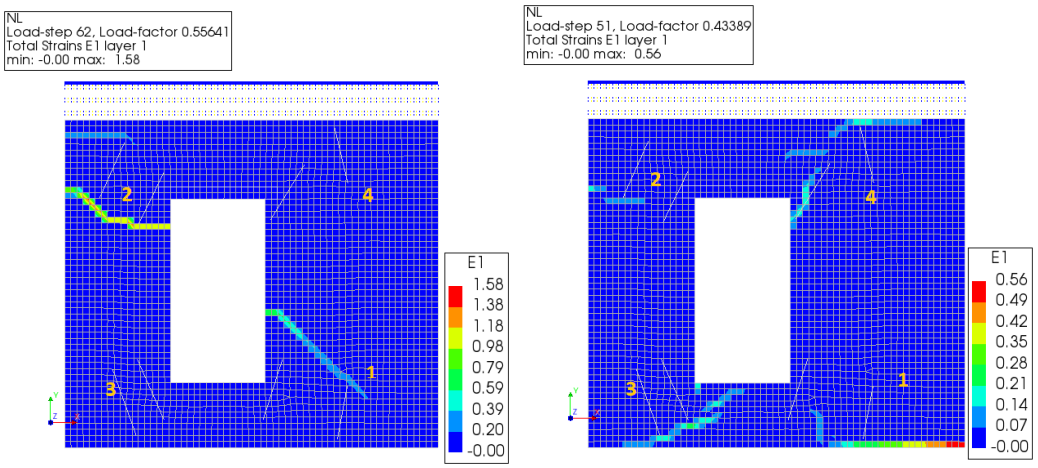

(a) Displacement = +44 mm

(b) Displacement = -34.5 mm (last converged step)

Figure 6-9: Retrofitted wall with only longer diagonal anchors, maximum principal strain

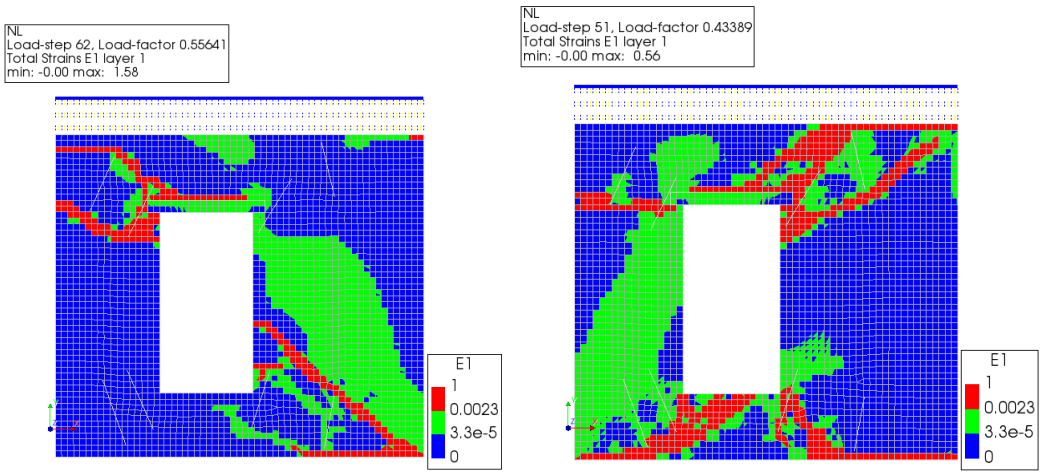

(a) Displacement = +44 mm (b) Displacement = -34.5 mm (last converged step)

Figure 6-10: Retrofitted wall with only longer diagonal anchors, scaled principal strain.

In conclusion, by applying longer diagonal anchors, the crack width cannot be limited. Larger crack width can be observed after retrofitting since the cracks are relocated to another location. Initiation and propagation of the cracks might change based on the location of the diagonal anchor. Furthermore, the same failure mechanisms compared with the URM wall are observed and the force capacity of the wall is increased slightly. So, this is not a reliable technique for retrofitting the URM wall.

Table 6-2: Numerical result summary. URM wall vs. Wall retrofitted with longer anchor

Model	Iterative Method	Peak-Load (+X) (kN)	Peak-Load (-X) (kN)	Crack Width Max. (+X) (mm)	Crack Width Max. (-X) (mm)
URM wall	Regular Newton-Raphson	24.85	22	147	48.80 (at 40 mm displacement)
Retrofitted wall with only longer diagonal anchor	Regular Newton-Raphson	26	23.90	114.55	40.30 (at 34 mm displacement. Divergence of the model)
Difference	-	**+4.5%**	**+8.15%**	**+22.07%**	-

6.3 The effect of only bed joint reinforcement on the seismic performance of the URM wall

In this part, the influence of *only* bed joint reinforcement on the seismic performance of the wall is investigated and the same reinforcement layout (Figure 6-11) applied in the experiment is modeled. Then the results are compared with the URM wall.

A combination of the Secant Method and Regular Newton Raphson Method is chosen to find the most suitable numerical results in terms of peak-load and crack patterns as follows (also see Appendix D).

- URM wall, for peak-load: the result of Regular Newton Raphson Method
- URM wall, for crack patterns and failure modes: the result of Regular Newton Raphson Method

- Retrofitted wall, for peak-load: the result of Regular Newton Raphson Method (divergence occurs at +50 mm)
- Retrofitted wall, for crack patterns and failure modes: the result of Secant Method (no problem with convergence/divergence)

Bed joint reinforcement changes the crack width. To study its effect on the crack width, the wall is divided into four quarters, quarter A to D, as can be seen in Figure 6-11. The crack width for both unreinforced masonry and the retrofitted wall is checked at some specific nodes corresponds to crack width in Y-direction.

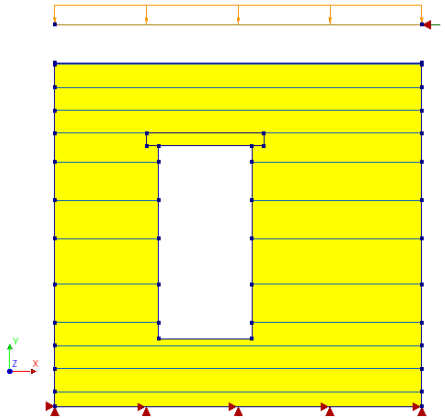

Figure 6-11: Bed joint reinforcement layout

Capacity curves (Figure 6-12) show that by applying bed joint reinforcement the behavior of the wall improves in terms of peak-load. A peak-load of 27.13 kN is reached by retrofitting of the wall that is 8.77 % higher than the URM wall for positive X-direction. In the opposite direction, the load is increased by 18.01% and reaches 25.98 kN. So, bed joint reinforcement is at least two times more effective than the longer diagonal anchors.

If we compare the retrofitted wall with only BJR and the retrofitted wall with BJR and diagonal anchors in terms of peak-load a slight difference of 1.22% is observed. It means we have the same increment with and without diagonal anchors.

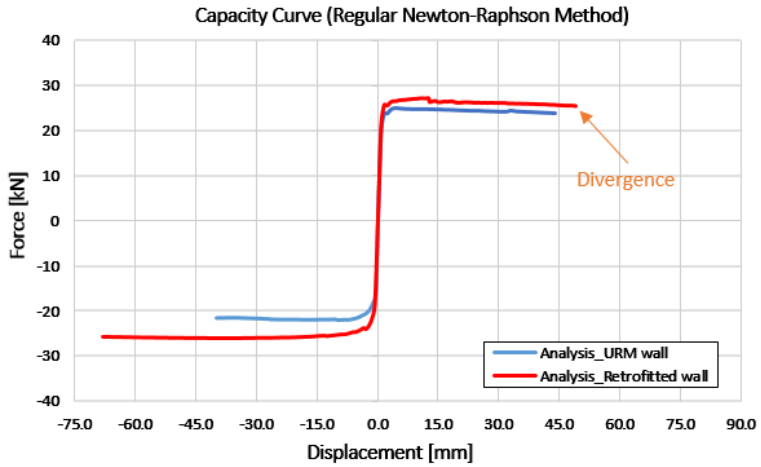

Figure 6-12: Capacity curve (Regular Newton-Raphson is used for iteration)

By applying the bed joint reinforcement (BJR), the failure mechanism of the structure is changed. Figure 6-13 shows the mechanisms that are recognized in both models. In the unstrengthened

wall, the main mechanism is rocking of the piers; for the retrofitted wall with only BJR initially rocking of the piers is observed but by increasing the deformation arch mechanism occurs in window bank and its adjacent. The arch effect is induced by the bed joint reinforcement. Reinforcement acts in tension to restrain crack opening. Figure 6-14 shows the von Mises stress in steel. As the maximum stress reaches 215.25 MPa, the yielding of the steel is observed in the model. Finally, compressive stress is very close to the compressive strength of the masonry at the bottom right corner of the wall that leads to toe-crushing when the wall is loaded in the positive X- direction.

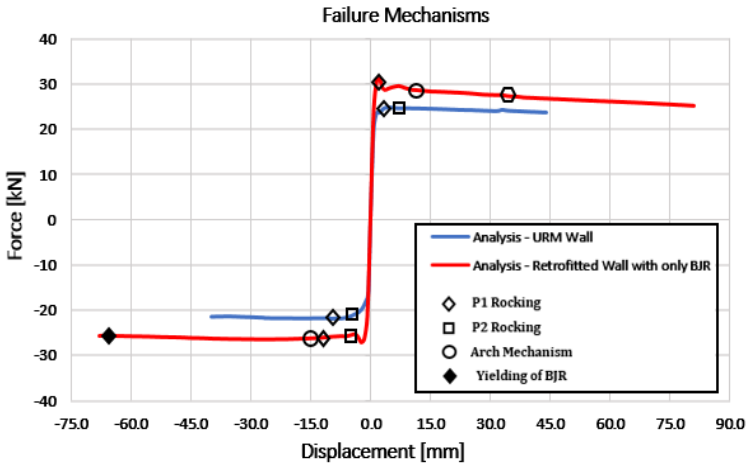

Figure 6-13: Capacity curve (Regular Newton-Raphson Method for the URM wall and Secant Method for the retrofitted wall is applied). P1 and P2 stand for pier1 (left pier) and pier 2 (right pier)

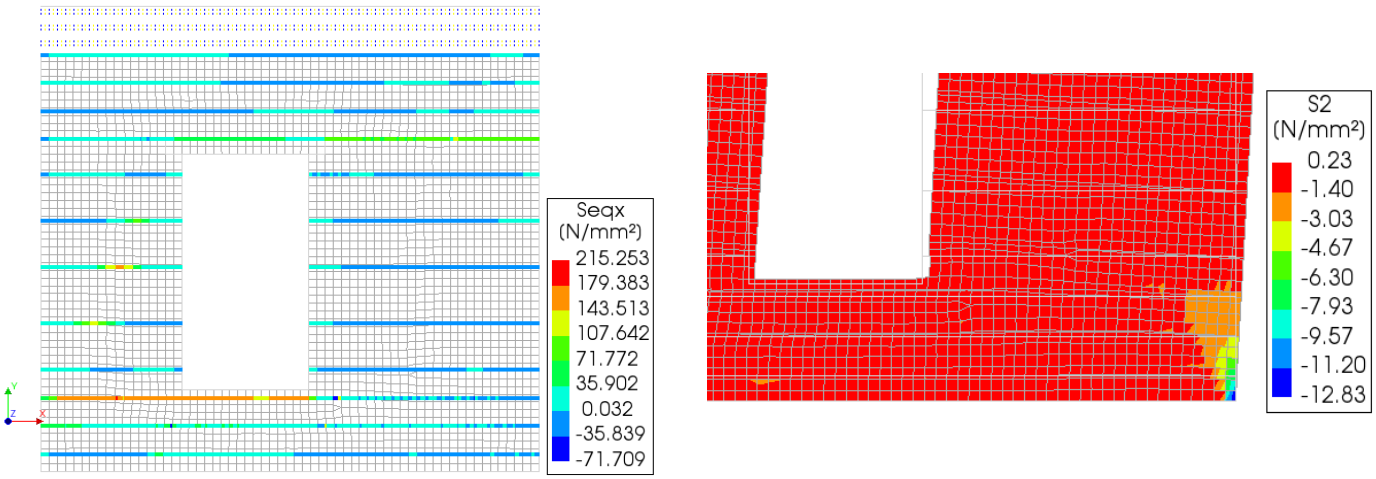

(a) (b)

Figure 6-14: von Mises stress in steel (a) and toe-crushing (b)

The crack pattern is another factor that changes in the retrofitted wall with only BJR. Figure 6-15 shows the influence of the bed joint reinforcement on the crack pattern.

A network of a staircase and horizontal cracks are produced below the window level (an arch mechanism) as a result of the longitudinal bars. In addition, wide shear cracks are recognized in the piers. The pure diagonal cracks observed in the URM wall are changed a bit in the retrofitted wall with only BJR with a smaller angle with respect to the horizon. Furthermore, crack width is dropped significantly as a result of bed joint reinforcement. This shows that the retrofitted wall

with only bed joint reinforcement has better performance than the retrofitted wall with only diagonal anchors.

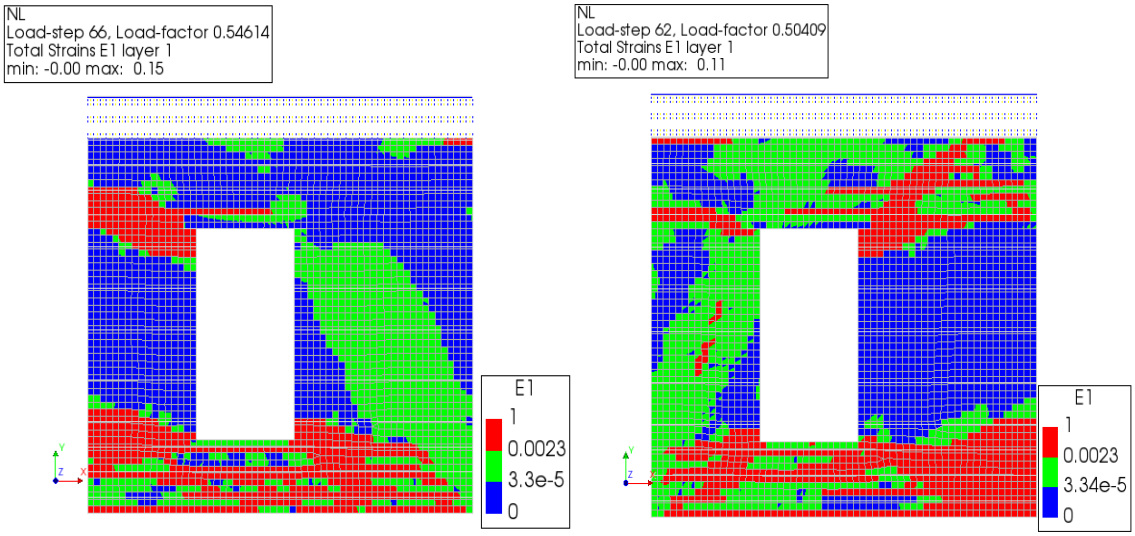

(a) Displacement = +81 mm (b) Displacement = -64 mm

Figure 6-15: Retrofitted wall with only bed joint reinforcement, scaled principal strain

It is fair to say that, by using only bed joint reinforcement, the crack width has been restricted both locally and globally. In the URM wall rocking failure of the piers is the main mechanism, however, by applying horizontal bars, apart from pier failure that occurs in higher lateral forces, an arch mechanism (a network of cracks below the window level) is recognized. In addition, the force capacity and ductility of the retrofitted wall are improved in both directions. Therefore, applying only bed joint reinforcement is an effective retrofitting technique for the URM wall since it improves the performance of the wall in terms of the force capacity and crack width.

Table 6-3: Numerical result summary. URM wall vs. Wall retrofitted with only bed joint reinforcement

Wall	**Iterative method**	**Peak load (+X) (kN)**	**Peak load (-X) (kN)**	**Crack Width Max. (+X) (mm)**	**Crack Width Max. (-X) (mm)**
URM wall	Combination of RNR and Secant Method	24.85	22	147	48.80
Retrofitted wall with only bed- joint reinforcement	Combination of RNR and Secant Method	27.15	26	17	12.50
Difference	-	**8.77%**	**16.59%**	**88.43%**	**118.38%**

6.4 The effect of layout of the reinforcement on the retrofitted wall performance

This section discusses the effect of the layout of the reinforcement on the performance of the retrofitted wall via a parametric study. The number of the bed joint reinforcement can vary in the thickness of the wall (1 or 2 bars) as well as along the height of the wall. For the former, the diameter of the rebar is kept constant (6mm) and for the latter 11 layouts are modeled as can be found in Figure 6-17. The length, diameter, and location of the diagonal anchors are the same in all 11 cases and similar to the experiment.

Table 6-4 shows the number of bars that are applied in 11 cases. In case 1 and case 2 only four layers of rebar are introduced. In former single bed joint reinforcement while in the latter double bed joint reinforcements are applied. One layer of bed joint is added above and below the opening from Case 3 to case 8. For odd numbers single and for even numbers double bed joint reinforcement is applied. Case 9 is as same as case 8 but with one additional single rebar layer in the piers. In case 10, bars are introduced evenly from bottom to the top and finally case 11 is as same as an experiment but with single rebar for all layers.

Results can be presented in terms of the percentage of the reinforcement as well. Due to opening, the cross-section of the wall is not constant so, the volume of the reinforcement over the volume of the masonry is used to show the percentage of the applied reinforcement.

The location of the maximum crack pattern, meanwhile, is checked. To do this, the wall is divided into 8 parts as can be seen in Figure 6-16.

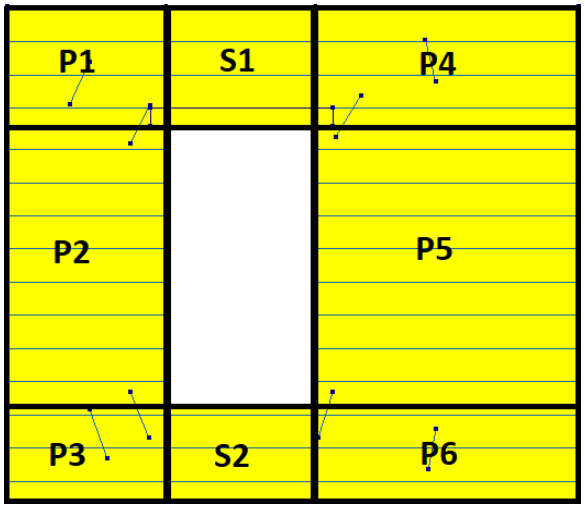

Figure 6-16: Division of the wall

Table 6-4: Number of bed joint reinforcement (BJR) for each model

Bar / Model	Single BJR (one bar per joint)	Double BJR (two bars per joint)	Total Number of BJR	Reinforcement Ration (%)	Location of BJR
Original	■	■	20	0.236	Everywhere
Case 1	■		4	0.049	Only above & below the opening
Case 2		■	8	0.098	Only above & below the opening
Case 3	■		6	0.074	Only above & below the opening
Case 4		■	12	0.147	Only above & below the opening
Case 5	■		8	0.098	Only above & below the opening
Case 6		■	16	0.196	Only above & below the opening
Case 7	■		9	0.110	Only above & below the opening
Case 8		■	18	0.221	Only above & below the opening
Case 9		■	19	0.230	Only above & below the opening
Case 10		■	30	0.698	Everywhere
Case 11	■		12	0.138	Everywhere

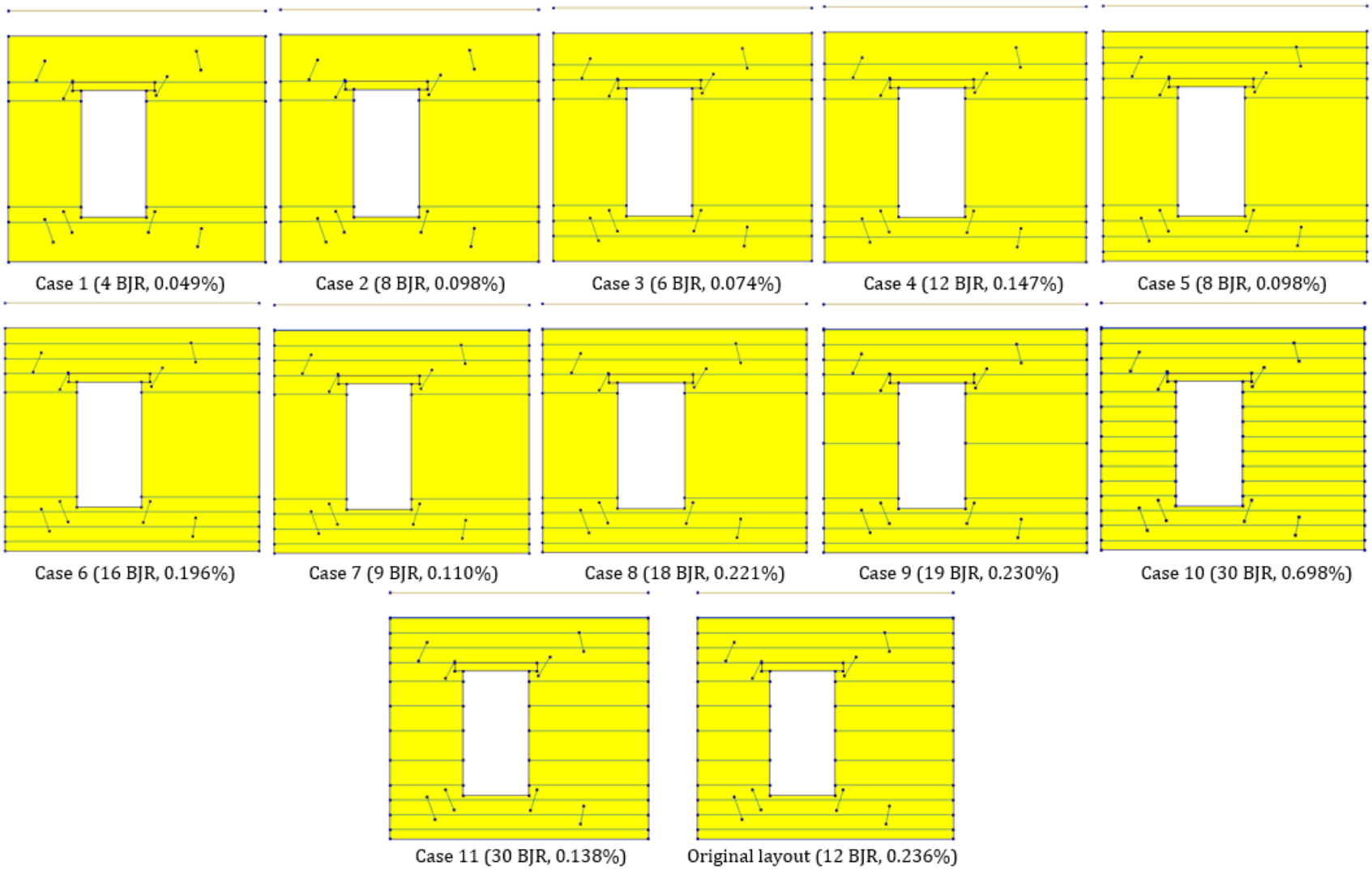

Figure 6-17: Layout of the bed joint reinforcement (BJR) for all cases, reinforcement ratio in %

In **case 1**, four layers of single bed joint reinforcement (BJR) are introduced just below and above the window opening since corners of the opening are the most vulnerable spots and remarkable diagonal cracks were observed at the opening corners in the URM wall.

Results are compared with the wall that is retrofitted with the original layout of the reinforcement to compare peak-load, maximum crack width, and failure modes.

In this model, although 16 bed joint reinforcements are removed only a difference of -2.22% in positive X-direction (from 31.43 to 30.74 kN) and -4.57% in negative X-direction (from 27.32 to 26.10 kN) is observed in the force capacity of the wall as can be seen in Figure 6-18.

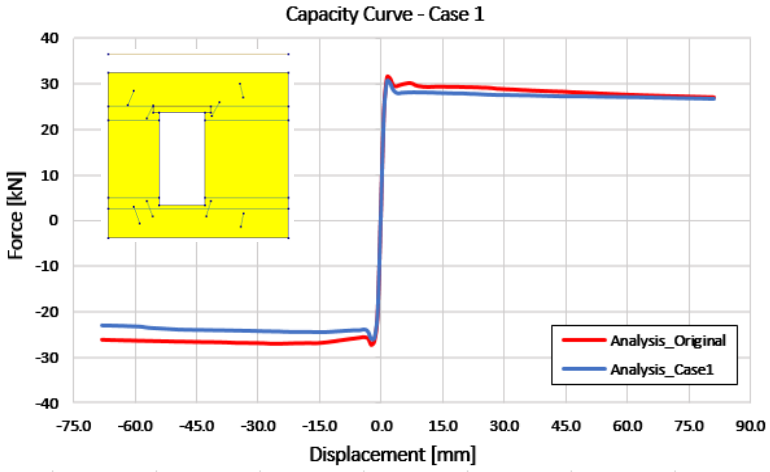

Figure 6-18: Capacity curve – case 1 (Secant Method is used for iteration)

The failure mechanism of the wall, however, changes a bit. The arch mechanism does not occur in the masonry below the opening level because the amount of reinforcement is too low and as a result, a lower compressive force is applied by rebar. The shear mechanism (Figure 6-19) is recognized in the piers. The absence of bars next to the opening can be the reason. Reinforcement acts in tension and as a result, restrains crack opening.

Crack patterns are nearly as same as the original layout but with a larger maximum crack width in both directions (a difference of +7.60% and +34.37% in positive and negative X-direction respectively). Since the arch mechanism is not observed lower cracks can be seen below the window level. Yielding of the BJR is observed in the model as steel acts in tension to restrains crack.

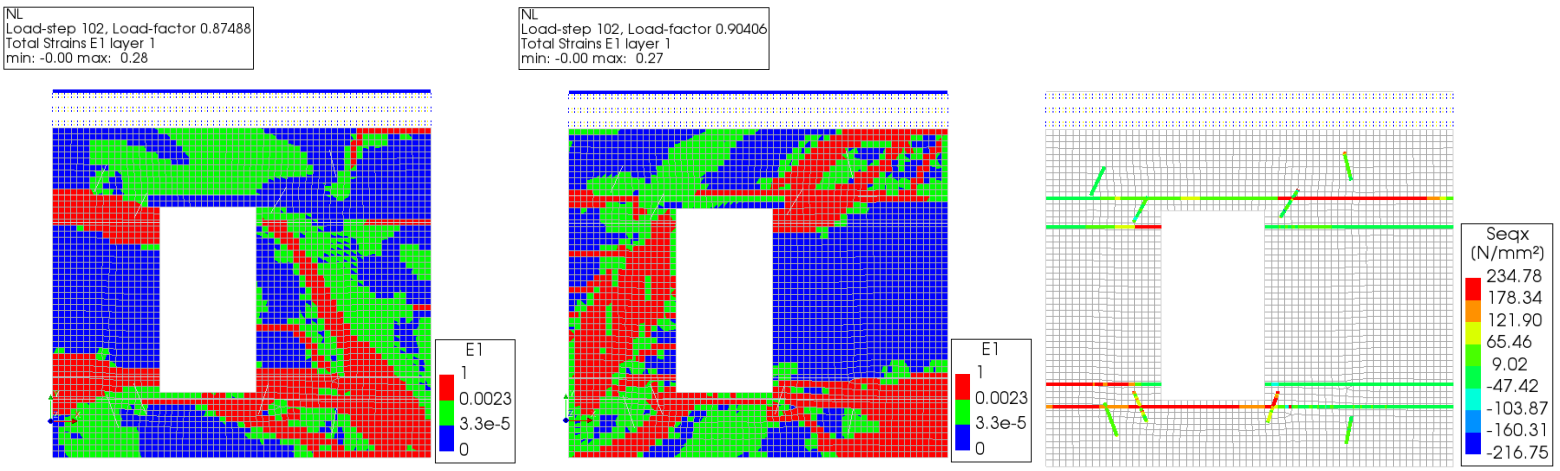

(a) Positive X-direction (b) Negative X-direction (c)

Figure 6-19: Retrofitted wall, case 1. Scaled principal strain (a) and (b), von Mises stress (c)

Table 6-5: Summary of results. Original layout vs. case 1

Model	Single BJR	Double BJR	Total Number of BJR	ρ (%) $(\frac{V_{bars}}{V_{wall}})$	F_{max} (+X) (difference to original) (kN)	F_{max} (-X) (difference to original) (kN)	Crack width Max. (location) (mm)
Original layout	■	■	**20**	**0.236**	**31.45**	**27.30**	(+x):19 (at P2) (-x):14.14 (at P5)
Case 1	■		4	0.049	30.75 (-2.22%)	26.10 (-4.57%)	(+x): 20.5 (at P2) (+7.60%) (-x):19 (at P5) (+34.37%)

Table 6-6: Failure modes. Original layout vs. case 1

Model	Failure Mechanism
Original layout	• Rocking of the piers • Arch mechanism • Toe-crushing • Sliding of the masonry above the window level with respect to the other portion of the wall
Case 1	• Rocking of the piers • Toe-crushing • Sliding of the masonry above the window level with respect to the other portion of the wall • Shear mechanism of piers

The location of the bars for C**ase 2**, is as same as case 1 (four layers of bed joint reinforcement) but with a double bar in each joint.

The capacity curve of this model (Figure 6-20) shows that double bar is much more effective than a single bar in terms of peak-load because only a difference of -1.12% and -0.088% in positive and negative X-direction compared with the original layout is observed while in the original layout 0.245% and in case 2 only 0.098% reinforcement is applied.

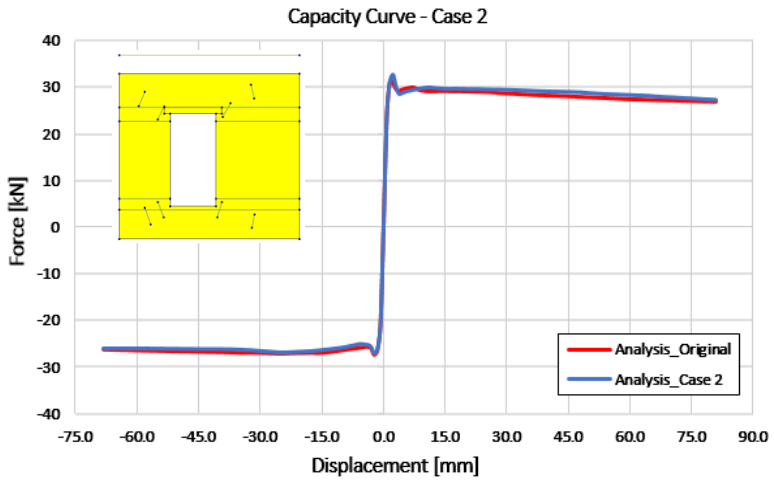

Figure 6-20: Capacity curve – case 2 (Secant Method is used for iteration)

The failure mode of case 2 is similar to case 1 but a moderate arch mechanism can be seen in the window bank as well. The reason is that more reinforcement is applied in the model. In addition, the shear mechanism of the piers is observed since reinforcement in the piers is not introduced to restrains crack opening (Figure 6-21).

Applying a double bar is more effective than the single bar in terms of maximum crack width as well. When this is compared with the original layout a difference of -11.11% (2 mm) in positive and +5.3% (0.75 mm) in the negative direction is observed. Due to very small differences, it is fair to say that the two models have the same crack width. As it was expected tensile force is generated in steel to control the crack opening. As a result, steel reaches yielding point as can be found in Figure 6-21.

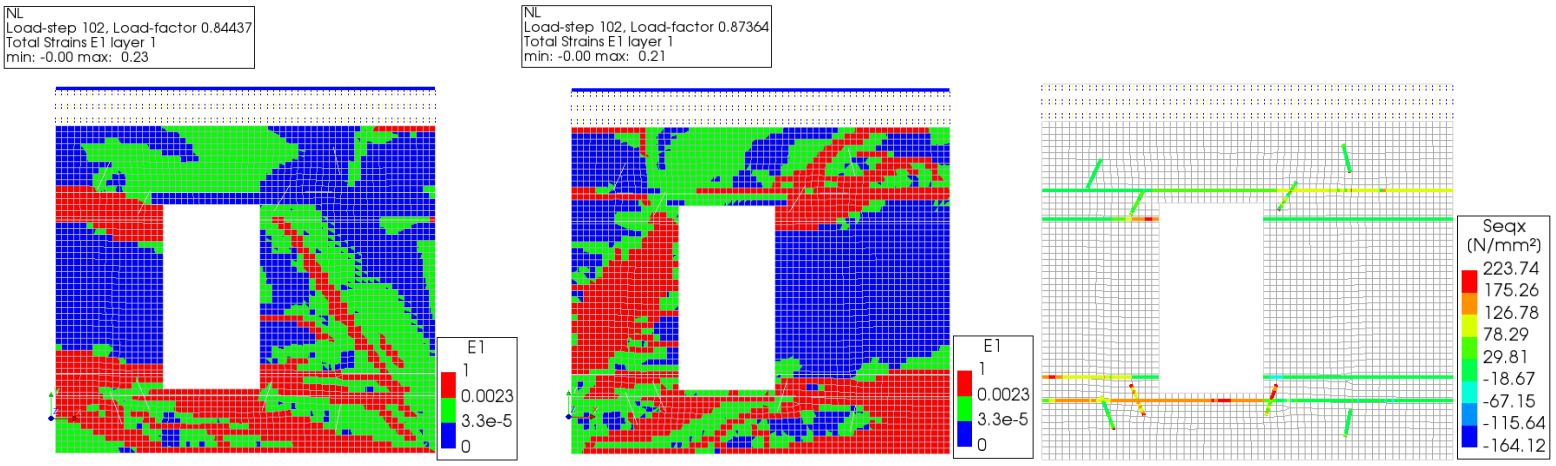

(a) Positive X-direction (b) Negative X-direction (c)

Figure 6-21: Retrofitted wall, case 2. Scaled principal strain (a) and (b). von Mises stress (c)

Table 6-7: Summary of results. Original layout vs. case 2

Model	**Single BJR**	**Double BJR**	**Total Number of BJR**	**ρ (%) $(\frac{V_{bars}}{V_{wall}})$**	**F_{max} (+X) (difference to original) (kN)**	**F_{max} (-X) (difference to original) (kN)**	**Crack width Max. (location) (mm)**
Original layout	■	■	**20**	**0.236**	**31.45**	**27.30**	(+x):19 (at P2) (-x):14.14 (at P5)
Case 2		■	8	0.098	31.10 (-1.12%)	27.10 (-0.088%)	(+x): 17 (at P2) (-11.11%) (-x):14.89 (at P5) (+5.3%)

Table 6-8: Failure modes. Original layout vs. case 2

Model	**Failure Mechanism**
Original layout	• Rocking of the piers • Arch mechanism • Toe-crushing • Sliding of the masonry above the window level with respect to the other portion of the wall
Case 2	• Rocking of the piers • Moderate arch mechanism • Toe-crushing • Sliding of the masonry above the window level with respect to the other portion of the wall • Shear mechanism of piers

In **case 3**, one layer of single bar is added at the top (in the spandrel) and bottom (window bank). Still, no reinforcement is introduced next to the opening.

A difference of -2.06% and -4.07% can be found in the peak-load of the wall compared with the original layout as can be found in Figure 6-22. In case 3, 0.074% while in the original layout 0.245% reinforcement is applied.

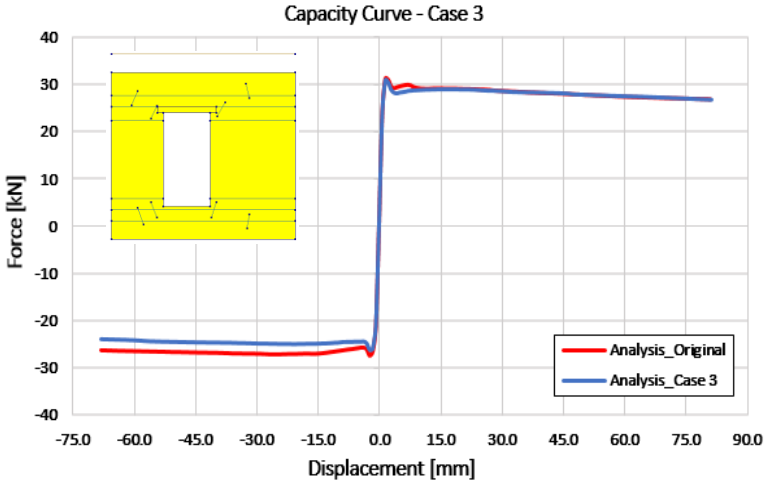

Figure 6-22: Capacity curve – case 3 (Secant Method is used for iteration)

The failure mechanism for case 3 is the same as the original layout with one difference: the shear mechanism is recognized in both piers (Figure 6-23) since reinforcement is not applied on the left and right side of the window opening.

Maximum crack width, meanwhile, is reduced by six bed joint reinforcement and a slight difference of +10% in negative X-direction is observed. In the positive direction, the maximum crack width of 19 mm (the same as the original layout) is recognized. Similar to other cases yielding of the reinforcement due to tension is observed in the model.

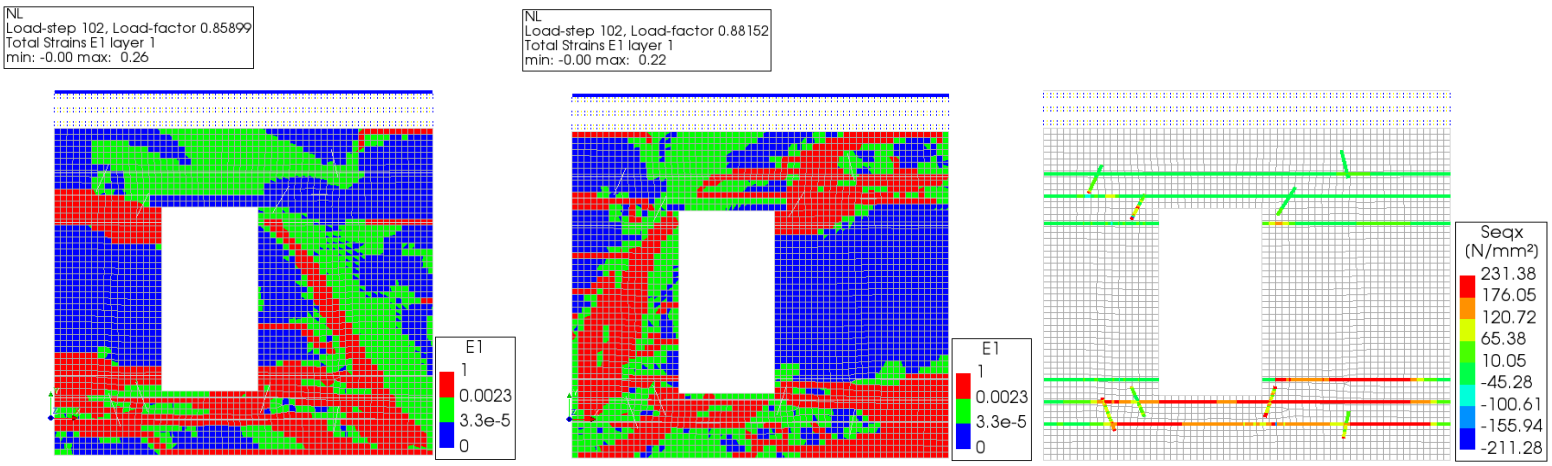

(a) Positive X-direction (b) Negative X-direction (c)

Figure 6-23: Retrofitted wall, case 3. Scaled principal strain (a) and (b). von Mises stress (c)

Table 6-9: Summary of results. Original layout vs. case 3

Model	Single BJR	Double BJR	Total Number of BJR	ρ (%) $(\frac{V_{bars}}{V_{wall}})$	F_{max} (+X) (difference to original) (kN)	F_{max} (-X) (difference to original) (kN)	Crack width Max. (location) (mm)
Original layout	■	■	**20**	**0.236**	**31.45**	**27.30**	(+x):19 (at P2) (-x):14.14 (at P5)
Case 3	■		6	0.074	30.80 (-2.06)	26.25 (-4.07%)	(+x):19 (at P2) (0%) (-x):15.56 (at P5) (+10%)

Table 6-10: Failure modes. Original layout vs. case 3

Model	Failure Mechanism
Original layout	• Rocking of the piers • Arch mechanism • Toe-crushing • Sliding of the masonry above the window level with respect to the other portion of the wall
Case 3	• Rocking of the piers • Arch mechanism • Toe-crushing • Sliding of the masonry above the window level with respect to the other portion of the wall • Shear mechanism of piers

Case 4 follows the same reinforcement pattern of case 3, but double bars are applied in each layer (12 bars is in total).

Force capacity of case 4 is almost the same as the original layout, while the amount of reinforcement is 40% lower in this model. In positive X-direction, a peak-load of 31.19 kN (-0.77 % difference) and in the negative direction an ultimate load of 27.16 kN is obtained (- 0.59% difference).

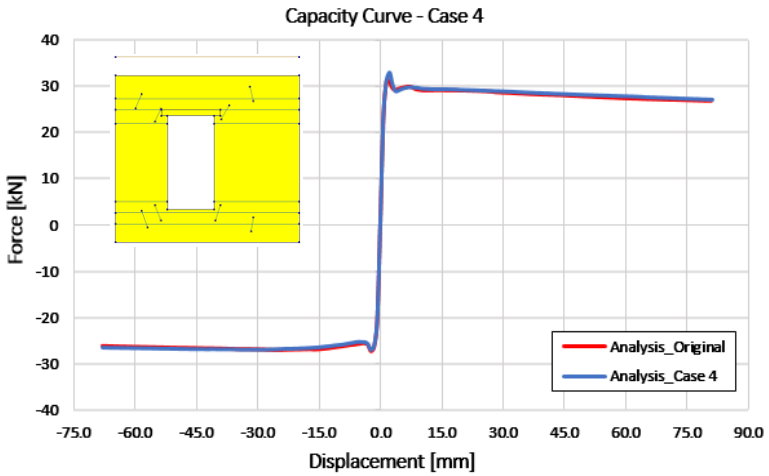

Figure 6-24: Capacity curve – case 4 (Secant Method is used for iteration)

The same failure mechanism as the original layout is recognized in model 4 apart from the shear mechanism of piers that occurs due to the absence of horizontal bars next to the window opening.

This amount of reinforcement (0.147%) is as effective as the original layout in terms of crack width. A difference of -19.97% and +5% in positive and negative direction can be seen. The yielding of the BJR is observed as it was expected.

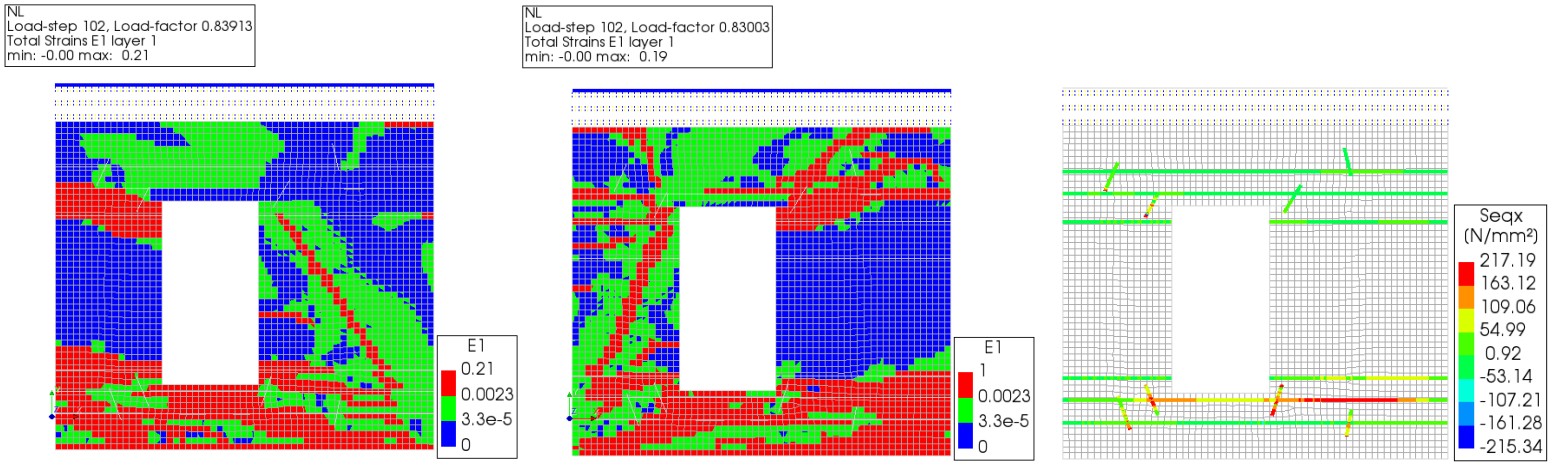

(a) Positive X-direction (b) Negative X-direction (c)

Figure 6-25: Retrofitted wall, case 4. Scaled principal strain (a) and (b). von Mises stress (c)

Table 6-11: Summary of results. Original layout vs. case 4

Model	**Single BJR**	**Double BJR**	**Total Number of BJR**	**ρ (%) ($\frac{V_{bars}}{V_{wall}}$)**	**F_{max} (+X) (difference to original) (kN)**	**F_{max} (-X) (difference to original) (kN)**	**Crack width Max. (location) (mm)**
Original layout	■	■	**20**	**0.236**	**31.45**	**27.30**	(+x):19 (at P2) (-x):14.14 (at P5)
Case 4		■	12	0.147	31.20 (-0.77%)	27.20 (-0.59%)	(+x):15.55 (at P2) (-19.97%) (-x):14.85 (at P5) (+5%)

Table 6-12: Failure modes. Original layout vs. case 4

Model	**Failure Mechanism**
Original layout	• Rocking of the piers • Arch mechanism • Toe-crushing • Sliding of the masonry above the window level with respect to the other portion of the wall
Case 4	• Rocking of the piers • Arch mechanism • Toe-crushing • Sliding of the masonry above the window level with respect to the other portion of the wall • Shear mechanism of piers

In **case 5** more reinforcement along the height of the wall is applied. Four single layers at the top and four single layers below the window level are introduced (0.098% reinforcement).

It is proved that a single layer of bar is less effective than a double layer. -2.02% difference in positive and -3.80% in negative X-direction is recognized compared with the original layout.

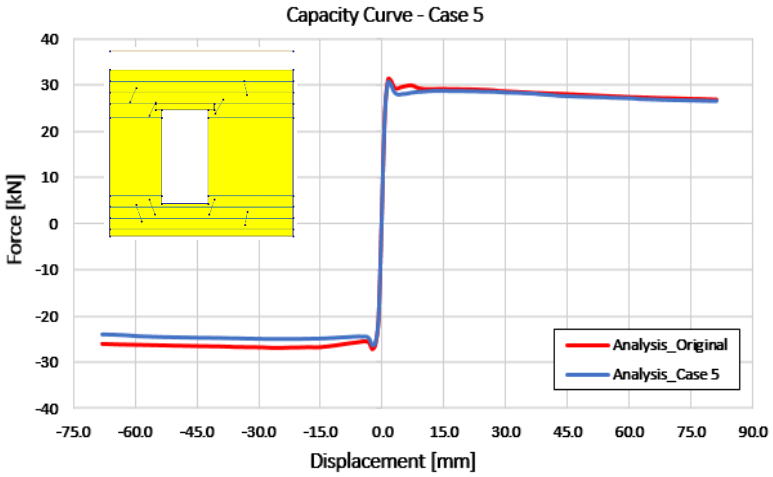

Figure 6-26: Capacity curve – case 5 (Secant Method is used for iteration)

The same failure modes and crack patterns are recognized in case 5 with only one difference similar to previous cases: shear failure of the piers due to removing bars next to the opening.

The same maximum crack width compared to the original layout is observed by increasing the layers of single bars. Almost all masonry portion above and below the opening is reinforced by horizontal bars and only a difference of +9.97% in maximum crack width in the negative direction is noticed. Reinforcement at the bottom of the wall acts in tension and reaches yielding stress as can be seen in Figure 6-27.

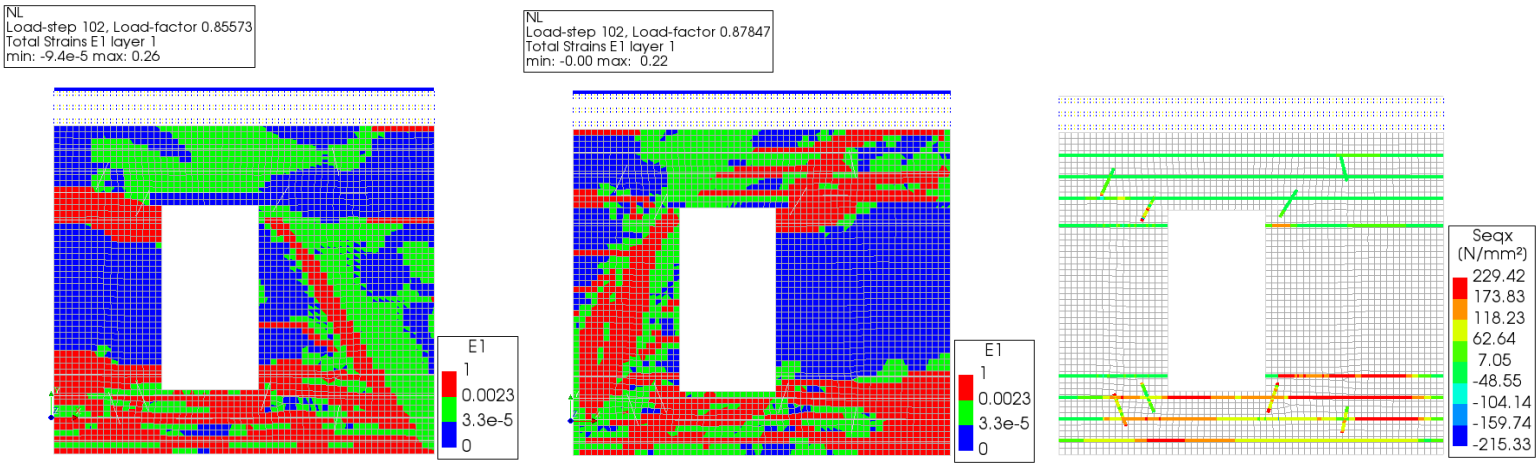

(a) Positive X-direction (b) Positive X-direction (c)

Figure 6-27: Retrofitted wall, case 5. Scaled principal strain (a) and (b). von Mises stress (c)

Table 6-13: Summary result. Original layout vs. case 5

Model	Single BJR	Double BJR	Total Number of BJR	ρ (%) $(\frac{V_{bars}}{V_{wall}})$	F_{max} (+X) (difference to original) (kN)	F_{max} (-X) (difference to original) (kN)	Crack width Max. (location) (mm)
Original layout	■	■	**20**	**0.236**	**31.45**	**27.30**	(+x):19 (at P2) (-x):14.14 (at P5)
Case 5	■		8	0.098	30.80 (-2.02%)	26.30 (-3.80%)	(+x):19 (at P2) (0%) (-x):15.55 (at P5) (+9.97%)

Table 6-14: Original layout vs. case 5

Model	Failure Mechanism
Original layout	• Rocking of the piers • Arch mechanism • Toe-crushing • Sliding of the masonry above the window level with respect to the other portion of the wall
Case 5	• Rocking of the piers • Arch mechanism • Toe-crushing • Sliding of the masonry above the window level with respect to the other portion of the wall • Shear mechanism of piers

The reinforcement pattern of case 5 is repeated for **Case 6** with a double bar in each joint (0.196% reinforcement). The results have revealed that a double bar is more effective than the single bar in terms of peak-load and maximum crack width.

A peak-load of 31.25 kN (positive direction) and 27.30 kN (negative direction) is reached in case 6 that is only -0.57% and -0.073% different compared with the original layout. As can be seen in Figure 6-28 models have the same patterns.

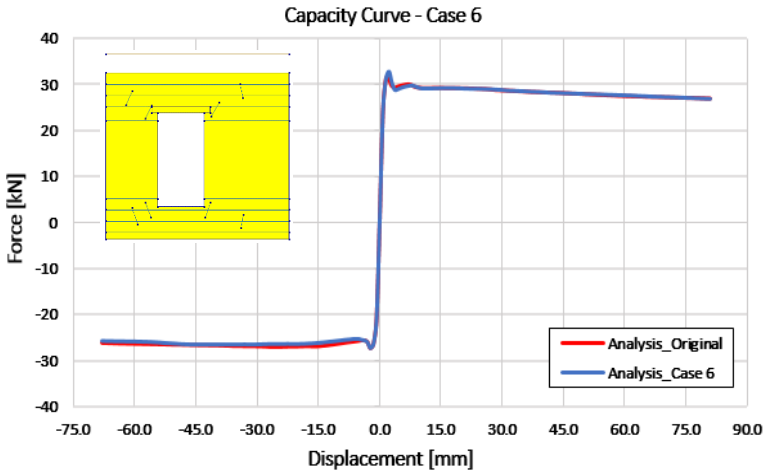

Figure 6-28: Capacity curve – case 6 (Secant Method is used for iteration)

Similar to previous cases, the shear mechanism of the piers is observed as cracks are much more developed in the left and the right piers since no bar is applied there.

In terms of maximum crack width, an improvement compared with a single layer of bar is observed, however, a difference of -19.97% and +5% compared with the original layout is recognized which are too small. Reinforcement located at the bottom of the wall yields due to tensile force generated in steel.

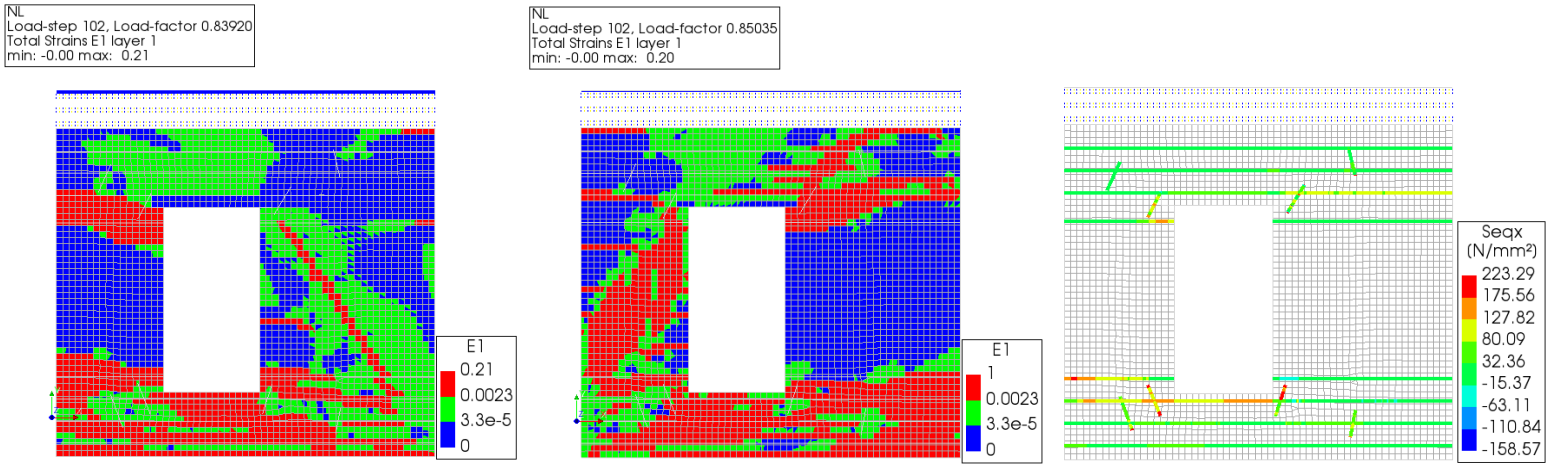

(a) Positive X-direction (b) Negative X-direction (c)

Figure 6-29: Retrofitted wall, case 6. Scaled principal strain (a) and (b). von Mises stress (c)

Table 6-15: Summary of results. Original layout vs. case 6

Model	**Single BJR**	**Double BJR**	**Total Number of BJR**	**ρ (%) $(\frac{V_{bars}}{V_{wall}})$**	**F_{max} (+X) (difference to original) (kN)**	**F_{max} (-X) (difference to original) (kN)**	**Crack width Max. (location) (mm)**
Original layout	■	■	**20**	**0.236**	**31.45**	**27.30**	(+x):19 (at P2) (-x):14.14 (at P5)
Case 6		■	16	0.196	31.25 (-0.57%)	27.30 (-0.073%)	(+x): 15.55 (at P2) (-19.97%) (-x):14.85 (at P5) (+5%)

Table 6-16: Original layout vs. case 6

Model	**Failure Mechanism**
Original layout	• Rocking of the piers • Arch mechanism • Toe-crushing • Sliding of the masonry above the window level with respect to the other portion of the wall
Case 6	• Rocking of the piers • Moderate arch mechanism • Toe-crushing • Sliding of the masonry above the window level with respect to the other portion of the wall • Shear mechanism of piers

The same reinforcement layout used in the experiment is applied in **case 7** with two differences: no bar is applied in the left and right-hand side of the opening and only one bar is introduced in each joint.

Results show a difference of -2.48% and -3.80% in the positive and negative direction for the ultimate load. This decrease is due to the number of bars in joints. It is observed that even 9 layers of single bars are less effective than 4 layers of double bars (case2 with 8 bars in total).

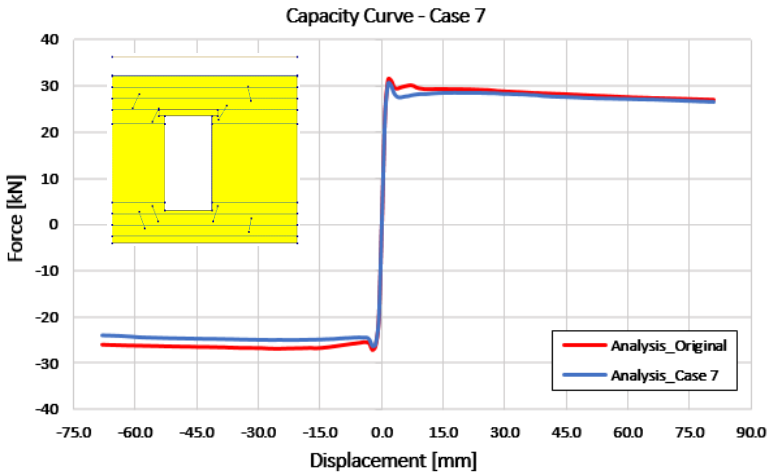

Figure 6-30: Capacity curve – case 7 (Secant Method is used for iteration)

The mechanism of the wall is the same as the previous cases and the shear mechanism of the piers is the only difference between case 7 and the original layout. The shear mechanism of the piers will be prevented by applying horizontal bars next to the opening.

Since a single layer of bar is introduced in the joints a difference of +9.97% in negative direction compared with the original layout is recognized. By applying single bars more bars yield as can be seen in Figure 6-31.

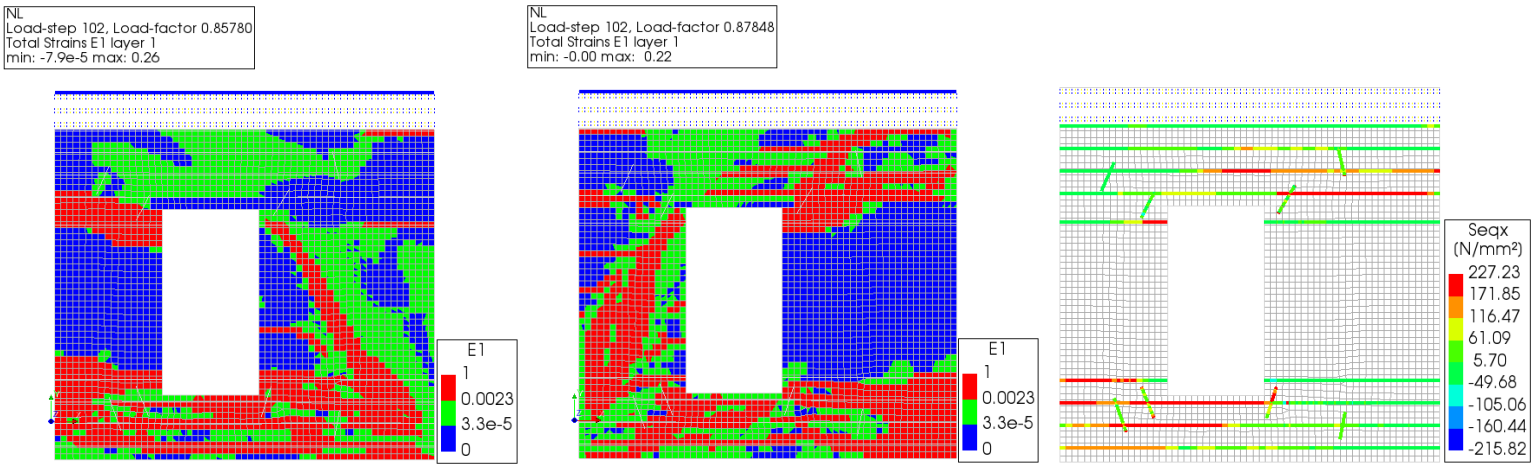

(a) Positive X-direction (b) Negative X-direction (c)

Figure 6-31: Retrofitted wall, case 7. Scaled principal strain (a) and (b). von Mises stress (c)

Table 6-17: Summary of results. Original layout vs. case 7

Model	Single BJR	Double BJR	Total Number of BJR	ρ (%) $(\frac{V_{bars}}{V_{wall}})$	F_{max} (+X) (difference to original) (kN)	F_{max} (-X) (difference to original) (kN)	Crack width Max. (location) (mm)
Original layout	■	■	**20**	**0.236**	**31.45**	**27.30**	(+x):19 (at P2) (-x):14.14 (at P5)
Case 7	■		9	0.110	30.65 (-2.48%)	26.30 (-3.80%)	(+x): 19 (at P2) (0%) (-x): 15.55 (at P5) (+9.97%)

Table 6-18: Original layout vs. case 7

Model	Failure Mechanism
Original layout	• Rocking of the piers • Arch mechanism • Toe-crushing • Sliding of the masonry above the window level with respect to the other portion of the wall
Case 7	• Rocking of the piers • Moderate arch mechanism • Toe-crushing • Sliding of the masonry above the window level with respect to the other portion of the wall • Shear mechanism of piers

Case 8 has the same pattern of case 7 but double bars are introduced in this model. The double bar has a positive effect on the maximum crack width and peak-load of the wall.

As can be seen in Figure 6-32, the force capacity of case 8 and the original layout are the same. A negligible difference of -0.19% and -0.037% in positive and negative X-direction can be found.

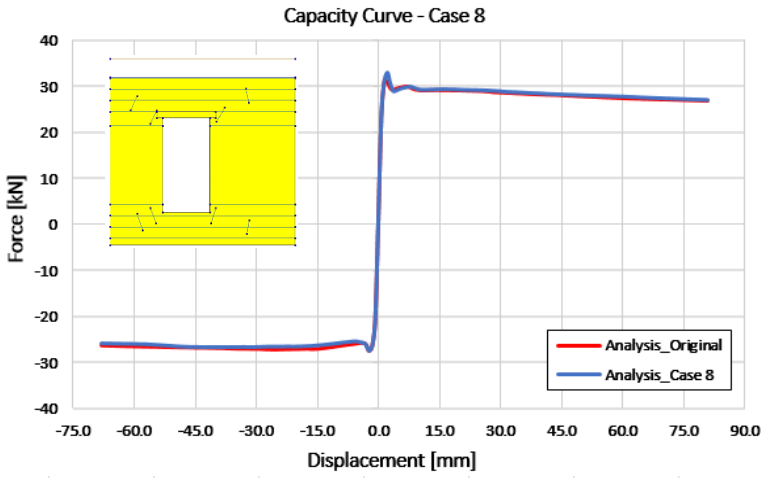

Figure 6-32: Capacity curve – case 8 (Secant Method is used for iteration)

The difference between the failure modes of the wall compared with the previous cases is not recognized. The shear mechanism in piers occurs due to the absence of bed joint reinforcement next to the opening.

The maximum crack width is a bit improved by applying double bars compared with case 7. Furthermore, a difference of -19.97% and +5% in positive and negative X-direction is recognized when it is compared with the original layout. Reinforcement at the bottom of the wall reaches the

yielding point, however, much less amount of reinforcement yields by applying a double bar as can be seen in Figure 6-33.

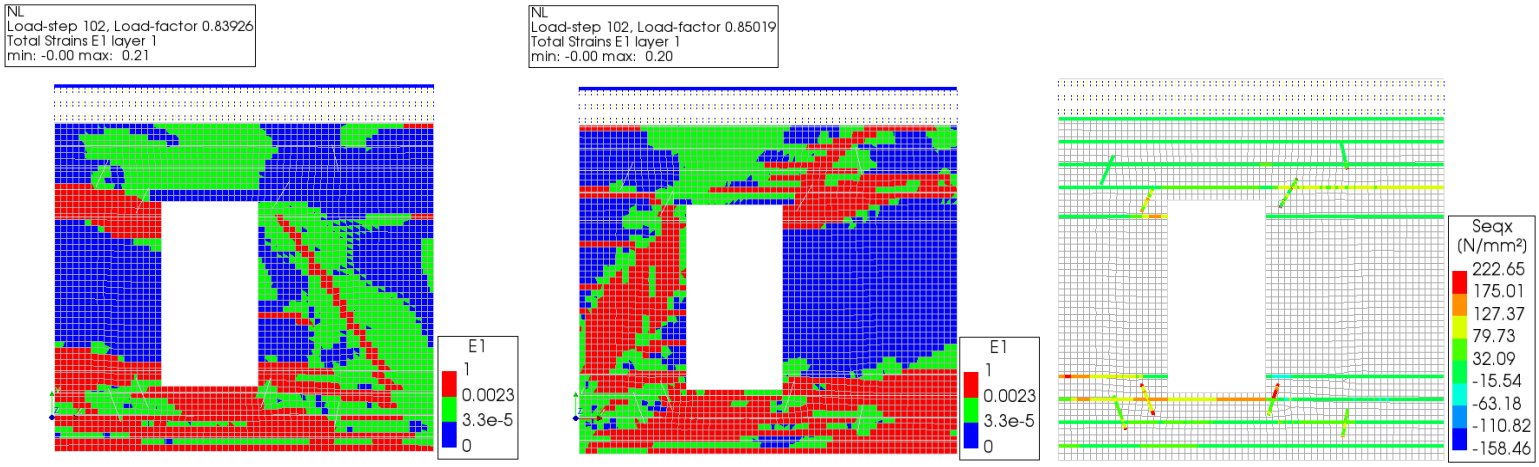

(a) Positive X-direction (b) Negative X-direction (c)

Figure 6-33: Retrofitted wall, case 8. Scaled principal strain (a) and (b). von Mises stress (c)

Table 6-19: Summary of results. Original layout vs. case 8

Model	**Single BJR**	**Double BJR**	**Total Number of BJR**	**ρ (%) ($\frac{V_{bars}}{V_{wall}}$)**	**F_{max} (+X) (difference to original) (kN)**	**F_{max} (-X) (difference to original) (kN)**	**Crack width Max. (location) (mm)**
Original layout	■	■	**20**	**0.236**	**31.45**	**27.30**	(+x):19 (at P2) (-x):14.14 (at P5)
Case 8		■	18	0.221	31.40 (-0.19%)	27.30 (-0.037%)	(+x):15.55 (at P2) (-19.97%) (-x):14.85 (at P5) (+5%)

Table 6-20: Original layout vs. case 8

Model	**Failure Mechanism**
Original layout	• Rocking of the piers • Arch mechanism • Toe-crushing • Sliding of the masonry above the window level with respect to the other portion of the wall
Case 8	• Rocking of the piers • Moderate arch mechanism • Toe-crushing • Sliding of the masonry above the window level with respect to the other portion of the wall • Shear mechanism of piers

Case 9 follows the same reinforcement pattern of case 8 but a single bar is added in the piers to observe if the shear mechanism of the piers can be prevented.

A negligible difference in terms of peak-load is obtained as can be seen in Figure 6-34. Case 9 reaches to 31.43 kN (+X) and 27.32 kN (-X) while these values are 31.43 kN (+X) 27.32 kN (-X) for the wall with the original layout.

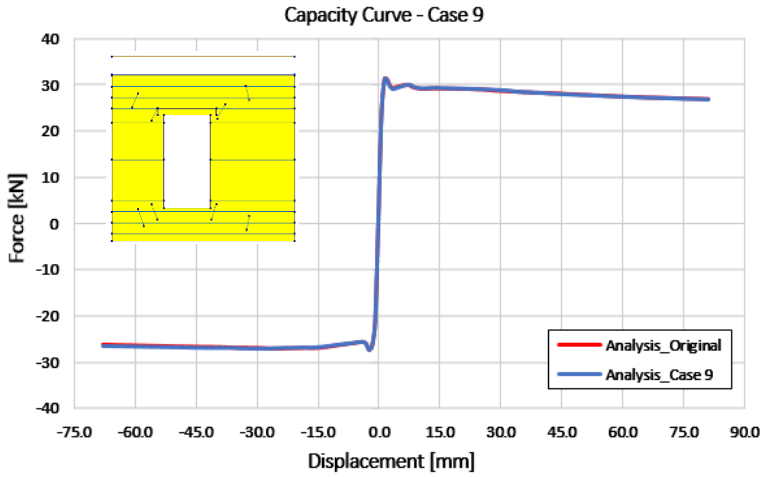

Figure 6-34: Capacity curve – case 9 (Secant Method is used for iteration)

Figure 6-35 shows that single bed joint reinforcement in the left and right-hand side of the window opening can prevent shear mechanism of the piers by restricting the development of the cracks that lead to yielding of the single BJR as it is showing in

Figure 6-35. However, it is observed that applying only one layer of the bar is not sufficient to prevent the shear failure of the piers as it is not controlled completely.

The maximum crack width in both directions does not change considerably compared with case 8 and is exactly the same as the original layout.

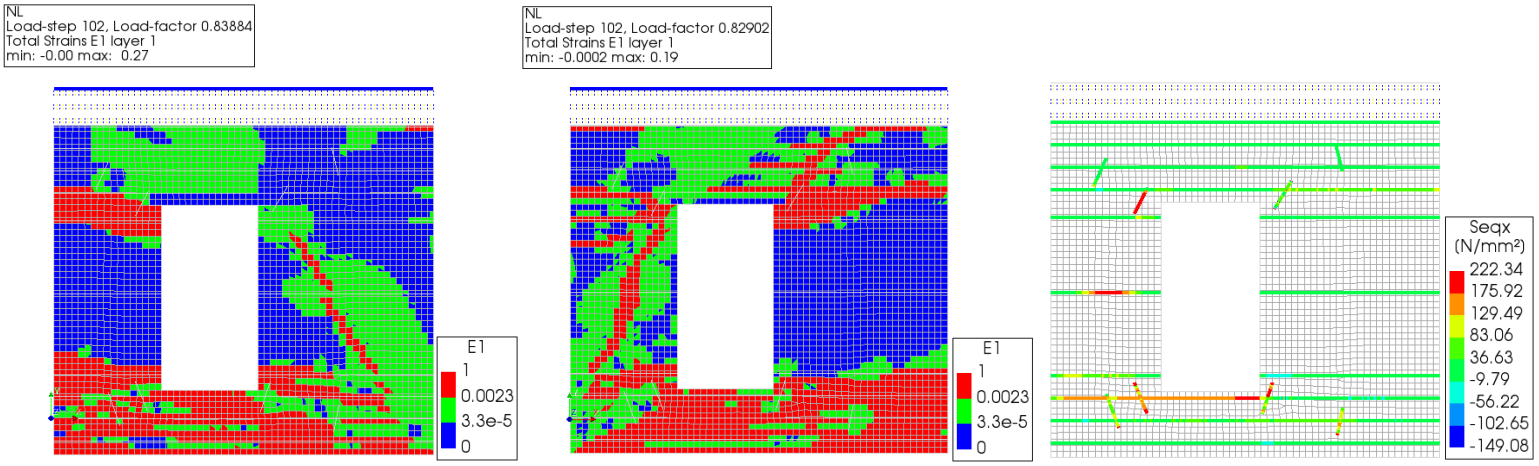

(a) Positive X-direction (b) Negative X-direction (c)

Figure 6-35: Retrofitted wall, case 9. Scaled principal strain (a) and (b). von Mises stress (c)

Table 6-21: Summary of results. Original layout vs. case 9

Model	Single BJR	Double BJR	Total Number of BJR	ρ (%) ($\frac{V_{bars}}{V_{wall}}$)	F_{max} (+X) (difference to original) (kN)	F_{max} (-X) (difference to original) (kN)	Crack width Max. (location) (mm)
Original layout	■	■	**20**	**0.236**	**31.45**	**27.30**	(+x):19 (at P2) (-x):14.14 (at P5)
Case 9	■	■	19	0.230	31.40 (-0.10%)	27.30 (-0.037%)	(+x):19 (at P2) (0%) (-x):14.14 (at P5) (0%)

Table 6-22: Original layout vs. case 9

Model	Failure Mechanism
Original layout	• Rocking of the piers • Arch mechanism • Toe-crushing • Sliding of the masonry above the window level with respect to the other portion of the wall
Case 9	• Rocking of the piers • Moderate arch mechanism • Toe-crushing • Sliding of the masonry above the window level with respect to the other portion of the wall • Shear mechanism of piers

An even distribution of double bed joint reinforcement with equal distance (180mm) is applied for **case 10**. In total, 30 bars (0.698% reinforcement) that are 10 layers more than the original layout (0.236% reinforcement) shows a small difference in terms of peak-load and maximum crack width.

An ultimate load of 31.55 kN (+0.38% difference to original) in positive and 27.44 kN (+0.44% difference to original) in negative X-direction is observed as can be found in Figure 6-36. This difference is obtained by a 200% increase in reinforcement that is not reasonable due to the considerable increase in the retrofitting cost.

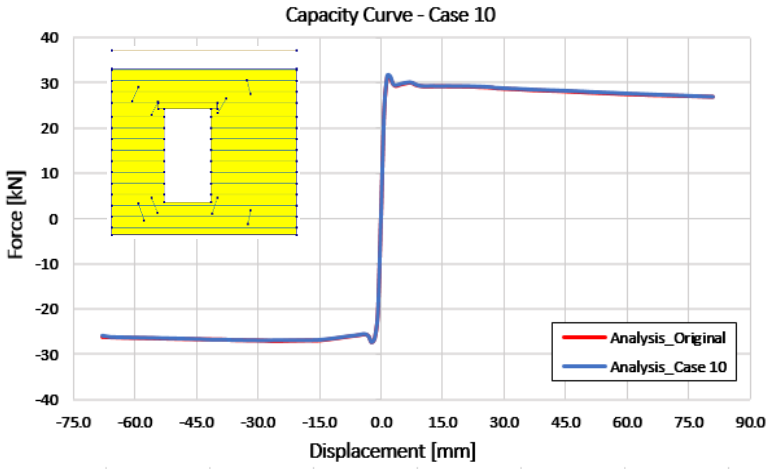

Figure 6-36: Capacity curve – case 10 (Secant Method is used for iteration)

The situation is the same for failure modes and crack width (Figure 6-37). The remarkable amount of reinforcement improves the maximum crack width slightly: -11.29 in positive X-direction but this value was obtained by lower reinforcement in previous cases. Furthermore, failure modes are the same as the original layout. It can be seen that with at least 3 horizontal bars in the left and right-hand side of the opening, shear mechanism of the piers is prevented and fully open cracks (red strain in contour) are restricted. Therefore, considering 12 bars that are applied next to the opening in case 10 is believed to be not an effective action.

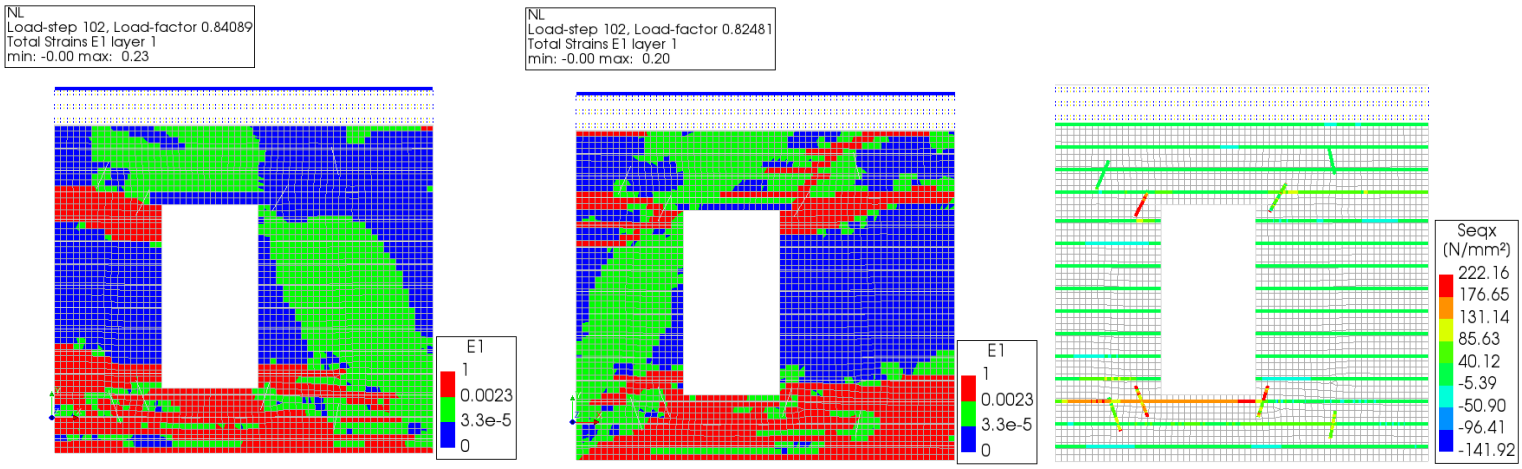

(a) Positive X-direction (b) Negative X-direction (c)

Figure 6-37: Retrofitted wall, case 10. Scaled principal strain (a) and (b). von Mises stress (c)

Table 6-23: Summary of results. Original layout vs. case 10

Model	**Single BJR**	**Double BJR**	**Total Number of BJR**	**ρ (%) $(\frac{V_{bars}}{V_{wall}})$**	**F_{max} (+X) (difference to original) (kN)**	**F_{max} (-X) (difference to original) (kN)**	**Crack width Max. (location) (mm)**
Original layout	■	■	**20**	**0.236**	**31.45**	**27.30**	(+x):19 (at P2) (-x):14.14 (at P5)
Case 10		■	30	0.698	31.55 (+0.38%)	27.45 (+0.44%)	(+x): 16.97 (at P2) (-11.29%) (-x):14.14 (at P5) (0%)

Table 6-24: Original layout vs. case 10

Model	**Failure Mechanism**
Original layout	• Rocking of the piers • Arch mechanism • Toe-crushing • Sliding of the masonry above the window level with respect to the other portion of the wall
Case 10	• Rocking of the piers • Moderate arch mechanism • Toe-crushing • Sliding of the masonry above the window level with respect to the other portion of the wall

Case 11 has the same reinforcement pattern of the original layout but with a single bar for each layer. The amount of applied reinforcement is decreased by 40% in this model.

By applying single rebar per layer, a decrease in peak-load is observed similar to previous cases that were modeled with a single layer of reinforcement. In the positive X-direction, ultimate loads decrease from 31.43 kN to 30.80 kN (a difference of -2.02%). In negative X-direction, a difference of -2.37% (from 27.32 kN to 26.68 kN) is recognized.

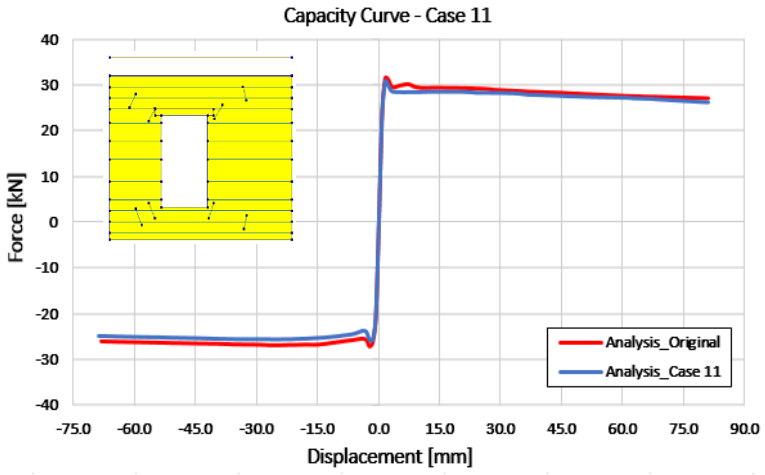

Figure 6-38: Capacity curve – case 11 (Secant Method is used for iteration)

Crack pattern and failure mode of case 11 and the original layout are the same (Figure 6-39). This is due to having a similar reinforcement layout along with the height of the wall. The maximum crack width, however, is more desirable in the original layout as double reinforcement is more effective for this parameter. A difference of +7.6% and +20% are recognized in positive and negative direction respectively. As explained before, by applying single BJR more plasticity is observed in the steel.

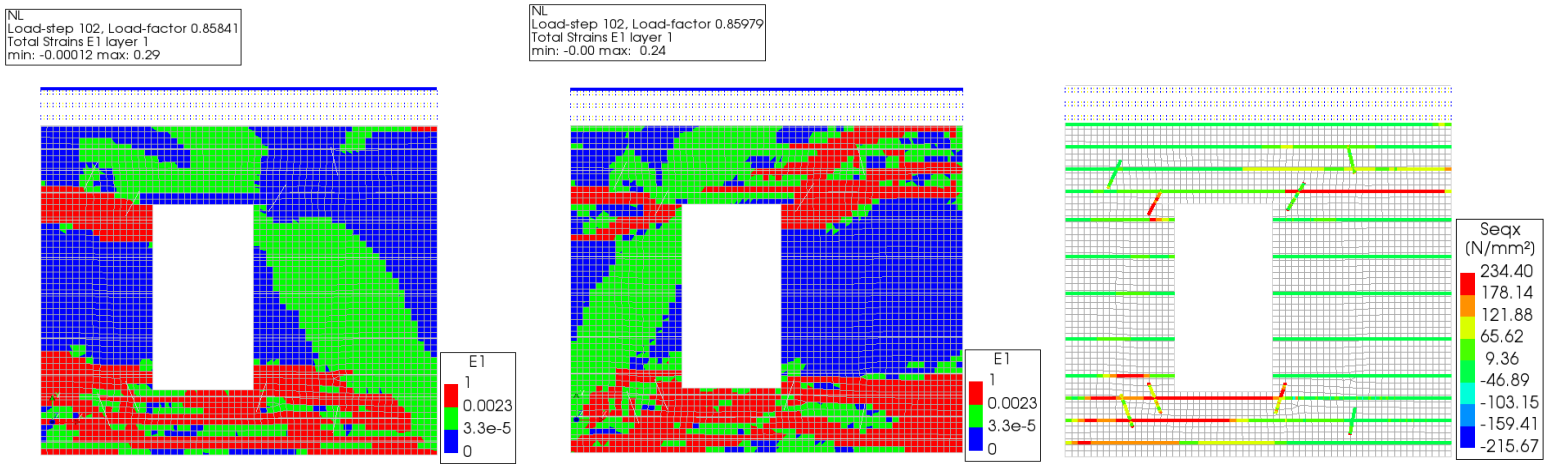

(a) Positive X-direction (b) Negative X-direction (c)

Figure 6-39: Retrofitted wall, case 11. Scaled principal strain (a) and (b). von Mises stress (c)

Table 6-25: Summary of results. Original layout vs. case 11

Model	Single BJR	Double BJR	Total Number of BJR	ρ (%) $(\frac{V_{bars}}{V_{wall}})$	F_{max} (+X) (difference to original) (kN)	F_{max} (-X) (difference to original) (kN)	Crack width Max. (location) (mm)
Original layout	■	■	**20**	**0.236**	**31.45**	**27.30**	(+x):19 (at P2) (-x):14.14 (at P5)
Case 11	■		12	0.138	30.80 (-2.02%)	26.70 (-2.37%)	(+x):20.5 (at P2) (+7.6%) (-x): 16.97 (at P5) (+20%)

Table 6-26: Original layout vs. case 11

Model	Failure Mechanism
Original layout	• Rocking of the piers • Arch mechanism • Toe-crushing • Sliding of the masonry above the window level with respect to the other portion of the wall
Case 11	• Rocking of the piers • Moderate arch mechanism • Toe-crushing • Sliding of the masonry above the window level with respect to the other portion of the wall

According to the numerical results, it can be concluded that double bed joint reinforcement (BJR) is slightly more effective than BJR in terms of peak-load as can be seen in Figure 6-43. By applying only 4 layers of double bed joint reinforcement (BJR) the peak-load of the original layout with a difference of -1% is obtained. The location of the BJR is essential. In the URM wall cracks mostly developed diagonally from the window corners. By applying BJR just below and above the opening (Figure 6-40) not only the maximum crack width drops but also the diagonal cracks are restricted and failure mechanism of the wall changes (Table 6-28 presents the failure modes for all cases). With this layout, the peak-load, the maximum crack width in principal direction, and failure modes are comparable with the original reinforcement layout with a substantial decrease in reinforcement ratio (0.245% vs. 0.098%). It can be observed that for the single and double BJR, by increasing the number of layers (thus the reinforcement ratio) of the reinforcements the force capacity of the wall does not change noticeably, Figure 6-43.

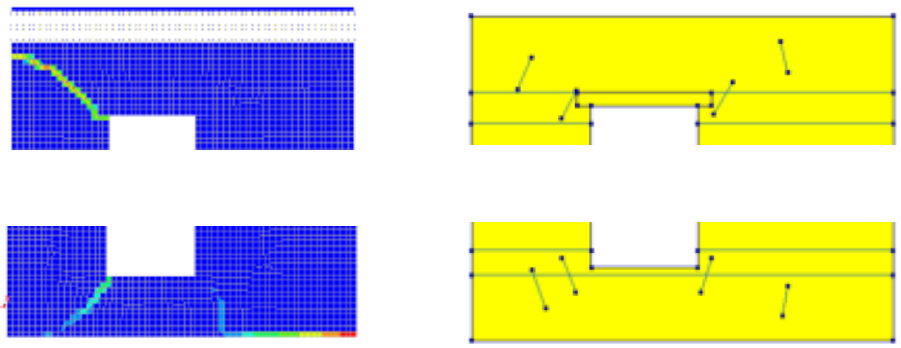

Figure 6-40: BJR just below and above the opening in order to prevent diagonal cracks

However, the absence of BJR that is introduced on the left and right-hand side of the opening might lead to the shear mechanism of the piers. Figure 6-41 presents this phenomenon and the necessary BJR.

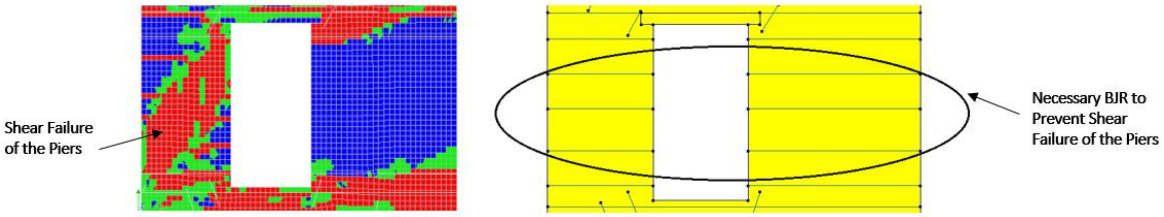

(a) (b)

Figure 6-41: Shear mechanism of the pier (a) and necessary BJR to prevent shear mechanism (b)

Tensile stress in the BJR is another property that can be measured by numerical modeling. Because of the spiral shape of the BJR, the results of the strain gauges obtained by the experiment are not reliable (Petersen et al., 2012). Bars act in tension to restrain the crack opening. By checking von Mises stress in the steel, it is observed that regardless of the number of the BJR in the thickness (single or double BJR) and along with the height of the wall, yielding point reaches in all 12 cases (from 217 to 234 MPa). However, by applying double BJR a decrease in the amount of plasticity in the steel is observed as shown in Figure 6-42 where cases 7 and 8 are presented as an example.

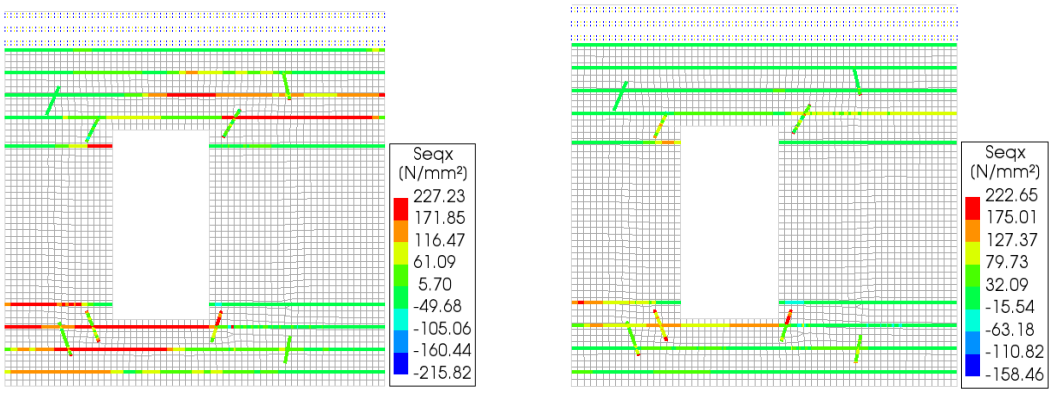

(a) (a)

Figure 6-42: Yielding of BJR. Case 7 single BJR (a) and case 8 double BJR (b)

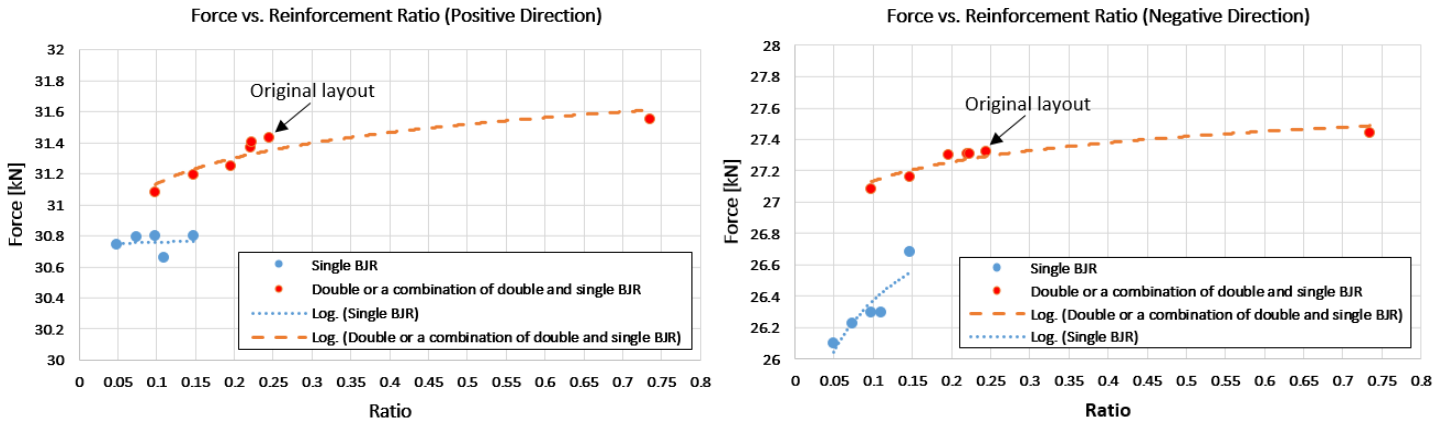

Figure 6-43: Peak-load vs. reinforcement ratio for all 12 cases

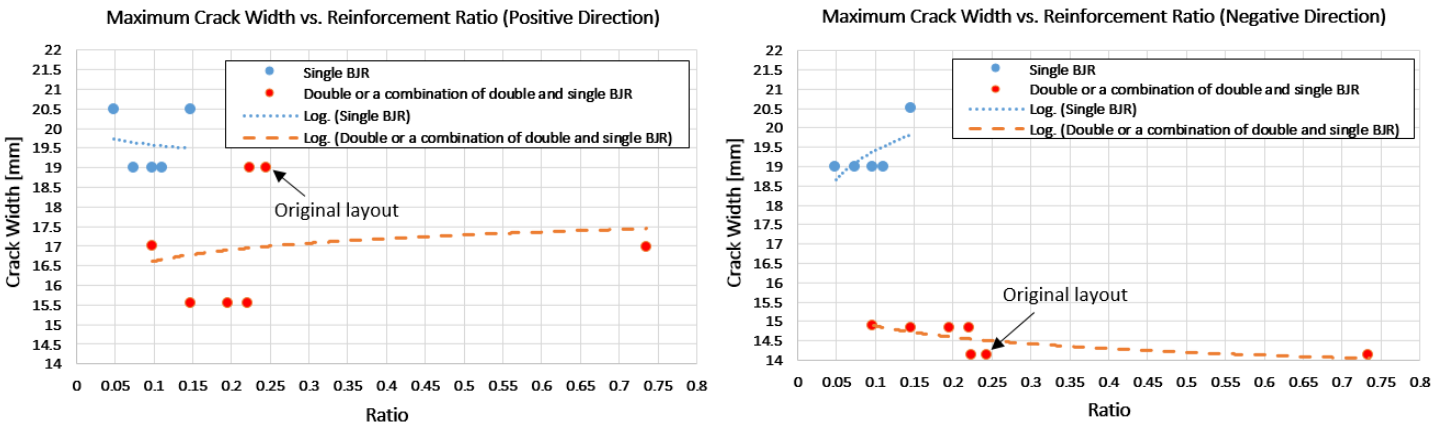

Figure 6-44: Maximum crack width in principal direction vs. reinforcement ratio for all 12 cases

Table 6-27: Summary of results of the parametric study. Reinforcement layout, percentage of reinforcement, peak-load and maximum crack width

Model	**Single BJR**	**Double BJR**	**Total Number of BJR**	**ρ (%) $(\frac{V_{bars}}{V_{wall}})$**	**F_{max} (+X) (diff. to original) (kN)**	**F_{max} (-X) (diff. to original) (kN)**	**Crack width Max. (location) (mm)**	**Crack width Max. diff. to original layout**
Original layout	■	■	**20**	**0.236**	**31.45**	**27.30**	**(+x):19 (at P2) (-x):14.14(at P5)**	**-**
Case 1	■		4	0.049	30.75 (-2.22%)	26.10 (-4.57%)	(+x): 20.5 (at P2) (-x):19 (at P5)	(+x): (+7.60%) (-x): (+34.37%)
Case 2		■	8	0.098	31.10 (-1.12%)	27.10 (-0.088%)	(+x): 17 (at P2) (-x):14.89 (at P5)	(+x): (-11.11%) (-x): (+5.3%)
Case 3	■		6	0.074	30.80 (-2.06)	26.20 (-4.07%)	(+x):19 (at P2) (-x):15.56 (at P5)	(+x): (0%) (-x): (+10%)
Case 4		■	12	0.147	31.20 (-0.77%)	27.15 (-0.59%)	(+x):15.55 (at P2) (-x):14.85 (at P5)	(+x): (-19.97%) (-x): (+5%)
Case 5	■		8	0.098	30.80 (-2.02%)	26.30 (-3.80%)	(+x):19 (at P2) (-x):15.55 (at P5)	(+x): (0%) (-x): (+9.97%)
Case 6		■	16	0.196	31.25 (-0.57%)	27.30 (-0.073%)	(+x): 15.55 (at P2) (-x):14.85 (at P5	(+x): (-19.97%) (-x): (+5%)
Case 7	■		9	0.110	30.70 (-2.48%)	26.30 (-3.80%)	(+x): 19 (at P2) (-x): 15.55 (at P5)	(+x): (0%) (-x): (+9.97%)
Case 8		■	18	0.221	31.40 (-0.19%)	27.30 (-0.037%)	(+x):15.55 (at P2) (-x):14.85 (at P5)	(+x): (-19.97%) (-x): (+5%)
Case 9	■	■	19	0.230	31.40 (-0.10%)	27.30 (-0.037%)	(+x):19 (at P2) (-x):14.14 (at P5)	(+x): (0%) (-x): (0%)
Case 10		■	30	0.698	31.55 (+0.38%)	27.45 (+0.44%)	(+x): 16.97 (at P2) (-x):14.14 (at P5)	(+x): (-11.29%) (-x): (0%)
Case 11	■		12	0.138	30.80 (-2.02%)	26.70 (-2.37%)	(+x):20.5 (at P2) (-x): 16.97 (at P5)	(+x): (+7.6%) (-x): (+20%)

Table 6-28: Failure mechanisms of the models

Model	Failure Mechanism
Original layout	• Rocking of the piers • Arch mechanism • Toe-crushing • Sliding of the masonry above the window level with respect to the other portion of the wall
Case 1	• Rocking of the piers • Toe-crushing • Sliding of the masonry above the window level with respect to the other portion of the wall • Shear mechanism of piers
Case 2	• Rocking of the piers • Moderate arch mechanism • Toe-crushing • Sliding of the masonry above the window level with respect to the other portion of the wall • Shear mechanism of piers
Case 3-9	• Rocking of the piers • Arch mechanism • Toe-crushing • Sliding of the masonry above the window level with respect to the other portion of the wall • Shear mechanism of piers
Case 10	• Rocking of the piers • Moderate arch mechanism • Toe-crushing • Sliding of the masonry above the window level with respect to the other portion of the wall
Case 11	• Rocking of the piers • Moderate arch mechanism • Toe-crushing • Sliding of the masonry above the window level with respect to the other portion of the wall

6.5 Retrofitted wall with proposed reinforcement layout

In this section, a desirable reinforcement layout is suggested based on the previous analyses. Peak-load, crack pattern, maximum crack width and failure modes are in a good agreement with the original reinforcement layout, however, the ration of the reinforcement is decreased by 30% in this model that is shown in Figure 6-45. Since diagonal anchors increase the retrofitting cost and do not affect the results remarkably, 8 anchors are removed in the suggested layout.

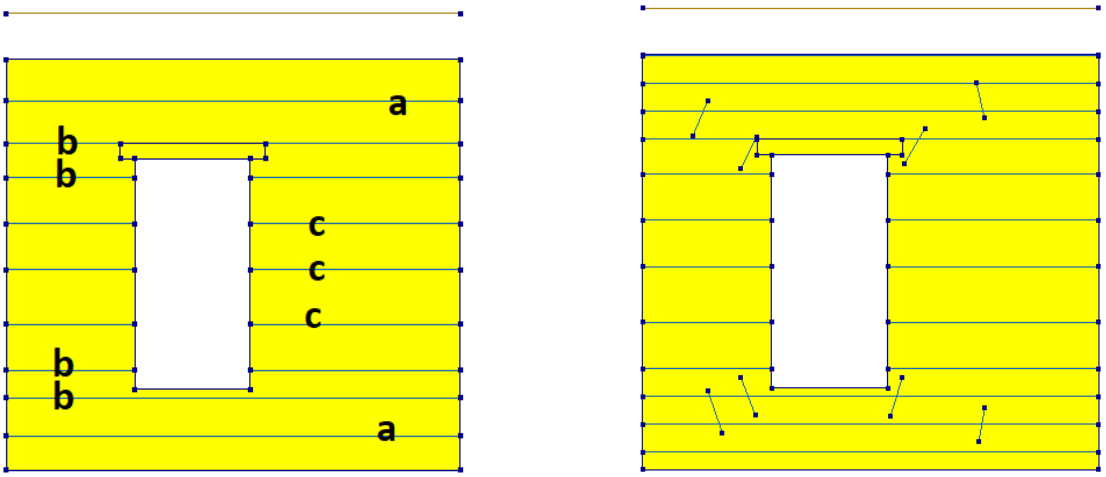

(a) (b)

Figure 6-45: suggested layout (a) and original layout (b)

Each layer of bed joint reinforcement (BJR) is applied for a certain reason. Layers are numbered with ***a***, ***b***, and ***c*** in Figure 6-45. The aim of the applying layers is as follows. Comparisons are made between the suggested layout and the original layout.

Layer *a*, that is a double BJR, does not change the peak-load, crack pattern and maximum crack width of the wall (one model without layers ***a*** was analyzed and results are the same as suggested layout*).* However, it prevents the possible sliding/failure of the masonry portion above the opening with respect to the rest of the wall. This phenomenon is not visible clearly in the model since a macro-modeling is applied for this research. Thus, it is suggested that do not leave the masonry above the lintel and below the opening unreinforced.

By contrast, **layer *b***, double BJR, is vital for improving the behavior of the wall. By applying these 4 layers (8 BJR) the results are is in good agreement with the original layout in terms of peak-load and maximum crack width.

Finally, single BJR **layer *c*** is necessary to prevent the shear mechanism of the piers (also see Figure 6-41). Neither force capacity nor maximum crack width of the model is improved by layer ***c***.

Figure 6-46, 47show the force capacity and crack pattern of the retrofitted wall with the proposed reinforcement layout. As can be seen, only a difference of -1.31 % is observed in the suggested reinforcement layout with respect to the original layout. Crack pattern and failure mechanisms are similar to the one obtained for the original reinforcement layout.

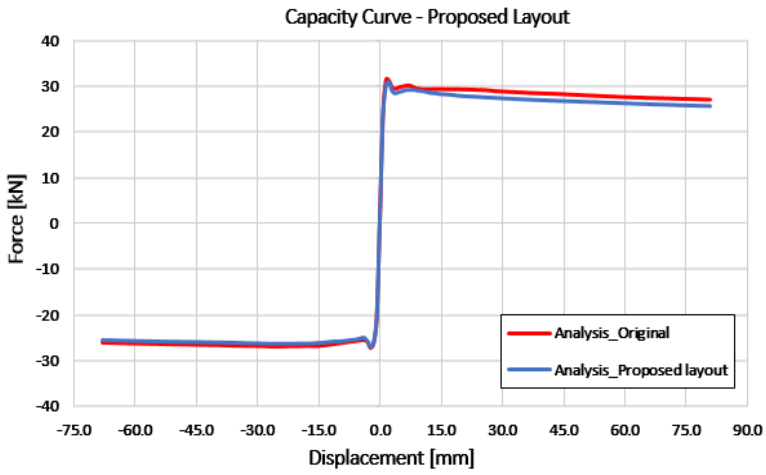

Figure 6-46: Force capacity – proposed reinforcement layout (Secant Method is used for iteration)

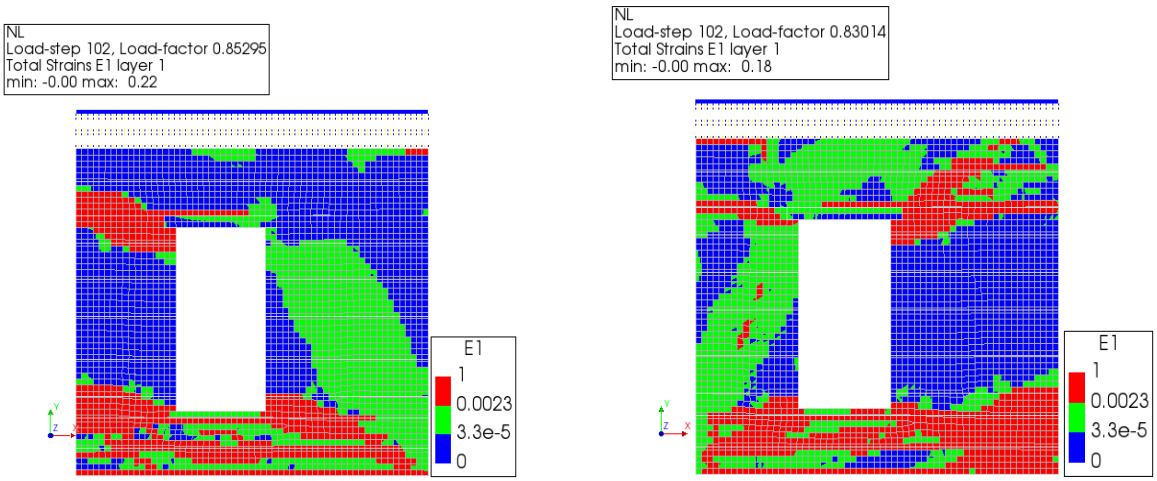

(a) Displacement = +81 mm (b) Displacement = -64 mm

Figure 6-47: Proposed reinforcement layout, scaled principal strain

Table 6-29: Summary of results. Original layout vs. proposed layout

Model	**Single BJR**	**Double BJR**	**Total Number of BJR**	**ρ (%) $(\frac{V_{bars}}{V_{wall}})$**	**F_{max} (+X) (difference to original) (kN)**	**F_{max} (-X) (difference to original) (kN)**	**Crack width Max. (location) (mm)**
Original layout	■	■	**20**	**0.245**	**31.45**	**27.30**	(+x):19 (at P2) (-x):14.14 (at P5)
Proposed layout	■	■	15	0.174	31 (-1.31%)	27.10 (-0.88%)	(+x): 16.26 (at P2) (-29.33%) (-x): 12.72 (at P5) (-10.5%)

6.6 Conclusions

The numerical analyses show that the improved performance of the retrofitted wall with respect to the URM wall is due to mainly the bed joint reinforcement. The application of only diagonal anchors (with both original and extended length) is not effective. In this case, the analyses show that the force capacity slightly increases but the failure modes (rocking of the piers) and maximum crack width almost do not change. In contrast, applying only bed joint reinforcement leads to a significant decrease in maximum crack width with respect to the one observed for the URM wall. This occurs because steel acts in tension and crack opening is restricted. In addition, the force capacity of the wall slightly increases (a difference of +9% in the positive and +17% in the negative X-direction is observed). Moreover, the wall retrofitted with only bed joint reinforcement shows a similar failure mechanism as the wall experimentally tested.

The numerical results of the different reinforcement layout show that double bed joint reinforcement (BJR) is slightly more effective than single BJR. By applying only 4 layers of double BJR (like case 2), similar peak-load can be reached comparing the results of the retrofitted wall with an original layout with a negligible difference. However, the location of the BJR is essential. To prevent the propagation of the diagonal cracks, BJR should be placed above and below the window opening. Crack width in principal direction can be restricted by the mentioned 4 layers as well. However, the absence of reinforcement in the masonry portion next to the window opening (piers) leads to the formation of shear cracks. For the studied wall, at least 3 layers of single BJR next to the window opening are necessary to prevent the shear failure of the piers. This may depend on the dimension (height) of the window opening.

An important property that can be measured by numerical modeling is tensile stress in the BJR. Bars act in tension to restrain the crack opening. For all the considered reinforcement layouts, yielding of the reinforcement occurred during the analysis. However, by applying double BJR, a decrease in plastic deformation is observed.

7

CONCLUSIONS and RECOMMENDATIONS

This chapter describes a summary of the research, including background problems, research questions, and the objective of the thesis. Then numerical results are presented in the conclusion section. Finally, the limitation of the models is discussed in the recommendation section.

7.1 Summary

Unreinforced masonry buildings located in the northern part of the Netherlands are damaged due to the gas-induced earthquakes. These types of buildings are vulnerable to seismic loads and effective action is required to be taken to improve the seismic resilience of these structures. In order to achieve this purpose, existing structures must be retrofitted. The retrofitting technique is determined by the importance of the building. For historical buildings, for instance, the appearance of the property may not be changed. An experimental campaign was conducted at Delft University of Technology (Licciardello & Esposito, 2019) to investigate whether bed joint reinforcement (BJR) can be implemented for seismic retrofitting of URM walls. The BJR is often used to repair damage in URM structures caused by settlement. This technique is of interest to historical buildings since does not alter the aesthetic of the structures. A cantilever asymmetric URM wall retrofitted with 12 layers of BJR and 8 diagonal anchors around the opening corner were tested. An in-plane quasi-static cyclic load was applied and results before and after retrofitting were compared. Experimental results of the retrofitted wall showed that the force capacity increased slightly and maximum crack width decreased noticeably compared with the URM wall.

In this thesis, the experimental test was investigated further via several numerical models. The most accurate finite element model for the URM and the retrofitted wall was obtained. Furthermore, the influence of the BJR and diagonal anchors on the in-plane behavior of the wall was studied. The influence of only diagonal anchor, its length and the effect of only BJR on the performance of the wall was checked. In addition, the sensitivity of the results to the variation of material properties was examined and finally, 11 reinforcement layouts were designed to investigate the effect of the number of BJR in the thickness as well as along with the height of the wall. Then a proposed reinforcement layout was provided accordingly.

7.2 Conclusions

1. Totals Strain Crack Model (**TSCM**) was adopted to model the unreinforced masonry (**URM**) and **retrofitted wall**. The numerical results showed that TSCM can predict the crack pattern, failure mechanisms, peak-load (with an accuracy of 12%), and initial stiffness of the structure in good agreement with the experiment. An acceptable simulation was found for diagonal stair-case cracks, rocking of the piers and bed joint cracks, toe-crushing and arch mechanism. Results obtained from the analyses showed that this isotropic material model is a good choice when an appropriate iterative method is applied.

2. Engineering Masonry Model (**EMM**) was also initially adopted in this study to model the **URM** and the **retrofitted wall**, nevertheless convergence problems were reported. The trend of the force-displacement curves are in good agreement with the experiment, however, due to the convergence problems, results cannot be considered after reaching the peak-load. Although various iterative methods, different material properties and extremely small load steps were applied, no convergent solution was found in this study. It must be mentioned that EMM was successfully used by other researchers at TU Delft and acceptable results were obtained.

3. Although numerical results are in good agreement with the experiment using **TSCM**, an influence of the **iterative method** on the results was reported. By reaching 50 mm displacement (the positive X-direction), **divergence** occurred when Regular Newton-Raphson method (RNR) was adopted. To solve this problem the Secant Method was applied and as a result, no divergence problem was experienced in the models. However, two problems arose: higher peak-loads were obtained in the models (within 25%) and no localization of cracks in one finite element was reported. Considering the scope of this project, the mathematics procedure involved in these two iterative methods was not investigated but according to a discussion with DIANA FEA support team, the number of cracked integration points might affect the peak-load. By applying the Secant Method, four times more cracked integration points compared with RNR were reported. Therefore, this research recommends more investigation and improvement in this iterative method by DIANA.

4. Numerical results showed that by applying **bed joint reinforcement (BJR),** the seismic performance of the wall was improved, however, diagonal anchors did not influence the results significantly. An increment of 13% was observed in the peak-load of the retrofitted wall. The maximum crack width was also affected by applying reinforcement. This parameter decreased by 87% in the positive and 70% in the negative X-direction at ultimate displacements. Bars acts in tension to restrain the cracks and by checking von Mises stress, the plasticity of steel was recognized. In the unstrengthened wall, rocking of the piers was the main mechanism. However, in the strengthened wall, apart from rocking of the piers that occurred initially, an arch mechanism (a network of cracks bellow the window level) was observed due to the presence of horizontal bars. In addition, toe-crushing at the bottom right corner of the retrofitted was noticed.

5. The **sensitivity analysis** revealed that results were insensitive to the variation of compressive strength, compressive fracture energy, and tensile strength. By contrast, results were affected by changing the modulus of elasticity and tensile fracture energy. The former affected the initial stiffness, peak-load, and maximum crack width while the latter changed peak-load and maximum crack width.

6. In the first and second parts of the **parametric study**, the influence of the retrofitted wall with **only diagonal anchors** and **extended diagonal anchors** were investigated. Numerical results showed a negligible difference in the force capacity of the structure without any changes in the failure mechanisms of the retrofitted walls. Applying the diagonal anchors led to a variation of initiation and propagation of the cracks and cracks smeared from the above and below the bars instead of the opening corners. In other words, the initiation, propagation and, location of the cracks were altered with the same crack width observed in the URM wall. Therefore, applying only diagonal anchors (even with extended length) was not an effective method for retrofitting of the wall.

7. The effect of **only bed joint reinforcement** (BJR) on the behavior of the wall was another parameter that was checked in the **parametric study**. The force capacity of the wall was improved by applying only BJR (a difference of +9% compared with the URM wall was observed). Furthermore, BJR has a substantial effect on the crack pattern,

maximum crack width, and failure mechanism of the retrofitted wall as well. In the URM wall, rocking of the piers was recognized as the main mechanism. By contrast, in the retrofitted wall, the same mechanism was observed initially, although increasing the deformation resulted in occurrence of an arch mechanism in the masonry portion bellow the window level. In addition, rocking of the piers took place with higher lateral loads. Since the cracks spread over the entire wall, a new crack pattern was developed in the structure. It was seen in this research that BJR decreased the crack width locally and globally. For the case of the URM wall, in positive X-direction, the maximum crack width of 147 mm was reported while this value dropped to 17 mm (88% difference) by applying BJR. Considering the opposite direction, a difference of 118% in the maximum crack width was reported (48 mm vs. 12 mm). This reduction in the crack width is due to tensile stress in steel. The diagonal anchors did not affect the result considerably and they could be ignored to reduce the retrofitting costs.

8. An extensive **parametric study** was performed to show the effect of the **reinforcement layout** on the performance of the retrofitted wall. 12 different reinforcement layouts (including the original reinforcement layout) were studied accordingly. It can be concluded that double bed joint reinforcement (BJR) is more effective than single BJR in terms of peak-load and maximum crack width. By applying only 4 layers of double BJR almost the same peak-load and maximum crack width were obtained comparing the results of the retrofitted wall with the original layout (with 12 BJR layers). The location of the BJR, however, was an important issue. It was vital to restrict diagonal cracks that initiated and propagated from window opening corners by horizontal bars so, BJR must be applied just below and above the opening accordingly. Furthermore, it was found that 3 single BJR next to the opening (in piers) were able to prevent shear failure of the piers. In the absence of these layers wide fully open diagonal cracks were recognized in the piers that might lead to shear failure.

9. Another property that can be measured by numerical modeling is the **tensile stress** of the **bed joint reinforcement (BJR)**. As explained before, BJR acts in tension to prevent crack opening and as a result, for all the considered reinforcement layouts, yielding of the reinforcement occurred during the analysis. By applying double BJR, plasticity decreased in bars and von Mises stress in steel was in a range of 225 MPa in the models.

10. By analyzing the numerical results, a proposed reinforcement layout can be presented: the mentioned 4 layers of double BJR and 3 layers of single BJR next to the opening were a good layout for retrofitting of the wall and diagonal anchors could be ignored. Conservatively, a layer of double BJR far above and below the window level should be applied. It is suggested to not to leave the masonry portion above the lintel and below the window opening unreinforced. In the proposed model the amount of reinforcement was decreased by 30%, however, the force capacity, crack patterns and failure modes of the model were comparable with the retrofitted wall with the original reinforcement layout.

7.3 Recommendations

1. The loading scheme of the experiment and the numerical model was not the same in this research. In the former cyclic load while in the latter monotonic load was applied. The different peak-loads between test and analysis might be solved by considering a cyclic load. Nevertheless, if a cyclic load is applied the Engineering Masonry Model should be adopted instead of The Total Strain Crack Model because the former adopts constitutive laws able to properly describe the energy dissipation of the material under cyclic loading. Consequently, the related convergence problem should be solved.

2. Engineering Masonry Model (EMM) is another material model that is more helpful for cyclic loads. Different head-joint failure types can be chosen by the user by applying EMM. So, after solving the convergence issue it can be a good material model to be used for simulating the crack patterns and failure modes of the wall.

3. This research focused on the in-plane behavior of the wall, however, in the near-collapse phase of the experimental test (displacement = -63 mm and +81 mm), the out-of-plane deformation of the retrofitted wall was reported. Although, this was not the governing failure mechanism of the sample more investigation in the numerical modeling is recommended through applying the shell element instead of the plane stress element.

BIBLIOGRAPHY

Breiholz, D. C. (1993). Centercore strengthening system for seismic hazard reduction of unreinforced masonry bearing wall buildings. *Structural Engineering in Natural Hazards Mitigation*, 319–324.

Campbell, J., & Durán, M. (2017). Numerical model for nonlinear analysis of masonry walls. *Revista de La Construccion*, *16*(2), 189–201. https://doi.org/10.7764/RDLC.16.2.189

Dashti, F., Dhakal, R. P., & Pampanin, S. (2017). Numerical Modeling of Rectangular Reinforced Concrete Structural Walls. *Journal of Structural Engineering (United States)*, *143*(6). https://doi.org/10.1061/(ASCE)ST.1943-541X.0001729

DIANA FEA. (2019). *DIANA FEA_Manuals*. https://dianafea.com/diana-manuals

Elgawady, M. A., & Lestuzzi, P. (2004). A review of conventional seismic retrofitting techniques for URM. *13th International Brick and Block Masonry Conference*, 1–10. http://imacwww.epfl.ch/GenieParasismique/EDOC_ST09/Course_6/old/89ElGA 13-IBMaC state of the art.pdf

Ghiassi, B., Soltani, M., & Tasnimi, A. A. (2012). Seismic evaluation of masonry structures strengthened with reinforced concrete layers. *Journal of Structural Engineering (United States)*, *138*(6), 729–743. https://doi.org/10.1061/(ASCE)ST.1943-541X.0000513

Korswagen, P. A., Longo, M., Meulman, E., & Rots, J. G. (2019). Crack initiation and propagation in unreinforced masonry specimens subjected to repeated in-plane loading during light damage. In *Bulletin of Earthquake Engineering* (Vol. 17, Issue 8). Springer Netherlands. https://doi.org/10.1007/s10518-018-00553-5

Licciardello, L., & Esposito, R. (2019). *EXPERIMENTAL STUDY ON UNREINFROCED MASONRY STRENGTHENED WITH BED JOINT REINFORCEMENT*.

Licciardello, L., Rots, J., & Esposito, R. (2020). Performance of unreinforced masonry strengthened with bed joint reinforcements. *12th International Conference on Structural Analysis of Historical Constructions (SAHC), 16-18 September, Barcelona, Spain*.

Lourenço, P., Rots, J., & Blaauwendraad, J. (1995). Two approaches for the analysis of masonry structures. *Heron*, *40*(4), 313–340.

M.A.N. Hendriks, Boer, A. de, & Belletti, B. (2017). *Guidelines for Nonlinear Finite Element Analysis of Concrete Structures*. http://homepage.tudelft.nl/v5p05/RTD 1016-1(2017) version 2.1 Guidelines for Nonlinear Finite Element Analysis of Concrete Structures.pdf%0Ahttp://www.dianausers.nl/pub/20120516 Guidelines NLFEA-final.pdf

Mulder, M., & Perey, P. (2018). Gas production and earthquakes in Groningen reflection on economic and social consequences. In *CEER Policy Papers. Centre for Energy Economics Research, University of Groningen* (Vol. 3, Issue 3). http://www.rug.nl/feb/

Petersen, R. B., Ismail, N., Masia, M. J., & Ingham, J. M. (2012). Finite element modelling of unreinforced masonry shear wallettes strengthened using twisted steel bars. *Construction and Building Materials*, *33*, 14–24. https://doi.org/10.1016/j.conbuildmat.2012.01.016

Schreppers, G. M. A., Garofano, A., Messali, F., & Rots, J. G. (2017). *DIANA Validation report for Masonry modelling*. 1–143.

van der Voort, N., & Vanclay, F. (2015). Social impacts of earthquakes caused by gas extraction in the Province of Groningen, The Netherlands. *Environmental Impact Assessment Review*. https://doi.org/10.1016/j.eiar.2014.08.008

FEMA. 2000. *Prestandard and Commentary for the Seismic Rehabilitation of Buildings*. FEMA 365

FEMA. 1998. *Evaluation of Earthquake Damaged Concrete and Masonry Wall Buildings: Basic Procedure Manuals.* FEMA 306

FEMA. 1997. *NEHRP Guidelines for the Seismic Rehabilitation of Buildings*. FEMA 273

APPENDICES

A

Appendix A

This appendix reports mesh refinement and its effect on the numerical result of the wall.

Mesh refinement is an important factor that can determine the accuracy of an FE result. Here 4 mesh sizes (100*100, 50*50, 25*25, and 12.5*12.5mm^2) are check to see which ones give the most accurate result. Also, the effect of mesh size on divergence is studied. The Regular Newton-Raphson Method for Iteration is used. Wall is only loaded leftwards and TSCM is used as the material model.

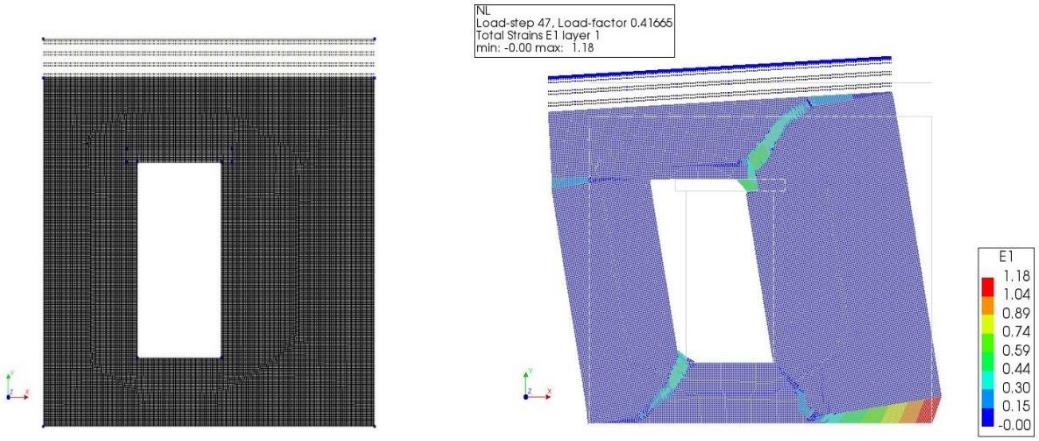

Mesh size 12.5 mm

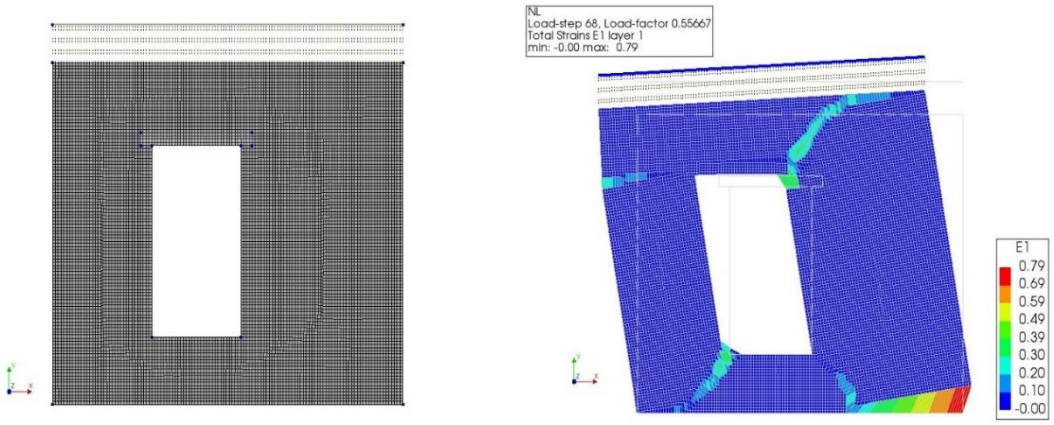

Mesh size 25 mm

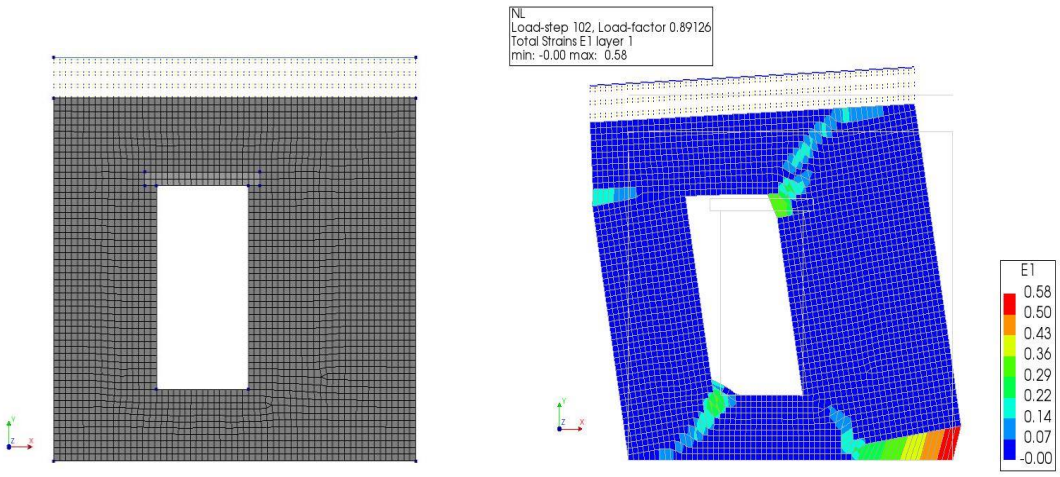

Mesh size 50 mm

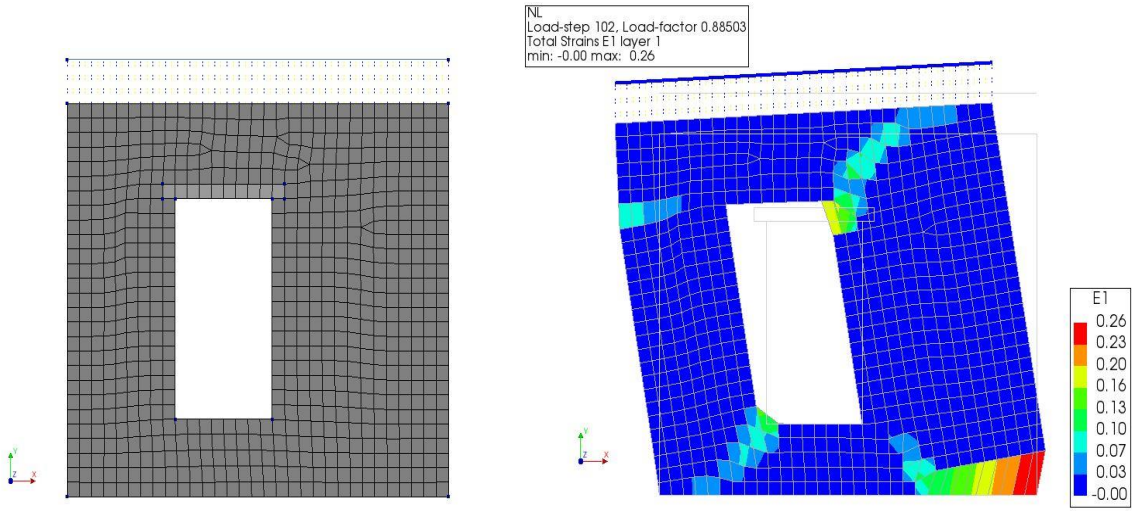

Mesh size 100

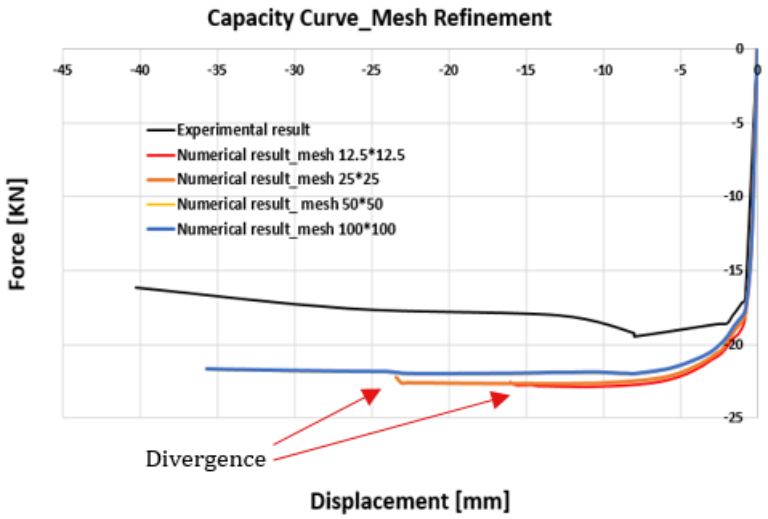

Capacity curve

Table 1

Model	Load step	Divergence	Peak-load (kN)	Difference to Test (peak load)
Experimental	N/A	N/A	19.40	N/A
Mesh 12.5*12.5	0.4 mm [0.01(100)]	Yes	22.90	**+15%**
Mesh 25*25	0.4 mm [0.01(100)]	Yes	22.70	**+14.40%**
Mesh 50*50	0.4 mm [0.01(100)]	No	22	**+11.70%**
Mesh 100*100	0.4 mm [0.01(100)]	No	22.30	**+12.95%**

From mesh refinement, it is concluded that coarse mesh not only gives less error in peak load but also prevents divergence in the model. The element size of 50*50 gives the most accurate result in terms of peak load. Regarding the cracking pattern, all models have the same result.

B

Appendix B

This appendix shows four possible head-joint failures when the wall is modeled by Engineering Masonry Model. Failure types are as follows.

Head-Joint Failure Not Considered: Based on the experimental results 0.107 MPa is chosen for bed joint strength and fracture energy in tension is 0.0085 $\frac{N}{mm}$.

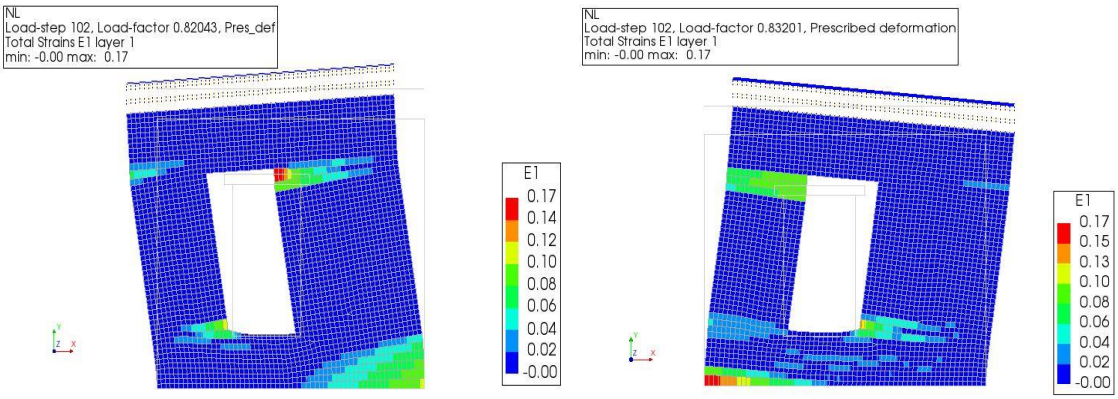

Secant Method E1, head joint failure not considered

Direct Input Head-Joint Tensile Strength: Direct head-joint and bed joint strength can be used for this model. Based on the experimental tests the former is 0.433 MPa and the latter is 0.107 MPa. Fracture energy in tension is 0.0085 $\frac{N}{mm}$.

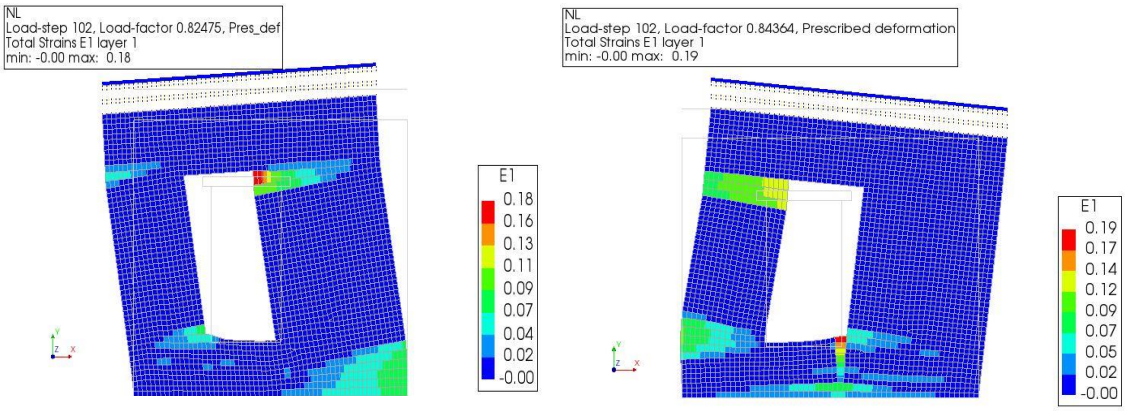

Secant Method E1, Direct Input Head-Joint Tensile Strength

***Diagonal Stair*-Case Cracks:** Bed joint tensile strength is set as 0.107 MPa. Fracture energy in tension is 0.0085 $\frac{N}{mm}$ and it is assumed that the angle between stepped diagonal crack and bed joint is 0.5 radians.

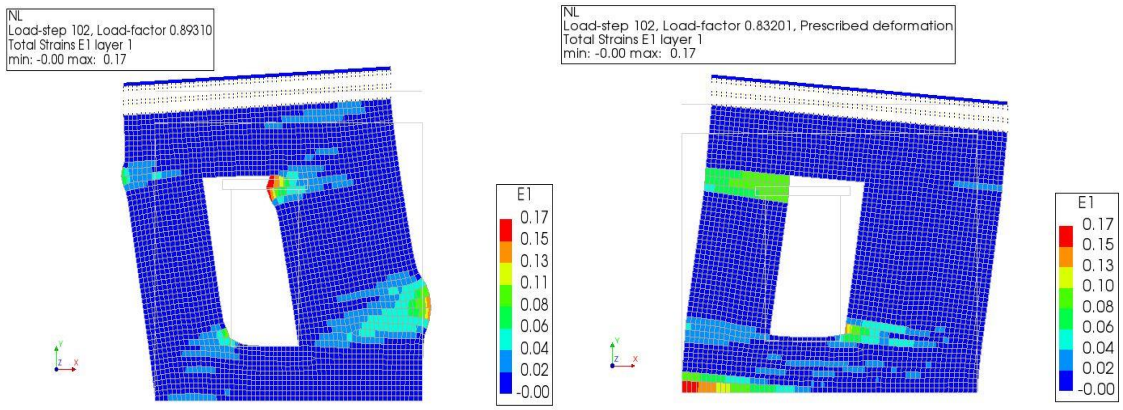

Secant Method E1, Diagonal Stair-Case Cracks

Tensile Strength Head-Joint Defined by Friction: In this model bed joint tensile strength and minimum head-joint tensile strength are considered as 0.107 MPa. Fracture energy in tension is 0.0085 $\frac{N}{mm}$ and it is assumed that the angle between stepped diagonal crack and bed joint is 0.5 radian.

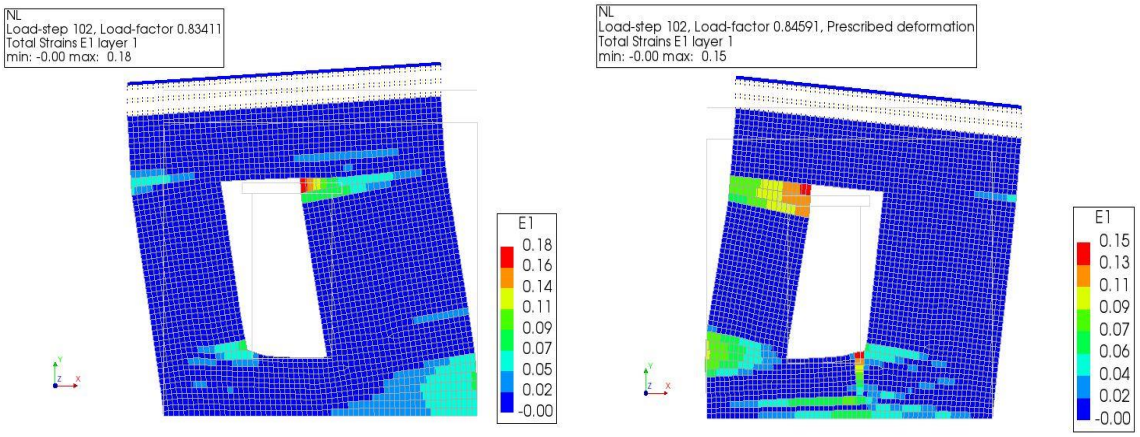

Secant Method E1, Tensile Strength Head-Joint Defined by Friction

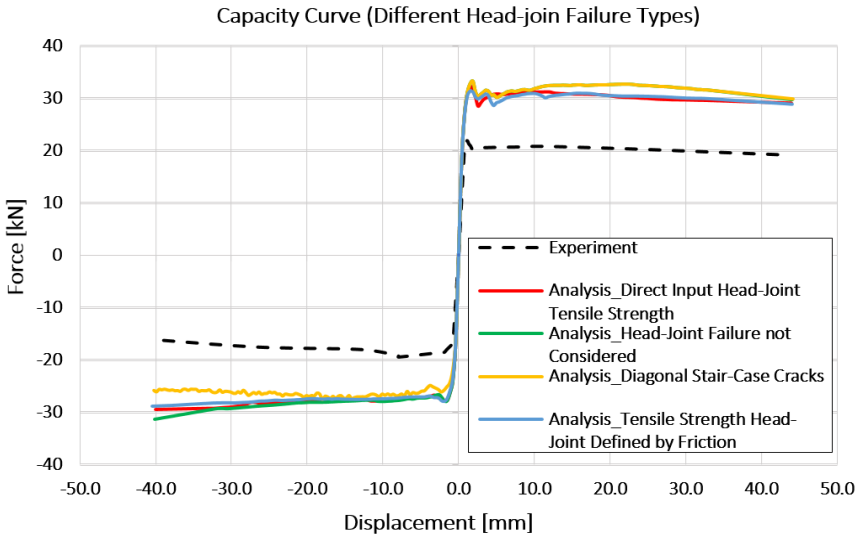

Capacity curve

Table 2

Element Type	Head-Joint Failure Type	Iterative Method	peak load (-X) (kN)	peak load (+ X) (kN)	Difference to Test (peak load) (+ X)	Difference to Test (peak load) (- X)	Crack pattern
Experiment	-----	-----	19.45	23.45	-----	-----	-----
Q8MEM	Head-Joint Failure not Considered	Quasi-Newton	29.55	33.25	**+41.70%**	**+52%**	**Non-converge solution**
Q8MEM	Direct Input Head-Joint Tensile Strength	Quasi-Newton	29.25	32.30	**+37.60%**	**+50.60%**	**Non-converge solution**
Q8MEM	Diagonal Stair-Case Cracks	Quasi-Newton	27.50	33.25	**+41.70%**	**+41.55%**	**Non-converge solution**
Q8MEM	Tensile Strength Head-Joint Defined by Friction	Quasi-Newton	28.40	31.30	**33.55%**	**46%**	**Non-converge solution**

C

Appendix C

This appendix shows the convergence history of the wall modeled by TSCM and EMM loaded in the negative and positive X-direction. The Python code provided by DIANA FEA BV (Arjen de Putter, MSc intern at DIANA FEA BV) is used to plot the convergence history of the models.

For both models 102 load steps are set. Convergence tolerance for energy and force norm are 0.001 and 0.01 respectively. A can be seen many load steps are not converged when EMM is used, however, TSCM provides an acceptable result.

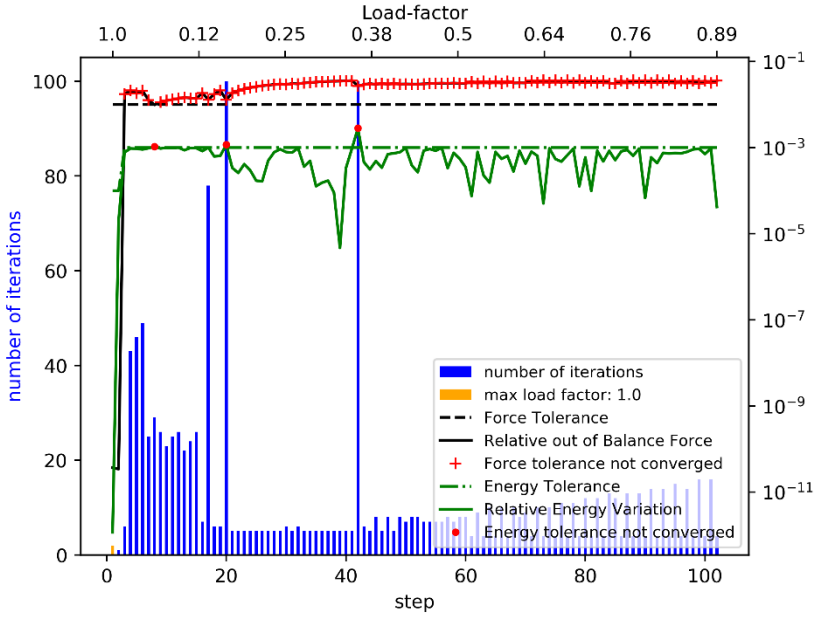

TSCM URM Wall (negative X-direction)

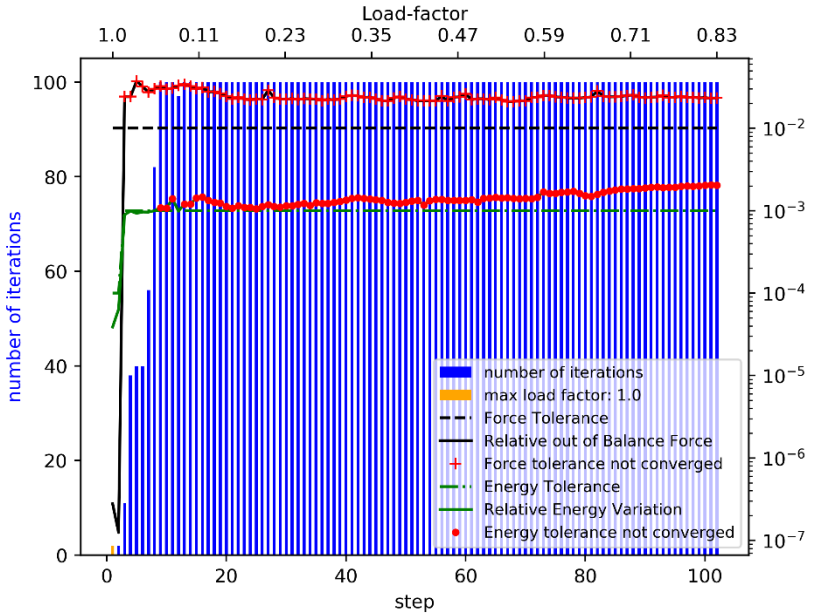

EMM URM Wall (negative X-direction)

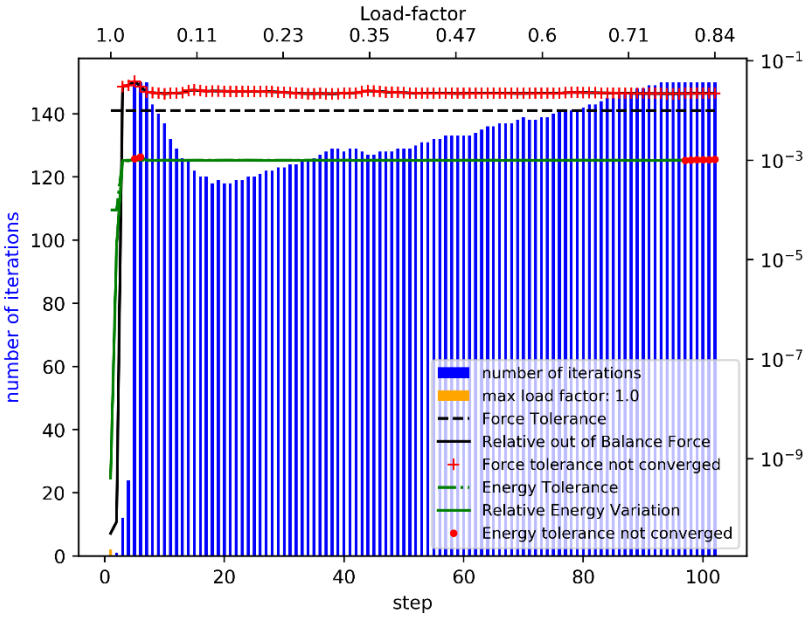

TSCM retrofitted Wall (positive X-direction)

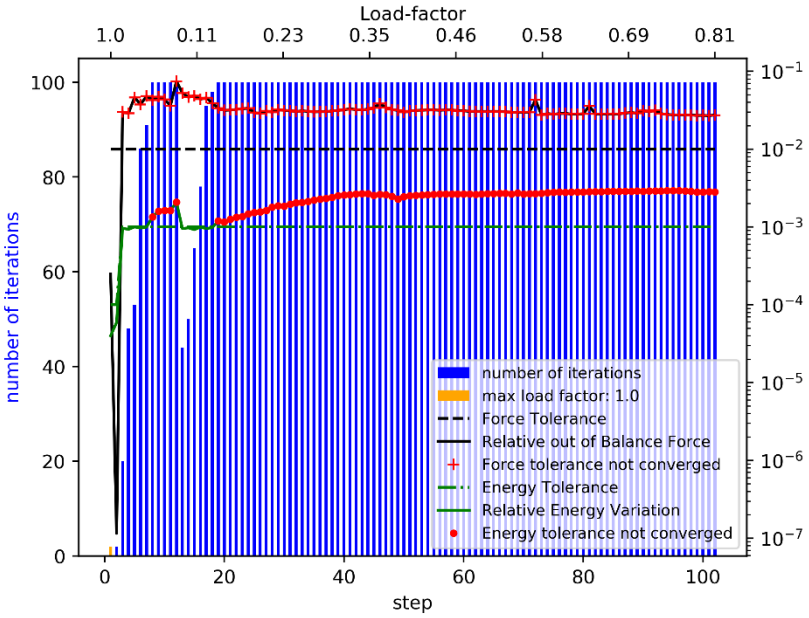

EMM retrofitted Wall (positive X-direction)

D

Appendix D

This appendix shows the influence of the iterative method on the numerical results when the URM wall and retrofitted wall only with bed joint reinforcement is studied.

Models are stopped at +44 and -40 mm displacement. By applying Secant Method, capacity curve is overestimated while Regular Newton – Raphson method provides an acceptable capacity curve. However, crack pattern is more desirable when it is estimated by Secant Method. We can use either of the methods based on what we need: accuracy in peak load or accuracy in crack pattern.

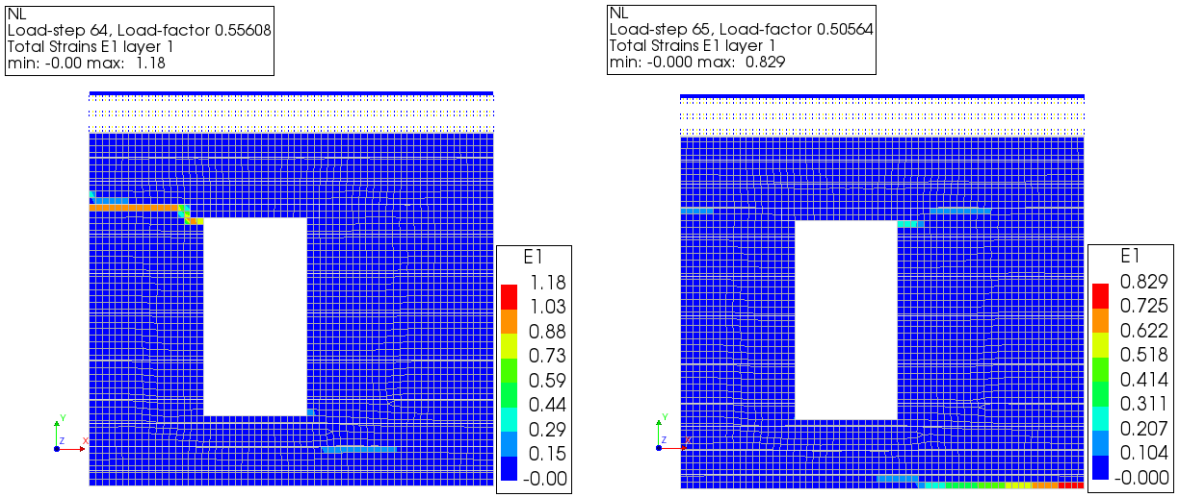

Regular Newton-Raphson Method

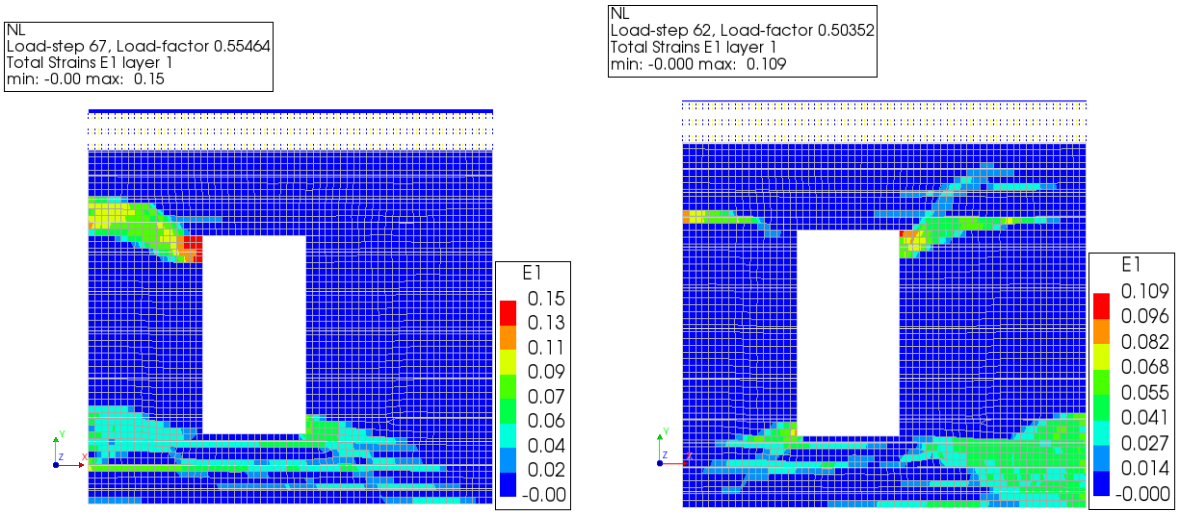

Secant Method

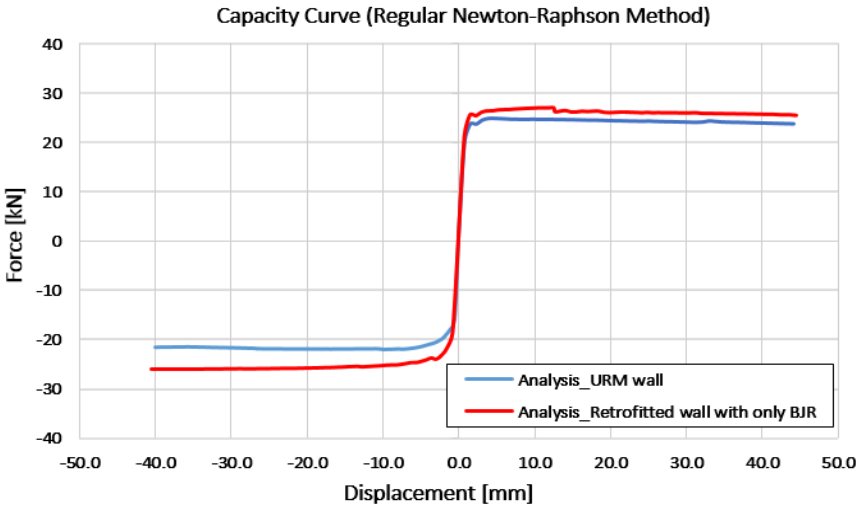

Capacity curve. Regular Newton-Raphson Method

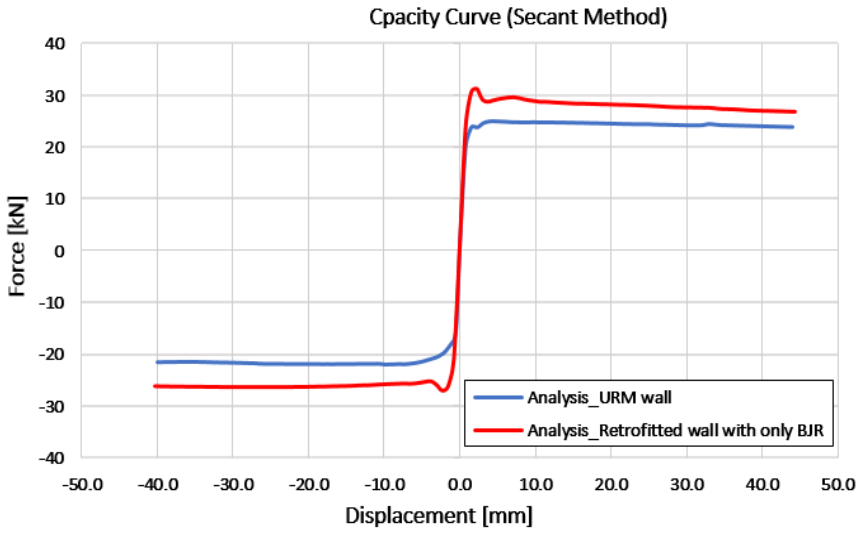

Capacity curve. Secant Method